# CO2 Capture by Metal-Organic Framework based Mixed Matrix Membranes (MMMs)

Sabetghadam, A.

**Citation (APA)**
Sabetghadam, A. (2019). *CO2 Capture by Metal-Organic Framework based Mixed Matrix Membranes (MMMs)*. [Dissertation (TU Delft), Delft University of Technology]. https://doi.org/10.4233/uuid:e3f848d9-9625-4f3c-a203-5e8e129022bf

**Important note**
To cite this publication, please use the final published version (if applicable).
Please check the document version above.

# $CO_2$ Capture by Metal-Organic Framework based Mixed Matrix Membranes (MMMs)

Propositions accompanying the PhD thesis:

**CO$_2$ Capture by Metal-Organic Framework based Mixed Matrix Membranes (MMMs)**

by Anahid Sabetghadam Esfahani

1. The solution-diffusion model is too simple to define the MOF-based MMMs performance.
   *Chapter 2 of this thesis, X. Ning, W. J. Koros, Carbon, 66 (2014) 511-522*

2. A high free volume matrix in MMMs creates alternative permeation routes for gas molecules to bypass the filler.
   *Chapter 2, 3 & 4 of this thesis*

3. Although high aspect ratio nanosheets are among the most promising MOF morphologies in MMMs, the orientation of the pores and pore topology should not be underestimated.
   *Chapter 2 & 5 of this thesis*

4. The assumption that MOFs would be ideal fillers for MMMs is still questionable.
   *Chapter 4 of this thesis & Hwang et al., Angew. Chem. Int. Ed. (2018), 57, 5156-5160*

5. The Robeson-type of graphing seems more generally applicable. E.g. take the example of quality versus quantity of published papers over time.

6. Writing a scientific paper is like a piece of art, from conceptual idea to the artistic final design.

7. Unlike in the past, people hardly neither realize nor understand the technological achievements that surround them.

8. There should be a limit to our activities that are controlled by deadlines.

9. High EQ (Emotional Quotient) is as essential as IQ (Intelligence Quotient) for success in both academic and industrial careers.

10. If there are two chefs, the soup will be too salty or tasteless.

These propositions are regarded as opposable and defendable, and have been approved as such by the promotors, prof. dr. F. Kapteijn and prof. dr. J. Gascon.

# CO$_2$ Capture by Metal-Organic Framework based Mixed Matrix Membranes (MMMs)

Proefschrift

Ter verkrijging van de graad van doctor

aan de Technische Universiteit Delft,

op gezag van de Rector Magnificus, prof.dr.ir. T.H.J.J. van der Hagen;

voorzitter van het College voor Promoties,

in het openbaar te verdedigen op

donderdag 31 Januari 2019 om 12:30 uur

door

Anahid SABETGHADAM ESFAHANI

chemische technologie, Iran University of Science and Technology, Iran

geboren te Tehran, Iran

Dit proefschrift is goedgekeurd door de promotoren.
Prof. dr. F. Kapteijn and Prof. dr. J. Gascón Sabaté

Samenstelling promotiecommissie bestaat uit:

| | |
|---|---|
| Rector Magnificus | voorzitter |
| Prof. dr. F. Kapteijn | Technische Universiteit Delft, promotor |
| Prof. dr. J. Gascón Sabaté | Technische Universiteit Delft /King Abdullah University of Science and Technology, promotor |

Onafhankelijke leden:

| | |
|---|---|
| Prof. dr. E. J. R. Sudhölter | Technische Universiteit Delft |
| Prof. dr. S.J. Picken | Technische Universiteit Delft |
| Prof.dr. J. Meuldijk | Eindhoven University of Technology |
| Dr. M. Carta | Swansea University, UK |
| Dr. I. Gascón Sabaté | University of Zaragoza, Spain |

Proefschrift, Technische Universiteit Delft
Met samenvatting in het Nederlands

An electronic version of this dissertation is available at
http://repository.tudelft.nl/.

*To all the kind people along the way*

# Table of Contents

*1*

# Introduction

*The key objective of this thesis, which forms a part of the large European project **M4CO2** in collaboration with over 16 academic and industrial partners, is to develop Mixed Matrix Membranes (MMMs) based on highly engineered Metal Organic Frameworks (MOFs) for carbon capture. In this regard, the membrane technology for capturing $CO_2$, along with the mechanisms of gas separation, will be introduced in this chapter. Finally, molecular transport in MOF-based MMMs, in which chemical compatibility, filler morphology and topology play key roles, will be discussed, and an outline of the chapters in this thesis are given.*

## 1.1 General introduction

The emergence of global warming as a significant environmental problem is likely to change the way the world produces and uses energy during the coming decades.[1, 2] Electrical power plants are responsible for 35-40% of global $CO_2$ emissions. There are approximately 5000 power plants around the world. The amount of $CO_2$ emitted by a given plant depends on the plant size and fuel feed; however, on average, a 500 megawatt electrical (MWe) power plant emits approximately 10,000 tons of $CO_2$ per day. Separating the $CO_2$ from these emissions, compressing the captured gas at high pressure (80-100 bar), and injecting it deep underground would go a long way towards mitigating the global warming problem.[1] Thus, according to the SET-Plan (European Strategic Energy Technology Plan) and the CCS (Carbon Capture and Sequestering) Technology Roadmap, the EU has agreed to deploy CCS after 2020 with the objective of 90% $CO_2$ capture at a cost of less than 23.5 euros per ton of $CO_2$ (25 euros per MWh), considering a coal power plants.[3-6] Conventional technologies such as cryogenic distillation, adsorption, condensation, and amine absorption require a gas-liquid phase change. This phase change adds a significant energy cost to the overall separation cost. In contrast, membrane gas separation offers a multitude of benefits over other separation technologies. [3, 7]

1. Membrane separation does not involve a phase change.
2. Membrane plants are smaller than amine stripping plants, and therefore have relatively smaller (physical) footprints.
3. Membrane separation processes are straightforward and allow continuous operation.

The increasing global demand for energy-efficient separations in carbon capture has prompted international action from governments and industries to establish collaborative programs to stimulate the search for novel, high-performance separation membranes.[8a] Membranes can be defined as engineered barriers that selectively control the passage of components from the feed to the permeate. This characteristic strongly depends on the use of materials with optimized structures to enhance the separation performance and reduce the energy cost required.[1, 9-11]

The primary difference between filtration and molecular separation is that a mechanical pressure gradient drives the fluid in the former, while in the latter a chemical potential gradient drives the flux through the membrane. Therefore, thermodynamic partitioning (sorption coefficient) and kinetic mobility (diffusion coefficient) are the key parameters controlling the molecular separation. Consequently, there is a clear need in materials science to engineer the chemical nature and structure of the membranes to tailor their sorption and diffusion properties and develop membrane-based processes that outperform current separation technologies.[9, 10, 12-14]
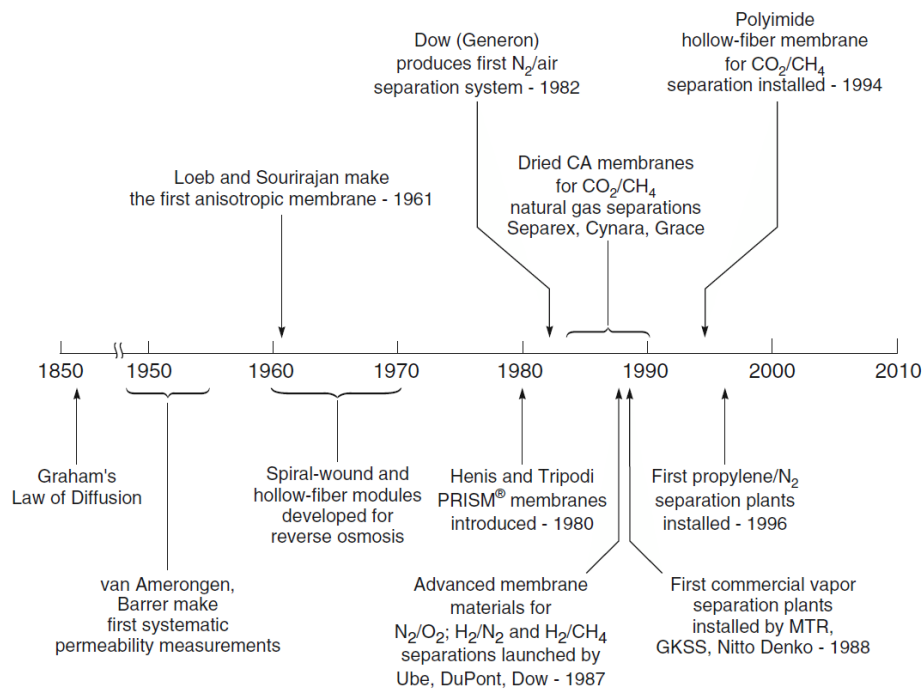
**Figure 1.1**. Milestones in the development of gas separation technologies up to 2010. Reproduced from ref [1]

## 1.2 Gas separation membranes and gas transport mechanism

Gas separation has become a major application for membrane technology over the past 30 years. However, the study of gas permeation has a long history which was started with Thomas Graham, who measured the permeation rates of several gases through different permeable diaphragms over a period of 20 years, and finally introduced the solution-diffusion model of gas permeation for the first time.[1] Figure 1.1 provides a summary of the development of gas separation technologies from 1850 to 2010.

The most important property of a membrane is its ability to selectively control the permeation of different components. Two models are used to describe permeation mechanisms: pore flow and solution-diffusion. In the pore flow model, the permeants are transported by pressure-driven convective flow through the pores of the membrane, while in the solution-diffusion model, the permeants are first dissolved in the membrane, and then diffuse through it due to the concentration gradient. In membranes for which molecular transport is best described by the solution-diffusion model, the free volume provided by the nanoscale spaces between polymer chains plays a key role. These spaces are created by the thermal motion of the polymer chains, and frequently form and collapse due to the movement of the permeants through the membranes. Figure 1.2 shows the results of a molecular dynamics simulation for a small-volume element of a polymer. [1]
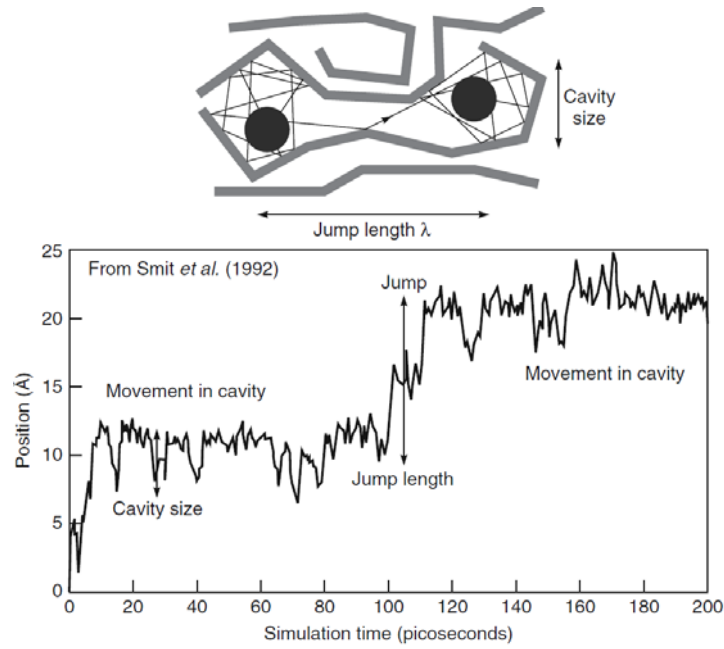
**Figure 1.2**. Motion of a carbon dioxide molecule in a 6FDA-4PDA polymer matrix. Reproduced from ref [15]

During gas separation, a gas mixture at a specific pressure ($p_o$) is applied to the feed side of the membrane, and the permeate at a lower pressure ($p_\ell$) is removed from the downstream side of the membrane. The pressure difference within the membrane is negligible, and the chemical potential gradient is often expressed (simplified) as the gradient in concentration/pressure of the feed and permeate side of the membrane. As the pressure on the feed side of the membrane is increased, the concentration at the feed-membrane interface increases, achieving a maximum value when the vapour pressure of component $i$ ($p_{i,o}$) reaches the saturation vapor pressure ($p_{i,sat}$). Similarly, the concentration at the membrane-permeate interface decreases with decreasing permeate pressure, reaching zero if a hard vacuum is applied on the permeate side of the membrane.[1]

$$p_{i,sat} \geq p_{i,0} \geq p_{i,l} \qquad\qquad (1)$$

Permeability is an intrinsic property of the membrane material, and can be expressed in an approximation as the product of diffusivity and solubility, as shown in Equation (2):

$$P_i = D_i \times S_i \qquad\qquad (2)$$

$$D_i = f_i \times \lambda_i^2 / 6 \qquad\qquad (3)$$

where $P_i$ represents the permeability of the component $i$. $D_i$ is the diffusivity, and is roughly correlated to $\lambda_i$ and $f_i$, which are defined as the random jump length and frequency of component $i$ molecules, respectively (Equation 3). $S_i$ is the sorption coefficient, and is equal to the

sorption concentration in the membrane relative to the partial pressure of component *i* in the feed.[9] The permeability unit is commonly expressed in the much used *Barrer* unit (1 Barrer = $1 \times 10^{-10}$ cm³ (STP) cm/(cm²·s·cmHg)). Another relation defining the permeability of component *i* is based on experimental data:

$$P_i = l \times N_i / \Delta p_i \qquad (4)$$

Where *L* is the membrane thickness (cm) and $N_i$ refers to the flux of component *i* through the membrane (cm³/s). Another parameter that is important for practical applications is the membrane permeance, which is expressed as:

$$J_i = P_i / l = N_i / \Delta p_i \qquad (5)$$

The permeance unit of the membrane is commonly given in GPU (Gas permeation unit), which is mainly used for thin layer membranes (1 GPU=$1 \times 10^{-6}$ cm³ (STP)/(cm²·s·cmHg)). The ideal selectivity of a membrane, which is the ratio of the permeability or permeance of the individual gases, can be defined as: [1, 9]

$$\alpha_{i,j} = P_i / P_j = J_i / J_j = (\Delta p_j \times N_i)/(\Delta p_i \times N_j) = \left[ S_i / S_j \right] \times \left[ D_i / D_j \right] \qquad (6)$$

The sorption selectivity is determined by the intrinsic chemical and structural properties of the penetrants and the penetrant-polymer interaction. These properties determine the solubility of the desired penetrant in the membrane, and therefore, the solubility selectivity can be adjusted by proper selection of the polymeric material. Instability of the functional groups that provide solubility selectivity is a problem that must be overcome for long-term operation. Penetrants sorb in the membrane matrix and diffuse in a size-dependant manner via jumps ($\lambda_i$) between the micropores and the polymer chains. These jumps are controlled by the enthalpy ($\Delta H_D$) needed for the creation of transient gaps that enable the jump to occur. Smaller penetrants require less energy, and therefore their diffusion is faster. For similarly sized penetrants, differences in vibrational and rotational movements result in different entropic factors ($\Delta S_D$), and subsequently different diffusion selectivities. The transition state theory of diffusion explains the importance of the relative dimensions of the *i* and *j* components. This theory confirms that diffusion selectivity is correlated to the ratios of the jump lengths of the respective components (size-dependence) and the exponential function of the difference in the free energies of activation, $\Delta G_{D(i,j)}$ (equation 7). [16, 17]

$$\frac{D_A}{D_B} = \left[ \frac{\lambda_i^2}{\lambda_j^2} \right] + \exp\left[ \frac{\Delta S_{D(i,j)}}{R} \right] \times \exp\left[ -\frac{\Delta H_{D(i,j)}}{RT} \right] \qquad (7)$$

## 1.3 Molecular transport in flexible and semi-rigid polymers

*Flexible polymers*: Rubbery polymers are classified as flexible polymers. In these polymers, the formation of penetrant-scale gaps occurs frequently due to the movement of the penetrants and the segmental motion of the polymer chains (Figure 1.3a, type III). The difference in the activation energies (enthalpies; $\Delta H_{D(i,j)}$) of the penetrants is responsible for the difference in the jump frequencies $f_i$ and $f_j$ (Equation 3) of the smaller molecule ($i$) versus the larger molecule ($j$), thereby providing diffusion selectivity. The flexible chains of the polymer lead to an insignificant difference between the entropic factors of the penetrants, as they do not inhibit their rotational and vibrational movements. As discussed in Section 1.2, the solubility selectivity of these polymers strongly depends on the interaction of the penetrants and the functional groups of the polymer. An additional limitation of flexible polymers is plasticization, which can be defined as the increase in the segmental motion of the polymer chains in the presence of a high concentration of the sorbed component, leading to a decrease in selectivity. One remedy to this phenomenon is crosslinking of the polymer chains, which limits their segmental motion. [18]

*Semi-rigid (glassy) polymers:* Semi-rigid polymers (Fig 1.3a, type II), such as polymers with intrinsic microporosity (PIM-1) and thermally rearranged (TR) polymers, have intermediate properties among those of flexible polymers and rigid molecular sieves.[19-21] The smaller scale of the gaps along the semi-rigid polymer chains may lead to the greater differences in the entropic factors of the permeants in comparison to the flexible polymers (equation (7)). Although the diffusion selectivity for dissimilarly sized penetrants is much greater than in flexible polymers, it is lower in comparison to rigid structures. In terms of solubility selectivity, the role of the functional groups of the polymer in adsorbing the desired penetrant is important. However, depending on the heat of adsorption, a higher desorption energy (activation energy) may be required for the penetrant to jump along the polymer backbone.

### 1.3.1 Overcoming the trade-off limit

As discussed previously, there are many applications in which the use of membranes is favored over other separation processes due to their lower energy consumption, simplicity, and smaller footprint. However, membranes are subject to a trade-off between permeability and selectivity, which is a hurdle to their application in industry.[8a] During the 1980s, permeability data for six common gases (He, $H_2$, $O_2$, $N_2$, $CO_2$, and $CH_4$) were used to quantify the trade-off relationship between permeability and selectivity. This trade-off relationship is related to an upper bound relationship where log of separation factor versus log of permeability of gas in the polymeric membranes yielded a limit called Robeson upper bound (Figure 1.3b). [8b]
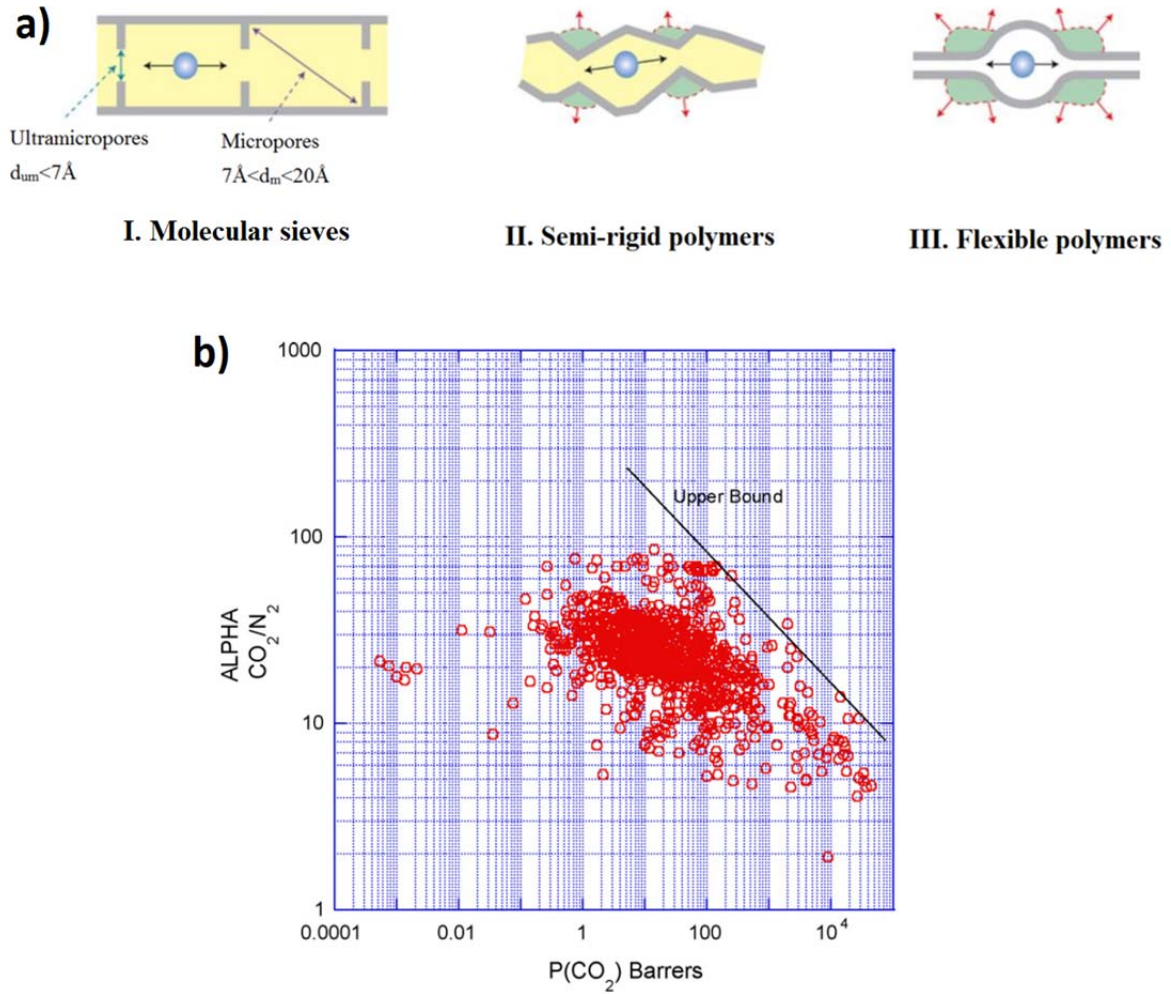
**Figure 1.3**. Molecular sieves with a rigid ultramicropore and micropore morphology (type I), Semi-rigid polymers with a distribution of connected pores created by segmental packing (type II), Flexible polymers with a transient gap distribution created by segmental packing and motion (type III) (a). Reproduced from ref [9], Upper bound correlation for $CO_2/N_2$ separation (b). Reproduced from ref [8b]

The upper-bound was acquired by adding the trend line to the experimental permeation performance data of the membranes that have the highest selectivity for a given permeability, following equation (8) and (9).[8c]

$$\alpha_{i,j} = \beta_{i,j} \cdot P_i^{-\lambda_{i,j}} \tag{8}$$

$$\lambda_{i,j} = \left(\frac{d_j}{d_i}\right)^2 - 1 \tag{9}$$

In these equations, $\lambda_{ij}$ depends on the diameters of the gas pair, while $d_j$ and $d_i$ are the kinetic diameters of the larger and smaller gas molecules, respectively. The parameter $\beta_{ij}$ is mainly correlated with the gas solubility and the polymer chain distance and stiffness.[8d] The Robeson

upper bound was revised in 2008 for more permeable and selective membranes, but only a modest shift was observed for most gas pairs. The shift in the upper-bound limit was mainly attributed to variation in $\beta_{ij}$, while the slope of the upper-bound ($\lambda_{ij}$) remained constant. Two classes of highly permeable polymers, PIMs (polymers of intrinsic microporosity) and thermally rearranged polymers, surpassed the upper-bound.[19, 8e] Examining the roles of glassy versus rubbery polymers, it is noteworthy that glassy polymers show higher gas solubility due to their higher free volume in comparison with rubbery polymers. The higher free volume results in additional sorption of the gases. Thus, glassy polymers dominated the upper-bound, mainly due to their higher gas solubility.[21, 8f] The upper bound will not indefinitely extended as the permeability of the gases increases. In fact the mechanism of permeability will change from solution-diffusion to molecular sieving in case of ladder-type polymer structures (PIMs) and then shift to Knudsen diffusion as the pore size of the membrane increases. The example of the latter is PTMSP with pore diameter in the range of 0.9-1.2 nm which offer the end permeability data of $CO_2$/$N_2$ 2008 upper bound. The upper bound relationship (equation (8)) is mainly diffusion-dominated as diffusion selectivity varies with permeability while solubility selectivity is invariant ($\beta_{ij}$). The transition from solution-diffusion to Knudsen diffusion is where diffusion selectivity of the membrane is equal to Knudsen diffusion selectivity. The Knudsen diffusion selectivity is equal to the square root of the molecular weight of the permeants ($\sqrt{(M_{N2}/M_{CO2})}$).[8b]

The exploration of efficient approaches to surpass the upper-bound are urgently required. One method to overcome the challenges associated with obtaining membrane performance well above the Robson upper-bound is to disperse molecular sieving fillers in polymers to prepare MMMs.[1]

## 1.4 Molecular transport in molecular sieves

The molecular sieve structure is presented in Figure 1.3a (Type I). Molecular sieves can be divided into two categories: crystalline and amorphous molecular sieves. Zeolites and metal organic frameworks (MOFs) are crystalline subgroups, and carbon molecular sieves belong to the amorphous category. These materials do not suffer from the plasticization issues that are observed for polymers. In most molecular sieves, the jump lengths of the penetrants in equation (7) are almost equal due to the rigidity of the structure. However, differences in their enthalpies and entropies both contribute to diffusion selectivity. Rigid molecular sieve structures are promising materials for the separation of many gas pairs.[22] In this case, the motion of the larger molecule is more hindered compared to the smaller one, leading to higher diffusion selectivity. Moreover, the relative condensability and partial pressure of the components in the feed are the important parameters for adjusting the separation selectivity of $CO_2$ and $N_2$ pairs. However, the strong sorption and greater condensability of one species (i.e., a hydrocarbon or $CO_2$) can

dramatically hinder the permeation of a smaller penetrant such as $H_2$ in $H_2$/hydrocarbon separation, which is unfavorable.[23, 24]

**MOFs**: MOFs are an important class of crystalline molecular sieves that consist of networks of metal ions/clusters and organic linkers.[25] The extraordinary structural variety of MOFs makes them unique among porous structures, and they are considered to be among the most sophisticated nanostructured material.[26] In addition to their high surface area and pore volume, their chemical nature can be engineered by independently selecting a suitable metal ion/cluster and organic linker to obtain an appropriate building block for the selective separation of gases.[3] Moreover, the porosity of MOFs is much higher than that of their inorganic counterpart (zeolites) and their facile functionalization makes them unique. In some cases, MOFs undergo structural changes upon the adsorption of certain species (breathing), confirming the potential advantages of framework design in creating dynamic porous materials.[27-29] Although MOFs can be structurally engineered to achieve high sorption selectivity, preserving the sorption selectivity at increased pressure is challenging due to saturation of the adsorptive sites. Therefore, to take advantage of the entropic factor differences in Equation (7), MOFs with smaller aperture sizes (<4-5 Å) are required to achieve size selective separations.[30-32] As reported by Zhang *et al*., zeolitic imidazolate framework-8 (ZIF-8) (aperture size of ~4.0 Å) is an attractive MOF for the separation of important gas pairs (for example, $O_2/N_2$, $CO_2/N_2$, $H_2/CH_4$, and $CO_2/CH_4$).[33] As reported by Rui *et al*, the strong $CO_2$ sorption of MOF-5 membranes at elevated pressures can enhance the $CO_2/CH_4$ selectivity of the membrane tremendously (up to 324) due to the blockage of the diffusion paths for the less-condensable $CH_4$ molecules.[34] These sieving characteristics open the way towards the fabrication of membranes with performances exceeding even those of crosslinked flexible or glassy polymers for gas separation. Thus, enhancement of diffusion selectivity by tuning the MOF aperture size and simultaneously improving the sorption selectivity by tuning the MOF chemistry is certainly a very attractive approach for MOF membrane development, although it must be mentioned that the larger structural flexibility of MOFs result in lower selectivities than for zeolites The main challenge in fabricating pure MOF membranes is to prepare defect-free membranes.[24]

**$CO_2$-philic site decorated MOFs**: By imparting open metal sites or ligands containing functional groups to a MOF (in most cases, MOFs with larger pores), $CO_2$ molecules can be selectively captured from dilute gas streams.[35-39] Jiang *et al.* reported the introduction of azide groups inside the pores of a Zr-MOF, which provided a new approach to introduce diverse functional groups into the pores of MOF.[40] Additionally, amine functional groups have been extensively studied, and represent a successful approach to enhance the $CO_2$-philicity of MOFs. Vaidhyanathan *et al.* systematically studied $CO_2$ sorption on amine groups in functionalized MOFs. They reported that a higher degree of amine functionalization did not enhance $CO_2$

sorption, since this can hinder $CO_2$ interaction to the amine groups.[41] Another approach to enhance the $CO_2$-philicity of a MOF is to add N-containing functional groups and O-containing hydroxyl groups. Cui *et al*. discussed the use of $CO_2$-philic multi-sites in the zeolite-like microporous tetrazole-based MOF framework. The multiple sites that were attractive for $CO_2$ molecules, including the *π*-electrons of aromatic tetrazole rings, nitrogen atoms of tetrazole rings, and the C-H bonds in the $O-(CH_2CH_2-)_2$ moiety, played a key role in enhancing the $CO_2$ capture and achieving excellent $CO_2/CH_4$ selectivity.[42] In general, MOFs that have a small pore aperture in the range of the kinetic diameter of the target molecules and a relatively high $CO_2$ adsorption capacity are the best candidates for membrane separation.[43]

## 1.5 Molecular transport in hybrid materials (MMMs)

Combining rigid and highly selective structures (type I) and a processable polymer matrix (type II or III) is advantageous for fabricating a membrane with considerable separation performance (Fig 1.4a). It is of primary importance to choose selective rigid structures with a separation performance well above the upper bound of the polymer. Secondly, the selected sieve structure should show good compatibility and matching with the continuous phase (polymer) to achieve the desired separation performance. By simply using Equation (10), the Maxwell relation[44] applied to mixed matrix membranes, and knowing the permeability of component *i* in the MMM ($P_{imm}$) and polymer ($P_{ic}$) and the dispersed sieve phase volume fraction ($\varphi_d$), it is possible to back-calculate the permeability of the dispersed sieve phase ($P_{id}$).[45] By using this equation, one can depict the variation of selectivity versus permeability for a specific sieve filler with various polymers to gain insight in to the influence of the permeation of each phase on the overall permeability of the hybrid membranes. According to the results shown in Figure 1.4b, the optimal selectivity *versus* permeability for the gas pair $C_3H_6/C_3H_8$ is achieved when the permeability ratio of the polymer to the sieve (in this case ZIF-8) is approximately 0.15. In this case, the selectivity of the hybrid membrane reaches its highest value.[9, 46, 47] It is worth emphasizing that the match between the sieve and the polymer and the proper permeability ratio of the components in the hybrid material are the key parameters for obtaining optimum performance.

$$P_{imm} = P_{ic} \left[ \frac{P_{id} + 2P_{ic} + 2\varphi_d \left( P_{ic} - P_{id} \right)}{P_{id} + 2P_{ic} - \varphi_d \left( P_{ic} - P_{id} \right)} \right] \qquad (10)$$

### 1.5.1 MOF-based MMMs

Although pure MOF membranes show enhanced selectivity, the main hurdle to achieving satisfactory permeation performance is the trade-off between permeability and selectivity.

Moreover, the fabrication of pure MOF membranes may result in a defective structure, which can dramatically influence the separation performance. One strategy to address these issues is to combine MOFs and polymers to create MOF-based mixed matrix membranes. Membranes produced by this strategy can outperform current pure polymeric and MOF membranes due to the combination of the intrinsic properties of polymers and MOFs (Figure 1.5). The first MOF-based MMM was reported by Yehia *et al.* in 2004, and comprised Cu-BPDC and poly(3-acetoxyethylthiophene) for $CO_2/CH_4$ separation. Subsequently, a great deal of research was conducted in this area.[48] The use of MOFs as the dispersed phase of the hybrid membranes might result in better compatibility between the MOFs and the polymers due to linker-polymer interactions, and may eventually avoid the formation of the so-called sieve in cage morphology in mixed matrix membranes.[28, 49, 50] Moreover, the adjustable size, shape, and functionality of the cavities can be tuned by choosing different ligands in order to obtain the desired structure.[51]

In addition, the densities of MOFs are commonly lower than that of zeolites due to their larger pore volume; therefore, their effect by weight percentage is more significant than that of zeolites. Although the incorporation of MOFs in polymers may considerably enhance the separation performance compared to the pure material in terms of selectivity and permeability, significant challenges still remain to obtain satisfactory results based on industrial standards. The strategies to overcome these challenges in mixed matrix membranes include post-treatment of the membrane, post-synthetic modifications, and improving the interfacial adhesion between the MOF and the polymer to reach industrial standards. However, defect formation in high loading of MOFs is still a major challenge in the preparation of MMMs that must be overcome. [43, 52, 53]
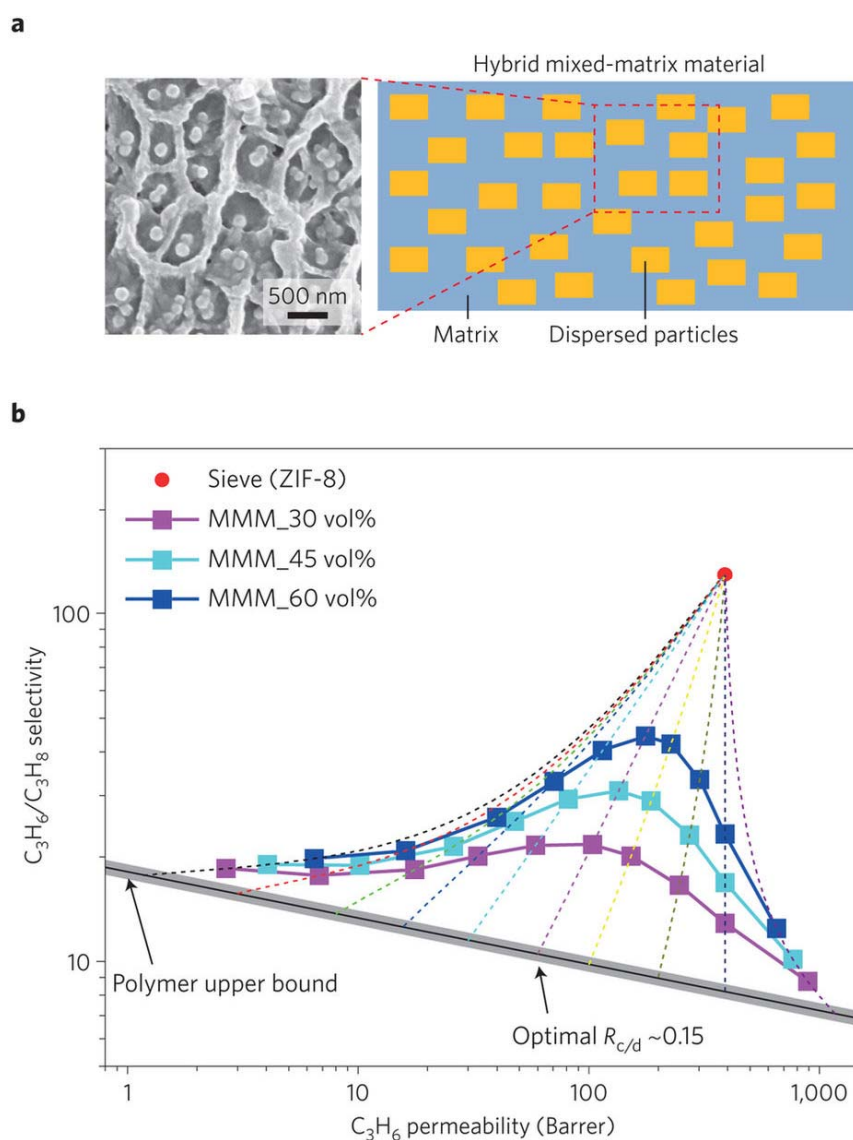
**Figure 1.4**. (a) Schematic and scanning electron microscope (SEM) images of MMMs, (b) Polymer–sieve matching for hybrid MMMs. The dotted lines represent the properties of mixtures of ZIF-8 with different polymers as the continuous phase that showed better performance than the polymer upper bound for $C_3H_6/C_3H_8$ separation. The ratio of polymer to sieve permeability is shown in range of 0.003-3.0 and the optimal ratio is around 0.15. Reproduced from ref [9]

*Polymer-MOF compatibility:* Obtaining optimum MMM separation performance strongly depends on the properties of the polymer and MOFs. The chemical structure, surface chemistry, particle size distribution, and aspect ratio are the parameters with the greatest influence in MOFs. To quantify the true effect of the filler in MMMs, a high loading of well-dispersed MOF is required. However, the fabrication of high-loading MMMs is quite challenging due to the weak interaction of the polymer chains around the agglomerated particles, creating non-selective voids. [54, 55]
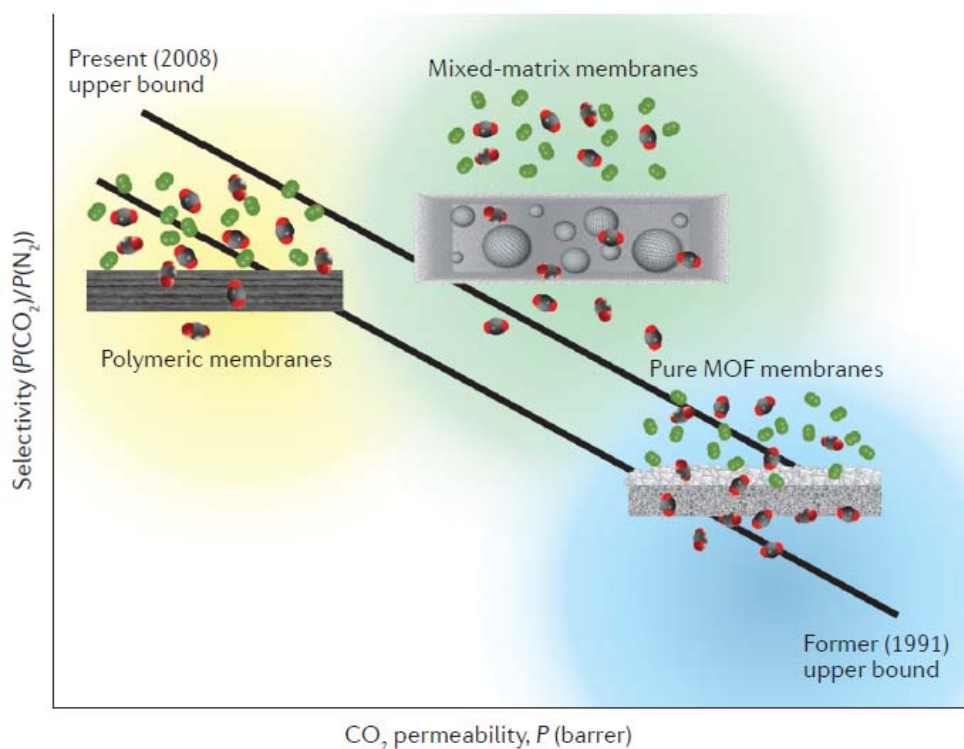
**Figure 1.5**. CO$_2$ and N$_2$ selectivity versus CO$_2$ permeability of pure polymeric, mixed-matrix, and pure MOF membranes versus Robeson upper bound. Reproduced from ref [43]

Thus, the interface of the filler and the polymer should first be assessed using known characterization techniques such as FIB-SEM tomography and IR characterizations or by available rigorous mathematical models that can predict the interfacial interactions between fillers and polymers in advance.[28, 56] Among various MOFs used in the preparation of MMMs and known polymers, ZIFs and MOFs containing amine groups show the best interactions for gas separation. In the case of ZIFs incorporated in polymers such as PBI, the similar ligand and polymer functional groups facilitate interaction between the polymer and the filler. As reported by Yao *et al*., incorporating up to 16 wt.% ZIF-11 in PBI improved both the permeability and selectivity of the MMMs for H$_2$/CO$_2$ separation.[57]

The same approach was followed by Zornoza *et al*., who used NH$_2$-MIL-53(Al) with amine functional groups as a filler to enhance the permeation performance of polysulfone membranes. Their results demonstrated an excellent adhesion of MOF with polysulfone Udel polymer due to the hydrogen bonding interaction.[27]
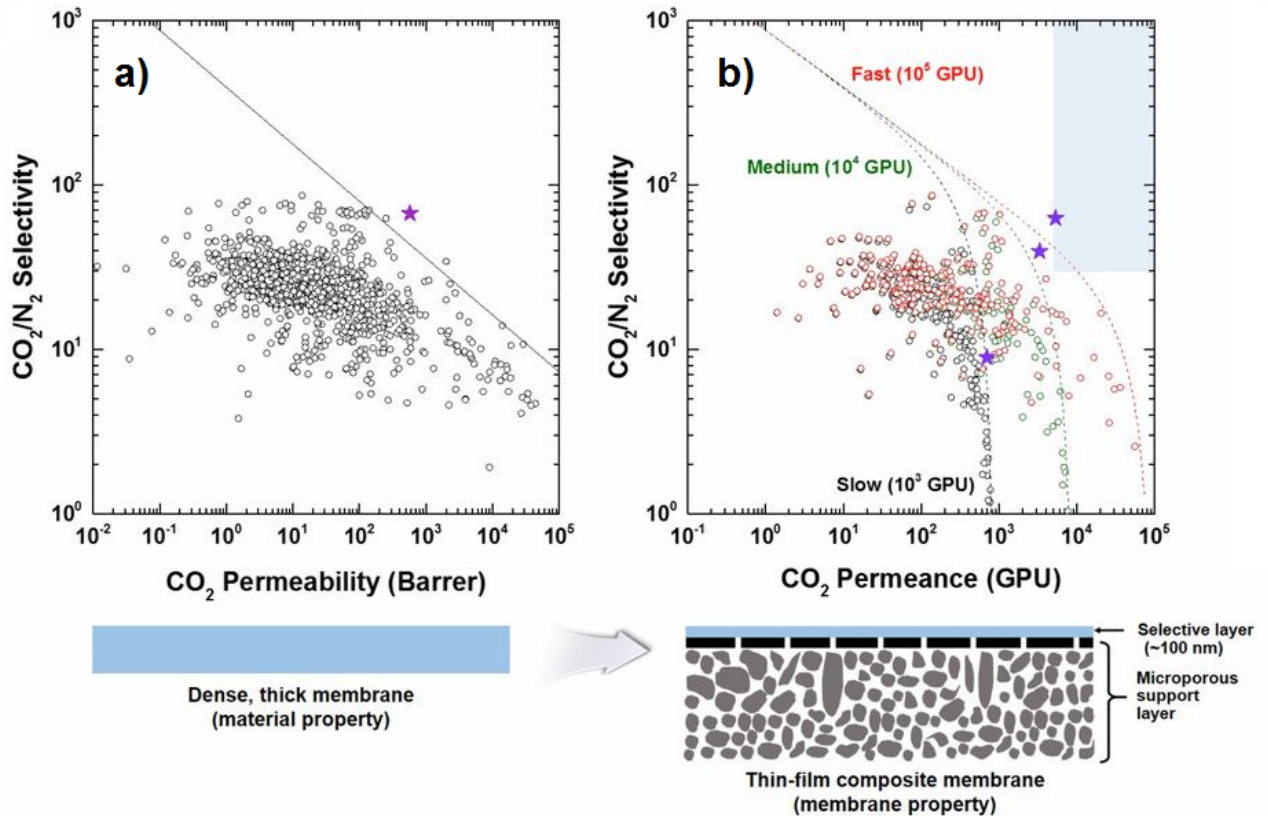
**Figure 1.6.** Robeson upper-bound data for $CO_2/N_2$ separation (a) and its translation into selectivity versus permeance, based on different support permeance (b). The star represents the permeability/selectivity of a hypothetical material with separation performance above the upper bound (a) and the permeance/selectivity of hypothetical thin-film composite membranes, using different supports (b), shaded region represents the post-combustion $CO_2$ capture target area. Reproduced from ref [8a].

*MOF morphology*: The morphology of the MOF can be easily tuned by specific modification of the synthesis procedure without changing the chemical properties of the MOF, and can extensively alter the MMM performance. Several studies have focused on loading nanoparticles in the membrane matrix for increased surface area, which allows a better interaction with the polymer chains.[46, 58] However, the appropriate dispersion of nanoparticles in a polymer is challenging due to the strong inter-particle interactions, which can lead to agglomerated nanoparticles or defect formation between the polymer and the dispersed phase.[3] In this regard, one strategy is to use high aspect ratio ultra-thin sheets that can efficiently enhance the performance of the MMMs. Anisotropically (e.g., sheet-like) shaped materials enhance the permeation performance of the MMMs compared to isotropically shaped materials.
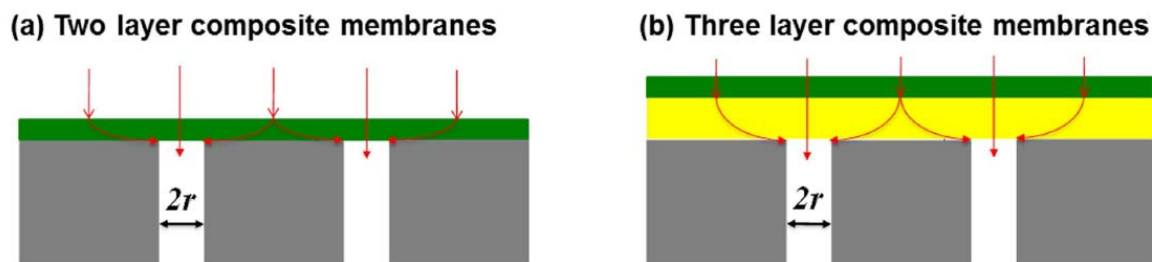
**Figure 1.7**. Schematic of thin film composite membranes: (a) with no PDMS gutter layer and (b) with PDMS gutter layer. Reproduced from ref [62]

Therefore, the incorporation of even a small amount of nanosheets (2-8 wt.%) in the membrane matrix could greatly enhance the separation performance of the membranes.[59, 60] When such high-aspect-ratio nanomaterials are incorporated in the polymer matrix, the resulting MMMs show enhanced separation performance due to the elimination of non-selective voids and effective molecular filtering of the gas transport in the membrane matrix.

## 1.6 Thin supported membranes

Although many studies have focused on improving the separation performance, the ultimate goal is to produce a membrane with a large flux (or permeance) together with good selective separation of the desired component for practical use. Therefore, a membrane with a thin separation layer coated on a low resistance porous support is needed to meet the criteria for large-scale application.

The influence of support resistance on the permeance of some composite membranes with upper-bound performances is shown in Figure 1.6b (the 2008 upper-bound for $CO_2/N_2$ separation has been translated to selectivity versus permeance for thin composite membranes). Supports can be categorized as slow ($10^3$ GPU), medium ($10^4$ GPU), or fast ($10^5$ GPU); these classifications are correlated to the resistance of the porous support to the permeation of gas molecules. The separation performances of supported thin layer membranes can be shifted towards the industrially desirable region (blue shaded area) by using a fast support.[61] Although the role of the support in mass transfer through the composite is considered negligible in some cases, this assumption becomes less valid as the thickness of the thin layer decreases and as the membrane becomes more permeable.[8a] The resistance of the support not only influences the permeance of the thin layer, but can also reduce the selectivity far below the intrinsic selectivity of the material. [62-64] The thickness of the thin membranes can be as little as 100 nm. Therefore, the support should be mechanically robust and inexpensive so that it can be utilized in the scaled-up production of composite membranes in industry. As it is illustrated in figure 1.7, a gutter layer with almost negligible mass transfer resistance can channel the flow and mitigate the geometric

restrictions of porous support. Moreover, as the thickness of the thin layer is very low (below ~100 nm), the distance that the penetrants must travel to reach the support pores is greater than the thickness of the thin layer, and the thin membrane cannot achieve its expected real flux. Thus, coating a highly permeable and thin gutter layer made of PDMS or PTMST between the support and thin layer is a simple solution to facilitate the molecular permeation pathway in the composite. Thus, designing new membranes without considering the influence of the support can lead to worse performance than self-standing membranes.[65]

## 1.7 Thesis outline

The main challenge that will be addressed in this thesis is the engineering of MOF-based MMMs to enhance their separation performance with the aim of $CO_2$ capture. To meet this objective, the MOF morphology, MOF pore structure (topology), polymer free volume and rigidity will play a key role. The above-mentioned study led to four research chapters, which are categorized into microscopic and macroscopic studies of MOFs and polymers as the main components of MOF-based MMMs. Finally, an approach towards industrial application is evaluated by fabricating thin composite MMMs using MOF nanosheets which will be thoroughly discussed. A brief overview of the following chapters is given below.

**Chapter 2** quantifies the role of the microscopic properties of MOFs, such as pore size, structure, and topology, on the MMM performance. Additionally, the solubility and diffusivity of $CO_2$ in the membrane matrix were investigated through adsorption studies and using the theoretical solution-diffusion model.

**Chapter 3** deals with the influence of the macroscopic properties of MOFs (size and morphology) on MMMs $CO_2$ separation performance. Three different morphologies of $NH_2$-MIL-53(Al), namely nanoparticles, microneedles, and nanorods, were synthesized and incorporated in low (Matrimid) and high (6FDA-DAM) free-volume membranes, which were tested under different feed pressures. This study highlights the importance of the crystal engineering of MOFs in the field of mixed matrix membranes.

**Chapter 4** focuses on the polymeric phase of the MMMs by doping glassy Matrimid® chains in to an ultra-high free volume PIM-1 matrix along with the addition of MOF fillers ($NH_2$-MIL-53(Al) and ZIF-94). Doping of the ultra-high and low free volume polymeric matrices resulted in a substantial enhancement of $CO_2$ permeability and $CO_2/N_2$ selectivity, and interestingly, reduced the initial aging of PIM-1. The obtained membrane performance exceeds the 2008 Robeson upper bound limit and reaches the economic target region for post-combustion $CO_2$ capture, even after 17 months of aging.

**Chapter 5** illustrates two different approaches in fabricating the supported thin layer MMMs comprising Cu-BDC nanosheets and the highly selective block co-polymer (Polyactive™). This

study presents the role of nanosheets in healing the defects of the thin membranes due to covering the lateral surface of the thin layer. Finally, the thin film composite TFC membranes performance was compared with theoretical models.

All chapters have been written as individual publications and can be read independently. Therefore, some overlap may be present.

# References

[1]     R.W. Baker, Membrane technology and application, second ed., John Wiley & Sons.Ltd, 2004.

[2]     S. Pacala, R. Socolow, Stabilization Wedges: Solving the Climate Problem for the Next 50 Years with Current Technologies, Science, 305 (2004) 968-972.

[3]     B. Seoane, J. Coronas, I. Gascon, M.E. Benavides, O. Karvan, J. Caro, F. Kapteijn, J. Gascon, Metal-organic framework based mixed matrix membranes: a solution for highly efficient CO2 capture?, Chemical Society Reviews, 44 (2015) 2421-2454.

[4]     F. Princiotta, Global Climate Change - The Technology Challenge, 1 ed., Springer Netherlands, 2011.

[5]     E. Publication, 2013 Technology map of the European Strategic Energy Technology Plan (SET-Plan), in: E. union (Ed.), EU Publication, 2013.

[6]     D.M. D'Alessandro, B. Smit, J.R. Long, Carbon Dioxide Capture: Prospects for New Materials, Angewandte Chemie International Edition, 49 (2010) 6058-6082.

[7]     P. Bernardo, E. Drioli, G. Golemme, Membrane Gas Separation: A Review/State of the Art, Industrial & Engineering Chemistry Research, 48 (2009) 4638-4663.

[8]     (a) H.B. Park, J. Kamcev, L.M. Robeson, M. Elimelech, B.D. Freeman, Maximizing the right stuff: The trade-off between membrane permeability and selectivity, Science, 356 (2017). (b) L.M. Robeson, The upper bound revisited, Journal of Membrane Science, 320 (2008) 390-400. (c) L.M. Robeson, Correlation of separation factor versus permeability for polymeric membranes, Journal of Membrane Science, 62 (1991) 165-185. (d) B.D. Freeman, Basis of Permeability/Selectivity Tradeoff Relations in Polymeric Gas Separation Membranes, Macromolecules, 32 (1999) 375-380. (e) P.M. Budd, N.B. McKeown, D. Fritsch, Free volume and intrinsic microporosity in polymers, Journal of Materials Chemistry, 15 (2005) 1977-1986. (f) L.M. Robeson, Q. Liu, B.D. Freeman, D.R. Paul, Comparison of transport properties of rubbery and glassy polymers and the relevance to the upper bound relationship, Journal of Membrane Science, 476 (2015) 421-431.

[9]     W.J. Koros, C. Zhang, Materials for next-generation molecularly selective synthetic membranes, Nature Materials, 16 (2017) 289.

[10]    W.J. Koros, R.P. Lively, Water and beyond: Expanding the spectrum of large-scale energy efficient separation processes, AIChE Journal, 58 (2012) 2624-2633.

[11]    R.W. Baker, Future Directions of Membrane Gas Separation Technology, Industrial & Engineering Chemistry Research, 41 (2002) 1393-1411.

[12]    W.J. Koros, G.K. Fleming, Membrane-based gas separation, Journal of Membrane Science, 83 (1993) 1-80.

[13]    W.J. Koros, G.K. Fleming, S.M. Jordan, T.H. Kim, H.H. Hoehn, Polymeric membrane materials for solution-diffusion based permeation separations, Progress in Polymer Science, 13 (1988) 339-401.

[14]    G.M. Geise, D.R. Paul, B.D. Freeman, Fundamental water and salt transport properties of polymeric materials, Progress in Polymer Science, 39 (2014) 1-42.

[15]    E. Smit, M.H.V. Mulder, C.A. Smolders, H. Karrenbeld, J. van Eerden, D. Feil, Modelling of the diffusion of carbon dioxide in polyimide matrices by computer simulation, Journal of Membrane Science, 73 (1992) 247-257.

[16]    X. Ning, W.J. Koros, Carbon molecular sieve membranes derived from Matrimid® polyimide for nitrogen/methane separation, Carbon, 66 (2014) 511-522.

[17]    A. Singh, W.J. Koros, Significance of Entropic Selectivity for Advanced Gas Separation Membranes, Industrial & Engineering Chemistry Research, 35 (1996) 1231-1234.

[18]    I.C. Omole, R.T. Adams, S.J. Miller, W.J. Koros, Effects of CO2 on a High Performance Hollow-Fiber Membrane for Natural Gas Purification, Industrial & Engineering Chemistry Research, 49 (2010) 4887-4896.

[19]    H.B. Park, C.H. Jung, Y.M. Lee, A.J. Hill, S.J. Pas, S.T. Mudie, E. Van Wagner, B.D. Freeman, D.J. Cookson, Polymers with Cavities Tuned for Fast Selective Transport of Small Molecules and Ions, Science, 318 (2007) 254-258.

[20]    N.B. McKeown, P.M. Budd, Polymers of intrinsic microporosity (PIMs): organic materials for membrane separations, heterogeneous catalysis and hydrogen storage, Chemical Society Reviews, 35 (2006) 675-683.

[21]    D.F. Sanders, Z.P. Smith, R. Guo, L.M. Robeson, J.E. McGrath, D.R. Paul, B.D. Freeman, Energy-efficient polymeric gas separation membranes for a sustainable future: A review, Polymer, 54 (2013) 4729-4761.

[22]    N. Kosinov, J. Gascon, F. Kapteijn, E.J.M. Hensen, Recent developments in zeolite membranes for gas separation, Journal of Membrane Science, 499 (2016) 65 - 79.

[23]    M.B. Rao, S. Sircar, Nanoporous carbon membranes for separation of gas mixtures by selective surface flow, Journal of Membrane Science, 85 (1993) 253-264.

[24]    v.d.B.L.J. P., B.W.J. W., K. Freek, M.J. A., Binary permeation through a silicalite-1 membrane, AIChE Journal, 45 (1999) 976-985.

[25]    M. O'Keeffe, O.M. Yaghi, Deconstructing the Crystal Structures of Metal–Organic Frameworks and Related Materials into Their Underlying Nets, Chemical Reviews, 112 (2012) 675-702.

[26]    S. Kitagawa, R. Kitaura, S.i. Noro, Functional Porous Coordination Polymers, Angewandte Chemie International Edition, 43 (2004) 2334-2375.

[27]    B. Zornoza, A. Martinez-Joaristi, P. Serra-Crespo, C. Tellez, J. Coronas, J. Gascon, F. Kapteijn, Functionalized flexible MOFs as fillers in mixed matrix membranes for highly selective separation of CO2 from CH4 at elevated pressures, Chemical Communications, 47 (2011) 9522-9524.

[28]    T. Rodenas, M.v. Dalen, E. García-Pérez, P. Serra-Crespo, B. Zornoza, F. Kapteijn, J. Gascon, Visualizing MOF Mixed Matrix Membranes at the Nanoscale: Towards Structure-Performance Relationships in CO2/CH4 Separation Over NH2-MIL-53(Al)@PI, Advanced Functional Materials, 24 (2014) 249-256.

[29]    T. Rodenas, M. van Dalen, P. Serra-Crespo, F. Kapteijn, J. Gascon, Mixed matrix membranes based on NH2-functionalized MIL-type MOFs: Influence of structural and operational parameters on the CO2/CH4 separation performance, Microporous and Mesoporous Materials, 192 (2014) 35-42.

[30]    A. Cadiau, K. Adil, P.M. Bhatt, Y. Belmabkhout, M. Eddaoudi, A metal-organic framework–based splitter for separating propylene from propane, Science, 353 (2016) 137-140.

[31]    C. Zhang, W.J. Koros, Tailoring the Transport Properties of Zeolitic Imidazolate Frameworks by Post-Synthetic Thermal Modification, ACS Applied Materials & Interfaces, 7 (2015) 23407-23411.

[32]    K. Eum, K.C. Jayachandrababu, F. Rashidi, K. Zhang, J. Leisen, S. Graham, R.P. Lively, R.R. Chance, D.S. Sholl, C.W. Jones, S. Nair, Highly Tunable Molecular Sieving and Adsorption Properties of Mixed-Linker Zeolitic Imidazolate Frameworks, Journal of the American Chemical Society, 137 (2015) 4191-4197.

[33]    C. Zhang, W.J. Koros, Zeolitic Imidazolate Framework-Enabled Membranes: Challenges and Opportunities, The Journal of Physical Chemistry Letters, 6 (2015) 3841-3849.

[34]    Z. Rui, J.B. James, A. Kasik, Y.S. Lin, Metal-organic framework membrane process for high purity $CO_2$ production, AIChE Journal, 62 (2016) 3836-3841.

[35]    A.-H. Lu, G.-P. Hao, Porous materials for carbon dioxide capture, 2013.

[36]    B. Li, Z. Zhang, Y. Li, K. Yao, Y. Zhu, Z. Deng, F. Yang, X. Zhou, G. Li, H. Wu, N. Nijem, Y.J. Chabal, Z. Lai, Y. Han, Z. Shi, S. Feng, J. Li, Enhanced Binding Affinity, Remarkable Selectivity, and High Capacity of $CO_2$ by Dual Functionalization of a rht-Type Metal–Organic Framework, Angewandte Chemie International Edition, 51 (2012) 1412-1415.

[37]    W. Lu, J.P. Sculley, D. Yuan, R. Krishna, Z. Wei, H.C. Zhou, Polyamine-Tethered Porous Polymer Networks for Carbon Dioxide Capture from Flue Gas, Angewandte Chemie International Edition, 51 (2012) 7480-7484.

[38]    H.J. Park, M.P. Suh, Enhanced isosteric heat of H2 adsorption by inclusion of crown ethers in a porous metal-organic framework, Chemical Communications, 48 (2012) 3400-3402.

[39]    F. Debatin, J. Mollmer, S.S. Mondal, K. Behrens, A. Moller, R. Staudt, A. Thomas, H.-J. Holdt, Mixed gas adsorption of carbon dioxide and methane on a series of isoreticular microporous metal-organic frameworks based on 2-substituted imidazolate-4-amide-5-imidates, Journal of Materials Chemistry, 22 (2012) 10221-10227.

[40]    H.-L. Jiang, D. Feng, T.-F. Liu, J.-R. Li, H.-C. Zhou, Pore Surface Engineering with Controlled Loadings of Functional Groups via Click Chemistry in Highly Stable Metal–Organic Frameworks, Journal of the American Chemical Society, 134 (2012) 14690-14693.

[41]    R. Vaidhyanathan, S.S. Iremonger, G.K.H. Shimizu, P.G. Boyd, S. Alavi, T.K. Woo, Competition and Cooperativity in Carbon Dioxide Sorption by Amine-Functionalized Metal–Organic Frameworks, Angewandte Chemie International Edition, 51 (2012) 1826-1829.

[42]    S.D. Burd, S. Ma, J.A. Perman, B.J. Sikora, R.Q. Snurr, P.K. Thallapally, J. Tian, L. Wojtas, M.J. Zaworotko, Highly Selective Carbon Dioxide Uptake by [Cu(bpy-n)2(SiF6)] (bpy-1 = 4,4′-Bipyridine; bpy-2 = 1,2-Bis(4-pyridyl)ethene), Journal of the American Chemical Society, 134 (2012) 3663-3666.

[43]    C.A. Trickett, A. Helal, B.A. Al-Maythalony, Z.H. Yamani, K.E. Cordova, O.M. Yaghi, The chemistry of metal–organic frameworks for $CO_2$ capture, regeneration and conversion, Nature Reviews Materials, 2 (2017) 17045.

[44]    J.C. Maxwell, Treatise on Electricity and Magnetism, University of Oxford, London, 1873.

[45]    J.H. Petropoulos, K.G. Papadokostaki, M. Minelli, F. Doghieri, On the role of diffusivity ratio and partition coefficient in diffusional molecular transport in binary composite materials, with special reference to the Maxwell equation, Journal of Membrane Science, 456 (2014) 162-166.

[46]    C. Zhang, Y. Dai, J.R. Johnson, O. Karvan, W.J. Koros, High performance ZIF-8/6FDA-DAM mixed matrix membrane for propylene/propane separations, Journal of Membrane Science, 389 (2012) 34-42.

[47]    S.J. Geier, J.A. Mason, E.D. Bloch, W.L. Queen, M.R. Hudson, C.M. Brown, J.R. Long, Selective adsorption of ethylene over ethane and propylene over propane in the metal-organic frameworks M2(dobdc) (M = Mg, Mn, Fe, Co, Ni, Zn), Chemical Science, 4 (2013) 2054-2061.

[48]    H. Vinh-Thang, S. Kaliaguine, Predictive Models for Mixed-Matrix Membrane Performance: A Review, Chemical Reviews, 113 (2013) 4980-5028.

[49]    B. Zornoza, C. Tellez, J. Coronas, J. Gascon, F. Kapteijn, Metal organic framework based mixed matrix membranes: An increasingly important field of research with a large application potential, Microporous and Mesoporous Materials, 166 (2013) 67-78.

[50]    R. Mahajan, R. Burns, M. Schaeffer, W.J. Koros, Challenges in forming successful mixed matrix membranes with rigid polymeric materials, Journal of Applied Polymer Science, 86 (2002) 881-890.

[51]    Z. Wang, S.M. Cohen, Postsynthetic modification of metal-organic frameworks, Chemical Society Reviews, 38 (2009) 1315-1329.

[52]    C. Duan, X. Jie, D. Liu, Y. Cao, Q. Yuan, Post-treatment effect on gas separation property of mixed matrix membranes containing metal organic frameworks, Journal of Membrane Science, 466 (2014) 92-102.

[53]    C. Zhang, K. Zhang, L. Xu, Y. Labreche, B. Kraftschik, W.J. Koros, Highly scalable ZIF-based mixed-matrix hollow fiber membranes for advanced hydrocarbon separations, AIChE Journal, 60 (2014) 2625-2635.

[54]    A. Car, C. Stropnik, K.-V. Peinemann, Hybrid membrane materials with different metal–organic frameworks (MOFs) for gas separation, Desalination, 200 (2006) 424-426.

[55]    M.J.C. Ordoñez, K.J. Balkus, J.P. Ferraris, I.H. Musselman, Molecular sieving realized with ZIF-8/Matrimid® mixed-matrix membranes, Journal of Membrane Science, 361 (2010) 28-37.

[56]    S. Mitchell, N.-L. Michels, K. Kunze, J. Pérez-Ramírez, Visualization of hierarchically structured zeolite bodies from macro to nano length scales, Nature Chemistry, 4 (2012) 825.

[57]    L. Li, J. Yao, X. Wang, Y.B. Cheng, H. Wang, ZIF-11/Polybenzimidazole composite membrane with improved hydrogen separation performance, Journal of Applied Polymer Science, 131 (2014).

[58]    T.H. Bae, J.S. Lee, W. Qiu, W.J. Koros, C.W. Jones, S. Nair, A High-Performance Gas-Separation Membrane Containing Submicrometer-Sized Metal–Organic Framework Crystals, Angewandte Chemie International Edition, 49 (2010) 9863-9866.

[59]    T. Rodenas, I. Luz, G. Prieto, B. Seoane, H. Miro, A. Corma, F. Kapteijn, F.X. Llabrés i Xamena, J. Gascon, Metal–organic framework nanosheets in polymer composite materials for gas separation, Nature Materials, 14 (2014) 48.

[60]    Y. Yang, K. Goh, R. Wang, T.-H. Bae, High-performance nanocomposite membranes realized by efficient molecular sieving with CuBDC nanosheets, Chemical Communications, 53 (2017) 4254-4257.

[61]    T.C. Merkel, H. Lin, X. Wei, R. Baker, Power plant post-combustion carbon dioxide capture: An opportunity for membranes, Journal of Membrane Science, 359 (2010) 126-139.

[62]    F.T. de Bruijn, L. Sun, Ž. Olujić, P.J. Jansens, F. Kapteijn, Influence of the support layer on the flux limitation in pervaporation, Journal of Membrane Science, 223 (2003) 141-156.

[63]    J.A.M. A. Cybulski, Structured catalysts and reactors, in:  Structured catalysts and reactors, CRC Taylor & Francis, Boca Raton, USA, 2006, pp. 700-746.

[64]    I. Pinnau, J.G. Wijmans, I. Blume, T. Kuroda, K.V. Peinemann, Gas permeation through composite membranes, Journal of Membrane Science, 37 (1988) 81-88.

[65]    M. Kattula, K. Ponnuru, L. Zhu, W. Jia, H. Lin, E.P. Furlani, Designing ultrathin film composite membranes: the impact of a gutter layer, Scientific Reports, 5 (2015) 15016.

# Influence of Filler Pore Structure and Polymer on the Performance of MOF-based Mixed Matrix Membranes for CO₂ Capture

**Abstract:** *In order to gain insight into the influence of metal-organic framework (MOF) filler and polymer on membrane performance, eight different composites are studied by combining four MOFs and two polymers. MOF materials (NH$_2$-MIL-53(Al), MIL-69(Al), MIL-96(Al) and ZIF-94) with various chemical functionalities, topologies, and dimensionalities of porosity were employed as fillers, while two typical polymers with different permeability-selectivity properties (6FDA-DAM and Pebax 1657) were deliberately selected as matrices. The best performing MOF-polymer composites were prepared by loading 25 wt.% of MIL-96(Al) as filler which improved the permeability and selectivity of 6FDA-DAM up to 32% and 10%, while for Pebax this enhancement was 25% and 18%, respectively. The observed differences in membrane performance in the separation of CO$_2$ from N$_2$ are explained on the basis of gas solubility, diffusivity properties and compatibility between the filler and polymer phases.*
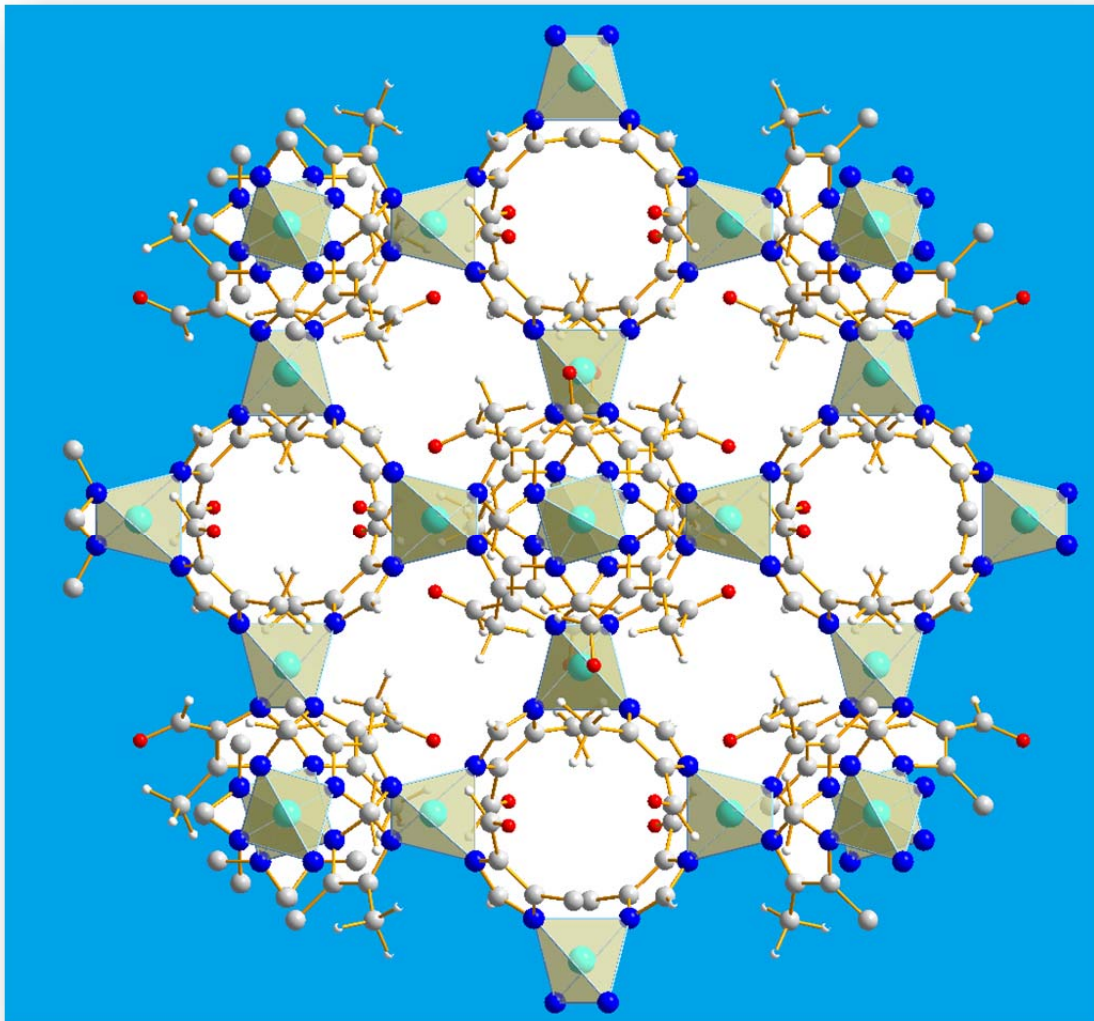
The image represents the structure of MOF ZIF-94.

## 2.1 Introduction

In recent times, the sharply rising atmospheric $CO_2$ concentration has generated widespread environmental concerns. [1-3] It is clear that the earth temperature has a direct dependence on the $CO_2$ concentration, and the climate will be significantly affected with a rise of a few degrees Celsius. [1] The excessive $CO_2$ emission stems predominantly from the increasing combustion of fossil fuels due to growing industrialisation. [1-3] Currently, the most frequent method for $CO_2$ capture from a post-combustion flue gas is chemical absorption. However, this process consumes considerable energy and poses additional environmental concerns.[4]

In contrast, membrane gas separation units are gaining increasing attention not only in terms of a relatively low energy consumption and ease of operation,[5, 6] but also because of environmental aspects. To date, polymeric membranes dominate the membrane market for industrial gas separation due to their easy processing and mechanical strength.[7] Nevertheless, the limited chemical and thermal stability of existing polymeric membrane materials limits their application range. Another drawback of polymeric membranes is the known Robeson upper bound limit. [8-10] Improvement in selectivity is always sacrificing permeability, and *vice versa*. Compared with polymeric materials, inorganic membrane materials (e.g., carbon, [11] zeolites [12, 13] and metal-organic frameworks [12, 13]) always provide superior performance and stability for gas separation. However, more research effort has to be devoted to inorganic membranes to overcome their inherent obstacles, such as high cost, brittleness and lack of reproducibility.

Mixed matrix membranes (MMMs), consisting of composites of inorganic or organic fillers dispersed in a polymer phase, are proposed as alternative materials delivering both the promising performance benefits from embedded fillers and the economical processing features of polymers. [4, 14, 15] Metal-organic frameworks (MOFs) have emerged as a family of outstanding porous crystalline materials. [16-19] Their rich chemistry and topological variety render MOFs as superior fillers to construct MMMs. [20-42] However, in spite of a clear explosion in the number of publications dealing with MOF based mixed matrix membranes, clear structural property relationships for these composites and the influence of MOF structure on pore dimensionality and accessibility have not yet been established. [41, 42] More comparative studies using diverse MOF fillers and polymers are required to determine the optimal combinations and ruling variables to facilitate the development of such structure/performance correlations.

In this study, four types of MOF materials ($NH_2$-MIL-53(Al), MIL-69(Al), MIL-96(Al) and ZIF-94) with different chemical functionalities and topologies were studied as fillers. Two typical polymers (polyimide 6FDA-DAM and poly(ether- block-amide) Pebax) were deliberately selected as matrices because of their outstanding separation performance (Figure 2,1). The morphology, $CO_2$ adsorption properties, crystalline structures of the MOF fillers and MOF-MMMs were

characterized, followed by gas permeation studies. The resulting membranes exhibit different performances in the separation of $CO_2$ / $N_2$ that can be rationalized on the basis of gas solubility and diffusivity in the MOF-MMMs, the interaction between both components of the composite and pore dimensionality.

NH$_2$-MIL-53(Al),[43] with a formula $Al(OH)[O_2C–C_6H_3NH_2–CO_2]$, is isoreticular to the well-known MIL-53. [44] This material is a microporous framework with diamond-shaped 1D channels (Figure 2.2a), which presents excellent properties for the selective adsorption of $CO_2$. [45] In this framework, dispersion forces control the flexibility of the structure: its narrow pore (*np*, window size ~3.4×16.0 Å$^2$) form is preferred at low $CO_2$ pressures, while the framework expands to its large pore (*lp*, window size ~8.5×12.0 Å$^2$) form at high $CO_2$ partial pressures. [46] NH$_2$-MIL-53 has been reported to display outstanding selectivity in the separation of $CO_2$ from natural gas or flue gas. [4,35]

For comparative studies, another MOF material with similar topology was selected, i.e. MIL-69(Al) (formulated $Al(OH)[O_2C–C_{10}H_6–CO_2]$). [47] This also is a microporous network with diamond-shaped 1D tunnels and a window size around 2.7×13.6 Å$^2$ in its narrow pore form upon hydrothermal synthesis, and 8.5x8.5 Å$^2$ in its anhydrous form (open square-like pore) which is called DUT-4 (Figure 2.2b). [48] In contrast to the breathing phenomenon encountered in the MIL-53 series, MIL-69(Al) displays a very limited flexibility upon adsorbate uptake and removal. [48]

Apart from MOFs with 1D channels, another type of MOF named as MIL-96(Al) was chosed ($Al_{12}O(OH)_{16}(H_2O)_5[btc]_6•29H_2O$, btc = 1,3,5-benzene-tricarboxylate). [49] This MOF is a trimesate microporous and its structure has been recently been refined and exhibits a 2D pore network. The MOF structure has three types of cavities. Of these cavities, only the B- and C-types are accessible, creating a "zigzag" 2D pore network with shared windows (4.5×3.6 Å$^2$) (Figure 2.2c). [49] After thermal activation, some water molecules, located on the μ$_3$-oxo Al trimer, are removed, which may increase the window diameter by approximately 2 Å.[51] MIL-96/Matrimid MMMs were developed showing higher $H_2$ and $CO_2$ permeabilities with slightly reduced $H_2$/$CO_2$ selectivities in comparison with the neat Matrimid membranes.[26]

ZIF-94 [52] (also termed as SIM-1 [53] and ZIF-8-MCIM [54]), with a formula Zn[mcim]$_2$ (mcim = 4-methylimidazolate-5-carbaldehyde), is an analogue of the extensively-studied ZIF-8.[55] It has a SOD topology with a 3D pore network and a window diameter of circa 2.6 Å (Figure 2.2d). ZIF-94 was selected against other ZIF materials due to its high $CO_2$ uptake at low pressure. [52] As it was reported by Aguado et al. [56] and Cacho-Bailo et al., [57] the ZIF-94 polycrystalline membranes exhibited good $CO_2$ selectivity over $N_2$ and $CH_4$.
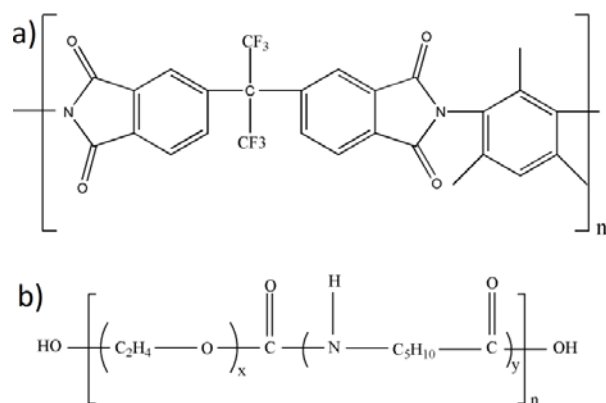
**Figure 2.1** Chemical structures of polymers 6FDA-DAM (a) and Pebax 1657 (b).
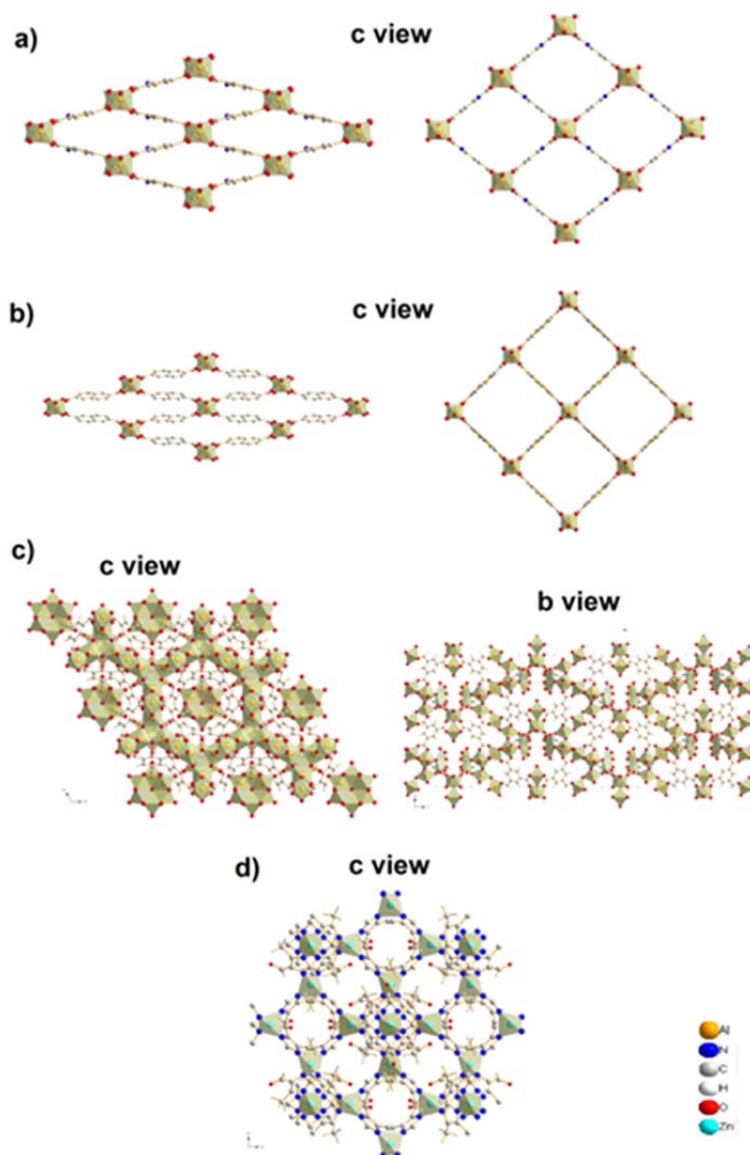


**Figure 2.2** Crystalline structures of NH$_2$-MIL-53(Al) (a, narrow and large pore forms), MIL-69(Al)/ DUT-4 (b, narrow and open pore forms), MIL-96(Al) (c) and ZIF-94 (d).
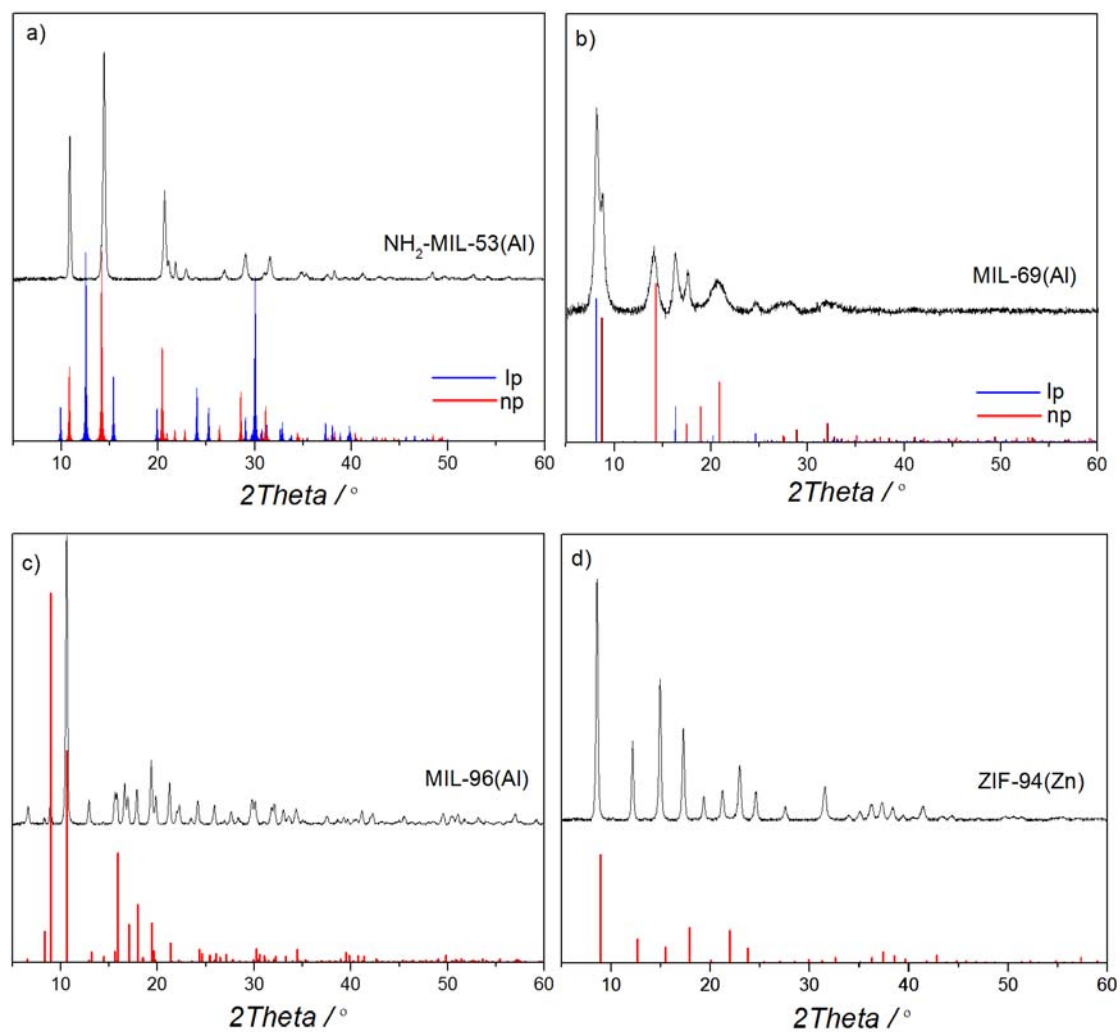
**Figure 2.3** The XRD and simulated patterns of NH$_2$-MIL-53(Al) (a), MIL-69(Al) (b), MIL-96(Al) (c) and ZIF-94(Zn) (d).

**Table 2.1.** CCDC codes of MOFs used in this study.

| MOF | CCDC or DOI | Ref. |
|---|---|---|
| **NH$_2$-MIL-53(Al)** | *lp*: 847255, *np*: 847256 | [59] |
| **MIL-69(Al)** | *np* (MIL-69(Al)): 1228352, *lp* (DUT-4): 691978 | [47,48] |
| **MIL-96(Al)** | 622598 | [50] |
| **ZIF-94(Zn)** | DOI: 10.1002/cctc.201000386 | [52] |
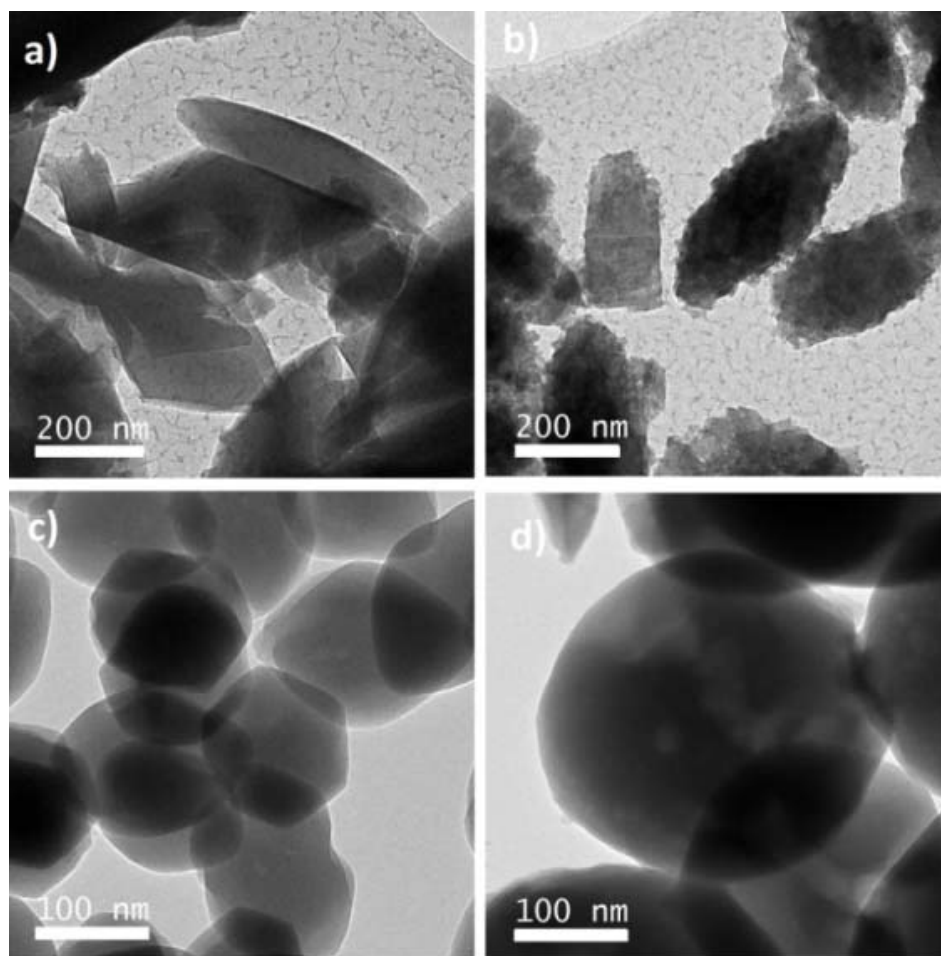
**Figure 2.4** TEM images of a) $NH_2$-MIL-53(Al), b) MIL-69(Al), c) MIL-96(Al) and d) ZIF-94.

Polyimide 6FDA-DAM is a representative glassy polymer (Figure 2.2a). 6FDA-DAM based membranes usually deliver a high $CO_2$ permeability and moderate $CO_2$ / $N_2$ selectivity. Pebax 1657 is a benchmark block copolymer, consisting of polyether blocks (flexible segments) and polyamide backbones (rigid segments) (Figure 2.2b). This polymer displays higher $CO_2$ / $N_2$ selectivity and a lower $CO_2$ permeability than 6FDA-DAM. [4]

## 2.2 Experimental Section

### 2.2.1 Synthesis of MOF crystals

$NH_2$-MIL-53(Al) sub-micrometer particles were synthesized according to a protocol reported earlier.[55] 1.5 g 2-amino-terepththalic acid (8.28 mmol, Sigma Aldrich, 99 %) and 1.97 g $AlCl_3·6H_2O$ (8.43 mmol, Sigma Aldrich, ≥ 99.0 %) were dissolved in a solution containing 18 mL deionized water and 2 mL N,N-dimethylformamide (DMF, Sigma Aldrich, >99.9%). Afterwards,

the solution was transferred to a Teflon-lined autoclave and heated at 423 K for 5 h in an oven under static conditions. After cooling, the resulting yellow powders were filtered under vacuum and washed with acetone. Subsequently, the powders were thoroughly activated in DMF at 423 K and methanol at 443 K for 15 h. Then, the powders were washed with acetone and dried at 393 K.

MIL-69(Al) submicrometer particles were synthesized under reflux for 5 h. 0.43 g 2,6-Naphthalenedicarboxylic acid (2 mmol, Alfa Aesar), 0.19 g NaOH (4.75 mmol, Acros organic, extra pur) and 1.50 g Al(NO$_3$)$_3$·9H$_2$O (4 mmol, Carlo Erba, 99+%) were dissolved in a 10 mL DMF (Carlo Erba, pur) and 10 mL H$_2$O. The reaction mixture was stirred under reflux for 5 h. The resulting product was filtered and washed with 30 mL DMF at 323 K under stirring for 5-6 h.

To synthesize MIL-96(Al), aluminium nitrate nonahydrate (4.5 g, 12 mmol) and trimesic acid (2.52 g, 12 mmol) were dissolved in 300 mL of a H$_2$O/DMF (50/50, vol./vol. ) mixture. Acetic acid (1.68 mL, 30 mmol) was added and the mixture was heated to reflux for 16 h. The resulting white mixture was centrifuged at 14500 rpm for 15 min, and then washed once with deionized water (100 ml), one more time with a H$_2$O/EtOH (50/50, vol./vol.) mixture (100 mL) and finally with EtOH (100 mL). The white powder was dried at room temperature and pure MIL-96(Al) particles were obtained.

Synthesis of ZIF-94 involved dissolving 0.4392 g Zn(CH$_3$COO)$_2$·2H$_2$O (2 mmol) in 20 ml methanol and 0.4404 g 4-methyl-5-imidazolecarboxaldehyde (mcim, 4 mmol) in 50 ml THF. After the solids were completely dissolved, Zn(CH$_3$COO)$_2$·2H$_2$O-methanol solution was poured slowly into the mcim-THF solution. The mixture was continuously stirred for 60 min at room temperature. The product was collected by centrifugation and washed with methanol three times before drying at room temperature.

### 2.2.2 Preparation of mixed-matrix membranes (MMMs)

Preparation of 6FDA-DAM based MMMs, is based on a previously reported method.[35] 6FDA-DAM (Mw ~272,000 Da, supplied by Akron) was degassed overnight at 453 K under vacuum. 0.40 g dried polymer was dissolved in 3.0 mL tetrahydrofuran (THF, Sigma Aldrich, ≥ 99.99 %). Then, 0.13 g of MOF crystals were suspended in 1.5 mL THF by ultrasonication and stirring. To attain better MOF and polymer interaction, firstly, a 10 % of the dissolved polymer was added to the MOF solution and the suspension was further stirred for 2 h (priming). Subsequently, the remaining amount of polymer solution was added to the MOF suspension and stirred overnight. The solution was poured on a glass plate and casted by Doctor Blade with a gap of 80 µm. Then, the membrane was covered with a top-drilled box and dried overnight under THF-saturated atmosphere at ambient temperature. Finally, the dried membranes were peeled off and treated under vacuum at 433 K for 24 h.

For the preparation of Pebax based MMMs, 0.18 g Pebax 1657 (supplied by Arkema) was dissolved in 3.0 ml water/ethanol (30/70 wt./wt.) mixture at 80 °C under reflux (2h) to achieve a polymeric solution. Then, 0.06 g MOF was added to 1.5 ml water/ethanol (30/70 wt./wt.), ultrasonicated and stirred. A similar procedure as described above was used for the casting of the membranes. Finally, the membranes were dried overnight in a top-drilled box in solvent saturated atmosphere, and then, treated under vacuum at 353 K for 24 h.

The MOF content in the above MMMs ($W_{MOF}/(W_{MOF}+W_{polymer})$) was 25 wt. % in all cases. As a reference, membranes based on the neat polymers were also prepared following an identical procedure. The thickness of all the membranes is around 30-40 μm, according to the measurements performed with a digital micrometer (Mitutoyo) at different locations within each membrane and then averaged.

## 2.3 Characterization

XRD patterns of MOF powders and the membranes were acquired in a Bruker-D8 Advance diffractometer using Co-$K_\alpha$ radiation ($\lambda$ = 1.78897Å, 40 KV, 30 mA). The *2θ* range (5-60°) was scanned using a step size of 0.02° and a scan speed of 0.2 s per step in a continuous scanning mode.

$N_2$ and $CO_2$ adsorption isotherms of MOFs and membranes were recorded in a Tristar II 3020 (Micromeritics) setup at 77 K and 295 K, respectively. Prior to the measurements, at least 100 mg of each sample (powder or membrane) were degassed at 423 K under vacuum for 16 h and used for adsorption measurements. The adsorption capacity of the MOF and membranes were acquired based on relative pressure and converted to absolute pressure (bar).

Scanning electron microscopy (SEM) experiments were performed in a Dual Beam Strata 235 (FEI) and AURIGA Compact (Zeiss) microscopes with a secondary electron detector operated at 5 kV. The membrane specimens were prepared by freeze-fracturing after immersion in liquid $N_2$ and coated with gold.

The TEM samples were prepared by applying a few drops of MOF dispersed in ethanol on a carbon-coated copper grid. TEM analysis was carried out in JEOL JEM-2010 microscope operated at 200 kV. An X-ray OXFORD detector, INCA energy TEM 100 model for microanalysis (EDS) and a bottom-mounted GATAN ORIUS SC600 imaging camera are equipped in the machine. Micrograph acquisition was performed with GATAN Digital Micrograph 1.80.70 software. By using TEM images, around 50 particles were selected and measured by Image J software to calculate the average particle size.

### 2.3.1 Gas permeation experiments

The $CO_2/N_2$ separation measurements were carried out in a home-made setup described elsewhere.[20] The membranes, with constant area (3.14 cm$^2$), were cut from the casted films and mounted in a flange between two Viton® O-rings. A macroporous stainless steel disc (316L, 20 µm nominal pore size) was used as support. All the evaluated membranes were in their fresh stage without aging. The permeation module was placed inside an oven, where the temperature was set to 298 K. A flow mixture (133 ml·min$^{-1}$, STP) of $CO_2$ (15 mol.%) and $N_2$ (85 mol.%) was applied as feed and helium (5 ml·min$^{-1}$, STP) as a sweep gas. The feed pressure was adjusted to 2 bar absolute using a back-pressure controller at the retentate side while the permeate side was kept at atmospheric pressure (1 bar) for all measurements. The permeation results of the membranes were recorded after stabilization overnight to ensure steady state permeation. An online gas chromatograph (Interscience Compact GC) equipped with a packed Carboxen® 1010 PLOT (30 m x 0.32 mm) column and TCD detector was used to analyse the permeate stream. Single gas $CO_2$ permeation tests were conducted at 295 K and 1 bar absolute feed pressure. Gas separation performance is defined by the selectivity ($\alpha$) or separation factor, and the gas permeability ($P$) of the individual components. The permeability for the component $i$ ($P_i$) was calculated as follows (Equation 1):

$$P_i = \frac{F_i \cdot \delta}{\Delta p_i \cdot A} \qquad\qquad (1)$$

where $F_i$ denotes the molar flow rate of compound $i$, $\delta$ is the thickness of the membrane, $\Delta p_i$ is the partial pressure difference of $i$ across the membrane, and $A$ is the membrane area. Although the SI unit for the permeability is mol·s$^{-1}$·m·m$^{-2}$·Pa$^{-1}$, gas permeabilities are reported in Barrer, where 1 Barrer = 3.35 x 10$^{-16}$ mol·s$^{-1}$·m·m$^{-2}$·Pa$^{-1}$. The mixed gas selectivity ($\alpha$) of $CO_2$ over $N_2$ was defined as the ratio of their permeabilities (Equation 2):

$$\alpha = \frac{P_{CO_2}}{P_{N_2}} \qquad\qquad (2)$$

The solubility ($S_{CO2}$) of $CO_2$ in the membranes (at 1 bar) was quantified from gas sorption measurements up to 1.2 bar at 295 K. The mmol/g unit was conversed to cm$^3$/cm$^3$·cmHg by applying the densities of MOFs and polymers (Table. S2) to calculate the density of MMMs based on 25 wt. % of MOF loading. The diffusivity ($D_{CO2}$) (at 1 bar) of $CO_2$ is calculated from the permeability and solubility (Equation 3):

$$D_{CO_2} = \frac{P_{CO_2}}{S_{CO_2}} \qquad\qquad (3)$$

## 2.4 Results and Discussion

### 2.4.1 MOF characterization

To get comparable results, the size of all synthesized MOF particles is in the sub-micrometer range (Figure 2.4). $NH_2$-MIL-53(Al) displays diamond- and rod-shapes with average particle size of 500 ± 90 nm. MIL-69(Al) adopts the shape of platelets (450 ± 90 nm), while MIL-96(Al) and ZIF-94 particles are of spherical shape (150 ± 90 and 300 ± 90 nm, in size, respectively). XRD patterns demonstrate the absence of additional phases for all four samples (Figure 2.3 & Table 2.1). The surface area and porosity of the MOF materials were assessed by measuring the $N_2$ adsorption isotherms at 77 K (Figure 2.5). The adsorption isotherms for the MOFs can be categorized as Type I, which confirms their permanent micro-porosity. According to the IUPAC classification, $N_2$ adsorption isotherms of all MOFs (except $NH_2$-MIL-53(Al)) are based on type I which is representative of microporous solid having mainly narrow micropores (pore width ≤ 1 nm). The steep uptake at very low pressure is due to strong adsorbent-adsorptive interaction which resulted in micropores filling at low pressure (micropores of molecular dimension). In case of the $NH_2$-MIL-53(Al), the isotherm is following the type III of IUPAC classification which is related to very weak adsorbent-adsorptive interaction and therefore, no significant monolayer formation. In this case the adsorbed molecules transform to cluster around the most favourable site of the solid. The BET analysis depicts that MIL-96(Al) has the highest surface area (Table 2.2), followed by ZIF-94 and MIL-69(Al). The BET areas of MIL-96(Al) and ZIF-94 are in line with previous studies. [51, 52] As previously reported, $NH_2$-MIL-53(Al) displays hardly any uptake of $N_2$ at 77 K in its *np* configuration. [59] The pores of $NH_2$-MIL-53(Al) start to open when *P* reaches a value of approximately 0.3 bar. Moreover, the $N_2$ desorption branch shows a pronounced hysteresis. Therefore, no BET area is given for this MOF. Adsorption properties are usually critical in determining membrane performance. For this reason, we measured $CO_2$ adsorption isotherms on all MOF samples, which display a large $CO_2$ capacity at moderate pressures (Figure 2.6 and Table 2.2).

### 2.4.2 MMM characterization

In order to benefit from the incorporation of MOF crystals in the polymeric matrix, membranes with a relatively high filler loading (25 wt. %) were prepared in this work. The SEM images in Figure 2.7 illustrate a good dispersion of the fillers independently of the MOF used. Differences in morphology can be appreciated when comparing 6FDA-DAM (Figure 2.7a, c, e and g), and Pebax membranes (Figure 2.7b, d, f and h), although this effect could be attributed to the more rigid nature of 6FDA-DAM, the formation of such cavities during cryo-fracturing of these membranes cannot be discarded.

**Table 2.2** BET area, pore volume, $CO_2$ uptake (@ 295 K, 1.0 bar), shape and size of the MOFs studied.

| MOF | $S_{BET}$ (m$^2$/g) | $V_{micro}$ (cm$^3$/g) | $CO_2$ uptake (mmol / g) | Shape | Particle size (nm) |
|---|---|---|---|---|---|
| NH$_2$-MIL-53(Al) | - | - | 1.6 | Diamond | 500 ± 90 |
| MIL-69(Al) | 275 | 0.09 | 1.5 | Platelet | 450 ± 90 |
| MIL-96(Al) | 670 | 0.24 | 3.5 | Sphere | 150 ± 90 |
| ZIF-94 | 545 | 0.20 | 2.3 | Sphere | 300 ± 90 |
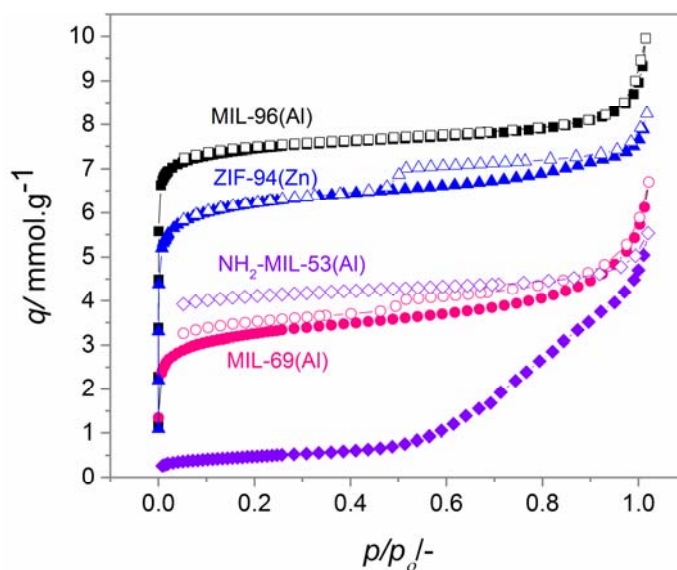


**Figure 2.5** N$_2$ (77 K) adsorption (solid symbols) and desorption isotherms (open symbols) for the MOF materials. The absolute pressure was transferred from the relative pressure.
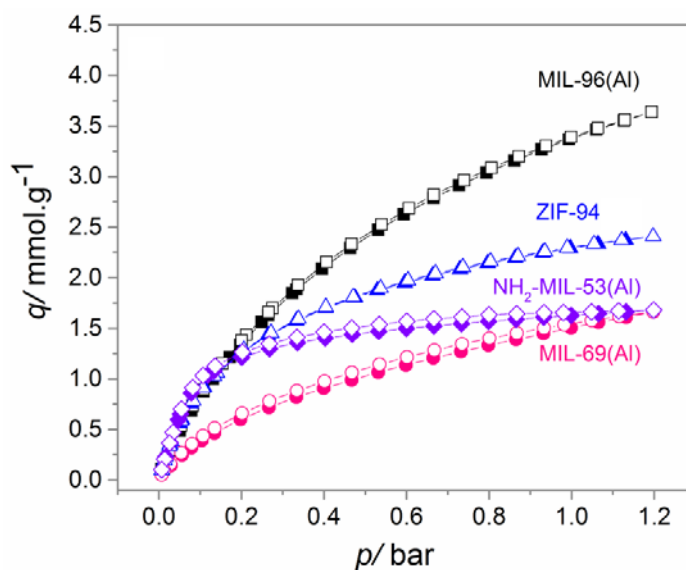


**Figure 2.6** CO$_2$ (295K) adsorption (solid symbols) and desorption isotherms (open symbols) for the MOF materials.

As already anticipated above, XRD patterns of the pure MOFs (Figure. 2.3), demonstrate the absence of other phases and are in good agreement with the simulated diffraction patterns for each MOF. [47, 50, 52, 60] The as-synthesized sub-micrometre $NH_2$-MIL-53(Al) powders display the expected narrow pore configuration (Figure 2.8a and Figure 2.8a).[58] In MIL-69(Al) the narrow and large pore configuration seem to co-exist (Figure 2.3). 6FDA-DAM is fully amorphous with a broad diffraction peak between 12-23 $^{o}$ (Figure 2.8), while Pebax shows a certain degree of crystallinity, as previously reported (Figure 2.9).[61] XRD patterns of the composites demonstrate that the crystalline structure of the MOFs was well retained upon MMM preparation.

It should be noted that pore expansion of $NH_2$-MIL-53(Al) occurs in the presence of Pebax (Figure 2.9a), suggesting polymer penetration in the MOF porosity.[34]

Figure 2.10 shows the $CO_2$ adsorption and desorption isotherms of MMMs with 6FDA-DAM as the continuous phase. All adsorption isotherms can be described as a linear combination (taking into account the ratio in the MMM) of the isotherms of their components (MOF and polymer), demonstrating that neither the MOF porosity nor the one related to the polymer are compromised upon membrane preparation.

The low free volume of Pebax is clearly exemplified in its corresponding $CO_2$ adsorption (Figure 2.11).[61] In this case, the calculated adsorption isotherms for the MMMs based on Pebax do not correspond with the experimentally measured data, except for MIL-69(Al) MMM. A similar effect was earlier observed for MOF containing silicone rubber based MMMs [41] and can be attributed to the partial blocking of the MOF fillers by polymer penetration, except for MIL-69(Al) in view of its narrower window size. [47] The increased contribution of the larger pore size in the MMM may be due to a solvent effect.

### 2.4 Gas permeation

The $CO_2$/$N_2$ (15/85, mol/mol) mixed gas permeation results of the neat polymeric membranes and MMMs were evaluated at 2 bar absolute and 298 K, and compared with the pure gas $CO_2$ permeation at 1 bar absolute displayed in Figure 2.12.
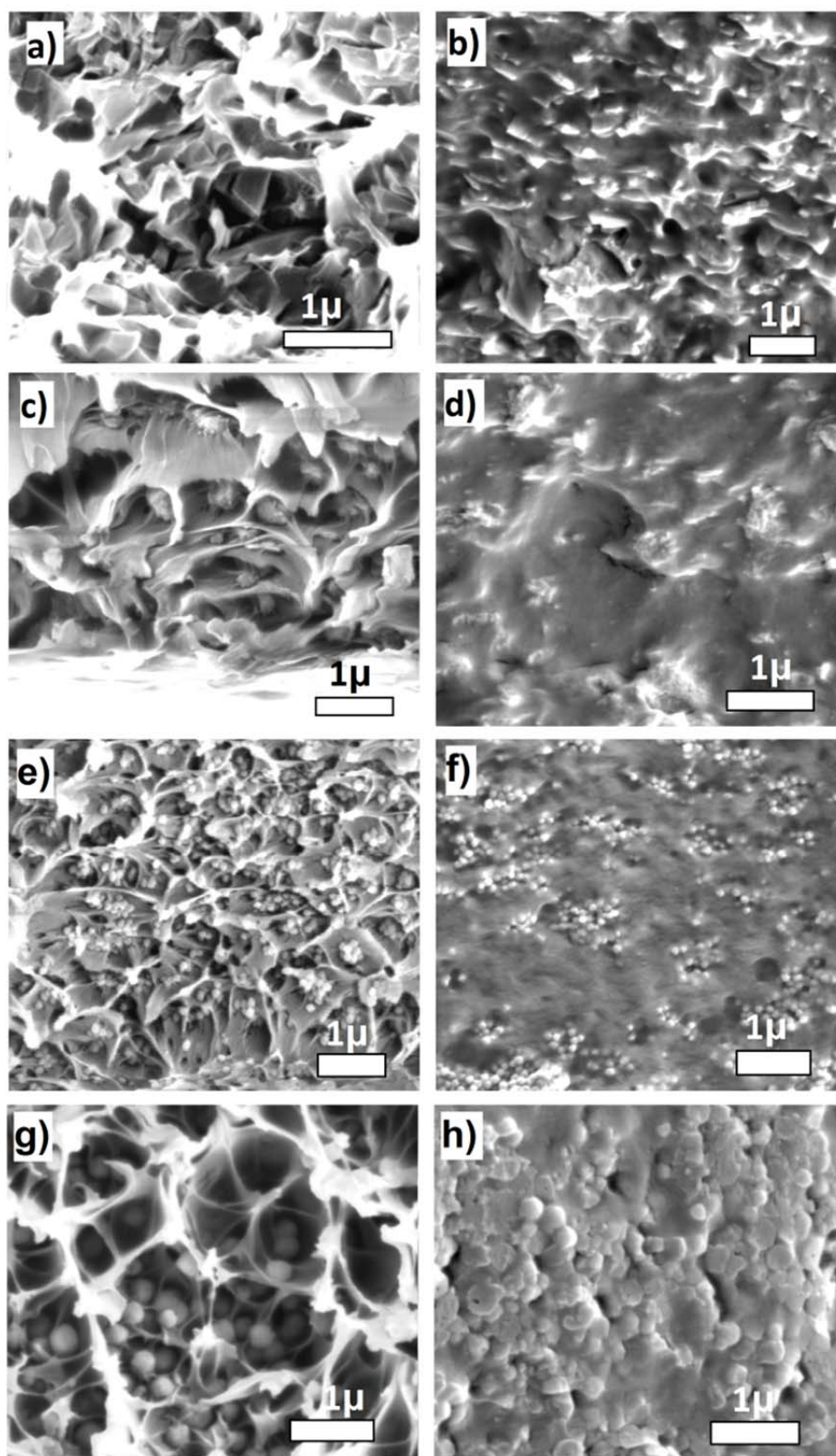
**Figure 2.7** Cross sectional SEM images of MOF-6FDA-DAM (*left column*) and MOF-Pebax membranes (*right column*), both with 25 wt. % filler loadings. The embedded MOF particles in these MMMs are NH$_2$-MIL-53(Al) (a, b), MIL-69(Al) (c, d), MIL-96(Al) (e, f) and ZIF-94 (g, h). The membrane specimens were prepared by cryo-fracturing after immersion in liquid N$_2$ and coated with gold.

The $CO_2$ permeabilities of the 6FDA-DAM membranes for the mixed gas are higher than for the pure gas feed experiments. The $CO_2$ pressure in the latter is higher, approaching a more saturated membrane and a lower apparent permeability, while the molar permeation flow through the membrane is higher. In the case of Pebax, this difference between the mixed gas and pure gas permeability is nearly absent, apart from MIL-69, so the diffusivity in the polymer phase will be the major controlling variable for these membranes. Although the relationship of Eq. (3) is therefore approximate, it helps interpreting the observations. The $CO_2$ solubility and diffusivity values are calculated in single gas (1.0 bar, Figure 2.12b and 2.12d) and mixed gas experiments (0.3 bar $CO_2$ partial pressure, Figure 2.13). Comparing these two cases, both the $CO_2$ solubility and diffusivity follow the same trend upon implanting various MOF fillers.

The $CO_2$ permeability of the bare 6FDA-DAM membranes was ca. 780 Barrer with a $CO_2/N_2$ mixture selectivity of 24 (Figure 2.12a). After addition of $NH_2$-MIL-53(Al), MIL-96(Al) and ZIF-94, the $CO_2$ permeability was enhanced (~35%, ~32% and ~42%, respectively) (Figure 2.12a) in virtue of the improved $CO_2$ solubility (Figure 2.12b and Figure 2.14a). The $CO_2$ diffusivity had hardly changed, with ZIF-94 as exception due to its 3D pore structure. The $CO_2/N_2$ selectivity is slightly increased, the most for MIL-69(Al). Although this MOF possesses similar diamond-shaped 1D channels as $NH_2$-MIL-53(Al), they are smaller in size,[47] explaining the higher selectivity, but lower permeability.

In comparison with neat 6FDA-DAM membranes, the bare Pebax membranes exhibit a higher CO2/N2 selectivity (~57) and lower $CO_2$ permeability (~44 Barrer) (Figure 2.13a). Due to the increased $CO_2$ solubility (Figure 2.13b and Figure 2.14b), the $CO_2$ permeability of MIL-96(Al) and ZIF-94 based MMMs was improved (around 25% and 33%, respectively) together with a slight improvement in selectivity (Figure 2.13a). Interpreting the results in terms of Eq. (3) suggests that the $CO_2$ diffusivity dropped sharply upon incorporation of MOF fillers (Figure 2.13b and Figure 2.14b). This effect can be attributed to the partial blocking of the fillers or even penetration of the flexible Pebax chains (polyether segments) into the MOF pores. Also, the interaction between filler and polymer matrix may disturb the packing and rotation mobility of the polymeric chains, thus influencing its overall diffusion properties. No obvious performance enhancement in terms of $CO_2$ permeability was observed for the addition of MIL-69(Al) although its $CO_2$ solubility was boosted. This did result in an increase in selectivity attributed to the narrow pores of this MOF. Furthermore, the reduced $CO_2$ permeability of the $NH_2$-MIL-53(Al)-Pebax membranes is a clear effect of polymer penetration.
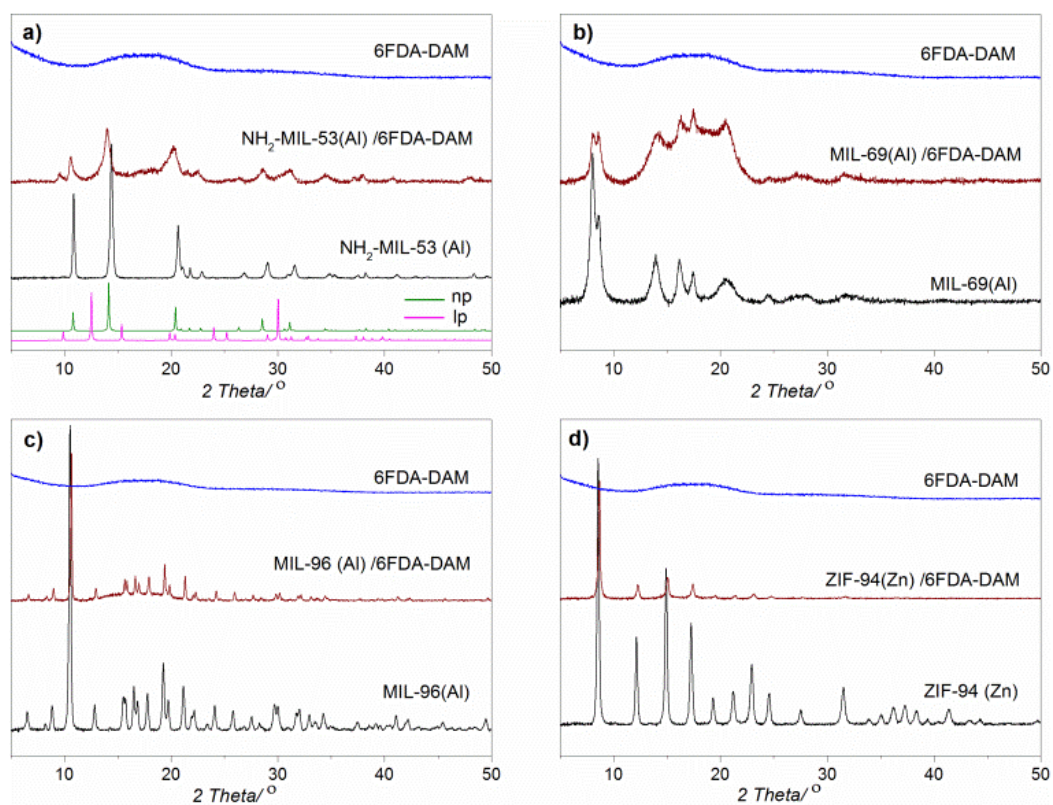
**Figure 2.8** The XRD patterns of the MOF fillers, neat 6FDA-DAM membranes and MMMs. The simulated XRD patterns of NH$_2$-MIL-53(Al) (*lp* and *np* forms) are shown for reference.
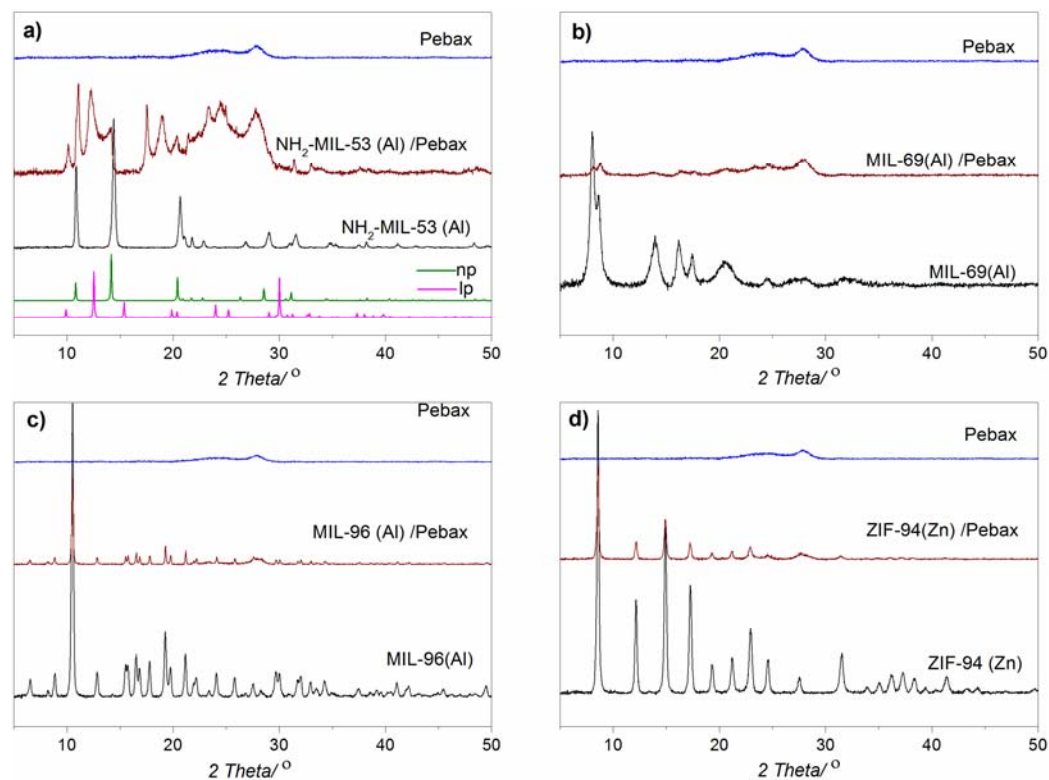


**Figure 2.9** The XRD patterns of the MOF fillers, neat Pebax membranes and MMMs. The simulated XRD patterns of NH$_2$-MIL-53(Al) (*lp* and *np* forms) are shown for reference.
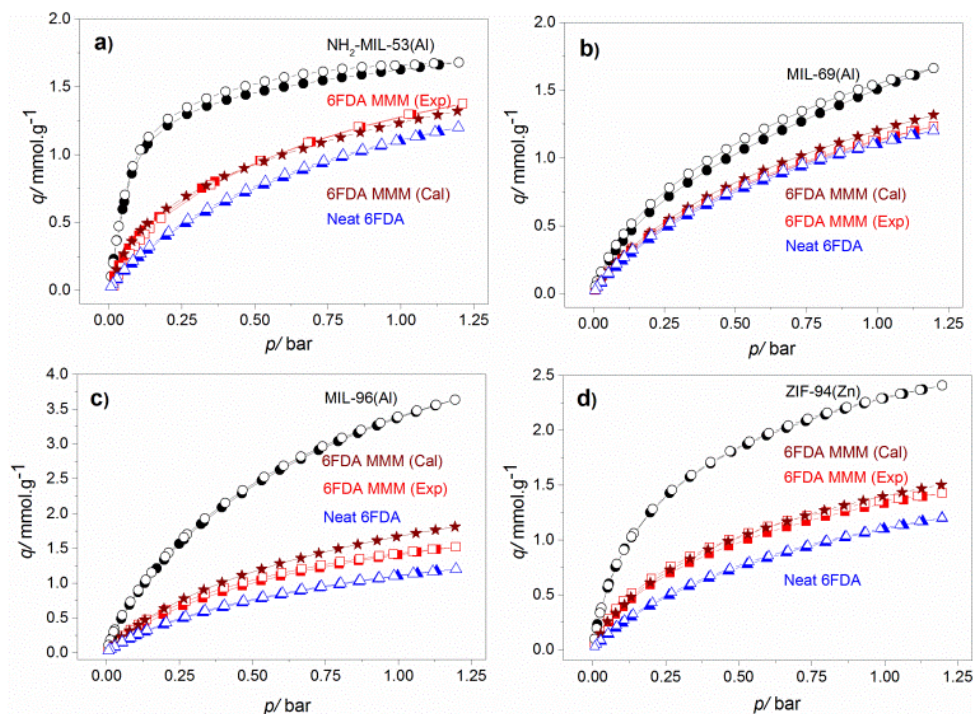
**Figure 2.10** Experimental $CO_2$ adsorption (solid symbols) and desorption (open symbols) isotherms of MOF fillers, neat 6FDA-DAM membrane and MMMs with filler loadings of 25 wt. % at 295 K. The calculated adsorption isotherms of MMMs are shown for comparison.
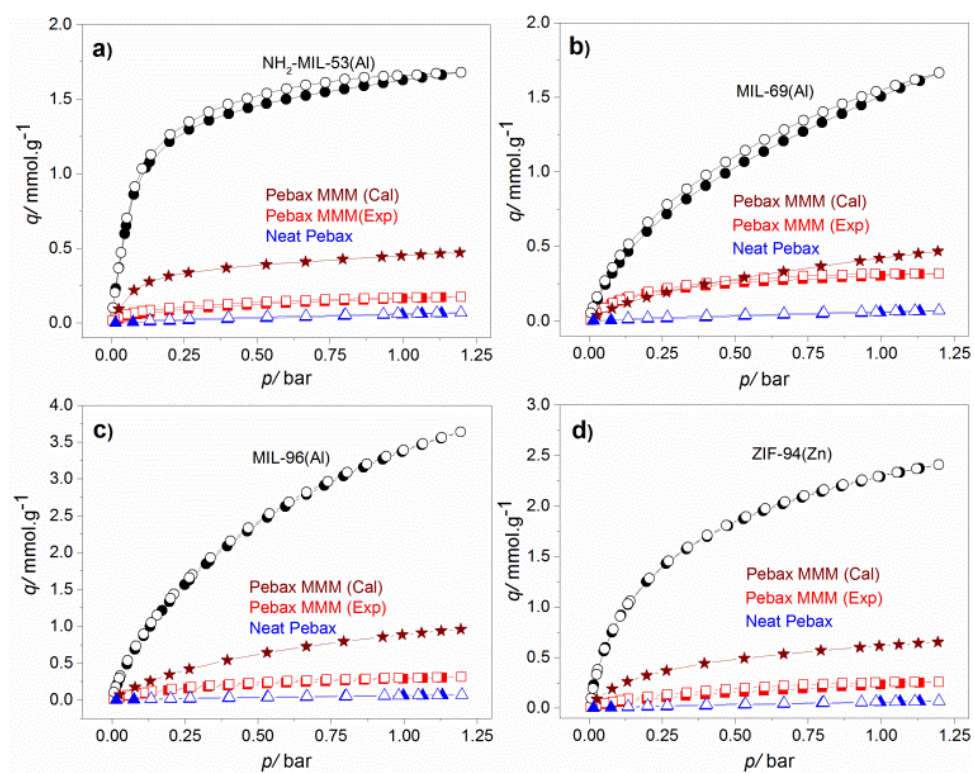


**Figure 2.11** Experimental $CO_2$ adsorption (solid symbols) and desorption (open symbols) isotherms of MOF fillers, neat Pebax membrane and MMMs with filler loadings of 25 wt. % at 295 K. The calculated adsorption isotherms of MMMs are shown for comparison.
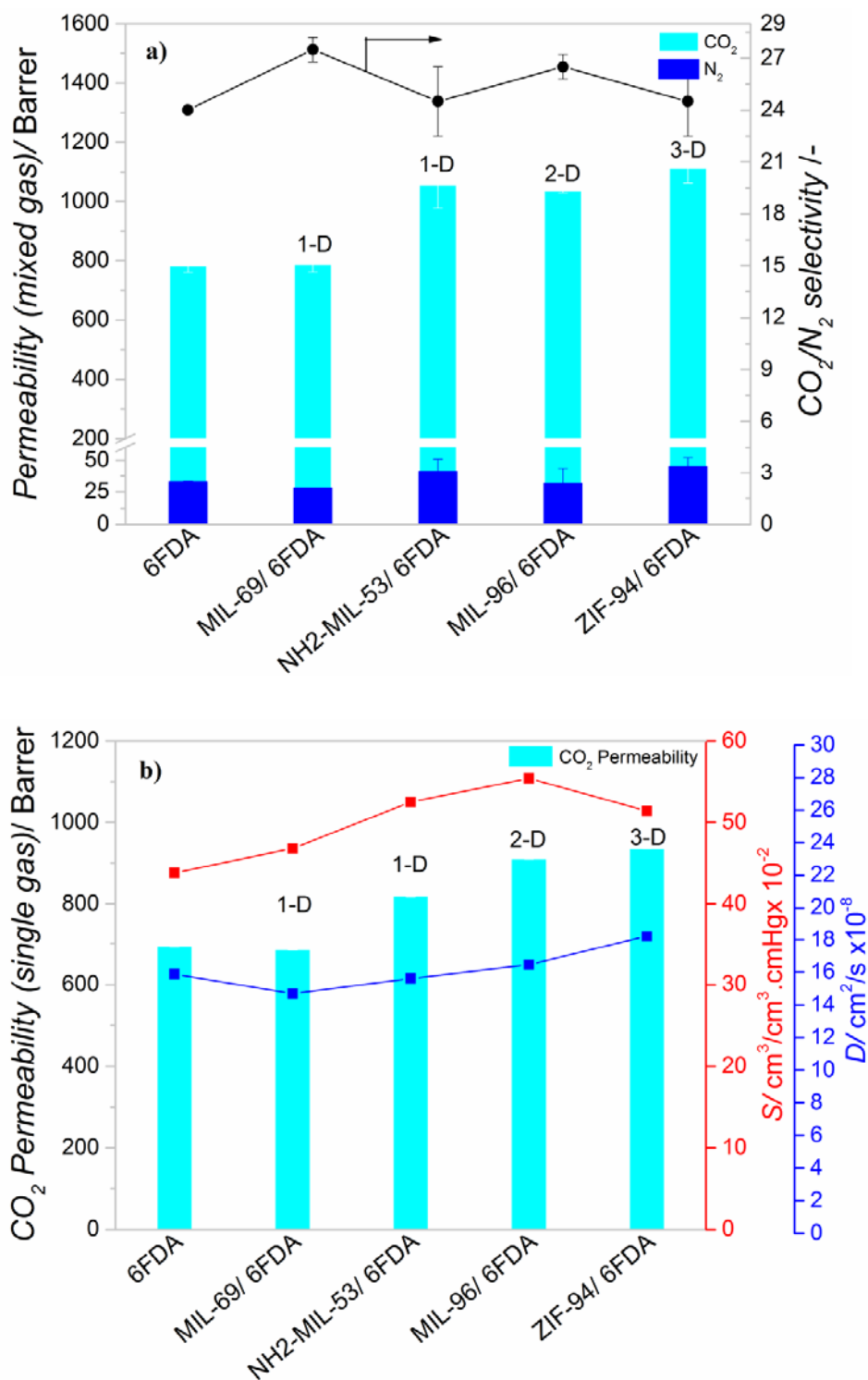
**Figure 2.12** $CO_2$ / $N_2$ mixed gas separation performance of 6FDA-DAM based membranes at 298 K and 2 bar absolute feed pressure (a). Single gas $CO_2$ permeability, solubility and diffusivity of 6FDA-DAM based membranes at 295 K and 1 bar absolute feed pressure (b). Error bars correspond to standard deviation of duplicate membranes.
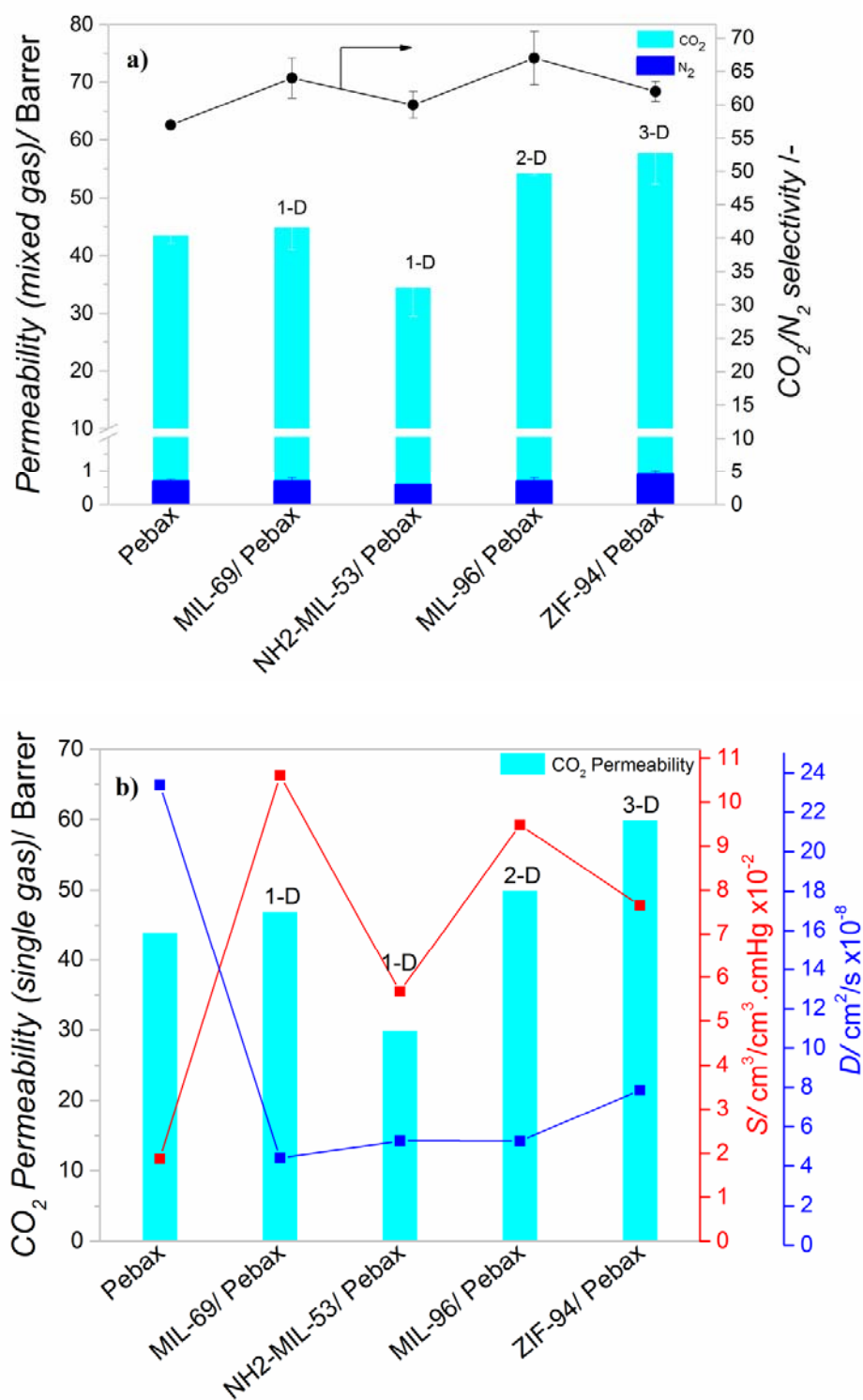
**Figure 2.13** $CO_2$ / $N_2$ mixed gas separation performance of Pebax 1657 based membranes at 298 K and 2 bar absolute feed pressure (a). Single gas $CO_2$ permeability, solubility and diffusivity of Pebax 1657 based membranes at 295 K and 1 bar absolute feed pressure (b). Error bars correspond to standard deviation of duplicate membranes.
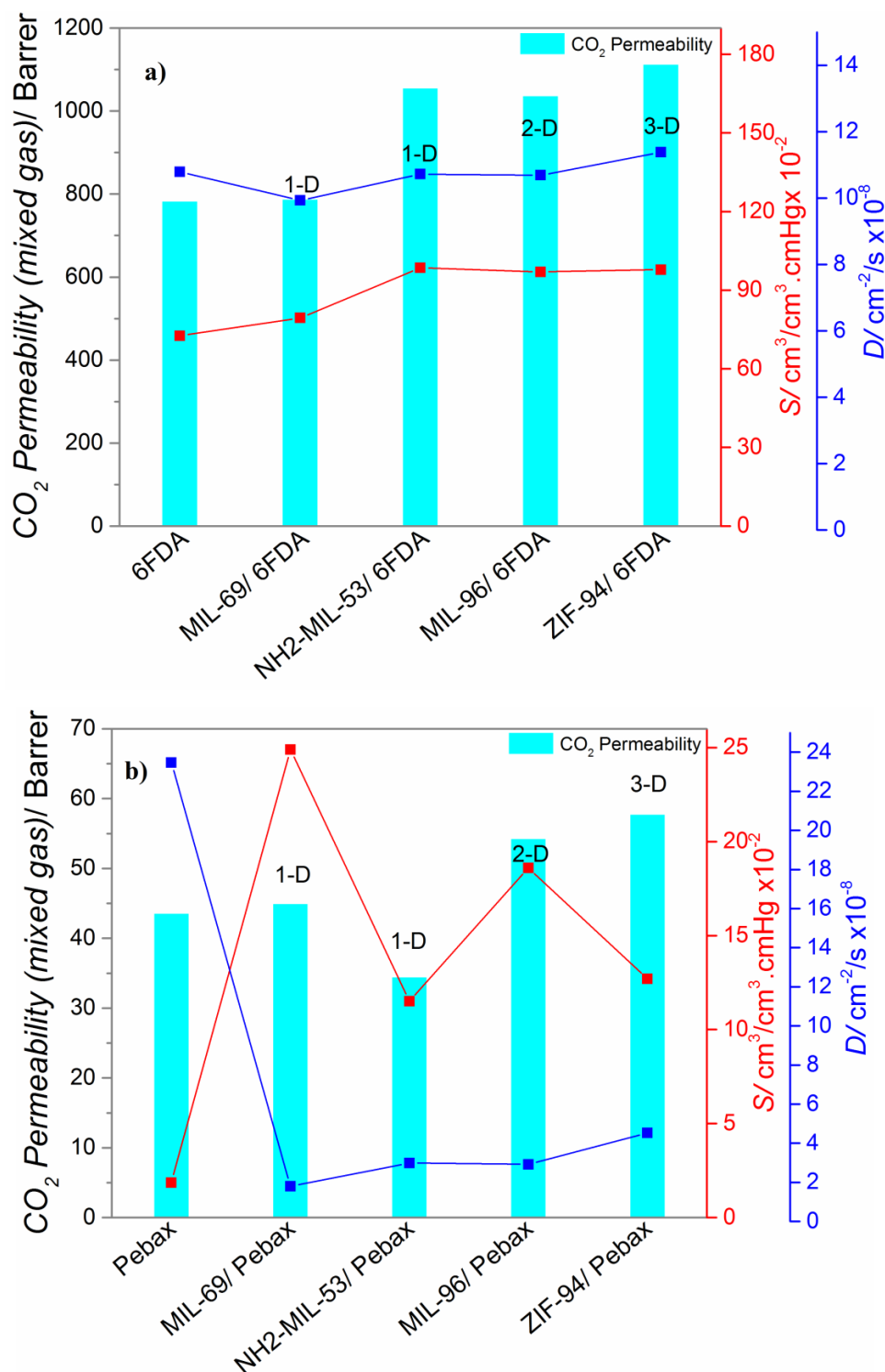
**Figure 2.14.** Single gas $CO_2$ permeability, solubility and diffusivity of 6FDA-DAM (a) and Pebax 1657 (b) based membranes at 295 K and 0.3 bar absolute feed pressure.

In order to benchmark and to give a more general overview of membrane performance, the most relevant permeation data are plotted in Figure 2.14 along with the Robeson upper bound ($CO_2/N_2$, 2008).[9] Addition of the nonflexible, small pore 1D MOF MIL-69 results for both polymers in a slight increase in selectivity at almost constant permeability. In case of $NH_2$-MIL-53,

with a similar topology but a flexible structure, interaction with the polymer results either in a decrease in permeability (Pebax) attributed to polymer penetration into the MOF structure or in an increase in permeability (6FDA-DAM) with hardly any improvement in selectivity, most likely related to a partial opening of the structure by the solvent upon membrane preparation.[60] Addition of the narrow pore, rigid, 2D-porous MIL-96 increases both permeability and selectivity for the two polymers. Finally, the 3D-porous ZIF-94 filler displays the largest increase in permeability for both polymers with a slight increase in selectivity only when Pebax is used as continuous phase. These results suggest that the MOF topology, dimensionality of porosity and interaction with the continuous polymer phase play key roles in determining membrane performance. The improved selectivity along with permeability (except for $NH_2$-MIL-53(Al)-Pebax) moves the MMM performance closer to the upper bound limit.

## 2.5 Conclusions

Mixed matrix membranes (MMMs) composed of diverse MOF fillers ($NH_2$-MIL-53(Al), MIL-69(Al), MIL-96(Al) and ZIF-94, 25 wt.% loading) and typical polymers (6FDA-DAM and Pebax) were developed for $CO_2/N_2$ separation. The large adsorption capacity of MOF fillers under moderate pressure and high porosity endows the 6FDA-DAM based MMMs with enhanced gas solubility and, consequently, an improved CO2 permeability (~ 35%, 32% and 42% for NH2-MIL-53(Al), MIL-96(Al) and ZIF-94, respectively, relative to ~780 Barrer for neat 6FDA-DAM) was observed together with a slightly increased selectivity. In the case of Pebax based MMMs, the CO2 permeability of MIL-96(Al) and ZIF-94 based MMMs was boosted (~ 25% and 33%, respectively; ~44 Barrer for neat Pebax) along with a slight enhancement of selectivity because of the improved CO2 solubility. The MMM performance are very close to the Robeson upper bound limit (2008, $CO_2/N_2$). The different topology of the MOF fillers, especially regarding their pore dimensionality, is responsible for the various performance modifications, although MOF-polymer interactions play another key role.
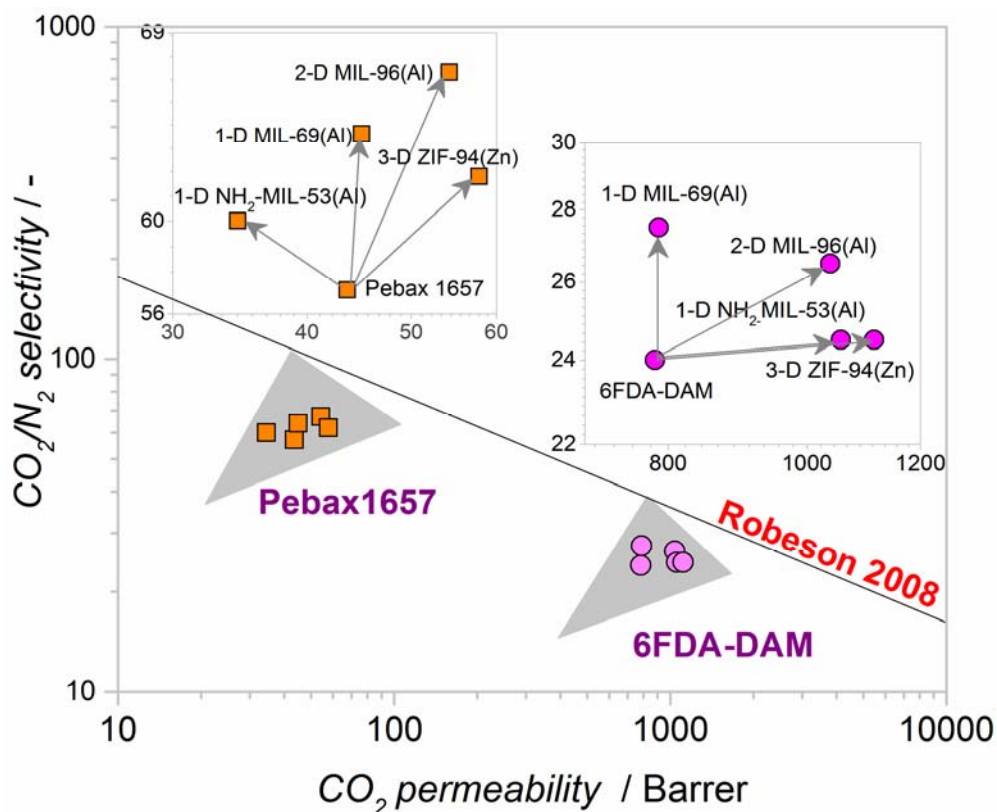
**Figure 2.14.** Robeson plot of $CO_2$ / $N_2$ separation performance of MOF-MMMs and neat 6FDA-DAM and Pebax membranes at 298 K and 2 bar absolute feed pressure (mixed gases). The insets are the enlarged views of thecorresponding membrane performance beneath. The Robeson upper bound (2008) is shown for reference. The loading of MOFs in all the MMMs is 25 wt. %.

# References

[1]     J.G. Vitillo, B. Smit, L. Gagliardi, Introduction: Carbon Capture and Separation, Chemical Reviews, 117 (2017) 9521-9523.

[2]     K. Sumida, D.L. Rogow, J.A. Mason, T.M. McDonald, E.D. Bloch, Z.R. Herm, T.-H. Bae, J.R. Long, Carbon Dioxide Capture in Metal–Organic Frameworks, Chemical Reviews, 112 (2012) 724-781.

[3]     A. Alvarez, A. Bansode, A. Urakawa, A.V. Bavykina, T.A. Wezendonk, M. Makkee, J. Gascon, F. Kapteijn, Challenges in the Greener Production of Formates/Formic Acid, Methanol, and DME by Heterogeneously Catalyzed CO2 Hydrogenation Processes, Chemical Reviews, 117 (2017) 9804-9838.

[4]     B. Seoane, J. Coronas, I. Gascon, M.E. Benavides, O. Karvan, J. Caro, F. Kapteijn, J. Gascon, Metal-organic framework based mixed matrix membranes: a solution for highly efficient CO2 capture?, Chemical Society Reviews, 44 (2015) 2421-2454.

[5]     W.J. Koros, R.P. Lively, Water and beyond: Expanding the spectrum of large-scale energy efficient separation processes, Aiche Journal, 58 (2012) 2624-2633.

[6]     D.E. Sanders, Z.P. Smith, R.L. Guo, L.M. Robeson, J.E. McGrath, D.R. Paul, B.D. Freeman, Energy-efficient polymeric gas separation membranes for a sustainable future: A review, Polymer, 54 (2013) 4729-4761.

[7]     P. Bernardo, E. Drioli, G. Golemme, Membrane Gas Separation: A Review/State of the Art, Ind Eng Chem Res, 48 (2009) 4638-4663.

[8]     L.M. Robeson, Correlation of Separation Factor Versus Permeability for Polymeric Membranes, Journal of Membrane Science, 62 (1991) 165-185.

[9]     L.M. Robeson, The upper bound revisited, Journal of Membrane Science, 320 (2008) 390-400.

[10]    B.D. Freeman, Basis of permeability/selectivity tradeoff relations in polymeric gas separation membranes, Macromolecules, 32 (1999) 375-380.

[11]    S.M. Saufi, A.F. Ismail, Fabrication of carbon membranes for gas separation - a review, Carbon, 42 (2004) 241-259.

[12]    J. Gascon, F. Kapteijn, B. Zornoza, V. Sebastian, C. Casado, J. Coronas, Practical Approach to Zeolitic Membranes and Coatings: State of the Art, Opportunities, Barriers, and Future Perspectives, Chem Mater, 24 (2012) 2829-2844.

[13]    N. Rangnekar, N. Mittal, B. Elyassi, J. Caro, M. Tsapatsis, Zeolite membranes - a review and comparison with MOFs, Chemical Society Reviews, 44 (2015) 7128-7154.

[14]    W.J. Koros, C. Zhang, Materials for next-generation molecularly selective synthetic membranes, Nature Materials, 16 (2017) 289-297.

[15]    J. Dechnik, J. Gascon, C.J. Doonan, C. Janiak, C.J. Sumby, Mixed-Matrix Membranes, Angew Chem Int Edit, 56 (2017) 9292-9310.

[16]    H.C. Zhou, J.R. Long, O.M. Yaghi, Introduction to Metal-Organic Frameworks, Chemical Reviews, 112 (2012) 673-674.

[17]    S. Kitagawa, R. Kitaura, S. Noro, Functional porous coordination polymers, Angew Chem Int Edit, 43 (2004) 2334-2375.

[18]    G. Ferey, Hybrid porous solids: past, present, future, Chemical Society Reviews, 37 (2008) 191-214.

[19]    A.J. Howarth, Y.Y. Liu, P. Li, Z.Y. Li, T.C. Wang, J. Hupp, O.K. Farha, Chemical, thermal and mechanical stabilities of metal-organic frameworks, Nat Rev Mater, 1 (2016).

[20]    T. Rodenas, I. Luz, G. Prieto, B. Seoane, H. Miro, A. Corma, F. Kapteijn, F.X.L.I. Xamena, J. Gascon, Metal-organic framework nanosheets in polymer composite materials for gas separation, Nature Materials, 14 (2015) 48-55.

[21]    X.L. Liu, Y.S. Li, G.Q. Zhu, Y.J. Ban, L.Y. Xu, W.S. Yang, An Organophilic Pervaporation Membrane Derived from Metal-Organic Framework Nanoparticles for Efficient Recovery of Bio-Alcohols, Angew Chem Int Edit, 50 (2011) 10636-10639.

[22]    T.H. Bae, J.S. Lee, W.L. Qiu, W.J. Koros, C.W. Jones, S. Nair, A High-Performance Gas-Separation Membrane Containing Submicrometer-Sized Metal-Organic Framework Crystals, Angew Chem Int Edit, 49 (2010) 9863-9866.

[23]    S. Sorribas, P. Gorgojo, C. Tellez, J. Coronas, A.G. Livingston, High Flux Thin Film Nanocomposite Membranes Based on Metal-Organic Frameworks for Organic Solvent Nanofiltration, Journal of the American Chemical Society, 135 (2013) 15201-15208.

[24]    G.X. Dong, H.Y. Li, V.K. Chen, Challenges and opportunities for mixed-matrix membranes for gas separation, J Mater Chem A, 1 (2013) 4610-4630.

[25]    S. Japip, K.S. Liao, T.S. Chung, Molecularly Tuned Free Volume of Vapor Cross-Linked 6FDA-Durene/ZIF-71 MMMs for H-2/CO2 Separation at 150 degrees C, Advanced Materials, 29 (2017).

[26]    A. Knebel, S. Friebe, N.C. Bigall, M. Benzaqui, C. Serre, J. Caro, Comparative Study of MIL-96(Al) as Continuous Metal-Organic Frameworks Layer and Mixed-Matrix Membrane, Acs Appl Mater Inter, 8 (2016) 7536-7544.

[27]    L. Diestel, X.L. Liu, Y.S. Li, W.S. Yang, J. Caro, Comparative permeation studies on three supported membranes: Pure ZIF-8, pure polymethylphenylsiloxane, and mixed matrix membranes, Micropor Mesopor Mat, 189 (2014) 210-215.

[28]    Y.J. Ban, Z.J. Li, Y.S. Li, Y. Peng, H. Jin, W.M. Jiao, A. Guo, P. Wang, Q.Y. Yang, C.L. Zhong, W.S. Yang, Confinement of Ionic Liquids in Nanocages: Tailoring the Molecular Sieving Properties of ZIF-8 for Membrane-Based CO2 Capture, Angew Chem Int Edit, 54 (2015) 15483-15487.

[29]    Q.L. Song, S. Cao, R.H. Pritchard, H. Qiblawey, E.M. Terentjev, A.K. Cheetham, E. Sivaniah, Nanofiller-tuned microporous polymer molecular sieves for energy and environmental processes, J Mater Chem A, 4 (2016) 270-279.

[30]    Z.G. Wang, D. Wang, S.X. Zhang, L. Hu, J. Jin, Interfacial Design of Mixed Matrix Membranes for Improved Gas Separation Performance, Advanced Materials, 28 (2016) 3399-3405.

[31]    J. Sanchez-Lainez, B. Zornoza, S. Friebe, J. Caro, S. Cao, A. Sabetghadam, B. Seoane, J. Gascon, F. Kapteijn, C. Le Guillouzer, G. Clet, M. Daturi, C. Tellez, J. Coronas, Influence of ZIF-8 particle size in the performance of polybenzimidazole mixed matrix membranes for pre-combustion CO2 capture and its validation through interlaboratory test, Journal of Membrane Science, 515 (2016) 45-53.

[32]    T.B. Nguyen, V.T. Hoang, X.Y. Chen, D. Rodrigue, S. Kaliaguine, Polymer functionalization to enhance interface quality of mixed matrix membranes for high CO2/CH4 gas separation, J Mater Chem A, 3 (2015) 15202-15213.

[33]    B. Zornoza, A. Martinez-Joaristi, P. Serra-Crespo, C. Tellez, J. Coronas, J. Gascon, F. Kapteijn, Functionalized flexible MOFs as fillers in mixed matrix membranes for highly selective separation of CO2 from CH4 at elevated pressures, Chem Commun, 47 (2011) 9522-9524.

[34]    T. Rodenas, M. van Dalen, E. Garcia-Perez, P. Serra-Crespo, B. Zornoza, F. Kapteijn, J. Gascon, Visualizing MOF Mixed Matrix Membranes at the Nanoscale: Towards Structure-Performance Relationships in CO2/CH4 Separation Over NH2-MIL-53(Al)@PI, Advanced Functional Materials, 24 (2014) 249-256.

[35]    A. Sabetghadam, B. Seoane, D. Keskin, N. Duim, T. Rodenas, S. Shahid, S. Sorribas, C. Le Guillouzer, G. Clet, C. Tellez, M. Daturi, J. Coronas, F. Kapteijn, J. Gascon, Metal Organic Framework Crystals in Mixed-Matrix Membranes: Impact of the Filler Morphology on the Gas Separation Performance, Advanced Functional Materials, 26 (2016) 3154-3163.

[36]    J. Ma, Y.P. Ying, X.Y. Guo, H.L. Huang, D.H. Liu, C.L. Zhong, Fabrication of mixed-matrix membrane containing metal organic framework composite with task specific ionic liquid for efficient CO2 separation, J Mater Chem A, 4 (2016) 7281-7288.

[37]    N.C. Su, D.T. Sun, C.M. Beavers, D.K. Britt, W.L. Queen, J.J. Urban, Enhanced permeation arising from dual transport pathways in hybrid polymer-MOF membranes, Energ Environ Sci, 9 (2016) 922-931.

[38]    S.R. Venna, M. Lartey, T. Li, A. Spore, S. Kumar, H.B. Nulwala, D.R. Luebke, N.L. Rosi, E. Albenze, Fabrication of MMMs with improved gas separation properties using externally-functionalized MOF particles, J Mater Chem A, 3 (2015) 5014-5022.

[39]    S.J.D. Smith, C.H. Lau, J.I. Mardel, M. Kitchin, K. Konstas, B.P. Ladewig, M.R. Hill, Physical aging in glassy mixed matrix membranes; tuning particle interaction for mechanically robust nanocomposite films, J Mater Chem A, 4 (2016) 10627-10634.

[40]    J. Shen, G.P. Liu, K. Huang, Q.Q. Li, K.C. Guan, Y.K. Li, W.Q. Jin, UiO-66-polyether block amide mixed matrix membranes for CO2 separation, Journal of Membrane Science, 513 (2016) 155-165.

[41]    T.H. Bae, J.R. Long, CO2/N-2 separations with mixed-matrix membranes containing Mg-2(dobdc) nanocrystals, Energ Environ Sci, 6 (2013) 3565-3569.

[42]    S. Kanehashi, G.Q. Chen, L. Ciddor, A. Chaffee, S.E. Kentish, The impact of water vapor on CO2 separation performance of mixed matrix membranes, Journal of Membrane Science, 492 (2015) 471-477.

[43]    J. Gascon, U. Aktay, M.D. Hernandez-Alonso, G.P.M. van Klink, F. Kapteijn, Amino-based metal-organic frameworks as stable, highly active basic catalysts, Journal of Catalysis, 261 (2009) 75-87.

[44]    C. Serre, F. Millange, C. Thouvenot, M. Nogues, G. Marsolier, D. Louer, G. Ferey, Very large breathing effect in the first nanoporous chromium(III)-based solids: MIL-53 or Cr-III(OH)center dot{O2C-C6H4-CO2}center dot{HO2C-C6H4-CO2H}(x)center dot H2Oy, Journal of the American Chemical Society, 124 (2002) 13519-13526.

[45] S. Couck, J.F.M. Denayer, G.V. Baron, T. Remy, J. Gascon, F. Kapteijn, An Amine-Functionalized MIL-53 Metal-Organic Framework with Large Separation Power for CO2 and CH4, Journal of the American Chemical Society, 131 (2009) 6326-6327.

[46] E. Stavitski, E.A. Pidko, S. Couck, T. Remy, E.J.M. Hensen, B.M. Weckhuysen, J. Denayer, J. Gascon, F. Kapteijn, Complexity behind CO2 Capture on NH2-MIL-53(Al), Langmuir, 27 (2011) 3970-3976.

[47] T. Loiseau, C. Mellot-Draznieks, H. Muguerra, G. Ferey, M. Haouas, F. Taulelle, Hydrothermal synthesis and crystal structure of a new three-dimensional aluminum-organic framework MIL-69 with 2,6-naphthalenedicarboxylate (ndc), Al(OH)(ndc)center dot H2O, Cr Chim, 8 (2005) 765-772.

[48] I. Senkovska, F. Hoffmann, M. Froba, J. Getzschmann, W. Bohlmann, S. Kaskel, New highly porous aluminium based metal-organic frameworks: Al(OH)(ndc) (ndc=2,6-naphthalene dicarboxylate) and Al(OH)(bpdc) (bpdc=4,4 '-biphenyl dicarboxylate), Micropor Mesopor Mat, 122 (2009) 93-98.

[49] M. Benzaqui, R.S. Pillai, A. Sabetghadam, V. Benoit, P. Normand, J. Marrot, N. Menguy, D. Montero, W. Shepard, A. Tissot, C. Martineau-Corcos, C. Sicard, M. Mihaylov, F. Carn, I. Beurroies, P.L. Llewellyn, G. De Weireld, K. Hadjiivanov, J. Gascon, F. Kapteijn, G. Maurin, N. Steunou, C. Serre, Revisiting the Aluminum Trimesate-Based MOF (MIL-96): From Structure Determination to the Processing of Mixed Matrix Membranes for CO2 Capture, Chem Mater, 29 (2017) 10326-10338.

[50] T. Loiseau, L. Lecroq, C. Volkringer, J. Marrot, G. Ferey, M. Haouas, F. Taulelle, S. Bourrelly, P.L. Llewellyn, M. Latroche, MIL-96, a porous aluminum trimesate 3D structure constructed from a hexagonal network of 18-membered rings and mu(3)-oxo-centered trinuclear units, Journal of the American Chemical Society, 128 (2006) 10223-10230.

[51] M. Maes, L. Alaerts, F. Vermoortele, R. Ameloot, S. Couck, V. Finsy, J.F.M. Denayer, D.E. De Vos, Separation of C-5-Hydrocarbons on Microporous Materials: Complementary Performance of MOFs and Zeolites, Journal of the American Chemical Society, 132 (2010) 2284-2292.

[52] W. Morris, N. He, K.G. Ray, P. Klonowski, H. Furukawa, I.N. Daniels, Y.A. Houndonougbo, M. Asta, O.M. Yaghi, B.B. Laird, A Combined Experimental-Computational Study on the Effect of Topology on Carbon Dioxide Adsorption in Zeolitic Imidazolate Frameworks, J Phys Chem C, 116 (2012) 24084-24090.

[53] S. Aguado, J. Canivet, D. Farrusseng, Facile shaping of an imidazolate-based MOF on ceramic beads for adsorption and catalytic applications, Chem Commun, 46 (2010) 7999-8001.

[54] X.L. Liu, Y.S. Li, Y.J. Ban, Y. Peng, H. Jin, W.S. Yang, K. Li, Synthesis of zeolitic imidazolate framework nanocrystals, Mater Lett, 136 (2014) 341-344.

[55] K.S. Park, Z. Ni, A.P. Cote, J.Y. Choi, R.D. Huang, F.J. Uribe-Romo, H.K. Chae, M. O'Keeffe, O.M. Yaghi, Exceptional chemical and thermal stability of zeolitic imidazolate frameworks, P Natl Acad Sci USA, 103 (2006) 10186-10191.

[56] S. Aguado, C.H. Nicolas, V. Moizan-Basle, C. Nieto, H. Amrouche, N. Bats, N. Audebrand, D. Farrusseng, Facile synthesis of an ultramicroporous MOF tubular membrane with selectivity towards CO2, New J Chem, 35 (2011) 41-44.

[57] F. Cacho-Bailo, M. Etxeberria-Benavides, O. Karvan, C. Tellez, J. Coronas, Sequential amine functionalization inducing structural transition in an aldehyde-containing zeolitic imidazolate framework: application to gas separation membranes, Crystengcomm, 19 (2017) 1545-1554.

[58] T. Rodenas, M. van Dalen, P. Serra-Crespo, F. Kapteijn, J. Gascon, Mixed matrix membranes based on NH2-functionalized MIL-type MOFs: Influence of structural and operational parameters on the CO2/CH4 separation performance, Micropor Mesopor Mat, 192 (2014) 35-42.

[59] S. Couck, E. Gobechiya, C.E.A. Kirschhock, P. Serra-Crespo, J. Juan-Alcaniz, A.M. Joaristi, E. Stavitski, J. Gascon, F. Kapteijn, G.V. Baron, J.F.M. Denayer, Adsorption and Separation of Light Gases on an Amino-Functionalized Metal-Organic Framework: An Adsorption and In Situ XRD Study, Chemsuschem, 5 (2012) 740-750.

[60] P. Serra-Crespo, M.A. van der Veen, E. Gobechiya, K. Houthoofd, Y. Filinchuk, C.E.A. Kirschhock, J.A. Martens, B.F. Sels, D.E. De Vos, F. Kapteijn, J. Gascon, NH2-MIL-53(Al): A High-Contrast Reversible Solid-State Nonlinear Optical Switch, Journal of the American Chemical Society, 134 (2012) 8314-8317.

[61] J.H. Kim, S.Y. Ha, Y.M. Lee, Gas permeation of poly(amide-6-b-ethylene oxide) copolymer, Journal of Membrane Science, 190 (2001) 179-193.

# Application of Engineered MOF Crystals to Mixed-Matrix Membranes: Impact of the Filler Morphology on the Gas Separation Performance

*Abstract:* *Mixed-matrix membranes (MMMs) comprising $NH_2$-MIL-53(Al) and Matrimid® or 6FDA-DAM have been investigated. $NH_2$-MIL-53(Al) with three different morphologies: nanoparticles, nanorods and microneedles have been dispersed in Matrimid®. The synthesized membranes have been tested in the separation of $CO_2$ from $CH_4$ in an equimolar mixture. At 3 bar and 298 K for 8 wt% MOF loading, incorporation of $NH_2$-MIL-53(Al) nanoparticles, leading to the largest improvement compared to nanorods and microneedles. The incorporation of the best performing filler, i.e. $NH_2$-MIL-53(Al) nanoparticles, to the highly permeable 6FDA-DAM has a larger effect, leading to a performance very close to the Robeson limit of 2008. Furthermore, a new non-destructive technique based on Raman spectroscopy mapping is introduced to assess the homogeneity of the filler dispersion in the polymer matrix. The MOF contribution can be calculated by modelling the spectra. The determined homogeneity of the MOF filler distribution in the polymer is confirmed by FIB-SEM analysis.*
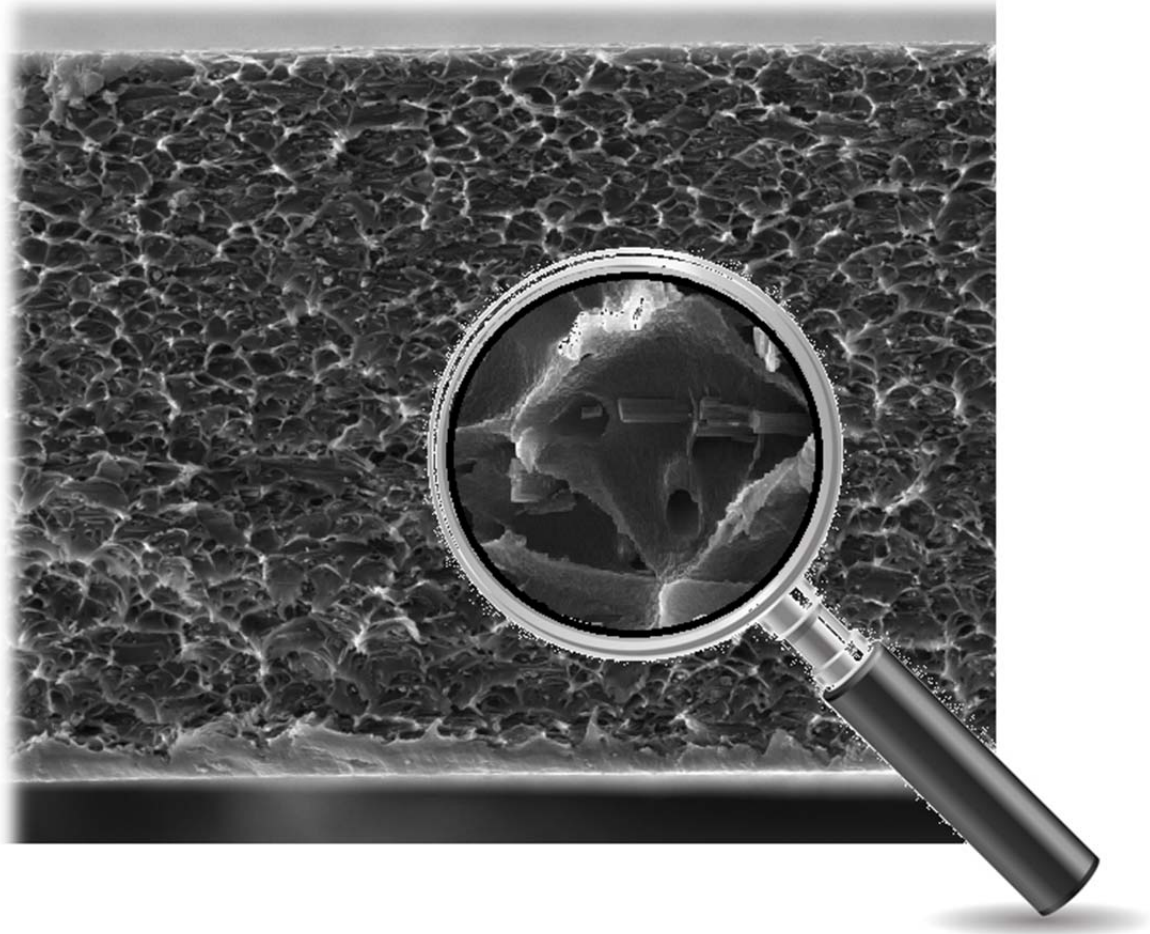
SEM cross-section image of MMM comprising rod-shape NH$_2$-MIL-53(Al)

### 3.1 Introduction

$CO_2$ is one of the most abundant contaminants in fuel gases such as natural gas and biogas. Its removal by gas upgrading is often necessary, not only to avoid releasing $CO_2$ to the atmosphere but also to increase fuels heating value and to prevent pipe corrosion.[1] Nowadays, liquid-phase absorption is the most applied technology for $CO_2$ capture.[2] In particular, the majority of the commercial large-scale absorption processes employ amine-based solutions, such as mono- and triethanolamine or Selexol® (a glycol-based solvent) and Rectisol® (refrigerated methanol) in case of high concentrations of $CO_2$. .[3] However, this technology presents a large energy penalty, since the need to heat and cool the recirculating fluids requires careful, well-monitored, expensive operating procedures. Furthermore, the degradation of the amine absorbent leads to corrosive mixtures. In this sense, alternative technologies such as selective adsorption or membrane separation may become more attractive.[4]

Membrane technology for gas separation is a promising method in both economic and energy saving terms.[5] In contrast to conventional technologies, such as cryogenic distillation or absorption processes, gas separation membranes do not involve a phase transition, thus being more energy efficient. Furthermore, gas separation membrane units lack of mechanical complexity, are safer and environmentally friendly and have, in general, smaller footprints than other types of plants like amine stripping.[6]

While ceramic or inorganic membranes may have applications in special cases due to their good permselectivity and high thermal and chemical stabilities, the vast majority of commercial gas separation membrane systems are based on polymers because of their easy processability and low cost.[7] However, for different gas pairs, polymeric membranes are known to have a well-established empirical trade-off between permeability and selectivity, which was quantified by Robeson initially in 1991 and then updated in 2008.[8, 9] Therefore, during the last few decades, several approaches have been followed to boost the performance of polymeric membranes. One promising approach is fabricating the so-called mixed matrix membranes (MMMs), which consists of a composite comprising two phases: a polymer matrix and a dispersed phase.[10, 11] The first MMMs were prepared using conventional fillers such as zeolites, carbon molecular sieves and silicas. However, over the last few years new materials have been incorporated, such as carbon nanotubes, clay-type layered silicates, metal organic frameworks (MOFs) or graphene.[11, 12]

Metal-organic frameworks (MOFs) are porous crystalline coordination compounds, extending in one, two or three dimensions, composed of metal atoms or clusters linked by organic ligands.[13] Next to a high surface area and pore volume,[14] their chemical functionality can be fine-tuned by different pre- and post-synthetic approaches; thus, enabling to specifically tailor MOF properties according to the different applications.[15] These properties, together with the flexibility of some structures upon external stimuli,[16] make MOFs ideal for their application in

different fields, from gas separation and storage to molecular sensing, catalysis and medical applications.[17, 18] When it comes to MMMs, MOFs have important advantages compared to other fillers.[18, 19] One of the main problems of zeolite-based MMMs is that they commonly suffer from poor polymer-filler compatibility, leading to the formation of defective membranes with non-selective voids at the polymer-filler interface.[20] In this sense, the use of MOFs as fillers might result in a breakthrough in the MMM field, since their partially organic nature provides an enhanced polymer-filler adhesion, preventing the resulting membranes to underperform.[21, 22]

Although MOF-based MMMs have experienced an exponential growth during the last years, few studies have been devoted to the study of the effect of the particle size and morphology on the membrane separation performance. Ge *et al.* compared the performance of MMMs comprising CuBTC with different sizes and poly(2,6-dimethyl-1,4-phenylene oxide) as polymer matrix. Smaller crystals (6 μm) were obtained by post-synthetic ultrasonic treatment and showed a better dispersion and interaction with the polymer than large CuBTC crystals (50 μm), giving rise to an improved separation performance.[23] Furthermore, Nordin *et al.* synthesized MMMs via phase inversion by dispersing ZIF-8 particles of different sizes (100, 300 and 500 nm) in polysulfone. Although the majority of the MMMs showed a decrease in selectivity compared to the bare polysulfone, the incorporation of ZIF-8 with the smallest size led to a 47 % improvement in the $CO_2/CH_4$ selectivity.[24] However, even though the incorporation of MOF nanoparticles into different polymers has led to outstanding results in the separation of different gas mixtures such as $H_2/CO_2$,[25] $CO_2/CH_4$[22, 26] and $CO_2/N_2$,[27] they are often difficult to disperse, complicating their incorporation within a polymer matrix.[28] In this spirit, we have recently reported the first study on the effect of the particle morphology on the MMMs' microstructure and performance. While bulk CuBDC crystals led to defective membranes with selectivities lower than those of the bare polymer, the dispersion of CuBDC nanosheets in the polymer gave rise to an enhancement of the $CO_2/CH_4$ selectivity from 60 for the neat polymer to 80 for 8 wt% MOF loading.[29] This behavior was attributed to the superior occupation and more uniform distribution of the filler in the membrane cross-section if nanosheets are used, showing that in the preparation of MMMs the particle morphology plays a key role.

$NH_2$-MIL-53(Al) is one of the most studied fillers in the preparation of MMMs together with ZIF-8, HKUST-1 and MIL-53 and it has been dispersed in different polymers, such as PSF,[30-33] 6FDA-based polyimides,[34-36] Matrimid®,[31, 32] poly(4 methyl-1-pentyne)[37] and poly(vinylidene fluoride). This MOF has been reported to display outstanding selectivities in the separation of $CO_2$ from equimolar mixtures of $CO_2$ and $CH_4$, being a good candidate for the preparation of MMMs.[38] Furthermore, MOFs functionalized with amino groups lead in general to good interaction with different polymer matrices, preventing the formation of voids at the filler-polymer interface, and thus, the fabrication of defective membranes.[35, 38] Herein, we study the effect of the $NH_2$-MIL-53(Al) crystal morphology on the MMMs microstructure and gas separation

performance for the first time. To this end, $NH_2$-MIL-53(Al) with three different crystal morphologies have been synthesized (nanoparticles, nanorods and microneedles) and used as fillers in the polyimide Matrimid®. The resulting membranes have been tested for $CO_2/CH_4$ separation and the influence of the MOF loading, crystal morphology and trans-membrane pressure difference on the membrane permeability and selectivity has been assessed. Furthermore, the best performing filler, *i.e.* $NH_2$-MIL-53(Al) nanoparticles, was also used as dispersed phase in a second polymer matrix, the highly permeable polyimide 6FDA-DAM. With this approach, membranes surpassing the Robeson limit of 1991, and being close to that of 2008, could be obtained upon 20 wt% MOF nanoparticles loading.

## 3.2 Experimental Section

### 3.2.1 Synthesis of $NH_2$-MIL-53(Al) nanoparticles

$NH_2$-MIL-53(Al) nanoparticles were synthesized under reflux conditions. In a typical synthesis, 1.902 g 2-aminoterephthalic acid (10.50 mmol, Sigma Aldrich, 99 %) was dissolved in 10.5 ml 2 M NaOH aqueous solution at room temperature. Then, 3.935 g $AlCl_3·6H_2O$ (16.30 mmol, Sigma Aldrich, ≥ 99.0 %) was added to a separated vial and both volumes were increased to a total of 7.5 ml by addition of distilled water. The reactants were mixed and treated at reflux temperature for 3 days without stirring. The resulting yellow powders were filtered under vacuum and activated to remove organic species trapped within the pores with N,N-dimethylformamide (DMF, Sigma Aldrich, > 99.8 %) at 403 K, and subsequently with methanol under reflux, overnight. Finally, the powder was thoroughly washed twice with ethanol and dried at 373 K under vacuum.

### 3.2.2 Synthesis of $NH_2$-MIL-53(Al) nanorods

$NH_2$-MIL-53(Al) nanorods were synthesized according to the method reported by Chin *et al*.[39] Two different solutions were prepared separately in 15.6 ml deionized water: 0.589 g 2-aminoterephthalic acid (3.25 mmol, Sigma Aldrich, 99 %) together with 0.898 g sodium acetate (10.95 mmol, Sigma Aldrich, 99 %), giving rise to a pale yellow solution, and 0.821 g $Al(NO_3)_3·9H_2O$ (2.20 mmol, Fluka, 98 %). Both solutions were mixed in a Teflon®-lined autoclave and the synthesis solution was treated at 393 K for 3 days in an oven under static conditions. The resulting powder was washed with acetone and centrifuged at 6000 rpm for 10 min. To efficiently eliminate the remaining linker occluded in the pores of the MOF, the solid was consecutively re-suspended in 30 ml N,N-dimethylformamide (DMF) and 30 ml methanol and treated at 403 K and 363 K overnight, respectively. Finally, the powder was centrifuged at 6000 rpm for 10 min, thoroughly washed twice with ethanol and dried at 353 K under vacuum.

### 3.2.3 Synthesis of NH$_2$-MIL-53(Al) microneedles

To synthesize NH$_2$-MIL-53(Al) microneedles the method reported by Chin *et al.*[39] was followed. Two different solutions were prepared in 15 ml DMF: 0.565 g 2-aminoterephthalic acid (3.12 mmol, Sigma Aldrich, 99 %) together with 3.783 g acetic acid (63 mmol, Sigma Aldrich, 99 %), giving rise to a pale yellow solution, and 0.788 g Al(NO$_3$)$_3$·9H$_2$O. Both solutions were mixed in a Teflon®-lined autoclave. The synthesis solution was then treated at 393 K for 3 days in an oven under static conditions. The washing and drying procedure was the same as for the nanorods.

### 3.2.4 6FDA-DAM polyimide synthesis

The monomers used for the polyimide synthesis –4,4'-(hexafluoroisopropylidene) diphthalic anhydride (6FDA, Sigma Aldrich, 99 %) and 2,4,6-trimethyl-*m*-phenylenediamine (DAM, Sigma Aldrich, 96 %) were purified by sublimation prior to their use. Besides, dimethylacetamide (DMAc, Acros Organics, 99.5 %), acetic anhydride and triethylamine (TEA, Sigma Aldrich, > 99 %) were used as received.

To synthesize the polyimide, a two-step procedure was followed. In the first step the diamine (1.5022 g, 10 mmol) was dissolved in DMAc (8 mL) in a moisture free flask under Ar atmosphere and 6FDA (4.4424 g, 10 mmol) was added in small portions together with another 8 mL of DMAc. Then, the mixture was stirred overnight and polyamic acid (PAA) was formed. In the second step PAA was chemically imidized using an equimolar, three-fold excess (based on the total amount of diamine monomers) of triethylamine/acetic anhydride mixture, and the mixture was heated up to 393 K for 30 min. After cooling, the polymer was precipitated in a 1:1 volume mixture of ethanol and distilled water, milled and washed with ethanol. The molecular weight of the synthesized polymer, as measured by gel permeation chromatography, was Mw = 123000 g/mol and Mn = 68000 g/mol.

### 3.2.5 Preparation of mixed-matrix membranes (MMMs)

Two different polyimides were used as polymeric matrices in the MMMs: Matrimid® 5218 (supplied by Huntsman Advanced Materials, Mw ≈ 80000 g/mol and Mn ≈ 11000 g/mol) and 6FDA-DAM (*vide supra*). Prior to the membranes synthesis, the polymers were degassed overnight at 453 K under vacuum in order to remove the adsorbed moisture. To prepare the MMMs, 0.4 g dried polymer was dissolved in 2.5 ml tetrahydrofuran (THF) and, in the case of 6FDA-DAM-based MMMs, the polymer solution was filtered through a syringe filter (PTFE membrane, 0.45 µm pore size). Then, MOF crystals were suspended in 1.55 ml THF under ultrasonication for 60 min. To this suspension, 10 % of the dissolved polymer amount was added

and the suspension further stirred for 4 h (priming). After that, the rest of the polymer solution was added to the MOF suspension and stirred overnight. The solvent/filler-polymer weight ratio was of 90/10 in all cases. The MOF content in this synthesis suspension was adjusted to achieve final desired MOF loadings in the resulting membranes. For comparison, membranes based on the neat polymers were also prepared following an identical procedure, but without MOF incorporation. The casting suspension was poured on the glass slide of a Doctor Blade setup to cast the membrane with 75 µm thickness. After casting, the membranes were covered with a top-drilled box (30.5 cm length x 15.5 cm height x 23.0 cm width) and dried overnight under THF-saturated atmosphere at room temperature (RT) by natural convective evaporation. Finally, membranes were treated under vacuum at 453 K during 24 h.

### 3.2.6 Characterization methods

XRD patterns of the prepared MOF powder and the membranes were recorded in a Bruker-D8 Advance diffractometer using Co-$K_\alpha$ radiation ($\lambda$ = 1.78897Å). The *2θ* range of 5–50° was scanned using a step size of 0.02° and a scan speed of 0.2 s per step in a continuous scanning mode.

High-pressure adsorption isotherms of $CO_2$ were measured for MOF powder samples with different types of morphologies. The $CO_2$ isotherms were determined using the volumetric technique with an apparatus from BEL Japan (Belsorp HP) at 273 K. Around 0.2 g $NH_2$-MIL-53(Al) nanoparticles was placed in the sample container. Before the measurement, the adsorbent was pretreated by increasing the temperature to 423 K at a rate of 10 K/min under $N_2$ flow and maintaining the temperature for 2 h. Furthermore, $CO_2$ isotherms were acquired for neat and mixed-matrix membranes. The different samples were first degassed under vacuum at 200 °C for 16 h and then analyze with a Tristar II 3020 (Micromeritics) apparatus using high purity $CO_2$ (Linde, 99.995 %).

For the TEM analysis the MOF powder samples were prepared by applying a few drops of MOF suspensions in ethanol on a carbon coated copper grid and dried. TEM analyses were carried out in JEOL JEM-2010 microscope operated at 200 keV. This microscope has an X-ray OXFORD detector, INCA energy TEM 100 model for microanalysis (EDS) and a bottom-mounted GATAN ORIUS SC600 imaging camera. Micrograph acquisition was performed with GATAN DigitalMicrograph 1.80.70 software. As for the MMMs, a portion of the membrane was embedded in an EpofixTM cold-setting embedding resin (in volume proportion, 15 parts of embedding resin and 2 parts of hardener) and cured for 24 h at room temperature. Afterwards, slices of 100 nm thickness were cut using a Leica EMUC7 ultramicrotome and placed on carbon copper. Membrane cross-sectional images were taken by transmission electron microscopy (TEM), with a Tecnai T20 operating at 200 kV.

Prior to the FIB-SEM analyses, the membranes were prepared by freeze-fracturing after immersion in liquid $N_2$ and coated with platinum. A trench was milled in the specimen by accelerating concentrated gallium ions (30 kV, 0.75 nA) using a Dual Beam 3 Nova 200 FIB. Several cross-sections of 15 x 10 $\mu m^2$ were exposed by FIB milling and individual SEM images of the exposed surfaces were recorded.

DSC measurements were performed using Perkin Elmer DSC 7 equipment to estimate glass transition temperature of the neat and MMMs. The scanning range was 25 – 425 °C at a heating rate of 10 °C/min under nitrogen atmosphere. Two consecutive runs were performed. A first DSC cycle was carried out to remove thermal history and adsorbed water from the samples. After cooling, a second cycle was performed following the same procedure. The glass transition temperature ($T_g$) value was taken from the middle point of the slope transition in the DSC curve.

Membrane thickness ($\mu m$), $l$, was determined using a digital micrometer Mitutoyo, with an accuracy of 1 $\mu m$. The measurement was performed at least at 10 different locations within each membrane and then averaged.

Raman experiments were conducted on the membranes in a Jobin Yvon Labram 300 confocal microscope equipped with a laser at 633 nm and a 1800 lines/mm grating. Alternatively, the spectrometer was also used to monitor the interferences of the laser light when passing through the membranes. From Equation 1, and by comparison with the measured membrane thickness (*vide supra*), either the membrane thickness or the refractive index of the material was calculated.

$$\ell = \frac{\Delta m}{2 \cdot n_A \cdot (\sigma_2 - \sigma_1)} \qquad (1)$$

Where $\Delta m$ is the number of periods between the wavenumbers $\sigma_1$ and $\sigma_2$, and $n_A$ is the refractive index of the material.

The homogeneity of the membranes for the dispersion of the filler in the polymer was estimated from the Raman intensities in the membrane compared to the spectra of the pure components. For this, at least 15 measurements were done at several spots (*ca.* 1 $\mu m^2$) on both sides of the membrane surface. All the spectra of the MMMs were then modeled by combining the same reference spectra of the pure MOF and polymer. The spectroscopic contribution of the MOF filler in the membrane was calculated using the spectrometer's software LabSpec 5. The numerical value of the calculated ratio was found to vary if different reference spectra were used for the modeling. However, for each set of common reference spectra, a similar evolution of the average ratios was obtained with the MOF loading.

### 3.2.7 Gas permeation experiments

Round membrane sheets with an area of 4.15 cm$^2$ were cut from the casted films placed on a macro-porous support 316L with 20 µm nominal pore size and mounted in a flange between Viton® O-rings. This flange fit in a permeation module was placed inside an oven using the permeation setup described elsewhere.[30] The $CO_2$/$CH_4$ separation measurements were carried out in a home-made setup employing a 1:1 flow mixture of $CO_2$ and $CH_4$ (50 ml·min$^{-1}$ of $CO_2$ and 50 ml·min$^{-1}$ of $CH_4$) as feed. Helium (3.3 ml·min$^{-1}$) was used as sweep gas for the permeate stream (atmospheric), while the trans-membrane pressure was adjusted in the range of 3-9 bar using a back-pressure controller at the retentate side. All the reported gas separation results were determined after at least 10 h of operation once the steady performance had been reached at each set of experimental conditions during the gas permeation experiments.[21] The temperature in the permeation module was 298 K. An on-line gas chromatograph (Interscience Compact GC) equipped with a packed Carboxen 1010 PLOT (30 m x 0.32 mm) column and TCD and FID detectors was used to periodically analyze the permeate stream. Each membrane was fabricated and measured at least two times to ensure the reproducibility of the results. In all cases, gas separation performance was evaluated after ensuring steady operation.

Gas separation performance was defined by the separation factor ($\alpha$) and the gas permeability ($P$) of the individual components. The permeability for the component $i$ ($P_i$) was calculated as follows (Equation 2):

$$P_i = \frac{F_i \cdot \delta}{\Delta p_i \cdot A} \tag{2}$$

Where $F_i$ denotes the molar flow rate of $i$-compound, $l$ is the thickness of the membrane, $\Delta p_i$ is the partial pressure difference of $i$ across the membrane and $A$ is the membrane area. The SI unit for the permeability is mol·s$^{-1}$·m·m$^{-2}$·Pa$^{-1}$. However, gas permeabilities are reported in the widely used non-SI unit Barrer, where 1 Barrer = 3.35 x 10$^{-16}$ mol·s$^{-1}$·m·m$^{-2}$·Pa$^{-1}$. The separation factor or mixed gas selectivity ($\alpha$) was calculated as the ratio of the permeability of the more permeable compound, $CO_2$, to the permeability of the less permeable compound, $CH_4$ (Equation 3).

$$\alpha = \frac{P_{CO_2}}{P_{N_2}} \tag{3}$$

## 3.3 Results and Discussion

### 3.3.1 Characterization of $NH_2$-MIL-53(Al)

$NH_2$-MIL-53(Al) crystals with three different morphologies ('nanoparticles' (NP), 'nanorods' (NR) and 'microneedles' (MN)) have been synthesized according to the method reported by Chin *et al*.[39] For comparison purposes, conventional MOF crystals in the submicrometer size range, hereafter referred to as submicron crystals, were also synthesized.[40] In order to examine the size and shape of the different MOFs crystals, TEM images were acquired. The nanoparticles and the nanorods possess the same width (*ca.* 15 nm) but differ in crystal length (Table 3.1 and Figure 3.1). While the average length of the nanoparticles is 46 ± 6 nm, the nanorods are 50 % longer with lengths of 67 ± 14 nm. As for the microneedles, the measured aspect ratio was one order of magnitude higher than for the other morphologies with lengths up to 4 ± 1 µm and widths of 80 ± 10 nm.

Figure 3.2 shows the XRD diffraction patterns obtained for the activated particles with different morphologies. The simulated XRD patterns for the large pore (*lp*) and narrow pore (*np*) $NH_2$-MIL-53(Al) configurations have also been included for comparison.[41] After activation, the reflections of the nanoparticles, nanorods and microneedles are consistent with a mixture of the *np* and *lp* forms in contrast to the $NH_2$-MIL-53(Al) submicron crystals, whose XRD pattern matches with the *np* form. These results are in agreement with previous findings on flexible MOFs, in which the open dried phase is stabilized by crystal downsizing.[42] Indeed, when it comes to high-pressure $CO_2$ adsorption, the shape of the isotherm is strongly affected by the particle morphology (see Figure 3.3) and just in the case of the microneedles a pronounced step could be observed.[39] This step has been commonly attributed to flexible MOFs exhibiting 'breathing behavior' or 'gate opening' upon external stimuli. Particularly, in the case of $NH_2$-MIL-53(Al) this step, taking place at *ca.* 7 bar at 273 K for MOF submicrometer crystals, is related to the breathing of the MOF, which changes from the narrow to the large pore configuration.[43] In the case of $NH_2$-MIL-53(Al) nanorods and nanoparticles the pressure at which the *lp* configuration starts forming is shifted towards higher pressures compared to the microneedles, the structural transformation taking place over a broader pressure range.[42]

### 3.3.2 Characterization and permeation results of $NH_2$-MIL-53(Al)-based MMMs

#### 3.3.2.1 $NH_2$-MIL-53(Al)@Matrimid® MMMs

*Characterization:* $NH_2$-MIL-53(Al)@Matrimid® MMMs with two different MOF loadings (8 and 16 wt%) have been prepared with 3 different crystal morphologies (*vide supra*) in order to assess the influence of the filler morphology and its loading on membrane structure and performance.
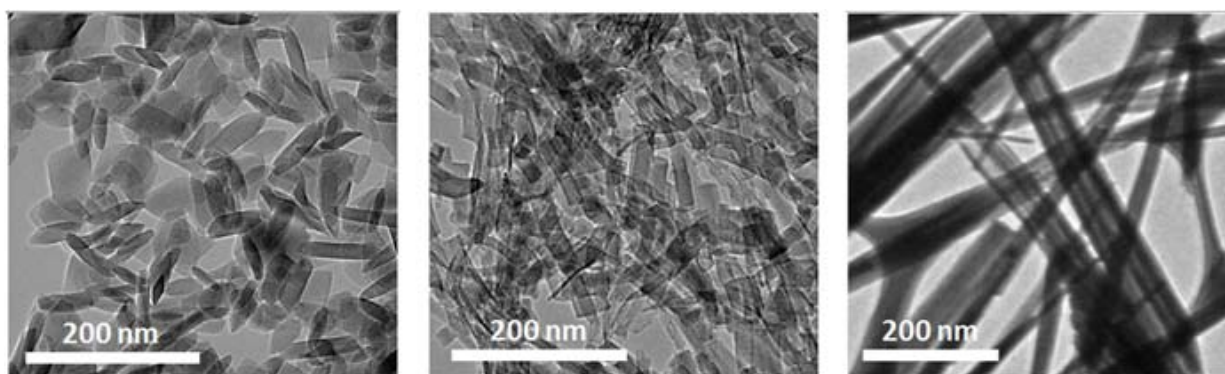
**Figure 3.1** TEM micrographs of a) NH$_2$-MIL-53(Al) nanoparticles, b) NH$_2$-MIL-53(Al) nanorods and c) NH$_2$-MIL-53(Al) microneedles. The dimensions of the particles can be found in Table 1.

**Table 3.1** Dimensions of NH$_2$-MIL-53(Al) nanoparticles, nanorods and microneedles.

| Particles | Length | Width | Aspect ratio |
|---|---|---|---|
| Nanoparticles | 46 ± 6 nm | 15 ± 1 nm | 3 ± 1 |
| Nanorods | 67 ± 14 nm | 15 ± 3 nm | 5 ± 1 |
| Microneedles | 4 ± 1 µm | 80 ± 10 nm | 12 |
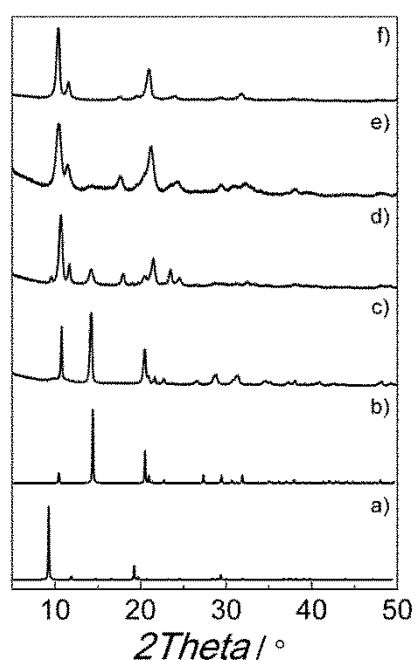


**Figure 3.2** Simulated XRD diffraction patterns for the a) large pore configuration and b) narrow pore configuration of NH$_2$-MIL-53(Al), and XRD diffraction patterns of the different NH$_2$-MIL-53(Al) crystals: c) submicron crystals synthesized according to the method reported by Ahnfeldt *et al.*,[40] d) nanoparticles, e) nanorods and f) microneedles.

The membrane preparation procedure does not affect the crystallinity of the MOF particles in the MMM. Moreover, the intensity of the reflections corresponding to the large pore configuration is higher for the MMM when compared with the activated MOF powder, in line with the results reported by Rodenas *et al*.[32] This behavior has been ascribed to the partial penetration of the polymer chains in the MOF pores during the different steps followed to disperse the filler in the polymer solution in order to prepare a homogeneous casting solution.[32]

In order to assess the filler dispersion on the cross section of the membrane and to evaluate the interaction between the continuous and the dispersed phase, SEM and TEM micrographs were acquired. Figure 3.5 shows that the distribution of the MOF crystals is homogeneous for the 8 wt% loading MMMs regardless the particle morphology. Furthermore, the TEM micrographs suggest a good interaction between the polymer and the MOF, in agreement with a good affinity between the filler and the polymer not only for the nanoparticles, which exhibit the highest surface to volume ratio, but also for the nanorods.

*Gas permeation performance:* Figure 3.6a depicts the $CO_2$ permeability and the $CO_2/CH_4$ separation factor of the membranes comprising $NH_2$-MIL-53(Al) crystals with different morphologies and Matrimid® as a function of the filler loading. The performance of the bare polymer has also been included for comparison. The gas separation performance of the MMMs is influenced by the morphology of the filler. While the $CO_2$ permeability of the NP-$NH_2$-MIL-53(Al)@Matrimid® MMMs increases upon 8 wt% loading, it decreases for both NR-$NH_2$-MIL-53 and MN-$NH_2$-MIL-53 (see Figure 3.6a). We speculate this behavior might be related to a better disruption of the polymer chains by the nanoparticles compared to the nanorods and the microneedles, providing more free volume in the polymeric matrix. As for the selectivity, at 3 bar pressure difference, it remains constant at 8 wt% MOF loading no matter the morphology used, in line with the work of Rodenas *et al*., who tested $NH_2$-MIL-53(Al)@Matrimid® MMMs in the separation of $CO_2$ from an equimolar $CO_2/CH_4$ at 35 ºC and $\Delta p$ = 3 bar and observed that the selectivity remained unchanged for MOF loadings up to 15 wt%.[32]
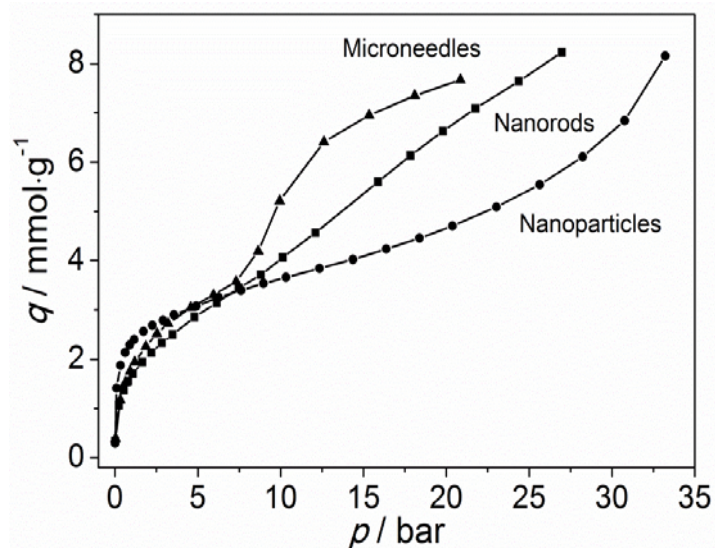
**Figure 3.3** $CO_2$ adsorption isotherms acquired at 273 K for $NH_2$-MIL-53(Al) MOF crystals with three different morphologies, *i.e.* nanoparticles, nanorods and microneedles.
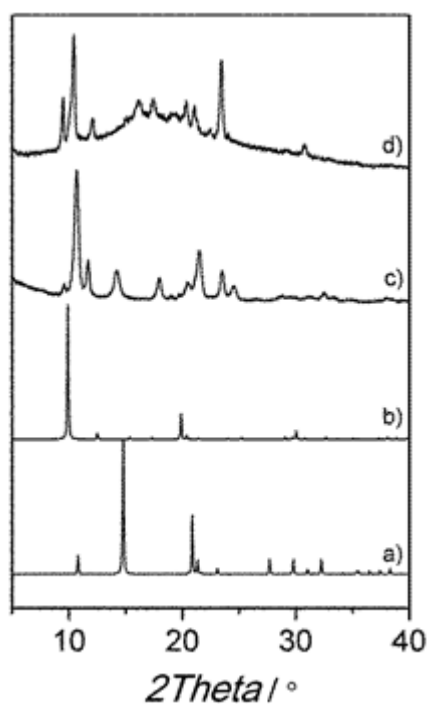


**Figure 3.4** Simulated XRD diffraction patterns of the a) narrow pore configuration and b) large pore configuration of $NH_2$-MIL-53(Al), and powder XRD of c) $NH_2$-MIL-53(Al) nanoparticles and d) of a NP-$NH_2$-MIL-53(Al)@Matrimid® MMM with 16 wt% MOF loading.
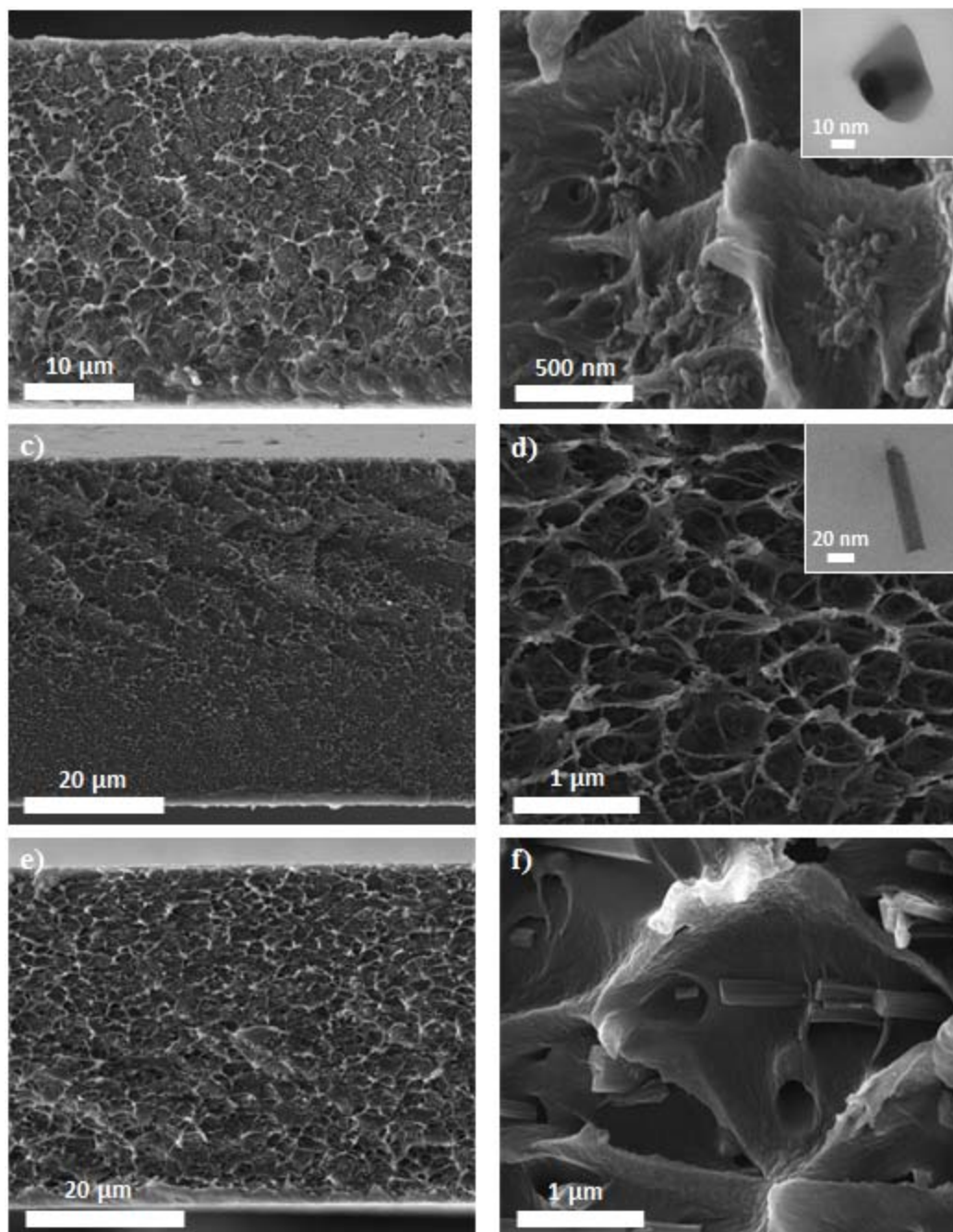
**Figure 3.5** SEM images of 8 wt% $NH_2$-MIL-53(Al)@Matrimid® MMMs synthesized using the three different crystal morphologies: a, b) nanoparticles (NP), c, d) nanorods (NR) and e, f) microneedles (MN). Inset: TEM micrographs of a particle embedded in Matrimid® acquired for the b) 8 wt% NP-$NH_2$-MIL-53(Al)@Matrimid® and d) 8 wt% NR-$NH_2$-MIL-53(Al)@Matrimid® MMMs.
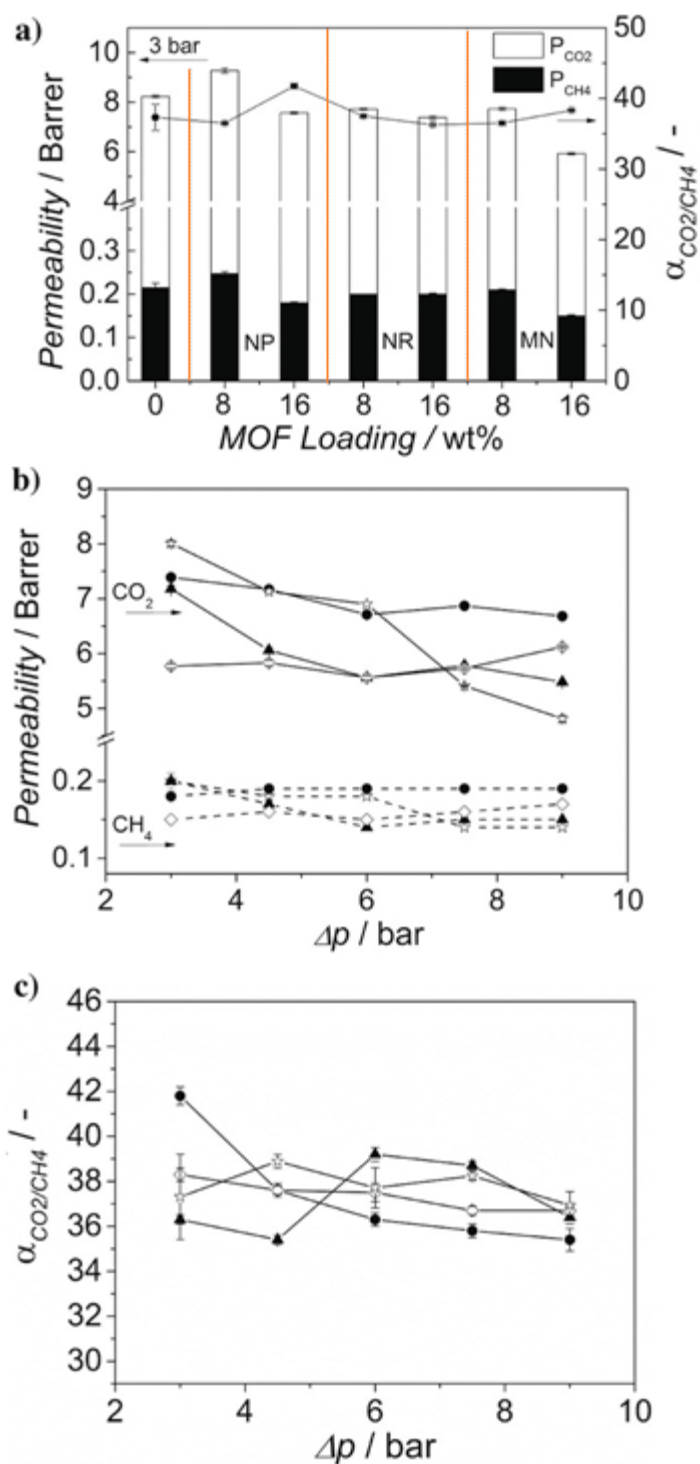
**Figure 3.6.** a) Permeation properties for the $CO_2/CH_4$ mixture (1:1) separation at 298 K and $\Delta p$ = 3 bar for MMMs comprising Matrimid® and $NH_2$-MIL-53(Al) MOF crystals with different morphologies (nanoparticles (NP), nanorods (NR) and microneedles (MN)) as a function of the filler loading. Effect of the trans-membrane pressure different on the b) $CO_2$ permeability and c) $CO_2/CH_4$ separation factor of the 16 wt% $NH_2$-MIL-53(Al)@Matrimid® MMMs prepared with different filler morphologies. The data are average values of at least two membranes and error bars correspond to standard deviation. ▲ Nanorods, ● nanoparticles, ◊ microneedles and   Matrimid®. ☆

**Table 3.2** Glass transition temperature ($T_g$) of different $NH_2$-MIL-53(Al)@ Matrimid® MMMs.

| Membrane | $T_g$ (°C) |
|---|---|
| Bare Matrimid® | 324 |
| 8 wt% NP-$NH_2$-MIL-53(Al)@Matrimid® | 325 |
| 16 wt% NP-$NH_2$-MIL-53(Al)@Matrimid® | 327 |
| 8 wt % NR-$NH_2$-MIL-53(Al)@Matrimid® | 324 |

This is in agreement with the general trend in MOF-based MMMs, in which the selectivities hardly change upon MOF addition, and with the previous observations of Bae *et al.* for membranes comprising low permeable polymers and highly permeable fillers. Indeed, there is a very large difference between $CO_2$ permeabilities reported for pure $NH_2$-MIL-53(Al) membranes (*ca.* 4400 Barrer) and that of the Matrimid® polymer.[22, 38, 44]

When the MOF loading is increased from 8 up to 16 wt%, the permeability decreases at constant or higher separation factors in agreement with reported results on MMMs containing $NH_2$-MIL-53(Al) as filler and Matrimid® as continuous phase.[32] This behavior is commonly attributed to rigidification of the polymer chains around the filler particles or to the partial blockage of the filler pores.[10] Considering the one-dimensional nature of the pores of the MIL-53 topology both effects would result in lower permeabilities.[45] However, given the fact that low MOF loadings result in higher permeabilities, pore blocking due to polymer penetration into the MOF porosity seems to be rather unlikely. On the other hand, the extent of polymer rigidification increases with increasing MOF loading, with an increase in the $T_g$ from 324 °C for pure Matrimid® to 327 °C for MMMs containing 16 wt% MOF loading  (see Table 3.2), leading to the observed lower permeabilities at higher filler content. Interestingly, the extent of this rigidification depends on $NH_2$-MIL-53(Al) crystal morphology, being smaller for nanorods than for nanoparticles (see Table 3.2). These results further confirm the better contact between nanoparticles and polymer.

Finally, the influence of the trans-membrane pressure difference (Δp) on the gas separation performance was studied for 16 wt% $NH_2$-MIL-53(Al)@Matrimid® MMMs synthesized with the three different crystal morphologies. The studied Δp range lies below the onset of plasticization, which for Matrimid® takes place above 12 bar of $CO_2$ at 25 ºC.[46] The decrease in $CO_2$ permeability of bare Matrimid® (Figure 3.6b) with pressure stems from the decreasing solubility of the polymer (gradual saturation of microvoids), following the predicted behaviour of the dual-mode sorption model.[47, 48]

In contrast, the $NH_2$-MIL-53-based MMMs show an almost constant permeability at higher pressures, as previously observed in literature and usually attributed to the restricted mobility of the polymer chains in the presence of a filler.[49] Furthermore, the separation factor remains almost constant regardless of the MOF particle morphology.

Table 3.3 Physical features of $NH_2$-MIL-53(Al)@6FDA-DAM MMMs.

| Loading [wt%] | Average thickness [μm] | | Refractive index, $n_A$ [c] [-] |
|---|---|---|---|
| | Micrometer [a] | Raman [b] | |
| 0 | 36.8 | 37.5 | 1.6 |
| 5 | 35.0 | 29.3 | 1.3 |
| 10 | 39.0 | 31.8 | 1.3 |
| 15 | 41.0 | 35.3 | 1.3 |

[a] Membrane thickness determined using a micrometer;

[b] Membrane thickness measured using a Raman spectra;

[c] $n_A$ = 1.544 for the pure 6FDA-DAM polymer.[50]

### 3.3.2.2 $NH_2$-MIL-53(Al)@6FDA-DAM MMMs

**Characterization:** Since a good match between the permeabilities of the continuous and dispersed phase has been reported to be of utmost importance in the preparation of MOF-based MMMs,[22] another polymer matrix, 6FDA-DAM, with higher $CO_2$ permeability was used with the best performing filler, *i.e.* $NH_2$-MIL-53(Al) nanoparticles. In particular, NP-$NH_2$-MIL-53(Al)@6FDA-DAM MMMs with four different MOF loadings (5, 10, 15 and 20 wt%) have been prepared.

The NP-$NH_2$-MIL-53(Al)@6FDA-DAM membranes were *ca.* 30 μm thick (see Table 4.3) according to the measurements performed with a micrometer device, showing no differences at several spots. In order to confirm the thickness of these membranes, laser interference measurements were performed using a Raman spectrometer. Assuming a constant refractive index ($n_A$ = 1.544),[50] the thicknesses determined by both methods for the pure 6FDA-DAM polymer are consistent. By contrast, the values determined for the MMMs were slightly lower than those measured by the micrometer (Table 3.3). This is likely due to a lowering of the refractive index in the MMM due to the presence of a porous phase.[50] Based on this the refractive indices of the composite membranes can thus be estimated, which turned out to be constant for the investigated NP-$NH_2$-MIL-53(Al) loadings, and approximately equal to 1.3.

Furthermore, the homogeneity of the filler dispersion in the polymer matrix was evaluated by the Raman spectra of the membranes. Spectra of the individual components and mixed matrix membranes $NH_2$-MIL-53(Al)@6FDA-DAM are shown in Figure 3.7. The MMMs did not show any additional absorbance compared to the pure components and the positions of the maxima were not significantly perturbed. Therefore, spectra of the MMMs could be modeled by combining the spectra of the pure components so that the (spectroscopic) contribution of the MOF filler in the membrane could be calculated. In this way comparison of the contributions obtained at different spots on the surface (*ca.* 1 μm$^2$) yields insight in the homogeneity of the membrane (Figure 3.8).
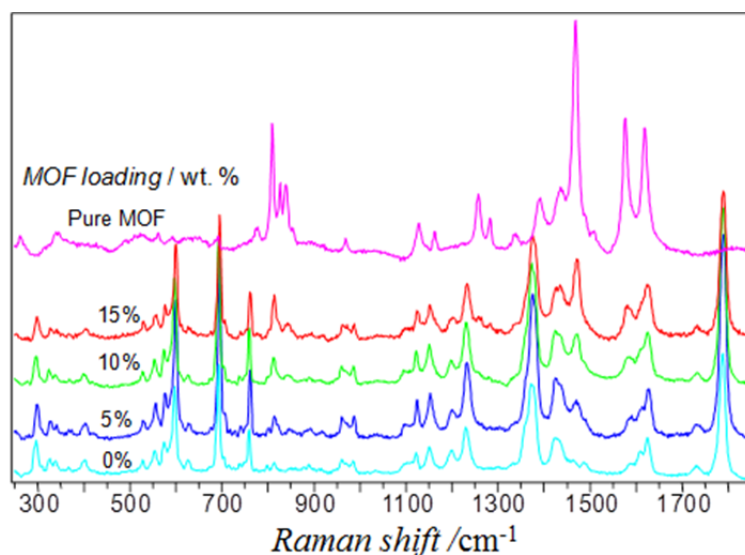
**Figure 3.7** Raman spectra of bare 6FDA-DAM (labelled as "0 %"), $NH_2$-MIL-53(Al) nanoparticles (labelled as "pure MOF") and NP-$NH_2$-MIL-53(Al)@6FDA-DAM MMMs with different loadings.

The analyses carried out at various positions on the NP-$NH_2$-MIL-53(Al)@6FDA-DAM membranes with different MOF loadings showed a rather good compositional homogeneity. Despite the small size of the spots analyzed, all three membranes showed only a limited variation in the calculated composition. In addition, separate measurements performed on each side of the membranes yielded similar results (Figure 3.8). The average values correlated with the nominal MOF loading, which confirms that the preparation of these membranes yielded a good dispersion of the MOF filler in the polymer. In order to corroborate these results, FIB-SEM (see Figure 3.9) micrographs were acquired for the cross sections of NP-$NH_2$-MIL-53@6FDA-DAM MMMs with 5 and 15 wt% MOF loading before and after FIB milling. In a previous publication we demonstrated the potential of this technique for the in depth characterization of complex composites such as mixed matrix membranes.[21] The images reveal a good spatial (homogeneous) distribution of the filler within the polymer matrix of the 6FDA-DAM-based membranes. Furthermore, the interaction between the continuous and dispersed phase is good and no defects could be observed at the interface. These results are comparable to those reported by Rodenas *et al.*,[21] who calculated void fractions as small as 0.11 % for 25 wt% MMMs comprising $NH_2$-MIL-53(Al) submicrometer crystals in Matrimid®.
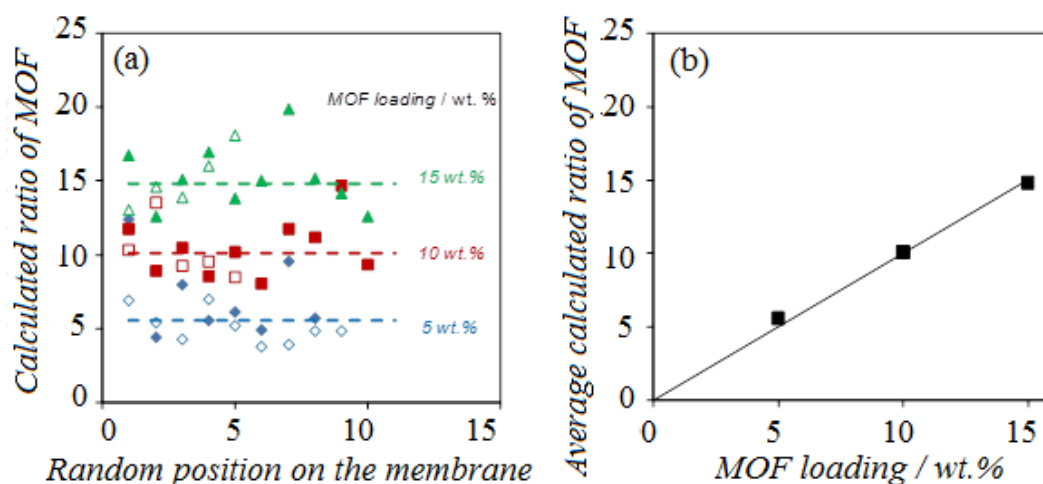
**Figure 3.8** Filler dispersion in the NH$_2$-MIL-53(Al)@6FDA-DAM MMMs evaluated by Raman spectroscopy. a) Contribution of NH$_2$-MIL-53(Al) in the modelled spectra at different locations on the membrane surface; b) comparison between the calculated spectroscopic ratio of NH$_2$-MIL-53(Al) and the nominal content in the membrane. In Figure a), full and empty symbols represent measurements on each side of the membrane; dotted lines show the average value for all measurements on each MMM.
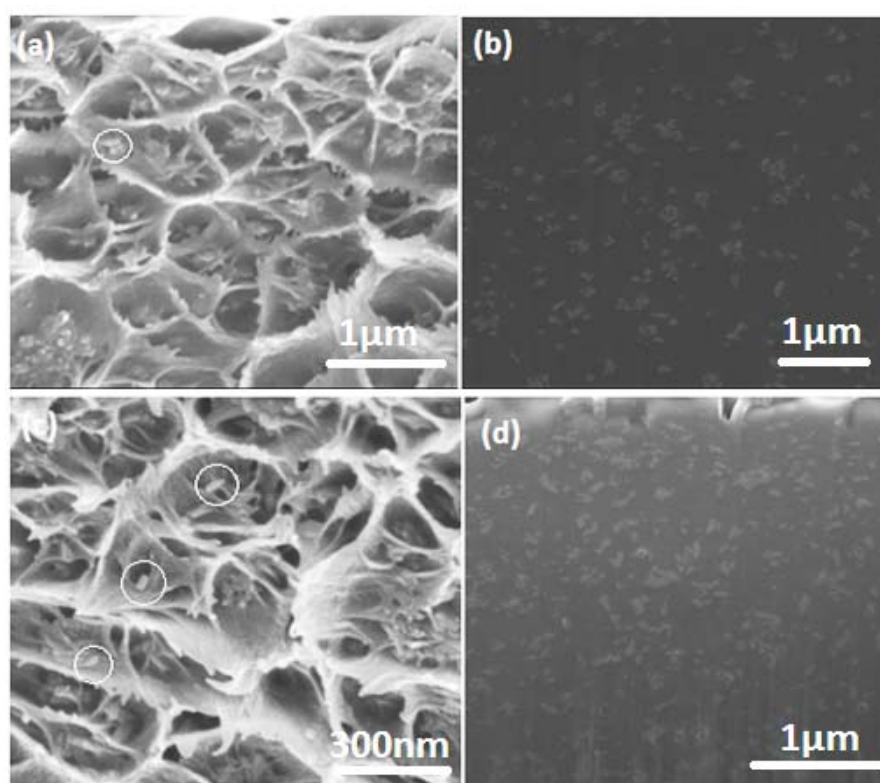


**Figure 3.9** SEM micrographs of MMMs comprising NH$_2$-MIL-53(Al) nanoparticles and 6FDA-DAM showing a, c) cross section of the membranes prepared by freeze fracturing without FIB milling for 5 and 15 wt% MOF loadings; and b, d) cross section of the composite membrane exposed via FIB milling for 5 and 15 wt% MOF loadings.
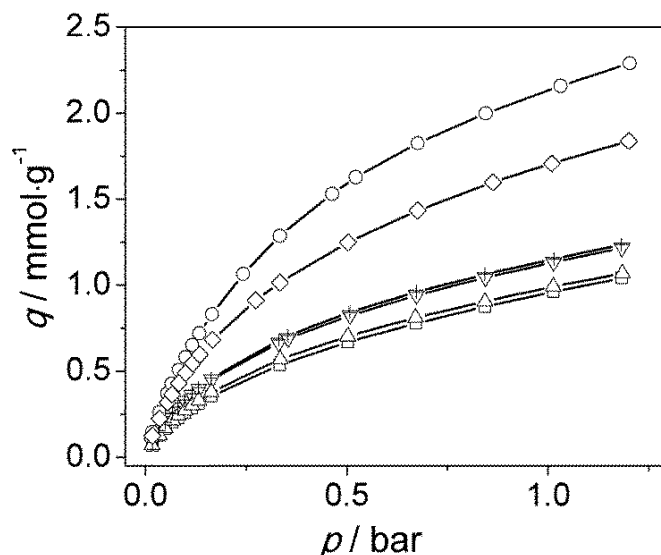
**Figure 3.10** $CO_2$ adsorption isotherms acquired at 273 K, ◇ bare 6FDA-DAM, ○ 8 wt% NP-NH$_2$-MIL-53(Al)@6FDA-DAM, □ bare Matrimid® and 8 wt% NH$_2$-MIL-53(Al)@ Matrimid® with +NP, △NR and MN.

Figure 3.10 shows the gas sorption measurements of $CO_2$ acquired at 273 K for bare 6FDA-DAM and Matrimid®, 8 wt% NP-NH$_2$-MIL-53(Al)@6FDA-DAM and 8 wt% NH$_2$-MIL-53(Al)@Matrimid® MMMs. The gas adsorption data confirm that the adsorption in Matrimid® is lower than in 6FDA-DAM, further verifying the high free volume and higher adsorption capacity of the latter. Interestingly, the amount of $CO_2$ uptake of both Matrimid® and 6FDA-DAM improved upon incorporation of NH$_2$-MIL-53(Al) with different morphologies, pointing to a higher solubility of $CO_2$ in the composite membranes.

*Gas permeation performance:* Figure 3.11 depicts the influence of the nanoparticle loading (wt%) in NP-NH$_2$-MIL-53(Al)@6FDA-DAM MMMs on both the permeability and separation factor. Upon increasing the MOF loading from 0 to 20 wt%, the $CO_2$ permeability increased from 360 up to 660 Barrer. As mentioned above, the nanoparticles might lead to some disruption of the polymer chains. The enhancement of the free volume, when compared to the bare polyimide, together with the MOF's porosity account for the increased flux through the composite. The enhanced $CO_2$ permeability can be partly attributed to the higher diffusivity of $CO_2$ through the MOF particles.[51] The separation factor remains unchanged for MOF loadings between 0 and 10 wt% and slightly decreases with further increase in loading, what could indicate that at such loadings voids are formed at the interface between polymer and MOF.

This differs from the constant selectivity reported for NH$_2$-MIL-53(Al)-based MMMs when PSF,[30] Matrimid®[32] and 6FDA-ODA[34, 36] are used as continuous matrix, but is similar to the published results when other 6FDA-based copolyimides are used instead.[35] Seoane *et al*. showed that depending on the flexibility of the polymers and their functional groups, the affinity between the dispersed and the continuous phase can be modified.[35] In this work, the use of the

relatively less flexible monomer DAM might account for defects formed at 15 wt% MOF loading.[52]

Moreover, the gas separation performance of the 20 wt% NP-NH$_2$-MIL-53(Al)@6FDA-DAM MMM was also determined for the separation of CO$_2$ from N$_2$ in a 15:85 mixture at 298 K and $\Delta p$ = 1 bar. Under these conditions both the CO$_2$/N$_2$ separation factor and the CO$_2$ permeability were slightly increased, from 25 and 715 Barrer for the neat polymer to 26.3 and 737 Barrer upon 20 wt% MOF loading. As we have previously shown, CO$_2$ adsorbs preferentially over CH$_4$ on NH$_2$-MIL-53(Al). This is due to the interaction between the amino and the hydroxyl groups within the NH$_2$-MIL-53(Al) framework, which stabilizes its narrow pore configuration, further hampering the diffusion of CH$_4$ through the MOF channels.[53]

Figures 3.11b and 3.11c show the performance of bare 6FDA-DAM and NP-NH$_2$-MIL-53(Al)@6FDA-DAM MMMs at different $\Delta p$. The permeability of the pure 6FDA-DAM and the MMMs decreased gradually with increasing $\Delta p$, what can be attributed to the saturation of Langmuir sites. Specifically, when the pressure is increased from 3 to 9 bar, the CO$_2$ permeability drops by 20 % for both the neat 6FDA-DAM membrane and the NP-NH$_2$-MIL-53(Al)@6FDA-DAM MMM with 20 wt% MOF loading, respectively. In contrast, the CH$_4$ permeability remained relatively constant, leading to a decrease in selectivity with pressure. Shahid et al.[48] reported that as the pressure is increased the permeability of CO$_2$ decreases more than that of CH$_4$ due to the saturation of the favorable Langmuir adsorption sites for CO$_2$. CH$_4$ being less affinitive to the neat polymer and MOF suffers relatively less change in its permeability. This behavior is similar as for zeolite membranes for mixtures of weakly and strongly adsorbing components.[54, 55]
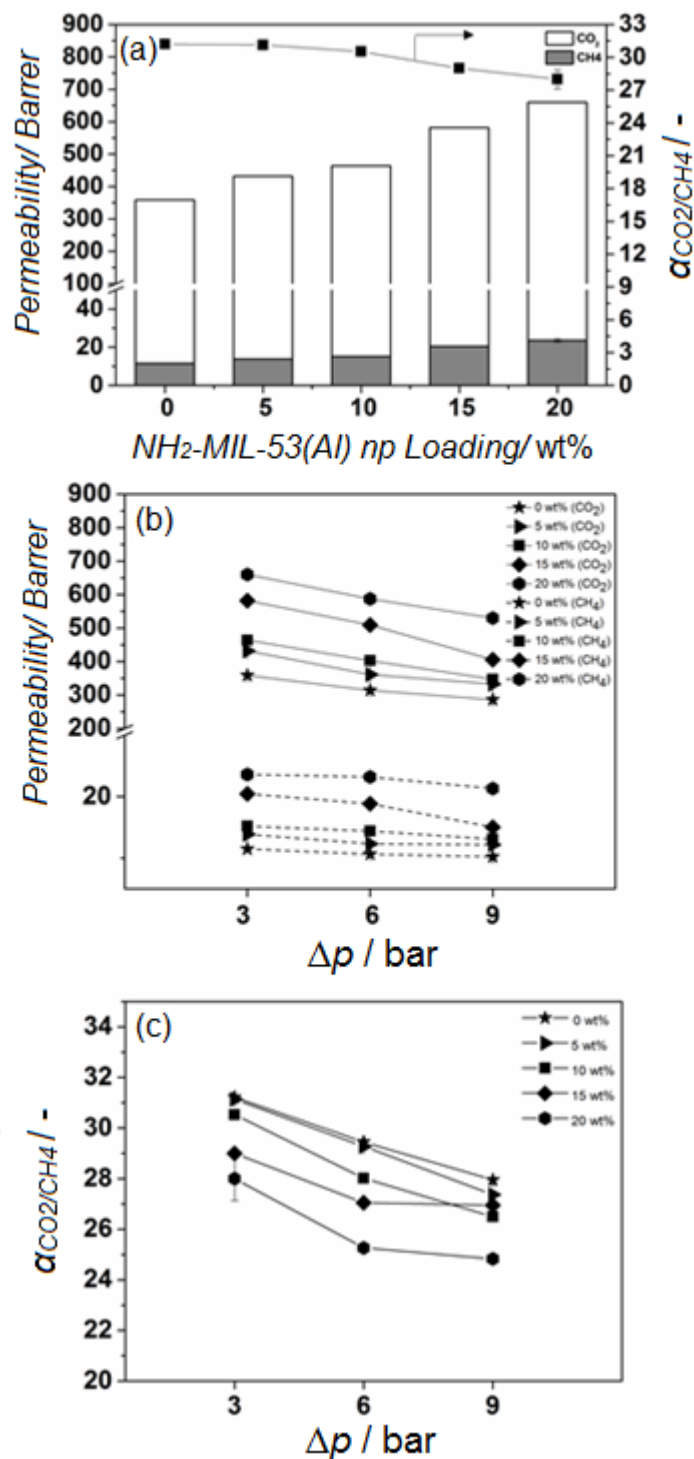
**Figure 3.11** a) $CO_2$ and $CH_4$ permeation properties measured for a 1:1 $CO_2/CH_4$ mixture at 298 K and $\Delta p$ = 3 bar of MMMs comprising 6FDA-DAM and $NH_2$-MIL-53(Al) MOF nanoparticles as a function of the filler loading, influence of the trans-membrane pressure difference ($\Delta p$ = 3, 6 and 9 bar), b) on the $CO_2$ permeability and c) on the selectivity of the $NH_2$-MIL-53(Al)@6FDA-DAM MMMs as a function of filler loading. The data are average values of at least two membranes and error bars correspond to standard deviation. ☆ bare 6FDA-DAM and ● 5 wt%, ▲ 10 wt%, ◊ 15 wt% and ■ 20 wt% $NH_2$-MIL-53(Al)@6FDA-DAM MMMs, respectively.
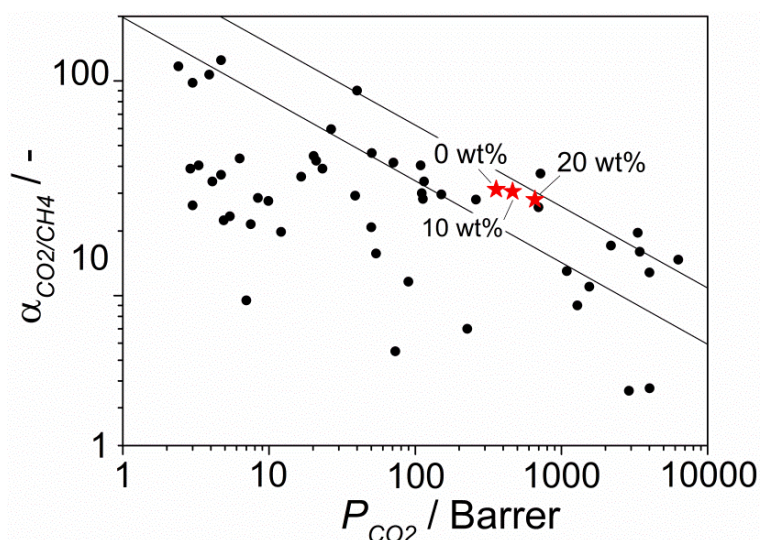
**Figure 3.12** Robeson plot for the separation of $CO_2$ from $CH_4$ showing the gas separation performance of pure 6FDA-DAM and of the MMMs prepared with 10 and 20 wt% of $NH_2$-MIL-53(Al) nanoparticles measured for a 1:1 $CO_2/CH_4$ mixture at 298 K and $\Delta p$ = 3 bar. Most relevant results reported in literature for MOF-based MMMs have also been included for comparison.

Putting the results obtained for the 6FDA-DAM MMMs containing $NH_2$-MIL-53(Al) nanoparticles in perspective using the customary Robeson plot (see Figure 3.12), the best results reported in this work surpass the Robeson limit of 1991 and are close to the revisited Robeson limit of 2008.[9] Note that the Robeson plot is constructed for ideal separation factors (based on unary permeation data) at room temperature and that for mixtures these usually deviate in positive or negative direction. In comparison with the most relevant results found in literature for $CO_2/CH_4$ separation by MOF-based MMMs,[38] our membranes place themselves among the best performing. This is attributed to the good match between the continuous and the dispersed phase, not only in terms in terms of permeability but also in terms of interaction at the interface. A proper choice of the MOF functional groups and particle morphology and aspect ratio is needed to attain better separation performance. These results highlight the importance of crystal engineering of MOFs in the field of mixed matrix membranes and the necessity of synthetic methods able to deliver a high degree of control over MOF formation at all relevant length-scales, from the framework topology and composition to crystal shape and size.

## 3.4 Conclusions

Mixed-matrix membranes (MMMs) comprising $NH_2$-MIL-53(Al) as filler and two different polymer matrices, the polyimides Matrimid® and 6FDA-DAM, have been investigated. For the Matrimid®-based MMMs, $NH_2$-MIL-53(Al) particles with three different crystal morphologies: nanoparticles, nanorods and microneedles were dispersed in the polymer matrix. The best results

were obtained for the $NH_2$-MIL-53(Al) nanoparticles, which led to an enhancement of the $CO_2$ permeability at constant selectivities in comparison with the bare Matrimid® membrane and the MMMs containing nanorods and microneedles. Our study reveals that the particle morphology has an impact on the permeation results. Moreover, by using the highly permeable polyimide 6FDA-DAM instead of Matrimid®, the permeability was increased up to 85 % upon $NH_2$-MIL-53(Al) nanoparticles addition, giving rise to membranes with a performance very close to the 2008 Robeson limit for $CO_2/CH_4$ separation.

A new non-destructive technique for the characterization (thickness and composition) of the MMMs based on Raman spectroscopy has been introduced. By modeling the polymer and MOF contributions to the Raman spectra of the composite membranes, the filler dispersion in the polymer matrix can be evaluated at different locations. The analysis confirmed the good distribution of the MOF filler in the 6FDA-DAM polymer, in agreement with FIB-SEM analysis.

# References

[1]     D. Andriani, A. Wresta, T.D. Atmaja, A. Saepudin, A Review on Optimization Production and Upgrading Biogas Through CO2 Removal Using Various Techniques, Applied Biochemistry and Biotechnology, 172 (2014) 1909-1928.

[2]     a) D. Jecha, J. Niesner, P. Stehlík, Biogas Upgrading Technologies: State of Art Review in Biogas Upgrading Technologies: State of Art Review in Biogas Biogas Upgrading Techniques: State of Art Review in European Region, 2013; b) J.D. Figueroa, T. Fout, S. Plasynski, H. McIlvried, R.D. Srivastava, Advances in $CO_2$ capture technology—The U.S. Department of Energy's Carbon Sequestration Program, International Journal of Greenhouse Gas Control, 2 (2008) 9-20.

[3]     F. Karadas, M. Atilhan, S. Aparicio, Review on the Use of Ionic Liquids (ILs) as Alternative Fluids for CO2 Capture and Natural Gas Sweetening, Energy & Fuels, 24 (2010) 5817-5828.

[4]     M. Tagliabue, D. Farrusseng, S. Valencia, S. Aguado, U. Ravon, C. Rizzo, A. Corma, C. Mirodatos, Natural gas treating by selective adsorption: Material science and chemical engineering interplay, Chemical Engineering Journal, 155 (2009) 553-566.

[5]     P. Bernardo, E. Drioli, G. Golemme, Membrane Gas Separation: A Review/State of the Art, Industrial & Engineering Chemistry Research, 48 (2009) 4638-4663.

[6]     X. He, M.-B. Hägg, Membranes for Environmentally Friendly Energy Processes, Membranes, 2 (2012) 706.

[7]     J. Gascon, F. Kapteijn, B. Zornoza, V. Sebastián, C. Casado, J. Coronas, Practical Approach to Zeolitic Membranes and Coatings: State of the Art, Opportunities, Barriers, and Future Perspectives, Chemistry of Materials, 24 (2012) 2829-2844.

[8]     L.M. Robeson, The upper bound revisited, Journal of Membrane Science, 320 (2008) 390-400.

[9]     L.M. Robeson, Correlation of separation factor versus permeability for polymeric membranes, Journal of Membrane Science, 62 (1991) 165-185.

[10]    T.-S. Chung, L.Y. Jiang, Y. Li, S. Kulprathipanja, Mixed matrix membranes (MMMs) comprising organic polymers with dispersed inorganic fillers for gas separation, Progress in Polymer Science, 32 (2007) 483-507.

[11]    G. Dong, H. Li, V. Chen, Challenges and opportunities for mixed-matrix membranes for gas separation, Journal of Materials Chemistry A, 1 (2013) 4610-4630.

[12]    P.S. Goh, A.F. Ismail, S.M. Sanip, B.C. Ng, M. Aziz, Recent advances of inorganic fillers in mixed matrix membrane for gas separation, Separation and Purification Technology, 81 (2011) 243-264.

[13]    a) S.R. Batten, N.R. Champness, X.-M. Chen, J. Garcia-Martinez, S. Kitagawa, L. Öhrström, M. O'Keeffe, M.P. Suh, J. Reedijk, Coordination polymers, metal–organic frameworks and the need for terminology guidelines, CrystEngComm, 14 (2012) 3001-3004; b) H. Li, M. Eddaoudi, M. O'Keeffe, O.M. Yaghi, Design and synthesis of an exceptionally stable and highly porous metal-organic framework, Nature, 402 (1999) 276.

[14]    O.K. Farha, I. Eryazici, N.C. Jeong, B.G. Hauser, C.E. Wilmer, A.A. Sarjeant, R.Q. Snurr, S.T. Nguyen, A.Ö. Yazaydın, J.T. Hupp, Metal–Organic Framework Materials with Ultrahigh Surface Areas: Is the Sky the Limit?, Journal of the American Chemical Society, 134 (2012) 15016-15021.

[15]    a) M. Eddaoudi, J. Kim, N. Rosi, D. Vodak, J. Wachter, M. O'Keeffe, O.M. Yaghi, Systematic Design of Pore Size and Functionality in Isoreticular MOFs and Their Application in Methane Storage, Science, 295 (2002) 469-472; b) Z. Wang, S.M. Cohen, Postsynthetic modification of metal–organic frameworks, Chemical Society Reviews, 38 (2009) 1315-1329.

[16]    a) G. Férey, C. Serre, Large breathing effects in three-dimensional porous hybrid matter: facts, analyses, rules and consequences, Chemical Society Reviews, 38 (2009) 1380-1399; b) B. Seoane, S. Sorribas, Á. Mayoral, C. Téllez, J. Coronas, Real-time monitoring of breathing of MIL-53(Al) by environmental SEM, Microporous and Mesoporous Materials, 203 (2015) 17-23.

[17]    a) J. Gascon, A. Corma, F. Kapteijn, F.X. Llabrés i Xamena, Metal Organic Framework Catalysis: Quo vadis?, ACS Catalysis, 4 (2014) 361-378; b) B. Liu, Metal–organic framework-based devices: separation and sensors, Journal of Materials Chemistry, 22 (2012) 10094-10101; c) L.E. Kreno, K. Leong, O.K. Farha, M. Allendorf, R.P. Van Duyne, J.T. Hupp, Metal–Organic Framework Materials as Chemical Sensors, Chemical Reviews, 112 (2012) 1105-1125.

[18]    M. Shah, M.C. McCarthy, S. Sachdeva, A.K. Lee, H.-K. Jeong, Current Status of Metal–Organic Framework Membranes for Gas Separations: Promises and Challenges, Industrial & Engineering Chemistry Research, 51 (2012) 2179-2199.

[19]    B. Zornoza, C. Tellez, J. Coronas, J. Gascon, F. Kapteijn, Metal organic framework based mixed matrix membranes: An increasingly important field of research with a large application potential, Microporous and Mesoporous Materials, 166 (2013) 67-78; b) H.B. Tanh Jeazet, C. Staudt, C. Janiak, Metal–organic frameworks in mixed-matrix membranes for gas separation, Dalton Transactions, 41 (2012) 14003-14027; c) I. Erucar, G. Yilmaz, S. Keskin, Recent Advances in Metal–Organic Framework-Based Mixed Matrix Membranes, Chemistry – An Asian Journal, 8 (2013) 1692-1704.

[20]    T.T. Moore, W.J. Koros, Non-ideal effects in organic–inorganic materials for gas separation membranes, Journal of Molecular Structure, 739 (2005) 87-98.

[21]    T. Rodenas, M.v. Dalen, E. García-Pérez, P. Serra-Crespo, B. Zornoza, F. Kapteijn, J. Gascon, Visualizing MOF Mixed Matrix Membranes at the Nanoscale: Towards Structure-Performance Relationships in $CO_2/CH_4$ Separation Over $NH_2$-MIL-53(Al)@PI, Advanced Functional Materials, 24 (2014) 249-256.

[22]    B. Tae-Hyun, L.J. Suk, Q. Wulin, K.W. J., J.C. W., N. Sankar, A High-Performance Gas-Separation Membrane Containing Submicrometer-Sized Metal–Organic Framework Crystals, Angewandte Chemie International Edition, 49 (2010) 9863-9866.

[23]    L. Ge, W. Zhou, V. Rudolph, Z. Zhu, Mixed matrix membranes incorporated with size-reduced Cu-BTC for improved gas separation, Journal of Materials Chemistry A, 1 (2013) 6350-6358.

[24]    N.A.H.M. Nordin, A.F. Ismail, A. Mustafa, R.S. Murali, T. Matsuura, The impact of ZIF-8 particle size and heat treatment on CO2/CH4 separation using asymmetric mixed matrix membrane, RSC Advances, 4 (2014) 52530-52541.

[25]    a) T. Yang, T.-S. Chung, High performance ZIF-8/PBI nano-composite membranes for high temperature hydrogen separation consisting of carbon monoxide and water vapor, International Journal of Hydrogen Energy, 38 (2013) 229-239;  b) L. Cao, K. Tao, A. Huang, C. Kong, L. Chen, A

highly permeable mixed matrix membrane containing CAU-1-NH$_2$ for H$_2$ and CO$_2$ separation, Chemical Communications, 49 (2013) 8513-8515;  c) S.N. Wijenayake, N.P. Panapitiya, S.H. Versteeg, C.N. Nguyen, S. Goel, K.J. Balkus, I.H. Musselman, J.P. Ferraris, Surface Cross-Linking of ZIF-8/Polyimide Mixed Matrix Membranes (MMMs) for Gas Separation, Industrial & Engineering Chemistry Research, 52 (2013) 6991-7001;  d) T. Yang, T.-S. Chung, Room-temperature synthesis of ZIF-90 nanocrystals and the derived nano-composite membranes for hydrogen separation, Journal of Materials Chemistry A, 1 (2013) 6081-6090.

[26]    a) A.F. Bushell, M. Attfield, C. Mason, P.M. Budd, Y. Yampolskii, L. Starannikova, A. Rebrov, F. Bazzarelli, P. Bernardo, J. Jansen, M. Lanč, K. Friess, V. Shantarovich, V. Gustov, V.I. Isaeva, Gas permeation parameters of mixed matrix membranes based on the polymer of intrinsic microporosity PIM-1 and the zeolitic imidazolate framework ZIF-8, 2013; b) J.O. Hsieh, K.J. Balkus, J.P. Ferraris, I.H. Musselman, MIL-53 frameworks in mixed-matrix membranes, Microporous and Mesoporous Materials, 196 (2014) 165-174.

[27]    a) T. Li, Y. Pan, K.-V. Peinemann, Z. Lai, Carbon dioxide selective mixed matrix composite membrane containing ZIF-7 nano-fillers, Journal of Membrane Science, 425-426 (2013) 235-242, b) V. Nafisi, M.-B. Hägg, Development of dual layer of ZIF-8/PEBAX-2533 mixed matrix membrane for CO2 capture, Journal of Membrane Science, 459 (2014) 244-255.

[28]    B. Seoane, V. Sebastián, C. Téllez, J. Coronas, Crystallization in THF: the possibility of one-pot synthesis of mixed matrix membranes containing MOF MIL-68(Al), CrystEngComm, 15 (2013) 9483-9490.

[29]    T. Rodenas, I. Luz, G. Prieto, B. Seoane, H. Miro, A. Corma, F. Kapteijn, F.X. Llabrés i Xamena, J. Gascon, Metal–organic framework nanosheets in polymer composite materials for gas separation, Nature Materials, 14 (2014) 48.

[30]    B. Zornoza, A. Martinez-Joaristi, P. Serra-Crespo, C. Tellez, J. Coronas, J. Gascon, F. Kapteijn, Functionalized flexible MOFs as fillers in mixed matrix membranes for highly selective separation of CO2 from CH4 at elevated pressures, Chemical Communications, 47 (2011) 9522-9524.

[31]    M. Valero, B. Zornoza, C. Téllez, J. Coronas, Mixed matrix membranes for gas separation by combination of silica MCM-41 and MOF NH$_2$-MIL-53(Al) in glassy polymers, Microporous and Mesoporous Materials, 192 (2014) 23-28.

[32]    T. Rodenas, M. van Dalen, P. Serra-Crespo, F. Kapteijn, J. Gascon, Mixed matrix membranes based on NH2-functionalized MIL-type MOFs: Influence of structural and operational parameters on the CO2/CH4 separation performance, Microporous and Mesoporous Materials, 192 (2014) 35-42.

[33]    P. Burmann, B. Zornoza, C. Téllez, J. Coronas, Mixed matrix membranes comprising MOFs and porous silicate fillers prepared via spin coating for gas separation, Chemical Engineering Science, 107 (2014) 66-75.

[34]    X.Y. Chen, V.-T. Hoang, D. Rodrigue, S. Kaliaguine, Optimization of continuous phase in amino-functionalized metal-organic framework (MIL-53) based co-polyimide mixed matrix membranes for CO2/CH4 separation, RSC Advances, 3 (2013) 24266-24279.

[35]    B. Seoane, C. Téllez, J. Coronas, C. Staudt, NH2-MIL-53(Al) and NH2-MIL-101(Al) in sulfur-containing copolyimide mixed matrix membranes for gas separation, Separation and Purification Technology, 111 (2013) 72-81.

[36]    X.Y. Chen, H. Vinh-Thang, D. Rodrigue, S. Kaliaguine, Amine-Functionalized MIL-53 Metal–Organic Framework in Polyimide Mixed Matrix Membranes for $CO_2/CH_4$ Separation, Industrial & Engineering Chemistry Research, 51 (2012) 6895-6906.

[37]    R. Abedini, M. Omidkhah, F. Dorosti, Highly permeable poly(4-methyl-1-pentyne)/$NH_2$-MIL 53 (Al) mixed matrix membrane for CO2/CH4 separation, RSC Advances, 4 (2014) 36522-36537.

[38]    B. Seoane, J. Coronas, I. Gascon, M.E. Benavides, O. Karvan, J. Caro, F. Kapteijn, J. Gascon, Metal-organic framework based mixed matrix membranes: a solution for highly efficient CO2 capture?, Chemical Society Reviews, 44 (2015) 2421-2454.

[39]    J.M. Chin, E.Y. Chen, A.G. Menon, H.Y. Tan, A.T.S. Hor, M.K. Schreyer, J. Xu, Tuning the aspect ratio of $NH_2$-MIL-53(Al) microneedles and nanorods via coordination modulation, CrystEngComm, 15 (2013) 654-657.

[40]    T. Ahnfeldt, D. Gunzelmann, T. Loiseau, D. Hirsemann, J. Senker, G. Férey, N. Stock, Synthesis and Modification of a Functionalized 3D Open-Framework Structure with MIL-53 Topology, Inorganic Chemistry, 48 (2009) 3057-3064.

[41]    S. Couck, E. Gobechiya, C.E.A. Kirschhock, P. Serra-Crespo, J. Juan-Alcañiz, A. Martinez Joaristi, E. Stavitski, J. Gascon, F. Kapteijn, G.V. Baron, J.F.M. Denayer, Adsorption and Separation of Light Gases on an Amino-Functionalized Metal–Organic Framework: An Adsorption and In Situ XRD Study, ChemSusChem, 5 (2012) 740-750.

[42]    Y. Sakata, S. Furukawa, M. Kondo, K. Hirai, N. Horike, Y. Takashima, H. Uehara, N. Louvain, M. Meilikhov, T. Tsuruoka, S. Isoda, W. Kosaka, O. Sakata, S. Kitagawa, Shape-Memory Nanopores Induced in Coordination Frameworks by Crystal Downsizing, Science, 339 (2013) 193-196.

[43]    P. Serra-Crespo, E. Gobechiya, E.V. Ramos-Fernandez, J. Juan-Alcañiz, A. Martinez-Joaristi, E. Stavitski, C.E.A. Kirschhock, J.A. Martens, F. Kapteijn, J. Gascon, Interplay of Metal Node and Amine Functionality in NH2-MIL-53: Modulating Breathing Behavior through Intra-framework Interactions, Langmuir, 28 (2012) 12916-12922.

[44]    Z. Feng, Z. Xiaoqin, G. Xue, F. Songjie, S. Fuxing, R. Hao, Z. Guangshan, Hydrogen Selective NH2-MIL-53(Al) MOF Membranes with High Permeability, Advanced Functional Materials, 22 (2012) 3583-3590.

[45]    H. Ren, J. Jin, J. Hu, H. Liu, Affinity between Metal–Organic Frameworks and Polyimides in Asymmetric Mixed Matrix Membranes for Gas Separations, Industrial & Engineering Chemistry Research, 51 (2012) 10156-10164.

[46]    A. Bos, I.G.M. Pünt, M. Wessling, H. Strathmann, $CO_2$-induced plasticization phenomena in glassy polymers, Journal of Membrane Science, 155 (1999) 67-78.

[47]    a) P.D. R., Gas Sorption and Transport in Glassy Polymers, Berichte der Bunsengesellschaft für physikalische Chemie, 83 (1979) 294-302; b) V. Stannett, The transport of gases in synthetic polymeric membranes — an historic perspective, Journal of Membrane Science, 3 (1978) 97-115.

[48]    S. Shahid, K. Nijmeijer, Performance and plasticization behavior of polymer–MOF membranes for gas separation at elevated pressures, Journal of Membrane Science, 470 (2014) 166-177.

[49]    S. Shahid, K. Nijmeijer, High pressure gas separation performance of mixed-matrix polymer membranes containing mesoporous Fe(BTC), Journal of Membrane Science, 459 (2014) 33-44.

[50]    J.H. Kim, W.J. Koros, D.R. Paul, Physical aging of thin 6FDA-based polyimide membranes containing carboxyl acid groups. Part I. Transport properties, Polymer, 47 (2006) 3094-3103.

[51]    E. Stavitski, E.A. Pidko, S. Couck, T. Remy, E.J.M. Hensen, B.M. Weckhuysen, J. Denayer, J. Gascon, F. Kapteijn, Complexity behind $CO_2$ Capture on NH2-MIL-53(Al), Langmuir, 27 (2011) 3970-3976.

[52]    S. Couck, J.F.M. Denayer, G.V. Baron, T. Rémy, J. Gascon, F. Kapteijn, An Amine-Functionalized MIL-53 Metal−Organic Framework with Large Separation Power for $CO_2$ and $CH_4$, Journal of the American Chemical Society, 131 (2009) 6326-6327.

[53]    S. Velioğlu, M.G. Ahunbay, S.B. Tantekin-Ersolmaz, Investigation of $CO_2$-induced plasticization in fluorinated polyimide membranes via molecular simulation, Journal of Membrane Science, 417-418 (2012) 217-227.

[54]    W. Zhu, P. Hrabanek, L. Gora, F. Kapteijn, J.A. Moulijn, Role of Adsorption in the Permeation of CH4 and CO2 through a Silicalite-1 Membrane, Industrial & Engineering Chemistry Research, 45 (2006) 767-776.

[55]    H. Voß, A. Diefenbacher, G. Schuch, H. Richter, I. Voigt, M. Noack, J. Caro, Butene isomers separation on titania supported MFI membranes at conditions relevant for practice, Journal of Membrane Science, 329 (2009) 11-17.

# 3

# Annex

## Application of Engineered MOF Crystals to Mixed-Matrix Membranes: Impact of the Filler Morphology on the Gas Separation Performance

**Table 3.4** Summary of the $CO_2/CH_4$ (1:1 mixture) separation performance at 298 K obtained for $NH_2$-MIL-53(Al)@Matrimid® and $NH_2$-MIL-53(Al)@6FDA-DAM MMMs with different filler loadings under several operation pressure conditions.

| Matrimid® | | | | | |
|---|---|---|---|---|---|
| **MOF loading** | 0 wt.% | | | | |
| **Thickness**[a] | 53 ± 1 µm | | | | |
| **Δp [bar]** | 3 | 4.5 | 6 | 7.5 | 9 |
| $P_{CO2}$ **[Barrer]** [b] | 8.01 ± 0.05 | 7.13 ± 0.00 | 6.90 ± 0.00 | 5.41 ± 0.01 | 4.81 ± 0.06 |
| $P_{CH4}$ **[Barrer ]**[b] | 0.20 ± 0.01 | 0.18 ± 0.00 | 0.18 ± 0.00 | 0.14 ± 0.00 | 0.14 ± 0.00 |
| **Selectivity [-]** | 37.3 ± 1.9 | 38.9 ± 0.3 | 37.7 ± 0.9 | 37.6 ± 0.2 | 35.4 ± 0.6 |

| $NH_2$-MIL-53(Al) Nanoparticles @ Matrimid® | | | | | | |
|---|---|---|---|---|---|---|
| **MOF loading** | 8 wt.% | | | | | |
| **Thickness**[a] | 50 ± 1 µm | | | | | |
| **Δp [bar]** | 3 | 4.5 | 6 | 7.5 | 9 | 3 |
| $P_{CO2}$ **[Barrer]** [b] | 9.03 ± 0.10 | 8.40 ± 0.09 | 7.97 ± 0.03 | 7.22 ± 0.04 | 7.28 ± 0.04 | 9.35 ± 0.09 |
| $P_{CH4}$ **[Barrer ]**[b] | 0.25 ± 0.01 | 0.22 ± 0.00 | 0.21 ± 0.00 | 0.19 ± 0.00 | 0.19 ± 0.00 | 0.27 ± 0.00 |
| **Selectivity [-]** | 36.5 ± 0.3 | 38.1 ± 0.4 | 38.5 ± 0.3 | 39.0 ± 0.4 | 37.8 ± 0.2 | 34.7 ± 0.4 |

| $NH_2$-MIL-53(Al) Nanoparticles @ Matrimid® | | | | | | |
|---|---|---|---|---|---|---|
| **MOF loading** | 16 wt.% | | | | | |
| **Thickness**[a] | 58 ± 1 µm | | | | | |
| **Δp [bar]** | 3 | 4.5 | 6 | 7.5 | 9 | 3 |
| $P_{CO2}$ **[Barrer]** [b] | 7.39 ± 0.04 | 7.17 ± 0.03 | 6.71 ± 0.05 | 6.87 ± 0.01 | 6.68 ± 0.03 | 8.28 ±0.03 |
| $P_{CH4}$ **[Barrer ]**[b] | 0.18 ± 0.00 | 0.19 ± 0.00 | 0.19 ± 0.00 | 0.19 ± 0.00 | 0.19 ± 0.00 | 0.26 ± 0.00 |
| **Selectivity [-]** | 41.8 ± 0.4 | 37.6 ± 0.3 | 36.3 ± 0.3 | 35.8 ± 0.3 | 35.4 ± 0.5 | 31.6 ± 0.5 |

| $NH_2$-MIL-53(Al) Nanorods @ Matrimid® | | | | | | |
|---|---|---|---|---|---|---|
| **MOF loading** | 8 wt.% | | | | | |
| **Thickness**[a] | 52 ± 1 µm | | | | | |
| **Δp [bar]** | 3 | 4.5 | 6 | 7.5 | 9 | 3 |
| $P_{CO2}$ **[Barrer]** [b] | 7.52 ± 0.03 | 6.73 ± 0.06 | 6.2 ± 0.02 | 5.65 ± 0.01 | 4.72 ± 0.1 | 8.5 ± 0.1 |
| $P_{CH4}$ **[Barrer ]**[b] | 0.2 ± 0.00 | 0.18 ± 0.00 | 0.16 ± 0.00 | 0.14 ± 0.00 | 0.11 ± 0.00 | 0.23 ± 0.00 |
| **Selectivity [-]** | 37.5 ± 0.4 | 37.9 ± 0.3 | 39.1 ± 0.6 | 40.3 ± 0.5 | 41.5 ± 1.4 | 37.5 ± 1.4 |

| $NH_2$-MIL-53(Al) Nanorods @ Matrimid® | | | | | | |
|---|---|---|---|---|---|---|
| **MOF loading** | 16 wt.% | | | | | |
| **Thickness**[a] | 60 ± 1 µm | | | | | |
| **Δp [bar]** | 3 | 4.5 | 6 | 7.5 | 9 | 3 |
| $P_{CO2}$ **[Barrer]** [b] | 7.18 ± 0.06 | 6.06 ± 0.03 | 5.56 ± 0.02 | 5.78 ± 0.04 | 5.48 ± 0.01 | 6.76 ± 0.05 |
| $P_{CH4}$ **[Barrer ]**[b] | 0.2 ± 0.00 | 0.17 ± 0.00 | 0.14 ± 0.00 | 0.15 ± 0.00 | 0.15 ± 0.00 | 0.19 ± 0.00 |
| **Selectivity [-]** | 36.3 ± 0.2 | 35.4 ± 0.2 | 39.2 ± 0.3 | 38.7 ± 0.2 | 36.4 ± 0.3 | 35.2 ± 0.1 |

| $NH_2$-MIL-53(Al) Microneedle @ Matrimid® | | | | | | |
|---|---|---|---|---|---|---|
| **MOF loading** | 8 wt.% | | | | | |
| **Thickness**[a] | 40 ± 1 µm | | | | | |
| **Δp [bar]** | 3 | 4.5 | 6 | 7.5 | 9 | 3 |
| $P_{CO2}$ **[Barrer]** [b] | 7.52 ± 0.06 | 7.02 ± 0.03 | 6.6 ± 0.03 | 6.48 ± 0.05 | 6.65 ± 0.04 | 8.14 ± 0.04 |
| $P_{CH4}$ **[Barrer ]**[b] | 0.21 ± 0.00 | 0.19 ± 0.00 | 0.18 ± 0.00 | 0.17 ± 0.00 | 0.18 ± 0.00 | 0.24 ± 0.00 |
| **Selectivity [-]** | 36.5 ± 0.4 | 37.8 ± 0.3 | 37.5 ± 0.3 | 37.7 ± 0.2 | 36.7 ± 0.2 | 33.3 ± 0.2 |

| $NH_2$-MIL-53(Al) Microneedle @ Matrimid® | | | | | | |
|---|---|---|---|---|---|---|
| **MOF loading** | 16 wt.% | | | | | |
| **Thickness**[a] | 57 ± 1 µm | | | | | |
| **Δp [bar]** | 3 | 4.5 | 6 | 7.5 | 9 | 3 |
| $P_{CO2}$ **[Barrer]** [b] | 5.77 ± 0.04 | 5.83 ± 0.05 | 5.56 ± 0.04 | 5.73 ± 0.02 | 6.12 ±0.02 | 6.68 ± 0.04 |
| $P_{CH4}$ **[Barrer ]**[b] | 0.15 ± 0.00 | 0.16 ± 0.00 | 0.15 ± 0.00 | 0.16 ± 0.00 | 0.17 ± 0.00 | 0.2 ± 0.00 |
| **Selectivity [-]** | 38.3 ± 0.3 | 37.6 ± 0.2 | 37.5 ± 0.4 | 36.7 ± 0.2 | 36.7 ± 0.2 | 33.3 ± 0.2 |

| 6FDA-DAM | | | |
|---|---|---|---|
| **MOF loading** | **0 wt.%** | | |
| **Thickness**[a] | **35 ± 1 µm** | | |
| **$\Delta$p [bar]** | **3** | **6** | **9** |
| **$P_{CO2}$ [Barrer]** [b] | 358.45 ± 0.08 | 313.42 ± 0.72 | 285.81 ± 0.21 |
| **$P_{CH4}$ [Barrer ]**[b] | 11.48 ± 0.00 | 10.64 ± 0.01 | 10.22 ± 0.01 |
| **Selectivity [-]** | 31.22 ± 0.03 | 29.45 ± 0.05 | 27.95 ± 0.01 |

| 6FDA-DAM | | | |
|---|---|---|---|
| **MOF loading** | **5 wt.%** | | |
| **Thickness**[a] | **38 ± 1 µm** | | |
| **$\Delta$p [bar]** | **3** | **6** | **9** |
| **$P_{CO2}$ [Barrer]** [b] | 431.58 ± 0.80 | 360.74 ± 0.88 | 332.63 ± 1.58 |
| **$P_{CH4}$ [Barrer ]**[b] | 13.87 ± 0.23 | 12.32 ± 0.01 | 12.16 ± 0.11 |
| **Selectivity [-]** | 31.14 ± 0.04 | 29.28 ± 0.05 | 27.37 ± 0.38 |

| 6FDA-DAM | | | |
|---|---|---|---|
| **MOF loading** | **10 wt.%** | | |
| **Thickness**[a] | **48 ± 1 µm** | | |
| **$\Delta$p [bar]** | **3** | **6** | **9** |
| **$P_{CO2}$ [Barrer]** [b] | 463.56 ± 0.43 | 402.72 ± 0.49 | 346.84 ± 0.98 |
| **$P_{CH4}$ [Barrer ]**[b] | 15.19 ± 0.00 | 14.39 ± 0.02 | 13.09 ± 0.01 |
| **Selectivity [-]** | 30.53 ± 0.07 | 28.02 ± 0.00 | 26.50 ± 0.07 |

| 6FDA-DAM | | | |
|---|---|---|---|
| **MOF loading** | **15 wt.%** | | |
| **Thickness**[a] | **44 ± 1 µm** | | |
| **$\Delta$p [bar]** | **3** | **6** | **9** |
| **$P_{CO2}$ [Barrer]** [b] | 581.78 ± 0.31 | 509.11 ± 1.28 | 405.25 ± 0.64 |
| **$P_{CH4}$ [Barrer ]**[b] | 20.46 ± 0.02 | 18.84 ± 0.00 | 15.03 ± 0.03 |
| **Selectivity [-]** | 29.00 ± 0.03 | 27.05 ± 0.00 | 26.94 ± 0.03 |

| 6FDA-DAM | | | |
|---|---|---|---|
| **MOF loading** | **20 wt.%** | | |
| **Thickness**[a] | **62 ± 1 µm** | | |
| **$\Delta$p [bar]** | **3** | **6** | **9** |
| **$P_{CO2}$ [Barrer]** [b] | 659.73 ± 0.87 | 586.80 ± 0.60 | 529.60 ± 1.68 |
| **$P_{CH4}$ [Barrer ]**[b] | 23.62 ± 0.87 | 23.23 ± 0.02 | 21.34 ± 0.06 |
| **Selectivity [-]** | 28.0 ± 0.87 | 25.26 ± 0.02 | 24.83 ± 0.03 |

[a] Thickness value corresponds to the average of 10 different measurements at different locations within each membrane after casting and activation and error corresponds to standard deviation;

[b] The permeability data are average values of at least two membranes and error corresponds to standard deviation.

# Towards High Performance MOF–Microporous Polymer Mixed Matrix Membranes: Addressing Compatibility and Limiting Aging Issues via Polymer Doping

*Abstract:* *Membrane separation for gas purification is an energy-efficient and environment-friendly technology. However, the development of high performance membranes is still a great challenge. In principle, mixed matrix membranes (MMMs) have the potential to overcome current materials limitations, but in practice there is no straightforward method to match the properties of fillers and polymers (the main components of MMMs) in such a way that the final membrane performance reflects the high performance of the microporous filler and the processability of the continuous polymer phase. This issue is especially important when high flux polymers are utilized. In this work, we demonstrate that the use of small amounts of a glassy polymer in combination with high performance PIM-1 allow for the preparation of MOF based MMMs with superior separation properties and low aging rates under humid conditions, meeting the commercial target for post-combustion $CO_2$ capture.*
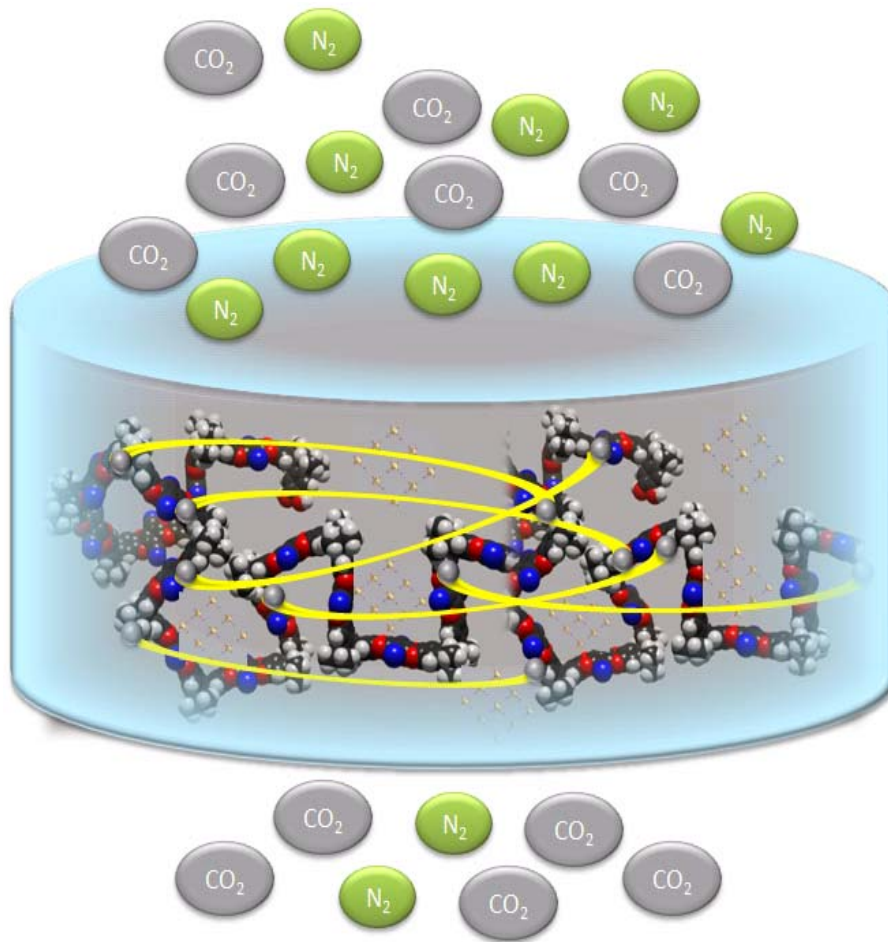
## 4.1 Introduction

Membrane technologies for gas separation are attractive due to their relatively low energy penalty and benign environmental aspects.[1] Currently, polymeric materials dominate the market for membrane gas separation thanks to ease of processing and mechanical strength.[1b] However, the performance of polymeric membranes is limited by the fact that improvements in permeability are always at the expense of selectivity, and *vice versa*.[2] This trade-off, defined by Robeson's upper bounds, still hampers the widespread application of membrane units.[2]

Recently, polymers of intrinsic microporosity (PIMs), [3] a subfamily of microporous polymers, have been identified as attractive candidates for high performance gas separation membranes. A prototypical example is PIM-1.[3d] The rigid and contorted ladder-like structure of PIM-1 leads to inefficient packing of polymer chains and to a high fractional free volume, providing highly permeable pathways for gas molecules but moderate selectivity and very fast physical aging.[3b] Various strategies including crosslinking,[4] post-modification[5] and polymer blending[6] have been employed to improve the membrane performance. Polymer blending has been recognized as a cost- and time-effective route,[7] which combines the advantages of different polymers.

Besides the above strategies, mixed matrix membranes (MMMs) are proposed to have even more potential, provided that properties from embedded fillers and the economical processing features of polymers can be properly matched.[8] [9] In the last few years, the effect of boosting gas adsorption[10] and diffusion,[10-11] incorporation of additional  polymer chains [12] and altering the matrix structure[13] have been explored by using metal-organic frameworks (MOFs),[10, 11b, 13] porous organic cages (POCs)[11a] and porous aromatic frameworks (PAFs)[12] as fillers. Nevertheless, simultaneous improvement of permeation and selectivity is challenging and there is not a large amount of data reported in literature showing this improvement. Table S1 shows data collected by Vinoba *et al*.[14] on membranes that have so far demonstrated an increase in both permeability and selectivity for $CO_2/N_2$ separation. Moreover, in most cases low permeation polymers are used. When it comes to microporous polymers, the main challenge to overcome in the field of MMMs is mostly the poor interfacial compatibility between the two phases.[15] As a result, performance improvements are marginal and membrane aging rates have been hardly reduced.

In this study, we demonstrate that the combination of doping glassy Matrimid® polymeric chains along with the addition of MOF fillers (*e.g.* $NH_2$-MIL-53(Al)) in PIM-1 (Scheme 1) results in both a substantial enhancement of $CO_2$ permeability and $CO_2/N_2$ selectivity under dry and humid conditions while greatly reducing aging. The obtained MMM performance transcends the 2008 Robeson upper bound limit and reaches the economic target region for post-combustion $CO_2$ capture,[16] even after 17 months of aging.
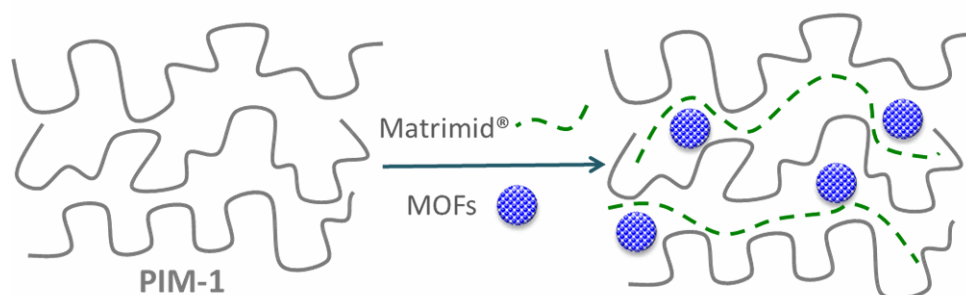
**Figure 4.1.** Scheme of doping Matrimid[®] and implanting MOFs into PIM-1 matrix.

**Table 4.1.** Improvement in $CO_2/N_2$ separation performance of reported MOF-based mixed matrix membranes relative to the neat membrane and comparison with this study.

| MOF | POLYMER | Filler (wt.%) | $P$ (bar) | $T$ (°C) | PF ($PCO_2$)[a] | SF ($\alpha CO_2/N_2$)[b] | Ref |
|---|---|---|---|---|---|---|---|
| UiO-66 | PEBAX | 2-20 | 3 | 25 | 1.95 | 1.41 | [45] |
| $NH_2$-UiO-66 | PIM-1 | 9.1 | 1 | 25 | 1.33 | 1.2 | [46] |
| $NH_2$-UiO-66 | Matrimid | 23 | 1 | RT | 3 | 1.32 | [47] |
| ZIF-7 | PEBAX | 34 | 3.75 | 25 | 1.54 | 2.85 | [48] |
| ZIF-8 | PVC-g-POEM | 30 | _ | 35 | 9.8 | 1.14 | [49] |
| ZIF-8 | [bmim][Tf2N] | 6 | 20 | 25 | 2.51 | 3.43 | [50] |
| Co-ZIF-108 | Psf | 0.037 | 1 | 25 | 17 | 1.57 | [51] |
| MIL-101(Cr) | SPEEK | 40 | 1 | 25 | 2.84 | 4 | [52] |
| Cu(BTC)2 | Matrimid | 30 | 10 | 35 | 1.65 | 1.27 | [53] |
| SIFSIX-3-Zn | XLPEO | 10 | 1 | 25 | 1.32 | 1.9 | [54] |
| HKUST-1 | 6FDA-Durene | 10 | 2 | 25 | 1.41 | 1.17 | [55] |
| $NH_2$-MIL-53(Al) | PIM/Matrimid | 25 | 2 | 25 | 1.1 | 1.47 | This work |

[a] PF is the permeability factor and is defined as MMM Permeability to the neat membrane permeability ratio.
[b] SF is the selectivity factor and is defined as MMM selectivity to the neat membrane selectivity ratio.

## 4.2 Experimental Section

Synthesis of $NH_2$-MIL-53(Al): Following to the protocol reported earlier,[29] 1.5 g 2-aminoterepththalic acid (8.28 mmol, Sigma Aldrich, 99 %) and 1.97 g $AlCl_3·6H_2O$ (8.43 mmol, Sigma Aldrich, ≥ 99.0 %) were dissolved in a mixture containing 18 mL deionized water and 2 mL N,N-dimethylformamide (DMF, Sigma Aldrich, >99.9%). The solution was transferred to a Teflon-lined autoclave and heated at 423 K for 5 h. The resulting yellow solution were filtered under vacuum to recover the powder and washed with acetone 3 times. Subsequently, the powders were thoroughly activated in DMF at 423 K and methanol at 443 K for 15 h. The activated powders were washed with acetone and dried at 393 K.

Synthesis of ZIF-94(Zn): A solution of 0.4392 g $Zn(CH_3COO)_2·2H_2O$ (2 mmol, Sigma Aldrich) in 20 ml methanol and one of 0.4404 g 4-methyl-5-imidazolecarboxaldehyde (aImeIm, 4 mmol, Maybridge) in 50 ml THF (Fisher Chemical) were prepared. After the reactant was completely dissolved in both mixtures, the first solution was poured slowly into the second solution. The final mixture was continuously stirred for 60 min at room temperature and the powder was collected by centrifugation and washed with methanol three times. The obtained product was dried at room temperature.

Synthesis of PIM-1: In a two-necked round bottom flask the exact stoichiometric amounts of bis-catechol (3.4 g, Sigma Aldrich) and 2,3,5,6-tetrafluoroterephthalonitrile (2 g, Sigma Aldrich) were added under dry nitrogen atmosphere, then dry dimethylformamide (DMF, 20 ml per gram of bis-catechol) was added to mix with the reactants. The mixture was heated at 65 °C, until the two starting materials were completely dissolved, then dry potassium carbonate (11.05 g, Sigma Aldrich) was added and the mixture was kept under stirring for 96 h. The solution was quenched with water (150 ml per gram of catechol) and the resulting precipitate were collected by filtration and washed repeatedly with water and acetone. The solid was dissolved in $CHCl_3$ or THF (15 ml per gram of solid), filtered through cotton wool and poured into a flask containing a mixture of acetone/methanol (2/1, vol./vol.), 40 ml per gram of polymer). The collected yellow solid was dried under vacuum overnight. Typically, the precipitation procedure is repeated twice. The molecular weight and polydispersity of synthesized PIM-1 is 300 kg/mol and 110 kg/mol, respectively.

MOF/PIMAT membrane preparation: to prepare the mixture of polymers, 0.10 g PIM-1 was dissolved in 4.0 ml chloroform (Sigma Aldrich, anhydrous ≥ 99.99 %) and then 0.010 g Matrimid® (Huntsman Advanced Materials, $M_W$: 80,000) was added and stirred for 2 h. Meanwhile, a certain amount of MOF $NH_2$-MIL-53(Al) or ZIF-94(Zn) (degassed at 373 K, 0.037 g) was dispersed in 1.5 ml of chloroform, followed by ultrasonication and stirring for 90 min. To attain a better MOF dispersion, firstly a 10 % of the dissolved polymers solution was added to the MOF solution After

After stirring, the remaining amount of polymer solution was added and stirred overnight. The homogeneous MOF/PIMAT solution was casted on a glass plate by Doctor Blade technique with a gap of 80 µm and covered with a top-drilled box and dried overnight under chloroform-saturated atmosphere. Finally, the dried membranes were peeled off and heat-treated under vacuum at 393 K for 24 h. The MOF content in both fabricated PIMAT membranes was kept at 25 wt.% ($W_{MOF}/(W_{MOF}+W_{PIMAT})$) for consistency. As reference, neat PIM-1, PIMAT ($W_{Mat}/(W_{Mat}+W_{PIM})$ = 9.1 wt.%), MOF/PIM-1 ($W_{MOF}/(W_{MOF}+W_{PIM})$ = 25 wt.%) membranes were prepared with the same approach. The thickness of all membranes was around 30-40 µm, measured by a digital micrometer (Mitutoyo, Japan, 1 µm) at different locations of each membrane.

## 4.3 Characterization

TEM analysis was carried out in JEOL JEM-2010 microscope operated at 200 keV. An X-ray OXFORD detector, INCA energy TEM 100 model for microanalysis (EDS) and a bottom-mounted GATAN ORIUS SC600 imaging camera are installed on the machine. Micrograph acquisition was performed with GATAN Digital Micrograph 1.80.70 software. To prepare the samples for imaging, a few drops of MOF dispersed in ethanol was applied on a carbon-coated copper grid and then it was placed on specimen. To calculate the average particle size using TEM images, around 50 particles were selected and measured by Image J software.

Focused Ion Beam-Scanning Electron Microscopy (FIB-SEM) was performed in the Dual Beam Strata 235 microscope (FEI) and an AURIGA Compact (Zeiss) microscope. A protective thin layer of Pt (0.3 µm thickness) was deposited on the surface of specimen using the gas injection system. The Ga ion beam (30 kV and 5000 pA), was used to mill surface with depth of ca. 3 µm. SEM micrographs of the milled cross-sections were recorded with a Secondary Electron Detector in the SEM operated at 5 kV. To get the cross section images of the membranes, some samples were immersed and fractured in liquid nitrogen and gold-coated prior to scanning and placed on the sample holder.

Atomic force microscopy (AFM) was performed with a Veeco Multimode Nanoscope 3A microscope operating in tapping mode. Prior to recording the membrane samples were placed onto a mica wafer substrate.

XRD patterns of MOF and the mixed matrix membranes were obtained in a Bruker-D8 Advance diffractometer using Co-$K\alpha$ radiation ($\lambda$ = 1.78897Å, 40 kV, 30 mA). The $2\theta$ range (5-60°) was scanned using a step size of 0.02° and a scan speed of 0.2 s per step in a continuous scanning mode.

$CO_2$ and $N_2$ adsorption isotherms of MOFs and membranes were recorded in a Tristar II 3020 (Micromeritics) setup at 273 K and 77 K, respectively. Prior to the measurements, the samples were degassed at 423 K under vacuum overnight.

Mechanical stability of the membrane samples were tested on a TA-Instruments DMA Q800 micro tensile tester. Samples of about 35x8x0.035 mm were tested in the tensile clamp setup with a constant speed of 100 µm/min. The recorded stresses and strains were used to calculate Young modulus, yield strength, tensile strength and ductility. The Young modulus was evaluated as the slope between 0.5 and 1% strain. Yield strength is defined as strength at which the sample start to deform plastically while tensile strength and ductility are the strength and strain at the point that sample was fractured.

ATR-IR spectra of the MOFs powder and membrane samples were acquired by NICOLET IS50-FT-IR (smart-Itx). The samples were placed on TR ID7/ITX AR coated diamond crystal (Product code: 869-168800). The resolution of the machine was 0.5 cm$^{-1}$ in the range of 4000-400cm$^{-1}$.

Gas permeation experiments and the separation of $CO_2$ and $N_2$ mixtures at 298 K was conducted in a home-made setup described elsewhere [29]. The membrane samples (area: 3.14 cm$^2$) were cut from the casted films and mounted in a flange between two Viton® O-rings. A macroporous stainless steel disc (316L, 20 µm nominal pore size) was used as support. To control the temperature, the permeation module was placed inside an oven. A flow mixture (133 ml·min$^{-1}$, STP) of $CO_2$ (15 mol.%) and $N_2$ (85 mol.%) was applied as feed and helium (5 ml·min$^{-1}$, STP) as a sweep gas. The feed pressure was adjusted to 2 bar (absolute pressure) using a back-pressure controller at the retentate side while the permeate side was kept at atmospheric pressure (1 bar absolute pressure) for all measurements. To reach the steady state, all the permeation results of the membranes were recorded after stabilization overnight. An online gas chromatograph (Interscience Compact GC) equipped with a packed Carboxen® 1010 PLOT (30 m x 0.32 mm) column and TCD detector was used to analyse the permeate stream.

Gas separation performance was defined by two terms: the separation factor ($\alpha$, or selectivity) and the gas permeability ($P$). The permeability for the component $i$ ($P_i$) was calculated as follows (Equation 1):

$$P_i = \frac{F_i \cdot \delta}{\Delta p_i \cdot A} \qquad\qquad (1)$$

where $F_i$ denotes the molar flow rate of compound $i$, $\delta$ is the thickness of the membrane, $\Delta p_i$ is the partial pressure difference of $i$ across the membrane, and $A$ is the membrane area. Although the SI unit for the permeability is mol·s$^{-1}$·m·m$^{-2}$·Pa$^{-1}$, gas permeabilities are reported in Barrer, where 1 Barrer = 3.35 x 10$^{-16}$ mol·s$^{-1}$·m·m$^{-2}$·Pa$^{-1}$.

The separation factor or mixed gas selectivity ($\alpha$) of $CO_2$ over $N_2$ was defined as the ratio of their permeabilities and can be expressed as follows:

$$\alpha = \frac{P_{CO_2}}{P_{N_2}} \qquad\qquad (2)$$

**Table 4.2.** $CO_2/N_2$ permeation performance of Matrimid® and PIM-1 blends at 2 bar feed pressure and 298 K.

| Membrane | $P_{CO2}$/Barrer | $P_{N2}$/Barrer | $\alpha_{CO2/N2}$ |
|---|---|---|---|
| PIM-1 | 3784 | 199 | 19 |
| 9.1 wt.% Matrimid in PIM-1 | 2220 | 90 | 25 |
| 20 wt.% Matrimid in PIM-1 | 2751 | 113 | 20 |
| 40 wt.% Matrimid in PIM-1 | 2412 | 168 | 14 |

## 4.3 Results and discussion

Matrimid®, in comparison to PIM-1, is a relatively flexible, and less contorted polymer that shows a higher degree of packing.[17] This results in higher selectivity, lower permeance and a very slow aging rate. Following previous reports, we used a Matrimid®/PIM-1 blending weight ratio of 9.1/90.9 to achieve a miscible mixture for membrane preparation (Table 4.2) [6]. Indeed, when using higher amounts of Matrimid® (Figure 4.2b, weight ratio 40/60), much rougher surfaces are observed by AFM than at the optimal ratio (Figure 4.2a). Such rough surfaces have been interpreted as phase segregation.[6]

$NH_2$-MIL-53 and ZIF-94 [18] as the promising MOF material, have been reported to display outstanding selectivity in the separation of $CO_2$ from $N_2$,[19] thus making it a good candidate for constructing MMMs.[20] Diamond and spherical shape of $NH_2$-MIL-53(Al) and ZIF-94 crystals with average particle size of 500-650 nm were prepared (Figure 4.3) to incorporate in MMM matrix. Surprisingly, the PIMAT composite is able to host high concentrations of MOF without compromising its structural properties. A relatively high filler content (25 wt.%, $W_{MOF}/(W_{MOF}+W_{PIMAT})$) was used. Indeed, such high loadings of filler in pure PIM-1 rendered brittle films with micro-cracks (Figure 4.4). The filler dispersion and morphology of the as-synthesized composite membrane was further studied by focused ion beam-scanning electronic microscopy (Figure 4.2 c,d) and (Figure 4.5). A homogeneous distribution of the MOF crystals in the PIMAT matrix illustrated a good adhesion between the filler and polymer phases.
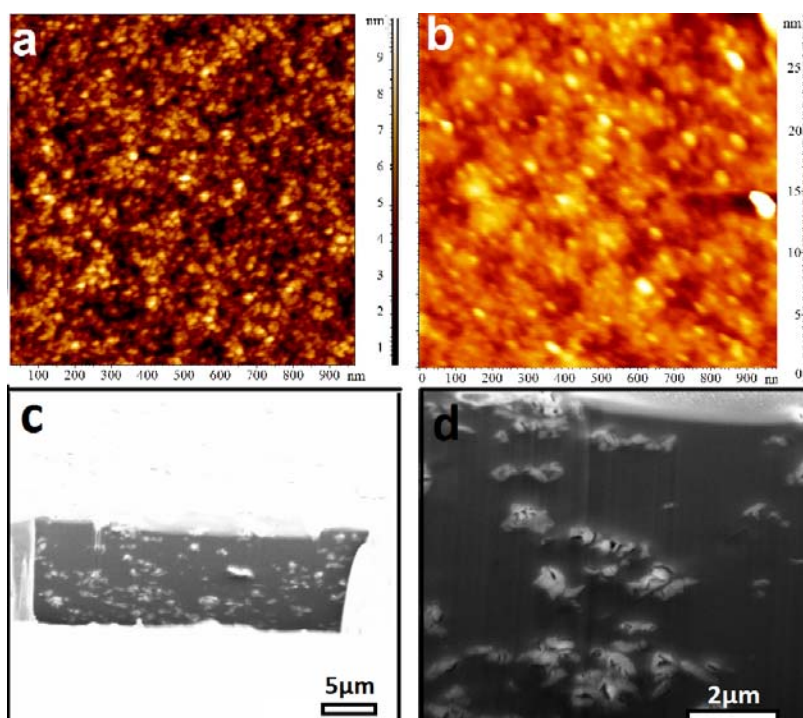
**Figure 4.2** Tapping-mode AFM topographical image of the surface of a) PIMAT (9.1 wt.%) and b) PIMAT (40 wt.%); The height profile (nm) is shown for reference. FIB-SEM images of 25 wt.% NH$_2$-MIL-53(Al)/PIMAT (9.1 wt.%) membrane: c) the trench created by FIB milling of the specimen and d) a representative cross-section of the membrane.
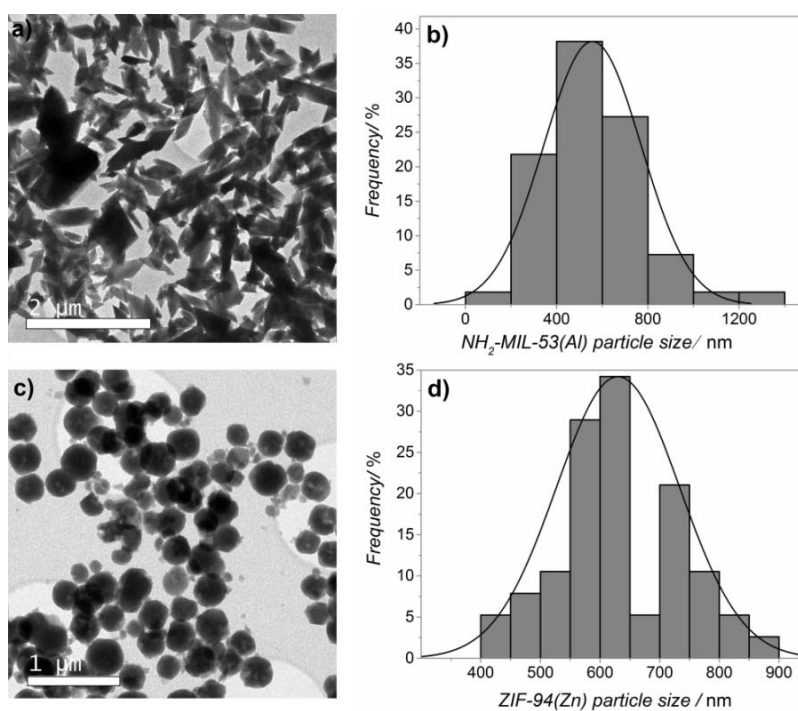


**Figure 4.3** TEM images and particle size distribution of NH$_2$-MIL-53(Al) (a, b) and ZIF-94(Zn) (c, d).
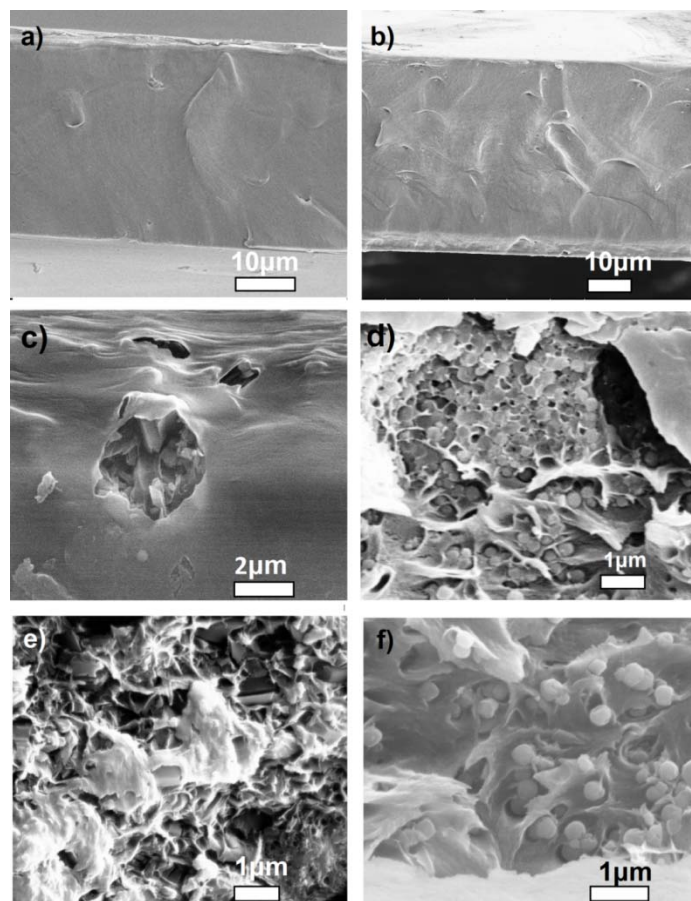
**Figure 4.4** Cross-section SEM images of PIM-1 (a), PIMAT (b), NH$_2$-MIL-53(Al)/PIM-1 (c), ZIF-94(Zn)/PIM-1 (d), NH$_2$-MIL-53(Al)/PIMAT (e), and ZIF-94(Zn)/PIMAT (f). The samples were prepared *via* freeze-fracturing of the membrane samples.
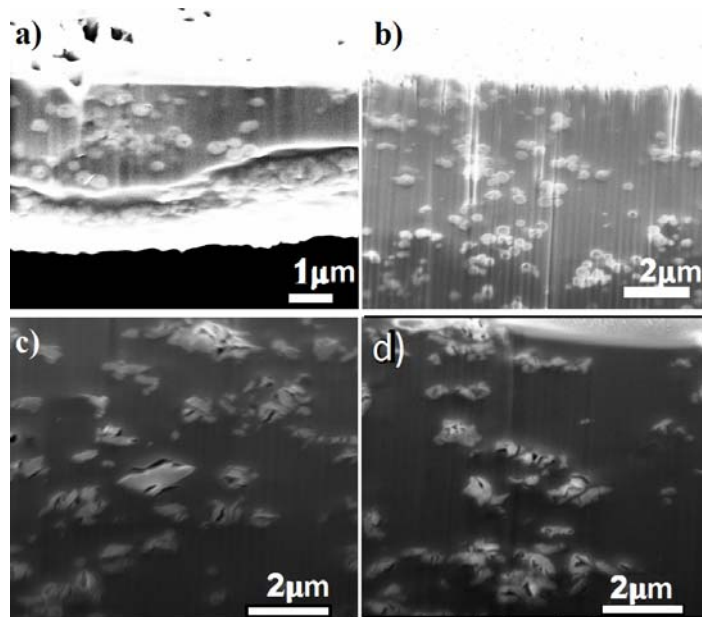


**Figure 4.5**. Cross-section FIB-SEM images of ZIF-94(Zn)/PIM-1 (a), ZIF-94(Zn)/PIMAT (b), NH$_2$-MIL-53(Al)/PIM-1 (c), and NH$_2$-MIL-53(Al)/PIMAT (d).
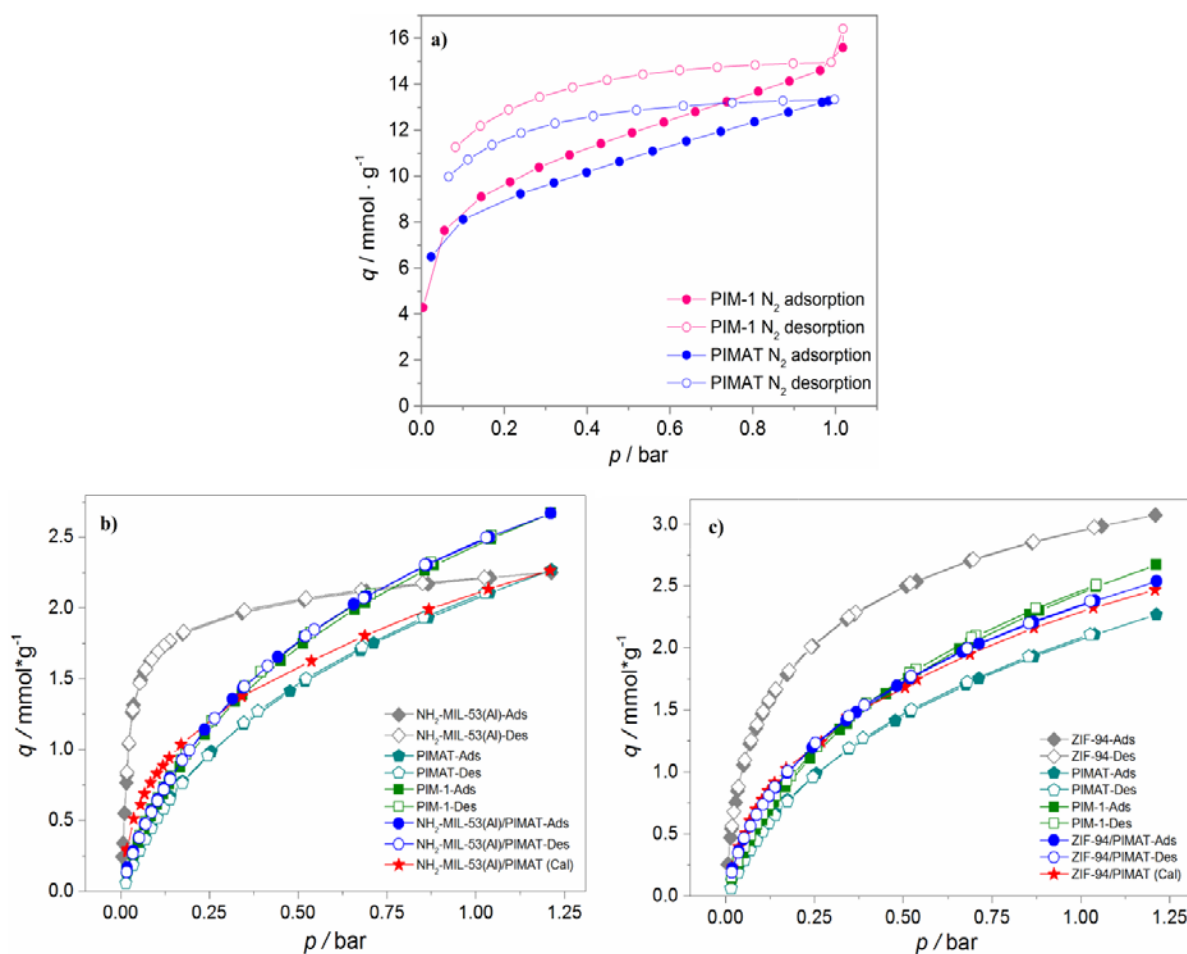
**Figure 4.6** Experimental $N_2$ adsorption (solid symbols) and desorption (open symbols) isotherms of PIM-1 and PIMAT membranes at 77 K (a), Experimental $CO_2$ adsorption (solid symbols) and desorption (open symbols) isotherms of $NH_2$-MIL-53(Al) and membranes at 273 K (b), Experimental $CO_2$ adsorption (solid symbols) and desorption (open symbols) isotherms of ZIF-94(Zn) and membranes at 273 K (c). The MOF particle loading in PIMAT is 25 wt.%. The Matrimid® loading in PIM-1 is 9.1 wt.%. The calculated isotherm is gained from a linear combination of the isotherms of $NH_2$-MIL-53(Al) and PIMAT based on their weight contribution.

$CO_2$ adsorption measurements on MOF materials and membranes were conducted at 273 K and up to 1.2 bar (Figure 4.6 b,c). A slight drop of $CO_2$ uptake on PIM-1 is observed upon blending Matrimid®, indicating a higher packing efficiency of polymer chains in PIMAT. Given the good miscibility of both polymers, the free volume of PIM-1 could be partially occupied by the threading Matrimid®. Also the reduced $N_2$ uptake on PIMAT membranes suggests this (Figure 4.6a). $NH_2$-MIL-53(Al) materials exhibit considerable $CO_2$ uptake even when its framework is in *np* configuration (Figure 4.6b).[19]
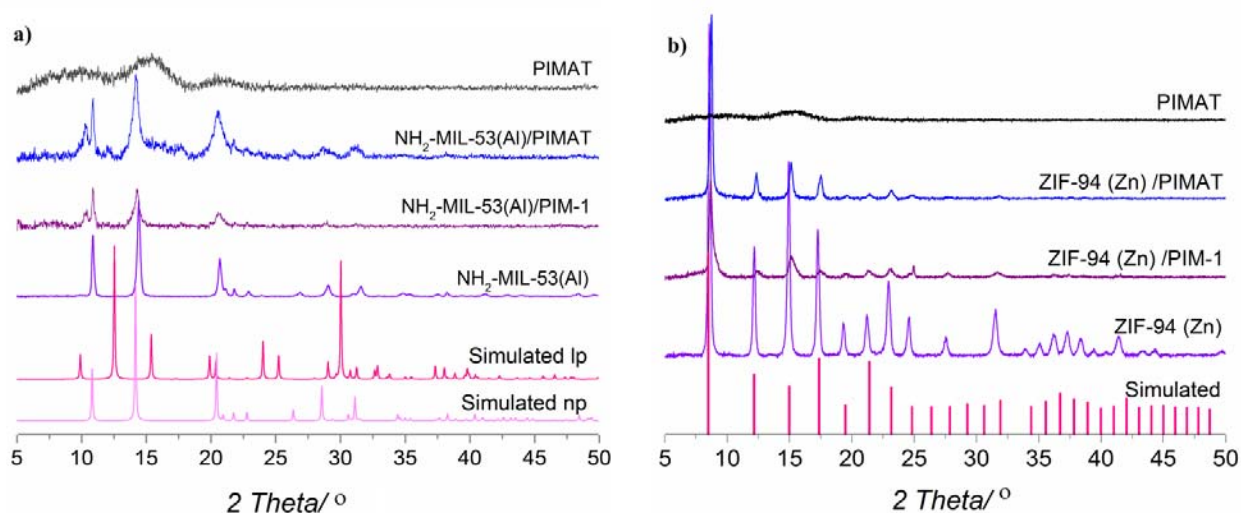
**Figure 4.7** The XRD patterns of $NH_2$-MIL-53(Al), PIMAT, $NH_2$-MIL-53(Al)/PIM-1 and $NH_2$-MIL-53(Al)/PIMAT. The simulated *lp* and *np* XRD patterns of $NH_2$-MIL-53(Al) are shown for reference (a); The XRD patterns of the ZIF-94(Zn), neat PIMAT membrane and MMMs. The simulated XRD pattern of ZIF-94(Zn) is shown for reference (b).[44]

For comparison, the ideal adsorption isotherm of $NH_2$-MIL-53(Al)/PIMAT and ZIF-94/PIMAT membranes were calculated from a linear combination of the isotherms of MOF and PIMAT based on their mass contribution. Since the $NH_2$-MIL-53(Al) in the membrane is in a *lp-np* configuration, the experimental $CO_2$ uptake is overall higher than the linear combination of both isotherms. In case of ZIF-94/PIMAT membranes, there was no significant variation between calculated and experimental isotherms.

The structures of the MOF powders and membranes were analyzed by XRD and the diffraction patterns are presented in Figure 4.7. $NH_2$-MIL-53 has a flexible framework, and displays a mixture of the narrow pore (*np*) and large pore (*lp*) configurations.[19] As-prepared $NH_2$-MIL-53 crystals show a diffraction pattern coherent with the *np* framework configuration, but diffractions ascribed to the *lp* MOF structure emerge in the pattern of the casted PIMAT membrane. The intensity ratio of the *lp/np* reflections in the $NH_2$-MIL-53(Al)/PIMAT is higher than $NH_2$-MIL-53(Al)/PIM-1 membrane, suggesting, as previously reported (Matrimid® in this case),[21] the partial penetration of Matrimid® into the MOF pores. The XRD patterns of ZIF-94 in PIM-1 and PIMAT membranes are compatible with the original pattern of ZIF-94 powder, showing that the crystallinity of the rigid ZIF-94 is preserved in the membrane.

To get insight into the polymer-MOFs interaction, ATR-IR spectra of the MMMs were acquired and compared to the original spectra of the MOF powder (Figure 4.8). In case of $NH_2$-MIL-53(Al) MMMs, a slight shift in the stretching vibration of $NH_2$-MIL-53(Al) carboxylic groups was observed.
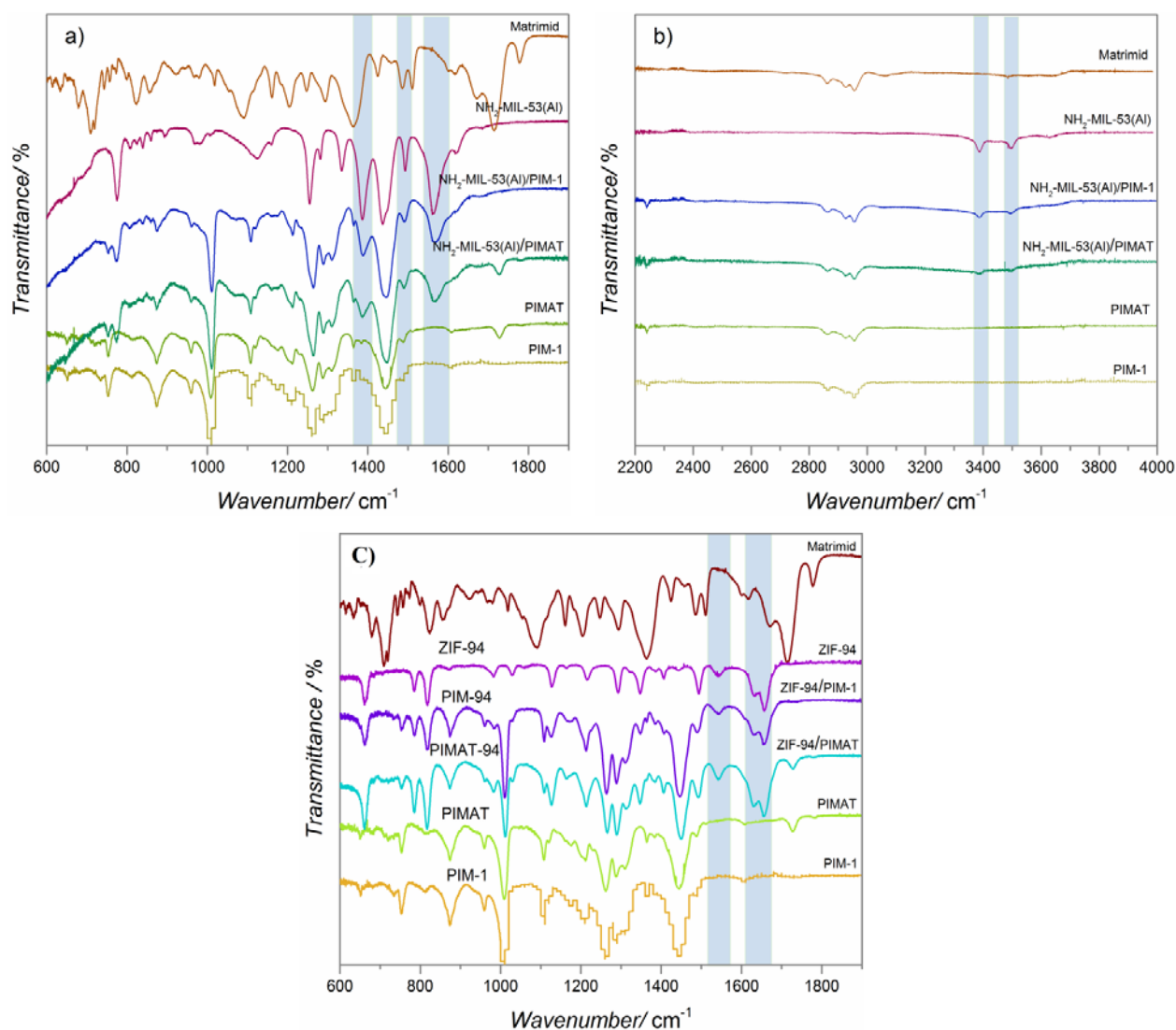
**Figure 4.8** ATR-FTIR spectra of NH$_2$-MIL-53(Al), PIM-1, PIMAT and MMMs between 600 and 1900 cm$^{-1}$ (a) 2200 and 4000 cm$^{-1}$ (b), and ATR-FTIR spectra of ZIF-94, PIM-1, PIMAT and MMMs between 600 and 1900 cm$^{-1}$ (c).

The shift in asymmetric (1500 cm$^{-1}$: blue shift and 1580 cm$^{-1}$: red shift) and symmetric (1410 cm$^{-1}$: red shift) stretching vibration is attributed to the interaction of carboxylic and amine groups in NH$_2$-MIL-53(Al) as reported by Chen *et al*.[22] Moreover, the peaks at 3500 and 3387 cm$^{-1}$ are attributed to the asymmetric and symmetric amine stretching of the MOF. The upward shift in the amine vibrations in PIMAT could be assigned to hydrogen bonding between MOF amine groups and free carbonyls in Matrimid® (Figure 4.8b).[23] Considering ZIF-94 MMMs (Figure 4.8c), there is no shift in the peak of –N-H bond vibration of the ZIF-94 (1665 cm$^{-1}$) by loading in PIM-1 and PIMAT MMMs.
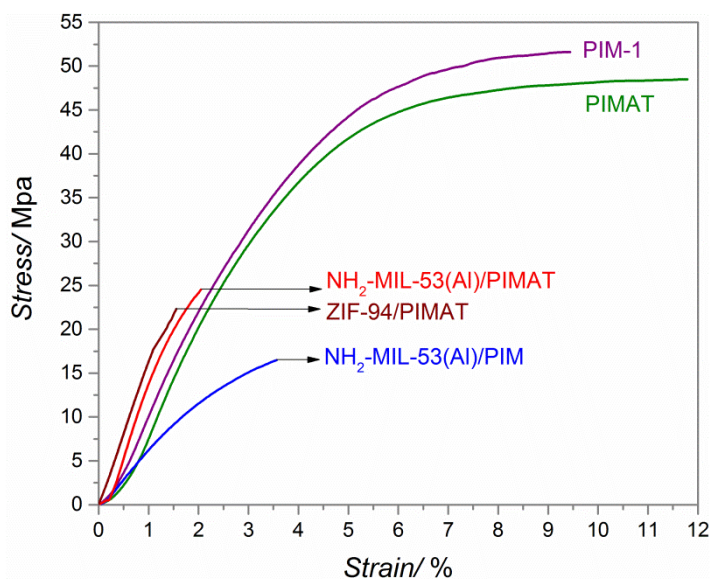
**Figure 4.9**. Stress versus strain curve of PIM-1, PIMAT, $NH_2$-MIL-53(Al)/PIMAT, ZIF-94/PIMAT and $NH_2$-MIL-53(Al)/PIM-1 membranes.

**Table 4.3.** Mechanical properties of PIM-1, PIMAT neat and MMMs.

| Membranes | Young modulus (GPa) | Yield strength (MPa) | Tensile strength (MPa) | Ductility (%) |
|---|---|---|---|---|
| PIM-1 | 1.28 | 18.78 | 51.62 | 9.50 |
| PIMAT | 1.06 | 22.70 | 48.48 | 11.80 |
| $NH_2$-MIL-53(Al)/PIMAT | 1.69 | 15.85 | 24.51 | 2.00 |
| $NH_2$-MIL-53(Al)/PIM-1 | 0.67 | 6.35 | 16.50 | 3.50 |
| ZIF-94/PIMAT | 1.64 | 11.96 | 22.30 | 1.50 |

The mechanical properties of the PIM-1 and PIMAT based membranes were assessed by tensile tests. The results are presented in Figure 4.9 and Table 4.3. As it was observed by simple flexing of the samples, PIMAT was more flexible than PIM-1. Accordingly, the tensile results showed that by addition of Matrimid® to PIM-1, not only the sample shows more plastic deformation (shown in Figure 4.9), but also the strain in the fracture point was higher than PIM-1, showing the flexibility of PIMAT membranes. However, loading of $NH_2$-MIL-53(Al) and ZIF-94 would result in a lower fracture point which is attributed to the brittleness of the membranes in comparison to the neat polymeric membranes. Despite this issue, the elastic modulus (stress to strain ratio) of the PIMAT based MMMs is much higher than the one measured for PIM-1 based MMMs, further demonstrating the benefits of polymer blending for the preparation of MMMs.[24]
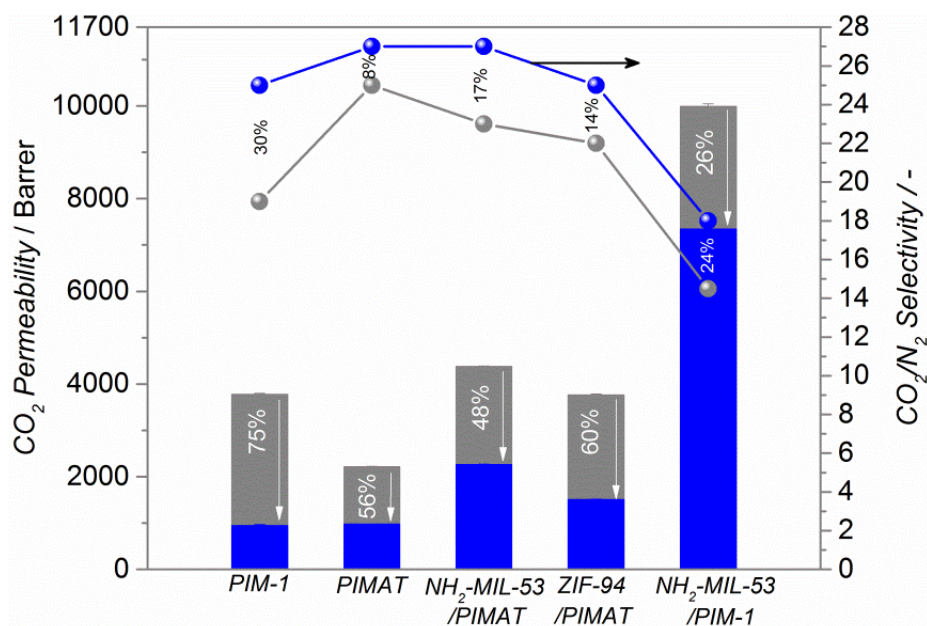
**Figure 4.10** $CO_2$ and $N_2$ gas separation performance of the fresh (grey symbols and bars) and 90 days aged membranes (blue symbols and bars) ($CO_2$ and $N_2$ (15/85 vol.%) mixture was used as feed at 298 K and 2 bar absolute).

The as-synthesized membranes were sealed in home-made modules and evaluated in the separation of $CO_2$ from $N_2$ at conditions relevant to pre-combustion $CO_2$ capture ($CO_2/N_2$ = 15/85 mol/mol mixture at 298 K and 2 bar absolute feed pressure (see the Supporting Information)). The performance is shown in Figure 4.10 and Figure 4.11a. The neat PIM-1 membrane exhibits a $CO_2$ permeability of ~3780 Barrer (1 Barrer = $1*10^{-10}$ cm$^3$ (STP) cm cm$^{-2}$ s$^{-1}$ cmHg$^{-1}$) and a $CO_2$ / $N_2$ selectivity of ~19, in line with previous reports.[6, 13] Upon threading the Matrimid®, a ~32% enhancement of gas selectivity was observed at the expense of ~41% reduction in $CO_2$ permeability, further confirming the higher polymer packing efficiency in PIMAT. By the addition of $NH_2$-MIL-53(Al) filler to PIMAT, the $CO_2$ permeability nearly doubled (~97% increase relative to PIMAT) with a slight drop in selectivity. This synergistic effect generates a simultaneous increase of selectivity (to 23) and $CO_2$ permeability (to 4380 Barrer) relative to PIM-1, driving the membrane separation performance over the Robeson upper bound limit (2008)[2] and reaching the economic target region.[16] For comparison, the performance of a $NH_2$-MIL-53(Al)/PIM-1 membrane was evaluated. As shown in Figure 4.11a, the membrane permeability increased by a 160% with 26% drop in selectivity relative to neat PIM-1. This is most probably the generation of micro-cracks in the polymer matrix due to the relatively high MOF loading (*vide supra*).

In order to gain insight into the influence on aging, membrane performance was evaluated after exposing the membranes to ambient conditions for 3 months. Results are shown in Figure 4.10. It is well known that during physical aging, the polymer chains of PIM-1 tend to pack more efficiently,[25] leading to a decrease in free volume and to the expected drop in permeability (75%) and an increase in selectivity from 19 to 25.

In contrast, in case of PIMAT, where Matrimid® occupies part of this free volume, $CO_2$ permeability decreases only by a 56% and selectivity slightly increases to 27. In case of $NH_2$-MIL-53(Al)/PIM-1, where a large fraction of permeability is due to the presence of micro-cracks, only a 26% drop in $CO_2$ flux is observed. Despite the substantial decrease (48%) in $CO_2$ permeability for the $NH_2$-MIL-53(Al)/PIMAT membrane upon aging, its performance, with a $CO_2$ permeability of 2260 Barrer and $CO_2/N_2$ selectivity of 27 lies on the Robeson upper bound (2008). This performance clearly improved over that observed for the fresh PIMAT and is better both in terms of selectivity and permeability than that of aged PIM-1.

In order to demonstrate the scope of our approach, we prepared additional membranes using ZIF-94(Zn) as filler, in virtue of its high $CO_2$ uptake at low pressure (Figure 4.6).[26] However, upon loading 25 wt.% ZIF-94(Zn) into PIM-1, very brittle membranes were obtained with no separation selectivity. As anticipated, a more selective ZIF-94(Zn)/PIMAT membrane was formed with the assistance of Matrimid® threading (Figure 4.10 and 4.11a). After 3 months aging, although the $CO_2$ permeability of ZIF-94(Zn)/PIMAT decreased by 60%, it is still higher than the aged PIM-1 with a comparable selectivity. These results further demonstrate the significance of our approach for composite membrane preparation.

Further, we have tested the aged PIM and PIMAT neat and MMM samples after 17 months (Figure 4.11a). The aging after 3 months mainly resulted predominantly in a decrease in permeation while after 17 months the aging shifted towards an increase in selectivity for the PIMAT membranes. In contrast, the PIM-1 membrane continued the trend of reduction in permeability after 17 months of aging. Interestingly, after 17 months of membranes aging in ambient conditions the PIMAT MMMs performance surpasses the upper bound.

The separation performance of PIM-1 and PIMAT neat and mixed matrix membranes was evaluated under humid conditions (2.3 mol.% water in feed) and compared with dry conditions (Figure 4.11b). PIMAT based membranes showed less reduction in permeability than PIM-1, while in both cases the selectivity increased by two points. However, the $NH_2$-MIL-53(Al)/PIMAT composites nearly preserved its high permeability of 4000 Barrer and improved $CO_2/N_2$ selectivity up to 28, the highest of all samples.

The results of this study (blue circles) demonstrate a superior performance in comparison to other PIMs (black open circles) and PIM blended (red open circles) membranes (Figure 4.11c). This confirms the influence of MOF loading in blended polymers and enhancing the $CO_2/N_2$ separation performance relative to the upper bound.
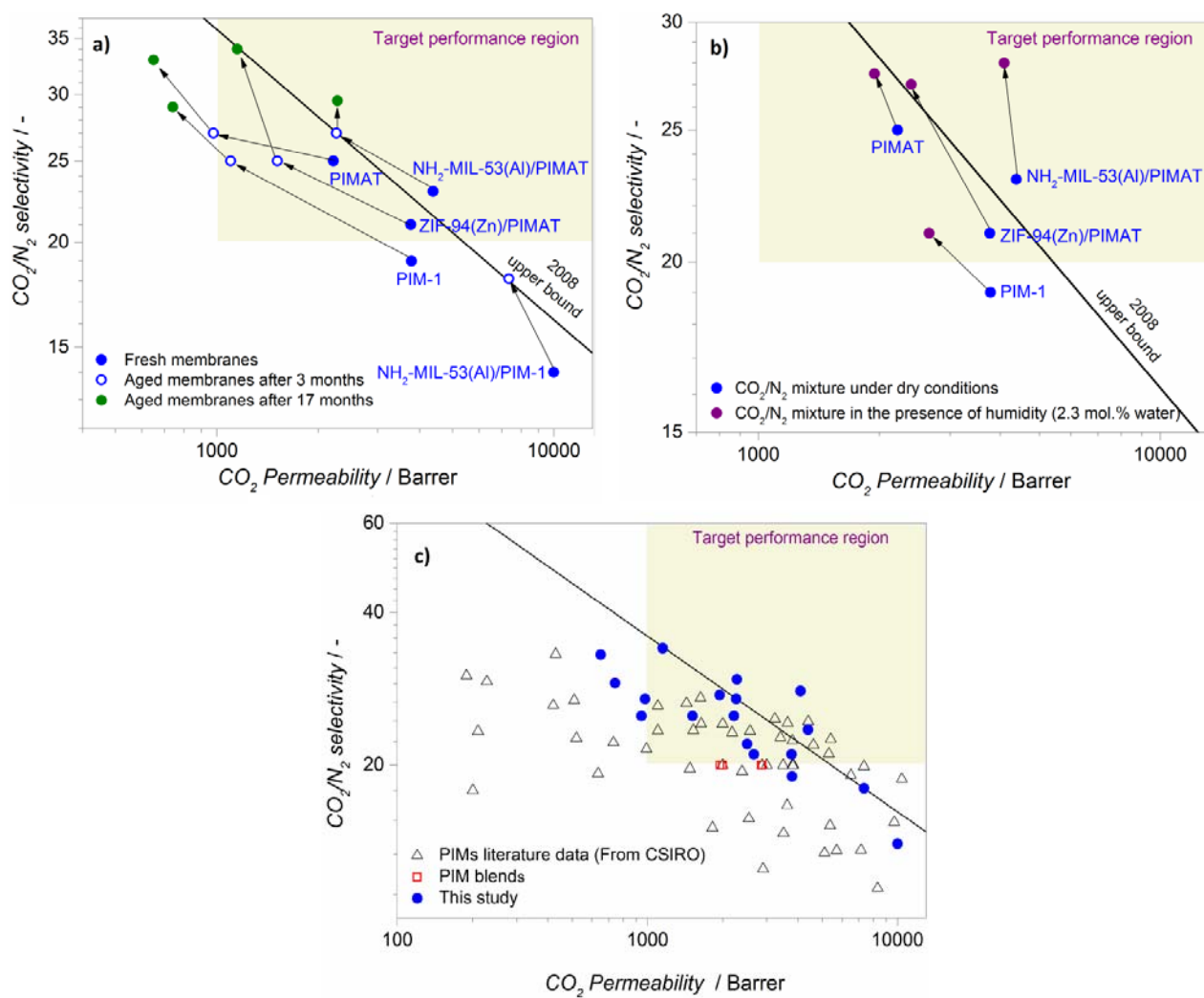
**Figure 4.11**. (a) Robeson plot of $CO_2/N_2$ separation performance of the fresh (*blue closed*), aged membranes after 3 months (*blue open*) and 17 months (*green closed squares*) tested under dry conditions. (b) Robeson plot of $CO_2/N_2$ separation performance of the fresh (*blue symbols*) membranes tested under dry and humid (2.3 mol.% water in feed, *purple symbols*) conditions. (c) Robeson plot of $CO_2/N_2$ mixed gas separation performance of this study (the fresh/aged membranes in dry and humid condition) and the literature data of microporous polymers taken from Commonwealth Scientific and Industrial Research Organization (CSIRO).[43] The Robeson upper bound (2008)[3] is shown for reference, as well as the target performance region for $CO_2$ capture from flue gas from Merkel *et al.* [30] assuming a membrane thickness of 1 μm. The MOF particle loading in PIMAT is 25 wt.%. The Matrimid® loading in PIM-1 is 9.1 wt.%. All the measurements were conducted at 298 K with 2 bar absolute feed pressure (mixed gases). 1 Barrer = $1*10^{-10}$ cm$^3$ (STP) cm cm$^{-2}$ s$^{-1}$ cmHg$^{-1}$.

## 4.4 Conclusions

In summary, by utilizing a second, less permeable polymer, in combination with a high performance PIM-1 microporous polymer, it was possible to manufacture MOF-based mixed matrix membranes showing enhanced phase compatibility, and consequently the improved membrane separation performance well above the Robeson upper bound. The permeation results indicated that $NH_2$-MIL-53(Al) was a promising MOF filler in terms of enhancing polymer and filler interaction due to its amine functional groups. Therefore, the superior permeation performance of the PIMAT MMM using $NH_2$-MIL-53(Al) as a filler led to surpassing $CO_2/N_2$ Robeson upper bound even after 17 months of ageing and under humid conditions. The versatility of the developed method was evidenced by using different MOF fillers, which can potentially incorporate in other rigid microporous polymer membranes.

# References

[1]    W.J. Koros, R.P. Lively, Water and beyond: Expanding the spectrum of large-scale energy efficient separation processes, AIChE J., 58 (2012) 2624-2633.

[2]    D.F. Sanders, Z.P. Smith, R. Guo, L.M. Robeson, J.E. McGrath, D.R. Paul, B.D. Freeman, Energy-efficient polymeric gas separation membranes for a sustainable future: A review, Polymer, 54 (2013) 4729-4761.

[3]    L.M. Robeson, The upper bound revisited, J. Membr. Sci., 320 (2008) 390-400.

[4]    X. Zhu, C. Tian, S.M. Mahurin, S.H. Chai, C. Wang, S. Brown, G.M. Veith, H. Luo, H. Liu, S. Dai, A superacid-catalyzed synthesis of porous membranes based on triazine frameworks for CO2 separation, J. Am. Chem. Soc., 134 (2012) 10478-10484.

[5]    S. Wang, X. Li, H. Wu, Z. Tian, Q. Xin, G. He, D. Peng, S. Chen, Y. Yin, Z. Jiang, M.D. Guiver, Advances in high permeability polymer-based membrane materials for CO2separations, Energy Environ. Sci., 9 (2016) 1863-1890.

[6]    M. Carta, R. Malpass-Evans, M. Croad, Y. Rogan, J.C. Jansen, P. Bernardo, F. Bazzarelli, N.B. McKeown, An efficient polymer molecular sieve for membrane gas separations, Science, 339 (2013) 303-307.

[7]    N.B. McKeown, P.M. Budd, Polymers of intrinsic microporosity (PIMs): organic materials for membrane separations, heterogeneous catalysis and hydrogen storage, Chem. Soc. Rev., 35 (2006) 675-683.

[8]    P.M. Budd, E.S. Elabas, B.S. Ghanem, S. Makhseed, N.B. McKeown, K.J. Msayib, C.E. Tattershall, D. Wang, Solution-Processed, Organophilic Membrane Derived from a Polymer of Intrinsic Microporosity, Adv. Mater., 16 (2004) 456-459.

[9]    I. Rose, C.G. Bezzu, M. Carta, B. Comesana-Gandara, E. Lasseuguette, M.C. Ferrari, P. Bernardo, G. Clarizia, A. Fuoco, J.C. Jansen, K.E. Hart, T.P. Liyana-Arachchi, C.M. Colina, N.B. McKeown, Polymer ultrapermeability from the inefficient packing of 2D chains, Nat. Mater., 16 (2017) 932-937.

[10]    Q. Song, S. Cao, R.H. Pritchard, B. Ghalei, S.A. Al-Muhtaseb, E.M. Terentjev, A.K. Cheetham, E. Sivaniah, Controlled thermal oxidative crosslinking of polymers of intrinsic microporosity towards tunable molecular sieve membranes, Nat. Commun., 5 (2014) 4813.

[11]    N. Du, H.B. Park, G.P. Robertson, M.M. Dal-Cin, T. Visser, L. Scoles, M.D. Guiver, Polymer nanosieve membranes for CO2-capture applications, Nat. Mater., 10 (2011) 372-375.

[12]    W.F. Yong, F.Y. Li, Y.C. Xiao, P. Li, K.P. Pramoda, Y.W. Tong, T.S. Chung, Molecular engineering of PIM-1/Matrimid blend membranes for gas separation, J. Membr. Sci., 407-408 (2012) 47-57.

[13]    D.R. Paul, S. Newman, Polymer Blends, Academic Press, New York,, (1978).

[14]    J. Dechnik, J. Gascon, C.J. Doonan, C. Janiak, C.J. Sumby, Mixed-Matrix Membranes, Angew. Chem. Int. Ed., 56 (2017) 9292-9310.

[15]    B. Seoane, J. Coronas, I. Gascon, M. Etxeberria Benavides, O. Karvan, J. Caro, F. Kapteijn, J. Gascon, Metal-organic framework based mixed matrix membranes: a solution for highly efficient CO2 capture?, Chem. Soc. Rev., 44 (2015) 2421-2454.

[16]   T. Rodenas, I. Luz, G. Prieto, B. Seoane, H. Miro, A. Corma, F. Kapteijn, I.X.F.X. Llabres, J. Gascon, Metal-organic framework nanosheets in polymer composite materials for gas separation, Nat. Mater., 14 (2015) 48-55.

[17]   T.H. Bae, J.S. Lee, W. Qiu, W.J. Koros, C.W. Jones, S. Nair, A high-performance gas-separation membrane containing submicrometer-sized metal-organic framework crystals, Angew. Chem. Int. Ed., 49 (2010) 9863-9866.

[18]   W.J. Koros, C. Zhang, Materials for next-generation molecularly selective synthetic membranes, Nat. Mater., 16 (2017) 289-297.

[19]   X.L. Liu, Y.S. Li, G.Q. Zhu, Y.J. Ban, L.Y. Xu, W.S. Yang, An organophilic pervaporation membrane derived from metal-organic framework nanoparticles for efficient recovery of bio-alcohols, Angew. Chem. Int. Ed., 50 (2011) 10636-10639.

[20]   N. Tien-Binh, H. Vinh-Thang, X.Y. Chen, D. Rodrigue, S. Kaliaguine, Crosslinked MOF-polymer to enhance gas separation of mixed matrix membranes, J. Membr. Sci., 520 (2016) 941-950.

[21]   A.F. Bushell, P.M. Budd, M.P. Attfield, J.T. Jones, T. Hasell, A.I. Cooper, P. Bernardo, F. Bazzarelli, G. Clarizia, J.C. Jansen, Nanoporous organic polymer/cage composite membranes, Angew. Chem. Int. Ed., 52 (2013) 1253-1256.

[22]   Q. Song, S. Cao, R.H. Pritchard, H. Qiblawey, E.M. Terentjev, A.K. Cheetham, E. Sivaniah, Nanofiller-tuned microporous polymer molecular sieves for energy and environmental processes, J. Mater. Chem. A, 4 (2016) 270-279.

[23]   C.H. Lau, P.T. Nguyen, M.R. Hill, A.W. Thornton, K. Konstas, C.M. Doherty, R.J. Mulder, L. Bourgeois, A.C. Liu, D.J. Sprouster, J.P. Sullivan, T.J. Bastow, A.J. Hill, D.L. Gin, R.D. Noble, Ending aging in super glassy polymer membranes, Angew. Chem. Int. Ed., 53 (2014) 5322-5326.

[24]   C.H. Lau, K. Konstas, A.W. Thornton, A.C. Liu, S. Mudie, D.F. Kennedy, S.C. Howard, A.J. Hill, M.R. Hill, Gas-separation membranes loaded with porous aromatic frameworks that improve with age, Angew. Chem. Int. Ed., 54 (2015) 2669-2673.

[25]   B. Ghalei, K. Sakurai, Y. Kinoshita, K. Wakimoto, Ali P. Isfahani, Q. Song, K. Doitomi, S. Furukawa, H. Hirao, H. Kusuda, S. Kitagawa, E. Sivaniah, Enhanced selectivity in mixed matrix membranes for $CO_2$ capture through efficient dispersion of amine-functionalized MOF nanoparticles, Nat. Energy, 2 (2017) 17086.

[26]   S.J. Smith, B.P. Ladewig, A.J. Hill, C.H. Lau, M.R. Hill, Post-synthetic Ti exchanged UiO-66 metal-organic frameworks that deliver exceptional gas permeability in mixed matrix membranes, Sci. Rep., 5 (2015) 7823.

[27]   M. Vinoba, M. Bhagiyalakshmi, Y. Alqaheem, A.A. Alomair, A. Pérez, M.S. Rana, Recent progress of fillers in mixed matrix membranes for CO 2 separation: A review, Sep. Purif. Technol., 188 (2017) 431-450.

[28]   S.J.D. Smith, C.H. Lau, J.I. Mardel, M. Kitchin, K. Konstas, B.P. Ladewig, M.R. Hill, Physical aging in glassy mixed matrix membranes; tuning particle interaction for mechanically robust nanocomposite films, J. Mater. Chem. A, 4 (2016) 10627-10634.

[29]   Z. Wang, D. Wang, S. Zhang, L. Hu, J. Jin, Interfacial Design of Mixed Matrix Membranes for Improved Gas Separation Performance, Adv. Mater., 28 (2016) 3399-3405.

[30]   T.C. Merkel, H. Lin, X. Wei, R. Baker, Power plant post-combustion carbon dioxide capture: An opportunity for membranes, J. Membr. Sci., 359 (2010) 126-139.

[31]   Y.D. Y. Xiao, T. S. Chung, M. D. Guiver, Effects of Brominating Matrimid Polyimide on the Physical and GasTransport Properties of Derived Carbon Membranes, Macromolecules, 38 (2005) 10042-10049.

[32]   J. Gascon, U. Aktay, M. Hernandezalonso, G. Vanklink, F. Kapteijn, Amino-based metal-organic frameworks as stable, highly active basic catalysts, J. Catal., 261 (2009) 75-87.

[33]   E. Stavitski, E.A. Pidko, S. Couck, T. Remy, E.J. Hensen, B.M. Weckhuysen, J. Denayer, J. Gascon, F. Kapteijn, Complexity behind CO2 capture on NH2-MIL-53(Al), Langmuir, 27 (2011) 3970-3976.

[34]   T. Rodenas, M. van Dalen, E. García-Pérez, P. Serra-Crespo, B. Zornoza, F. Kapteijn, J. Gascon, Visualizing MOF Mixed Matrix Membranes at the Nanoscale: Towards Structure-Performance Relationships in CO2/CH4 Separation Over NH2-MIL-53(Al)@PI, Adv. Funct. Mater., 24 (2014) 249-256.

[35]   A. Sabetghadam, B. Seoane, D. Keskin, N. Duim, T. Rodenas, S. Shahid, S. Sorribas, C.L. Guillouzer, G. Clet, C. Tellez, M. Daturi, J. Coronas, F. Kapteijn, J. Gascon, Metal Organic Framework Crystals in Mixed-Matrix Membranes: Impact of the Filler Morphology on the Gas Separation Performance, Adv. Funct. Mater., 26 (2016) 3154-3163.

[36]   A. Sabetghadam, X. Liu, M. Benzaqui, E. Gkaniatsou, A. Orsi, M.M. Lozinska, C. Sicard, T. Johnson, N. Steunou, P.A. Wright, C. Serre, J. Gascon, F. Kapteijn, Influence of Filler Pore Structure and Polymer on the Performance of MOF-Based Mixed-Matrix Membranes for CO2 Capture, Chem. Eur. J., 24 (2018) 7949-7956.

[37]   X.Y. Chen, V.-T. Hoang, D. Rodrigue, S. Kaliaguine, Optimization of continuous phase in amino-functionalized metal–organic framework (MIL-53) based co-polyimide mixed matrix membranes for CO2/CH4 separation, RSC Adv., 3 (2013) 24266.

[38]   X.Y. Chen, H. Vinh-Thang, D. Rodrigue, S. Kaliaguine, Amine-Functionalized MIL-53 Metal–Organic Framework in Polyimide Mixed Matrix Membranes for CO2/CH4 Separation, Ind. Eng. Chem. Res., 51 (2012) 6895-6906.

[39]   I.S. Flyagina, E.M. Mahdi, K. Titov, J.-C. Tan, Thermo-mechanical properties of mixed-matrix membranes encompassing zeolitic imidazolate framework-90 and polyvinylidine difluoride: ZIF-90/PVDF nanocomposites, APL Materials, 5 (2017) 086104.

[40]   X.Q. Cheng, K. Konstas, C.M. Doherty, C.D. Wood, X. Mulet, Z. Xie, D. Ng, M.R. Hill, L. Shao, C.H. Lau, Hyper-Cross-Linked Additives that Impede Aging and Enhance Permeability in Thin Polyacetylene Films for Organic Solvent Nanofiltration, ACS Appl. Mater. Interfaces, 9 (2017) 14401-14408.

[41]   W. Morris, N. He, K.G. Ray, P. Klonowski, H. Furukawa, I.N. Daniels, Y.A. Houndonougbo, M. Asta, O.M. Yaghi, B.B. Laird, A Combined Experimental-Computational Study on the Effect of Topology on Carbon Dioxide Adsorption in Zeolitic Imidazolate Frameworks, J. Phys. Chem. C, 116 (2012) 24084-24090.

[42]    M. Etxeberria-Benavides, O. David, T. Johnson, M.M. Łozińska, A. Orsi, P.A. Wright, S. Mastel, R. Hillenbrand, F. Kapteijn, J. Gascon, High performance mixed matrix membranes (MMMs) composed of ZIF-94 filler and 6FDA-DAM polymer, J. Membr. Sci., 550 (2018) 198-207.

[43]    https://membrane-australasia.org/polymer-gas-separation-membranes/.

[44]    W. Morris, N. He, K.G. Ray, P. Klonowski, H. Furukawa, I.N. Daniels, Y.A. Houndonougbo, M. Asta, O.M. Yaghi, B.B. Laird, A Combined Experimental-Computational Study on the Effect of Topology on Carbon Dioxide Adsorption in Zeolitic Imidazolate Frameworks, The Journal of Physical Chemistry C, 116 (2012) 24084-24090.

[45]    J. Shen, G. Liu, K. Huang, Q. Li, K. Guan, Y. Li, W. Jin, UiO-66-polyether block amide mixed matrix membranes for CO2 separation, Journal of Membrane Science, 513 (2016) 155-165.

[46]    M.R. Khdhayyer, E. Esposito, A. Fuoco, M. Monteleone, L. Giorno, J.C. Jansen, M.P. Attfield, P.M. Budd, Mixed matrix membranes based on UiO-66 MOFs in the polymer of intrinsic microporosity PIM-1, Separation and Purification Technology, 173 (2017) 304-313.

[47]    S.R. Venna, M. Lartey, T. Li, A. Spore, S. Kumar, H.B. Nulwala, D.R. Luebke, N.L. Rosi, E. Albenze, Fabrication of MMMs with improved gas separation properties using externally-functionalized MOF particles, Journal of Materials Chemistry A, 3 (2015) 5014-5022.

[48]    T. Li, Y. Pan, K.-V. Peinemann, Z. Lai, Carbon dioxide selective mixed matrix composite membrane containing ZIF-7 nano-fillers, Journal of Membrane Science, 425-426 (2013) 235-242.

[49]    C.W. Seok, K.S. Jin, L. Seung-Joon, B. Youn-Sang, K.J. Hak, Enhanced Performance of Mixed-Matrix Membranes through a Graft Copolymer-Directed Interface and Interaction Tuning Approach, ChemSusChem, 8 (2015) 650-658.

[50]    B. Yujie, L. Zhengjie, L. Yanshuo, P. Yuan, J. Hua, J. Wenmei, G. Ang, W. Po, Y. Qingyuan, Z. Chongli, Y. Weishen, Confinement of Ionic Liquids in Nanocages: Tailoring the Molecular Sieving Properties of ZIF-8 for Membrane-Based CO2 Capture, Angewandte Chemie International Edition, 54 (2015) 15483-15487.

[51]    B. Yujie, L. Yanshuo, P. Yuan, J. Hua, J. Wenmei, L. Xinlei, Y. Weishen, Metal-Substituted Zeolitic Imidazolate Framework ZIF-108: Gas-Sorption and Membrane-Separation Properties, Chemistry – A European Journal, 20 (2014) 11402-11409.

[52]    Q. Xin, J. Ouyang, T. Liu, Z. Li, Z. Li, Y. Liu, S. Wang, H. Wu, Z. Jiang, X. Cao, Enhanced Interfacial Interaction and CO2 Separation Performance of Mixed Matrix Membrane by Incorporating Polyethylenimine-Decorated Metal–Organic Frameworks, ACS Applied Materials & Interfaces, 7 (2015) 1065-1077.

[53]    S. Basu, A. Cano-Odena, I.F.J. Vankelecom, MOF-containing mixed-matrix membranes for CO2/CH4 and CO2/N2 binary gas mixture separations, Separation and Purification Technology, 81 (2011) 31-40.

[54]    H. Gong, T.H. Nguyen, R. Wang, T.-H. Bae, Separations of binary mixtures of CO2/CH4 and CO2/N2 with mixed-matrix membranes containing Zn(pyrz)2(SiF6) metal-organic framework, Journal of Membrane Science, 495 (2015) 169-175.

[55]    R. Lin, L. Ge, H. Diao, V. Rudolph, Z. Zhu, Ionic Liquids as the MOFs/Polymer Interfacial Binder for Efficient Membrane Separation, ACS Applied Materials & Interfaces, 8 (2016) 32041-32049.

# 5

# Thin mixed matrix and dual layer membranes containing metal-organic framework nanosheets and Polyactive™ for CO₂ capture

**Abstract:** *Preparation methods are presented of thin dual layer membranes (DLM's) and mixed matrix membranes (MMM's) based on nanosheets of the Cu-BDC metal-organic framework (MOF, lateral size range 1-5 μm, thickness 15 nm) and commercially available poly(ethylene oxide)–poly(butylene terephthalate) (PEO–PBT) copolymer (Polyactive$^{TM}$) and their performances are compared in $CO_2/N_2$ separation. The MMMs and DLMs represent two extremes, on the one hand with well-mixed components and on the other hand completely segregated layers. Compared to the free-standing membranes, the thin PAN- and zirconia-alumina-supported MMMs showed significant enhancement in both permeance and selectivity. The support properties affect the obtained selective layer thickness and its resistance impacts the $CO_2/N_2$ selectivity. The permeance of thin DLM's is among the highest reported literature data of MOF based thin MMMs, but have a modest selectivity. Addition of the nanosheets in the thin MMMs improves the $CO_2/N_2$ selectivity of the already selective polymer further to 77. The nanosheets in the thin MMMs make a gutter layer on the PAN support superfluous. The small pore support $ZrO_2$-alumina does not need a gutter layer.*
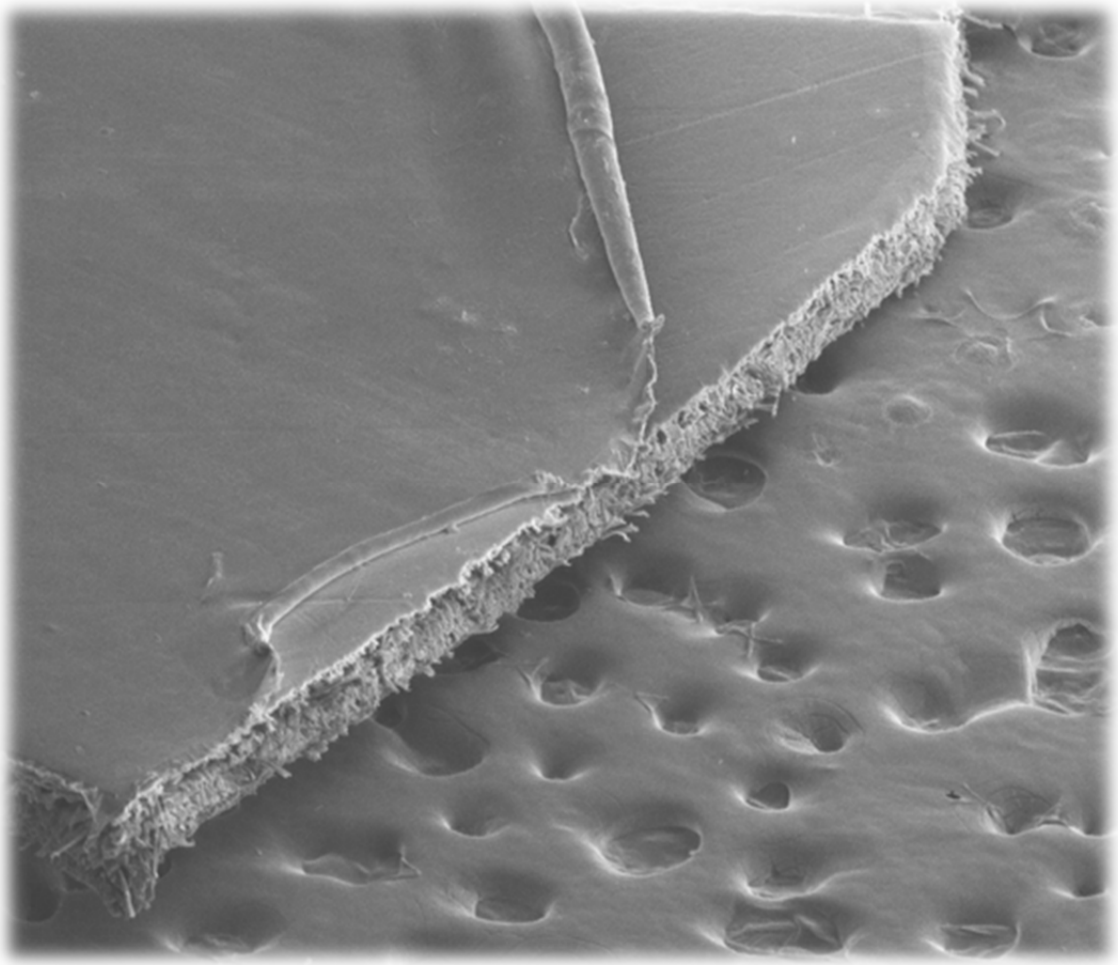
SEM image of the thin membrane on PAN support

### 5.1 Introduction

The increasing global demand for energy-efficient separations in carbon capture has prompted international actions on searching for novel, high-performance separation membranes.[1] For industrial scale applications such as natural gas sweetening [2], $CO_2$ capture from flue gas[3] and $H_2$ separation from syngas [4], the use of highly permeable and selective membranes is essential. Industrial-scale gas separation applications require production of large membrane areas (e.g., $10^5$ to $10^7$ m$^2$) with low defect densities (e.g., below 1 m$^2$ per $10^5$ m$^2$ of membrane surface area).[5] Such a scale-up is often quite challenging and requires the production of thin, defect free membranes using industrial membrane fabrication methods.[6] Membranes with very thin selective layers (asymmetric or composite structure) typically in the range of 0.1–2 µm are required. The first thin asymmetric membrane was made by phase inversion and reported by Loeb-Surirajan in 1959. The asymmetric structure consisted of a 0.2-0.5 µm thin skin layer supported by a porous substructure with 0.1-1.0 µm pore size.[7] Another class of thin membranes can be prepared by coating a thin selective layer on a porous support which are known as thin supported membranes.[8] These membranes are cheaper to manufacture on industrial scale due to the lower consumption of material for the selective layer preparation and the use of commercial porous supports. The most widely used methods for preparing thin supported membranes are drop-casting,[9] dip-coating [10] and spin coating.[11]

Commonly, thin membranes may also have an intermediate layer known as gutter layer between the porous support and the selective layer. The gutter layer is mainly chosen from highly permeable polymers such as PDMS [9] or PTMSP [12] to afford a smooth and flat coating surface while preventing the upper selective layer penetration into the support. This method also heals defects in the support layer improving the membrane quality, constituted a breakthrough in the application of polymeric membranes.

To improve the separation performance of thin polymeric membranes, a feasible approach is further the incorporation of fillers (e.g., micro- or nanoparticles) in the polymeric matrix to form mixed matrix membranes (MMMs).[13] However, thin MMMs potentially suffer from defect formation during the fabrication process due to a poor compatibility between filler and matrix, which makes their large-scale production quite challenging. One strategy to prepare defect free ultra-thin mixed matrix membranes is using polymers that address the compatibility and ageing issues. Glassy-rubbery block copolymers such as Pebax® have been widely studied to make the defect-free MMMs due to their low glass transition temperature and chain flexibility, filling the gaps between filler and polymer.[14-16] Using Pebax® 1657 as the continuous matrix resulted in MMMs featuring moderate $CO_2$ permeability and relatively high selectivity over $N_2$ and $CH_4$, making it an attractive polymer for defect free thin membrane formation.[10, 17-21] Polyactive™, composed of poly(ethylene oxide) (PEO) and poly(butylenes terephthalate) (PBT) segments, is

another promising block copolymer for $CO_2$ separation which has been fabricated as thin membrane and used in pilot scale modules.[22] To fabricate defect-free thin membranes the use of high molecular weight polymer was needed.[23]

Considering the compatibility issues in mixed matrix membranes, metal-organic frameworks are known as potential candidate with improved polymer-filler interaction. This is mainly ascribed to the organic linker functional groups which can interact with the polymer chains.[24, 25]

Another approach to address difficulties in fabricating large-scale, defect-free thin MMMs is the use of nanomaterials with a high aspect ratio (e.g., carbon nanotubes [26], graphene [27], 2D zeolites [28] and MOF nanosheets [29]) as fillers.[30, 31] In this regard MOFs offer a number of advantages, since their morphology can be tuned in a relatively straightforward manner. As example, different morphologies of $NH_2$-MIL-53(Al) such as nanorod, microneedle, nanoparticle and nanosheet were synthesized via using various synthetic approaches.[32, 33] Cu-BDC bulk and nanosheet morphologies were compared by Rodenas *et al.* [34] and even the preparation of non-lamellar MOF nanosheets has recently been reported.[33] In general, two different synthesis routes have been reported for 2D MOF materials which are globally (*i*) top-down and (*ii*) bottom-up synthesis approaches. The first approach relies on exfoliation of 3D materials which has some drawbacks such as crystal or morphological damage and re-aggregation of the exfoliated material.[35, 36] The second approach is preferably used in synthesis of ultra-thin sheets in which the aspect-ratio is possible to be tuned by either anisotropic crystal growth or thermodynamically limiting the layer stacking.[37-39] The main driving force for the bottom-up synthesis is the diffusion of the metal and ligand sources into the intermediate spacer layer which can be tuned by temperature as reported by Shete *et al.* [40]

Recently, an advancement of free-standing 2D MOF MMMs has been achieved by incorporating the Cu-BDC and $NH_2$-MIL-53(Al) nanosheets in Matrimid® and 6FDA-DAM membranes, showing a significant enhancement of $CO_2/CH_4$ selectivity relative to the pristine membranes.[33, 34, 40, 41] This confirms the role of lamellar morphology of the fillers with high aspect ratio that could facilitate a perpendicular pore orientation and shorter diffusion paths for desired components, while increasing that for undesired components making their permeation pathway more tortuous.[42] More recently, the synthesis of thin 2D MOF MMMs has been reported by Cheng *et al.*[11]

Here, we report the scaled-up synthesis of Cu-BDC nanosheets and fabrication of free-standing and thin supported membranes comprising these Cu-BDC nanosheets and commercially available PEO-PBT block copolymer (Polyactive™). In order to demonstrate the scope of this approach, the influence of different fabrication methods on the permeation performance of two membrane extremes, *viz.* thin MMMs with well mixed and DLMs with completely segregated components, was studied in relation to $CO_2$ capture.

### 5.1 Experimental

#### 5.2.1 Synthesis

***Cu-BDC nanosheet scaled-up synthesis:*** Cu-BDC nanosheets were prepared following the bottom-up route introduced by Rodenas *et al.*[32] In this study, the nanosheet synthesis was modified and scaled up where the amount of reactants and solvent was multiplied by 50. The linker layer was prepared by dissolving 1.5 g terephthalic acid (Sigma Aldrich, 99 %) in a mixture of 100 mL N,N-dimethylformamide (DMF, Sigma Aldrich, >99 %) and 50 mL acetonitrile (Sigma Aldrich, analytical grade) and was added to the 500 mL Duran® bottle as the bottom layer. The intermediate layer (spacer) consisted of 100 mL DMF and 100 mL acetonitrile and was added gently to the bottle. The top layer was prepared by dissolving 1.5 g $Cu(NO_3)_2 \cdot 3H_2O$ (Sigma Aldrich) in a mixture of 100 mL acetonitrile and 50 mL DMF and was added to the bottle without mixing. Then, the bottle was kept in the oven at 40 °C for 24h. The as-synthesized nanosheets were collected by centrifugation and after removing the supernatant, the solvent were replaced with fresh DMF. This procedure was repeated three times and the next step was using tetrahydrofuran (THF, Sigma Aldrich, >99 %) to centrifuge samples via identical procedure as DMF washing (in this study both chloroform and THF were used for comparison). Finally, the synthesized nanosheets were dispersed in chloroform (Sigma Aldrich, anhydrous) for membrane preparation.

***Free-standing MMMs preparation via solution-casting:*** to fabricate the free-standing membranes, Polyactive$^{TM}$ ($M_w$~35000 g/mol, Polyvation, NL) granules were degassed for 2 h at 353 K under vacuum and then, 0.2 g dried polymer was dissolved in 2.5 mL chloroform. The proper amount of Cu-BDC nanosheet suspension in chloroform were ultrasonicated for 20 min. Then, 10 % of dissolved polymer was added to the suspension and was stirred for 2 h. The rest of the polymer solution was added to the mixture and stirred overnight. The solvent/filler-polymer weight ratio was kept constant (95/5) in all cases. The casting solution was poured on the Teflon petri dish and was covered with a top-drilled box (30.5 cm length x 15.5 cm height x 23.0 cm width) overnight under chloroform-saturated atmosphere. Finally, the membranes were treated under vacuum at 353 K for 24 h. The neat membranes were also prepared with identical approach, without the addition of nanosheets.

***Thin supported MMMs preparation via dip-coating:*** to prepare the thin supported MMMs, polyacrylonitrile (PAN; supplied from AMT® Co. Ltd) porous UF membrane with pore size around 100 nm and $ZrO_2$ coated alumina (supplied from Fraunhofer IKTS, Germany) with pore size around 3 nm were used as support. The dip-coating method was used to coat the supports with the polymer/nanosheet mixture (4 and 8 wt.% nanosheet in Polyactive$^{TM}$ solution). The mixture used for dip-coating was prepared in a similar way as for the free-standing membranes. However,

the amounts were increased by 12 times to prepare the required volume for dip-coating process. The PAN support was pretreated by washing firstly with demi water, and keeping it in the mixture of water and ethanol (50/50) overnight to fill the pores of support. Prior to dip-coating, water droplets were smoothly wiped off from the surface of the support by filter paper. The support was sealed on the Teflon plate by Kapton® tape and was deeply soaked in 3 wt.% PDMS in hexane solution (*Sylgard*® 184 Silicone Elastomer). In order to cure the PDMS gutter layer, the support was heat-treated at 100 °C for 30 min. Then, the PDMS coated support was soaked in the polymer/nanosheet mixture vertically and left to dry in a closed Petri dish at room temperature for 24 h. The same procedure was used to prepare the thin membranes on the $ZrO_2$-alumina support. For the sample identification, the *x*ns-*y*PA-PDMS-MMM abbreviation was used where *x* represents the weight percentage of nanosheet based on polymer and *y* refers to the polymer concentration in the coating solution.

*Thin supported DLM preparation via drop-casting*: to fabricate the thin dual layer membranes (DLM), the PAN support was firstly mounted in the vacuum filtration apparatus and was coated with 1 mL highly diluted Cu-BDC nanosheet suspension (0.05 wt.%). After drying, the surface of the nanosheets layer was coated with PDMS for the membranes with gutter layer, as described above. Then, 1 mL Polyactive$^{TM}$ solution (0.25 to 0.5 wt.% in Chloroform) was dropwise added on the PDMS or nanosheet layer and the membranes were dried at room temperature for 24 h. Similarly as above for the sample identification the *x*ns-*y*PA-PDMS-DLM abbreviation was used.

### 5.2.2 Characterization

Transmission electron microscopy (TEM) analysis was carried out using a JEOL JEM-2010 microscope operated at 200 keV. Micrograph acquisition was performed with GATAN Digital Micrograph 1.80.70 software. A few drops of MOF dispersed in chloroform were added on a carbon-coated copper grid and then after drying it was placed on the specimen.

Field emission scanning electron microscopy (FE-SEM) was performed in Nova NanoSEM 450 (Thermo Fisher Scientific) operated at 10 kV. To get the cross section images of the membranes, the samples were immersed and fractured in liquid nitrogen and gold-coated prior to scanning.

Atomic force microscopy (AFM) was performed with a Veeco Multimode Nanoscope 3A microscope operating in tapping mode.

XRD patterns of nanosheets and MMMs were obtained in a Bruker-D8 Advance diffractometer using Co-*Kα* radiation (*λ* = 1.78897Å, 40 kV, 30 mA). The range of 5-60° of 2Ө was scanned using a step size of 0.02° and a scan speed of 0.2 s per step in a continuous scanning mode. The

XRD patterns of thin MMMs were obtained by Bruker-D8 Discovery diffractometer and using Cu-$K\alpha$ radiation ($\lambda$ = 1.54059 Å, 40 kV, 30 mA).

$CO_2$ and $N_2$ adsorption isotherms of Cu-BDC nanosheets were recorded in a Tristar II 3020 (Micromeritics) setup at 273 and 77 K, respectively. Prior to the measurements, the samples were degassed at 423 K under vacuum overnight.

### 5.2.3 Gas permeation experiments

The separation of $CO_2$ and $N_2$ mixtures at 298 K was conducted in a home-made setup described elsewhere.[43] The membrane samples (area: 1.13 or 3.14 $cm^2$) were prepared and mounted in a flange between two Viton® O-rings. A macroporous stainless steel disc (316L, 20 µm nominal pore size) was used as support. The permeation module was placed inside a convection oven for controlling the temperature. A mixture (133 ml·$min^{-1}$, STP) of $CO_2$ (15 mol.%) and $N_2$ (85 mol.%) flow was used as feed and helium (3 ml·$min^{-1}$, STP) was used as a sweep gas. The feed pressure was adjusted to 2 bar (absolute pressure) using a back-pressure controller at the retentate side while the permeate side was kept at atmospheric pressure (1 bar absolute pressure) for all measurements. An online gas chromatograph (Interscience Compact GC) equipped with a packed Carboxen® 1010 PLOT (30 m x 0.32 mm) column and TCD detector was used to analyse the permeate stream.

Gas separation performance was defined by two parameters: the separation factor ($\alpha$, or selectivity) and the gas permeability or permeance. The thin membranes performance mainly defined by permeance which is the pressure normalized flux of the membrane and is reported in Gas Permeation Unit (GPU) where 1 GPU = $1 \times 10^{-6}$ $cm^3$ (STP)/($cm^2$·s·cmHg) or $3.35 \times 10^{-12}$ mol·$s^{-1}$·$m^{-2}$·$Pa^{-1}$. The permeance for the component $i$ ($P_i$) was calculated as follows (Equation 1):

$$P_i = \frac{F_i}{\Delta p_i \times A} \qquad (1)$$

Where $F_i$ denotes the molar flow rate of compound $i$, $\Delta p_i$ is the partial pressure difference of $i$ across the membrane, and $A$ is the membrane area.

The separation factor or mixed gas selectivity ($\alpha$) of $CO_2$ over $N_2$ was defined as the ratio of their permeance and can be expressed as follows:

$$\alpha_{CO_2,N_2} = \frac{P_{CO_2}}{P_{N_2}} \qquad (2)$$

Where $P_{CO_2}$ and $P_{N_2}$ represent the permeance of $CO_2$ and $N_2$, respectively.
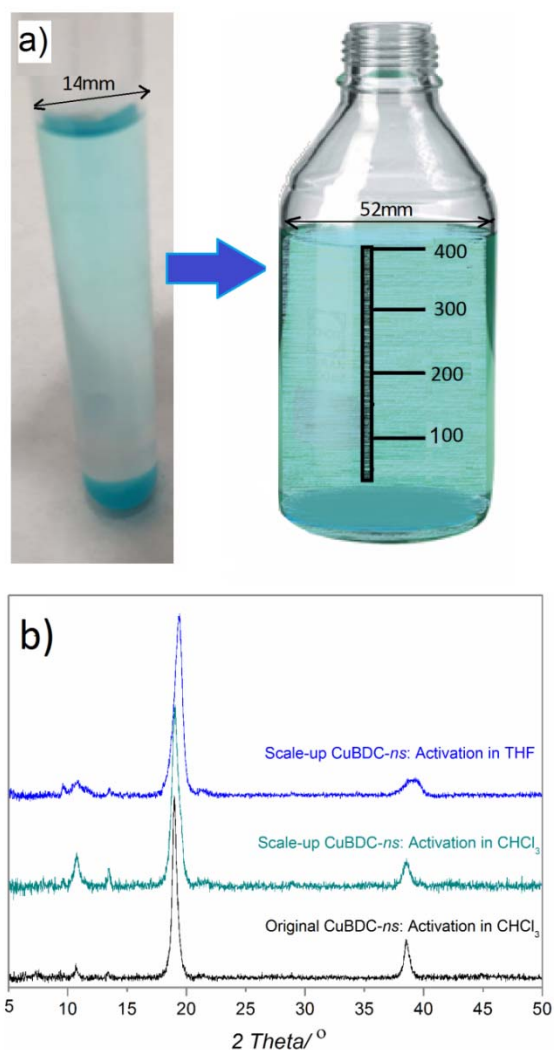
**Figure 5.1.** Cu-BDC nanosheet original and scaled-up synthesis (a), XRD patterns of original and scaled-up synthesis using chloroform and THF (b). [34]

## 5.2 Results and discussion

### 5.3.1 Characterization scaled-up Cu-BDC nanosheets

Scaled up synthesis of Cu-BDC nanosheet was successfully performed by using the layered route (Figure 5.1a) reported by our group.[39]  XRD results of the sample before and after washing with THF indicate no significant difference in crystallinity (Figure 5.1b).Transmission electron microscopy (TEM) and electron diffraction show the morphology and plane orientation of nanosheets. The equal *d*-spacing of the basal planes in the *xy* direction indicates the tetragonal projection of the crystal structure. (Figure 5.2a and 5.2b).[40]
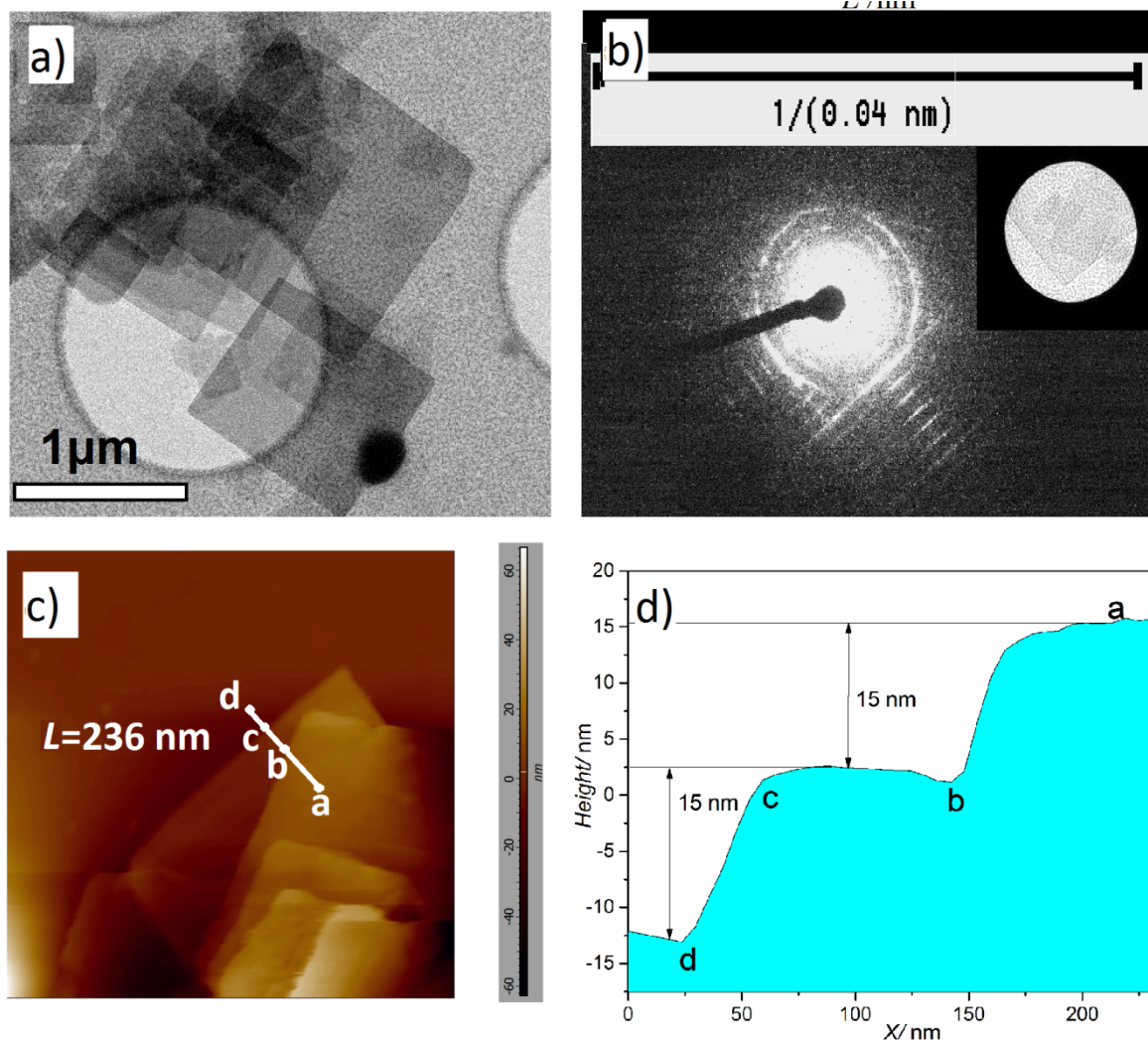
**Figure 5.2.** TEM images and electron diffraction pattern of region shown in inset (a, b), AFM image showing the thickness of Cu-BDC nanosheets (c, d).

Atomic force microscopy (AFM) images of the nanosheets presented in Figure 2c show the square platelet structures with lateral sizes of 1-5 µm and an approximate thickness of 15 nm (Figure 5.2d). $CO_2$ and $N_2$ adsorption of the scaled-up sample (Figure 5.3a, 5.3b) show an uptake of $CO_2$ of 0.8 mmol·$g^{-1}$ at 1 bar and a BET area of 55 $m^2$·$g^{-1}$. These results are in good agreement with the reported adsorption capacity and BET area of the samples of the original synthesis.[34] The calculated yield of the scaled up synthesis, however, was lower than original synthesis (4% *vs.* 8%), which might be attributed to the dominant influence of the interfacial area in the three layers approach. Although the amount of reactants was increased up to 50 times, the interface area in scaled-up synthesis was approximately 3.8 times larger than in the original synthesis (Figure 5.1a). This confirms the key role of interface area in promoting the yield of reaction by providing the sufficient surface to contact the reactants by diffusional transport.
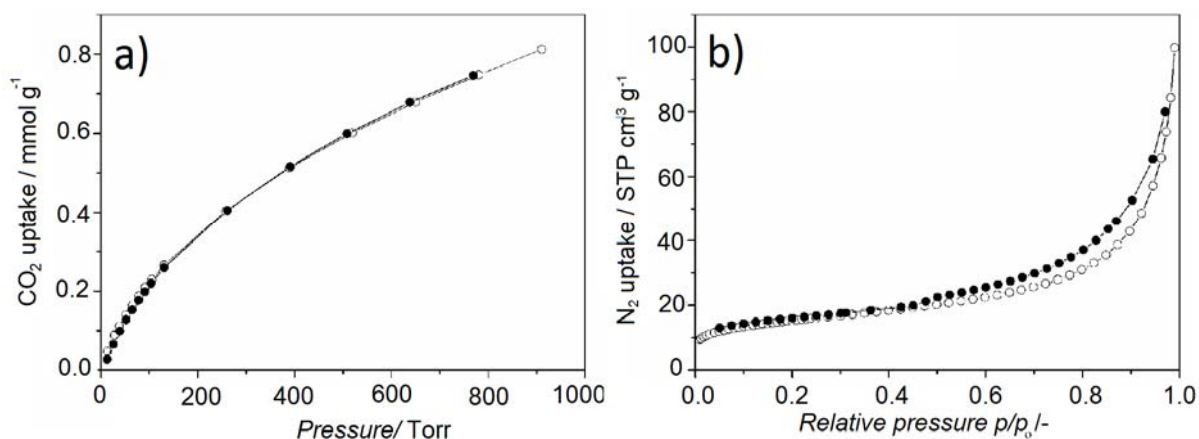
**Figure 5.3.** $CO_2$ and $N_2$ adsorption of Cu-BDC nanosheets at 273 and 77 K (g, h) (the open and closed symbols represent the adsorption and desorption data, respectively.

### 5.3.2 MMM characterization

Thin supported membranes comprising Cu-BDC nanosheets and Polyactive[TM] were prepared on porous PAN and $ZrO_2$-alumina supports using two approaches; *i*) Dip-coating and, *ii*) Drop-casting to obtain mixed matrix and dual layer thin membranes, respectively (Figure 5.4 & 5.5).

2D and 3D AFM images of thin MMM (8ns-3PA; 8 wt.% nanosheets in 3 wt.% Polyactive[TM] solution) prepared *via* dip-coating are shown in Figure 6a & 6b. Cross-sectional FE-SEM images of this membrane coated on $ZrO_2$-alumina and PAN supports (without PDMS gutter layer) are shown in Figure 5.6(c-f). The cross-sectional FE-SEM images reveal that the thin layer formation was successful without polymer penetration in to the finger-like pores of the PAN support, which could be attributed to the fast solvent ($CHCl_3$) evaporation and vertical orientation of membrane during drying (Figure 5.5).[44] Comparing the thin MMMs coated on PAN and on $ZrO_2$-alumina revealed that the thickness was 50% lower in case of $ZrO_2$-alumina support (351 *vs.* 708 nm) (Figure 5.6c & 5.6d). This is ascribed to the lower top surface roughness of $ZrO_2$-alumina (pore size ~3 nm) and adherence of less coating solution to the support.

In contrast, using drop-casting resulted in a smooth surface of the thin membranes, representing horizontally aligned nanosheets by vacuum filtration on the support (Figure 5.7a & 5.7b) and an adequate coverage of the nanosheets by the polymer layer (Figure 5.7c & 5.7d).
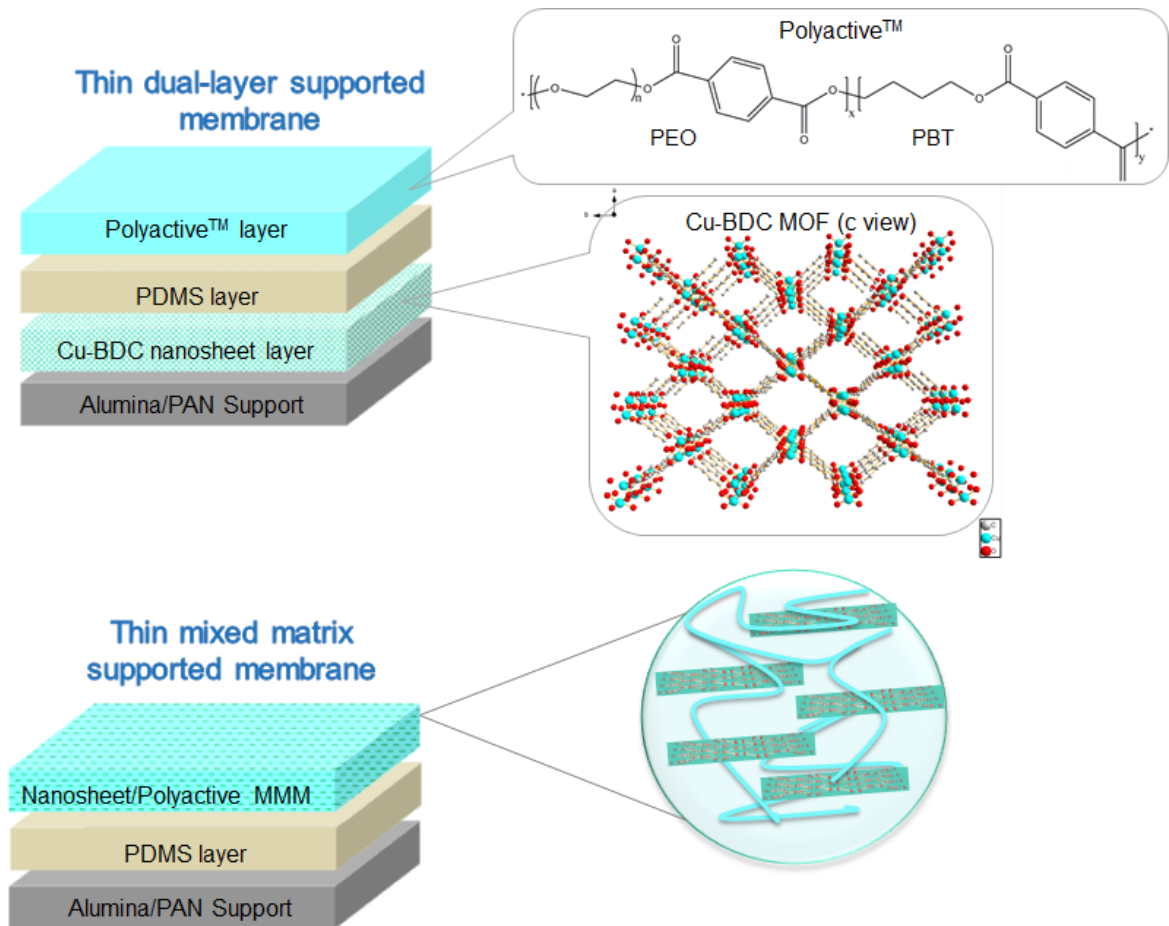
**Figure 5.4.** Scheme of thin supported dual layer (*top*) and mixed matrix (*bottom*) membranes prepared *via* dip-coating and drop-casting methods.
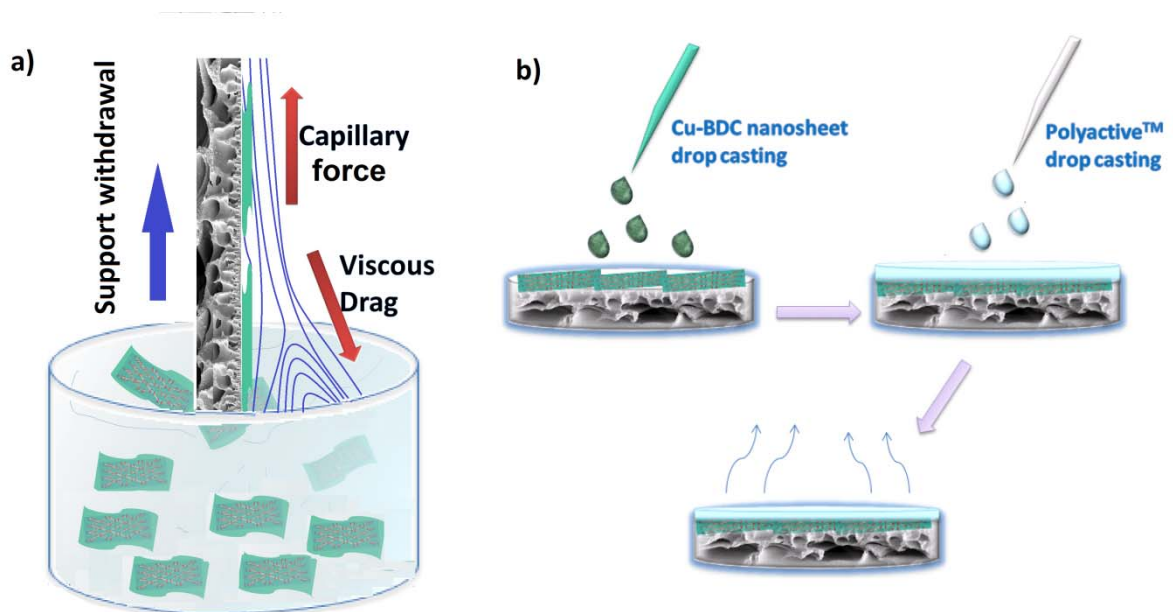


**Figure 5.5.** Scheme of various driving forces in dip-coating process a) and drop casting procedure b).

XRD patterns of Cu-BDC nanosheets and free-standing membranes are compared in Figure 8a. Polyactive[TM] neat membrane shows a certain degree of crystallinity [45]. However, by addition of Cu-BDC nanosheets into Polyactive[TM], the reflections of the polymer that appeared in the range of $2\Theta$ ~22-27° became wider and overlapped (Figure 5.8a). Moreover, the polymer reflection slightly shifted to higher $2\Theta$ (lower $d$-spacing), showing reduction in polymer chains spacing as was previously reported by Zornoza *et al*. [43, 46] Further, the typical reflections of Cu-BDC nanosheets which were indexed as (-2 0 1) and (-4 0 2) shifted slightly and their intensity decreased. In turn, the reflections of the (1 1 0), (0 4 0) planes (Figure 8c & 8d), are more visible in the MMMs. These results indicate a change in the orientation of the nanosheets in free-standing MMMs which might have arisen from shear forces during membrane preparation and solvent evaporation.[11, 47] In contrast, thin supported neat Polyactive[TM] membranes and the relevant thin MMMs showed different patterns as indicated in Figure 8b. This might be attributed to the ultrafast drying of the thin layer during the dip-coating process, changing the polymer chain packing and resulting in broadened reflections of thin supported membranes compared to free-standing membranes. The addition of nanosheets to the polymer slightly changed the crystallinity of the neat membrane and the nanosheet reflections corresponding to (-2 0 1) and (1 1 0) planes with direction toward pore accessibility were observed. However, the reflections attributed to (0 0 1), (0 4 0) and (-4 0 2) planes were not strong enough which might be due to the less loading of nanosheets or different orientation in the thin membranes.
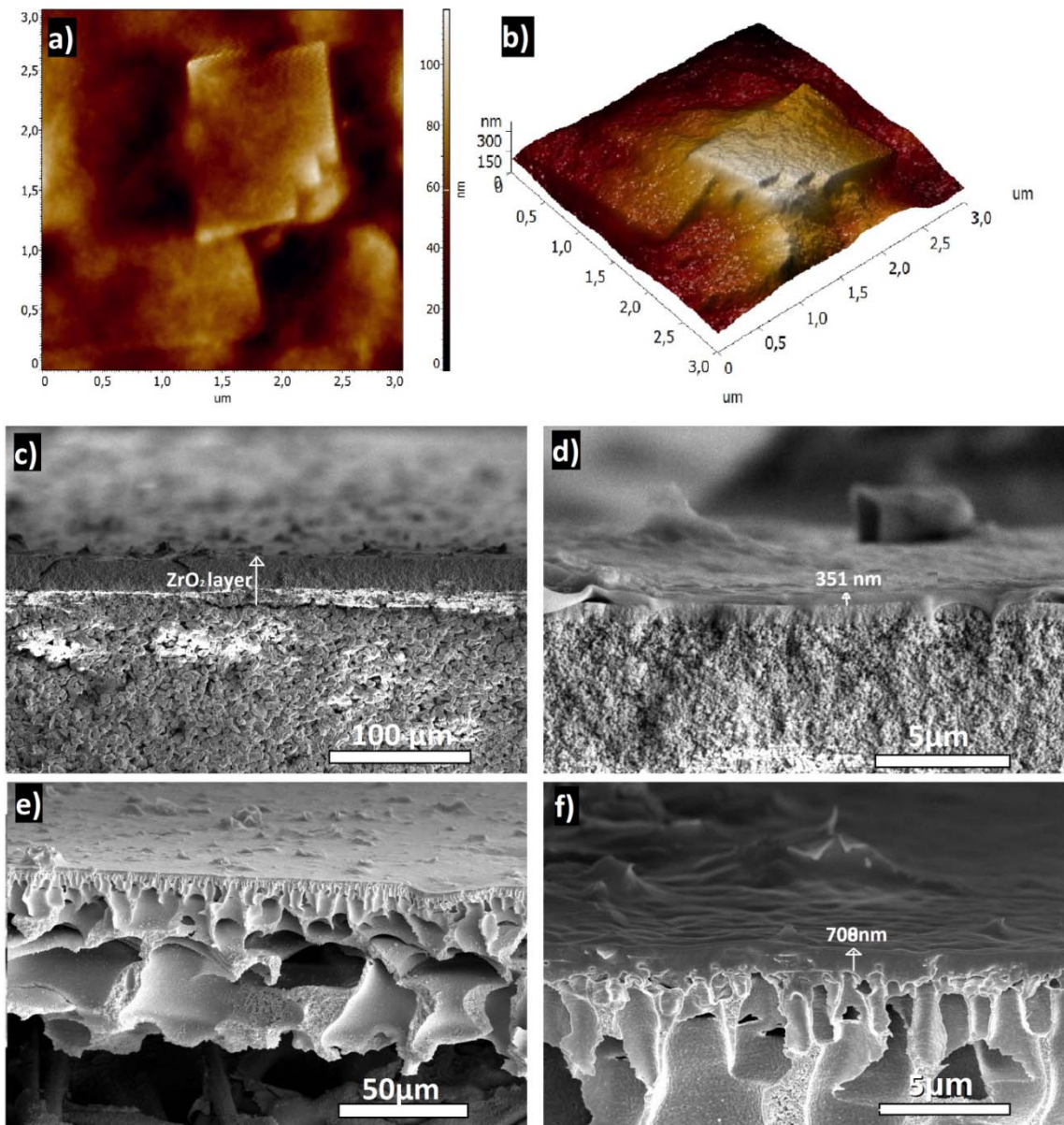
**Figure 5.6.** AFM  2D and 3D topography images (a, b) and FE-SEM images of thin MMMs on ZrO₂-alumina (c, d) and PAN support (e, f) prepared by dip-coating in the mixture of 8 wt.% nanosheet in Polyactive™ (8ns-3PA-MMM).
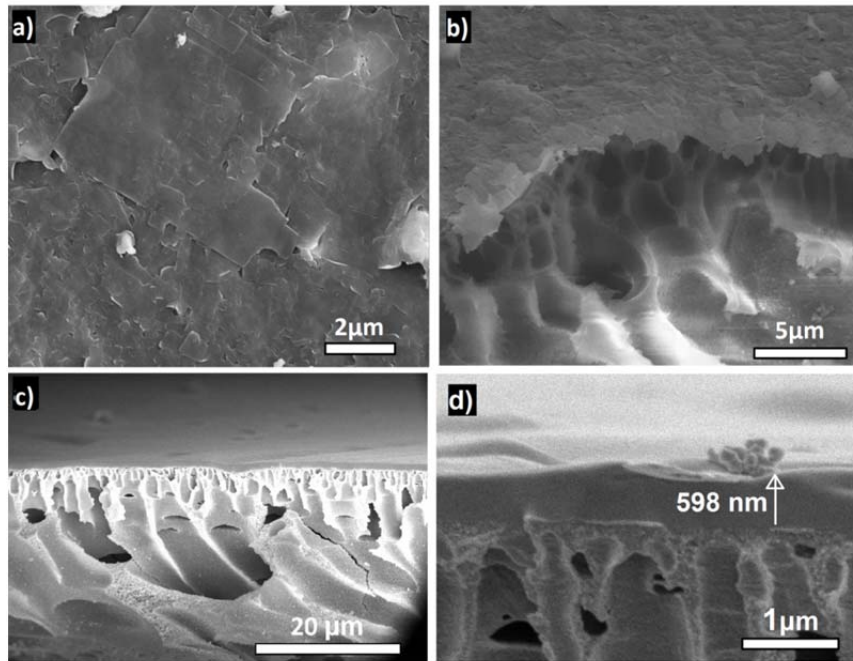
**Figure 5.7.** FE-SEM images of surface (a) and cross-section (b) of nanosheets coated on PAN and cross-section images of dual layer thin membranes on PAN prepared by drop-casting (ns-0.25PA-PDMS-DLM) (c, d).
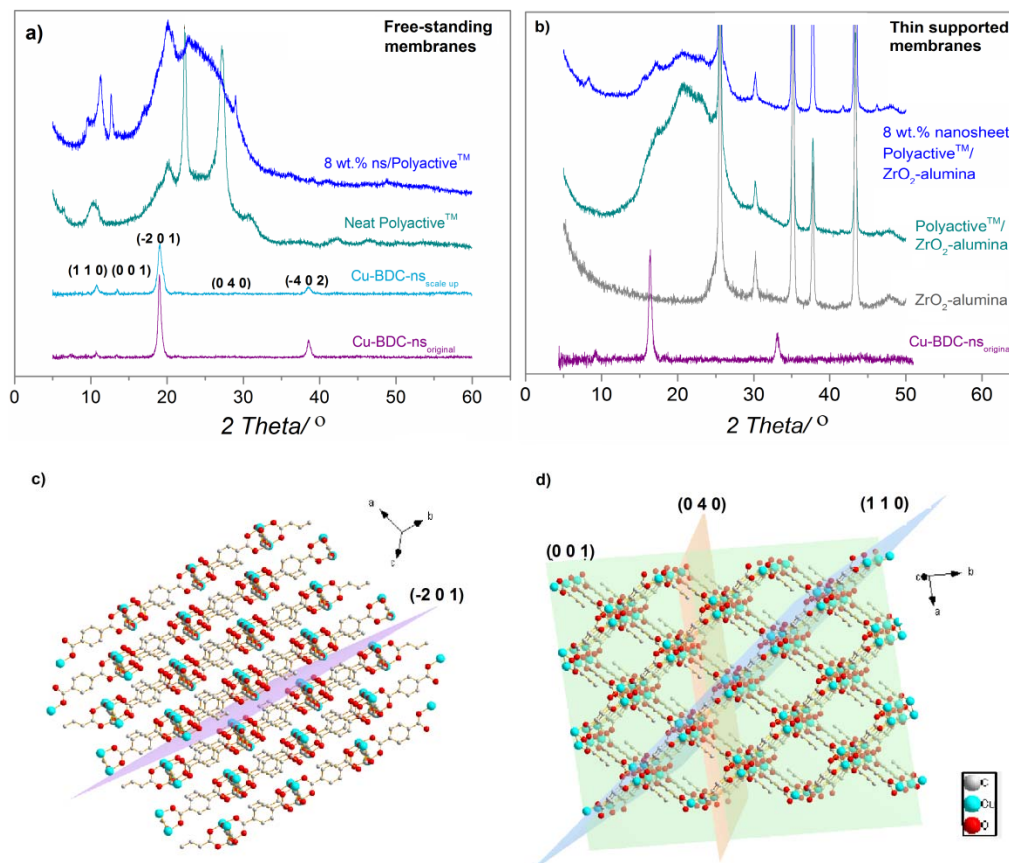


**Figure 5.8.** XRD patterns of Cu-BDC nanosheets, free-standing membranes (using Co-*Kα*) (a) and thin membranes (using Cu-*Kα*-radiation) (b), crystal structure of Cu-BDC showing (-2 0 1) (c) and (1 1 0), (0 4 0) and (0 0 1) planes (d).

### 5.3 Gas separation performance

The free-standing membranes fabricated by solution casting were tested under identical condition as reported previously.[25] Table 1 shows their $CO_2$ and $N_2$ separation performance parameters. The increase in nanosheet loading (from 0 to 16 wt.%) resulted in a monotonous improvement in selectivity (from 56 to 66) along with a decrease of gas permeance. The obtained permeation results are in good agreement with reported data of MMMs using Cu-BDC nanosheets with Matrimid® or 6FDA-DAM as the continuous matrix.[34, 40, 41] The decrease in permeance of the MMMs is in line with XRD patterns of the free-standing membranes, showing reduction in polymer chains distance and a partial change in orientation of nanosheets towards non-accessible porosity of MOF in MMMs. Further, the flexible polymer chains might penetrate into pores of the nanosheets and partially block the porosity of MOF.[45]

The thin membranes prepared by two different approaches (dip-coating and drop-casting methods) were tested under identical conditions as for the free-standing membranes. The permeation results of thin supported MMMs prepared by dip-coating with and without using PDMS as gutter layer are presented in Figure 5.9a. The selectivity of the neat thin membrane was very low (~10) which could be attributed to the large pore size of the PAN support and defect formation. Coating with a PDMS gutter layer improved slightly the selectivity. In order to fabricate a thin neat Polyactive™ membrane with expected intrinsic selectivity, a double coating approach was applied. However, a considerable drop in $CO_2$ permeance to ~6 GPU resulted (still above the free standing sample) along with an increase in selectivity to 54, similar as for the pure Polyactive™ membrane. For thin MMMs prepared under identical conditions with single coating, an increase in selectivity (ranging from 58 to 72) was achieved even with an improvement of permeance. The performance of thin MMMs prepared with PDMS gutter layer was only slightly different from the membranes without gutter layer. Therefore, high aspect ratio fillers (nanosheets) could make the PDMS gutter layer and its optimization superfluous with the advantage of obtaining higher selectivity.[1, 48] Interestingly, using a lower concentration of polymer solution (3 wt.%) resulted in certain improvement in permeance of the thin MMM (to ~40 GPU) and increasing the selectivity up to 77 (Figure 5.9a; purple symbol). The selectivity is even higher than the optimized free standing MMM (table 1) which might be attributed to the different polymer chains packing and nanosheet orientation as revealed by XRD studies. [11]

To investigate the role of support properties, $ZrO_2$-alumina with much smaller pore size (~3 nm) was used to prepare thin membranes via dip-coating (Figure 5.9b). The neat thin Polyactive™ membrane without PDMS gutter layer was apparently defect-free showing higher selectivity and permeance than the PAN supported membrane. The thin MMMs coated on $ZrO_2$-alumina showed a simultaneous improvement in permeance and in selectivity, whereas the

**Table 5.1.** Permeation performance of the free-standing MMMs comprising Cu-BDC nanosheets and Polyactive[TM] at 2 bar and 25 °C.

| Membrane | $CO_2$ Permeance (GPU) | $N_2$ Permeance (GPU) | $\alpha_{CO2/N2}$ - | $\delta$ (µm) |
|---|---|---|---|---|
| Neat PA | 3.9 ± 0.2 | 0.07 ± 0.00 | 56 ± 2 | 28 ± 1 |
| 4 wt.% ns/PA | 2.6 ± 0.1 | 0.04 ± 0.00 | 59 ± 1 | 37 ± 1 |
| 8 wt.% ns/PA | 2.5 ± 0.2 | 0.04 ± 0.00 | 62 ± 0 | 35 ± 1 |
| 16 wt.% ns/PA | 3.3 ± 0.2 | 0.05 ± 0.00 | 66 ± 2 | 20 ± 1 |

relevant PAN supported thin MMMs (without PDMS gutter layer) only showed improvement in selectivity and decrease in permeance. The thin MMMs coated on PAN, however, showed a higher selectivity using the same formulation, which might be attributed to the influence of support resistance on selectivity by Knudsen diffusion as reported by Kattula *et al*. for polymeric membranes [1, 48] and by Kapteijn *et al*. for zeolite membranes.[49] Decreasing the polymer concentration from 5 to 3 wt.% in the $ZrO_2$-alumina supported thin MMMs resulted in a further increase in permeance to ~40 GPU while selectivity hardly changed (65) (Figure 9b; purple symbol). Considering the thickness, the FE-SEM images (Figure 5.10) showed a 50-60% reduction in the thickness of the thin membranes. The same dilution for the PAN supported membranes resulted in an improvement of permeance from 25 to 40 GPU and selectivity from 72 to 77. This higher selectivity is attributed to the lower resistance of the PAN support compared to the small pore size $ZrO_2$-alumina support.[1, 50] Finally, 3 wt.% was found the lower limit for diluting the polymer concentration using dip-coating; at lower concentrations no defect-free thin film was obtained.

To utilize the morphological advantages of high aspect ratio nanosheets more efficiently in thin film formation, thin PAN-supported dual layer membranes (DLMs) were prepared by drop-casting (Figure 5.4).  Their permeation properties are indicated in Figure 5.9c. The higher permeance of the thin DLMs than MMMs confirms that the polymer chains packing and the orientation of the nanosheets were not influenced. However, the selectivity of the dip-coated thin MMMs was higher than the thin DLMs, which signifies the role of spatial distribution of nanosheets and the polymer chains distance on the selectivity in thin MMMs.[51] A PDMS gutter layer had a more pronounced influence on the permeation performance of thin dual layer membranes. The permeance with a PDMS gutter layer was 66% higher than without PDMS while the selectivity did not change significantly (Figure 9c; blue & green arrows). Decreasing the Polyactive[TM] concentration in the drop-casting solution from 0.5 to 0.25 wt.% further improved the permeance (2.5 times) of the thin membranes while selectivity was slightly decreased (16%). As a result, it can be concluded that preparing thin dual layer membranes via drop-casting is promising in terms of permeance. However, the spatial distribution of nanosheets, like in MMMs, is an essential parameter to effectively improve the selectivity of the thin membranes.
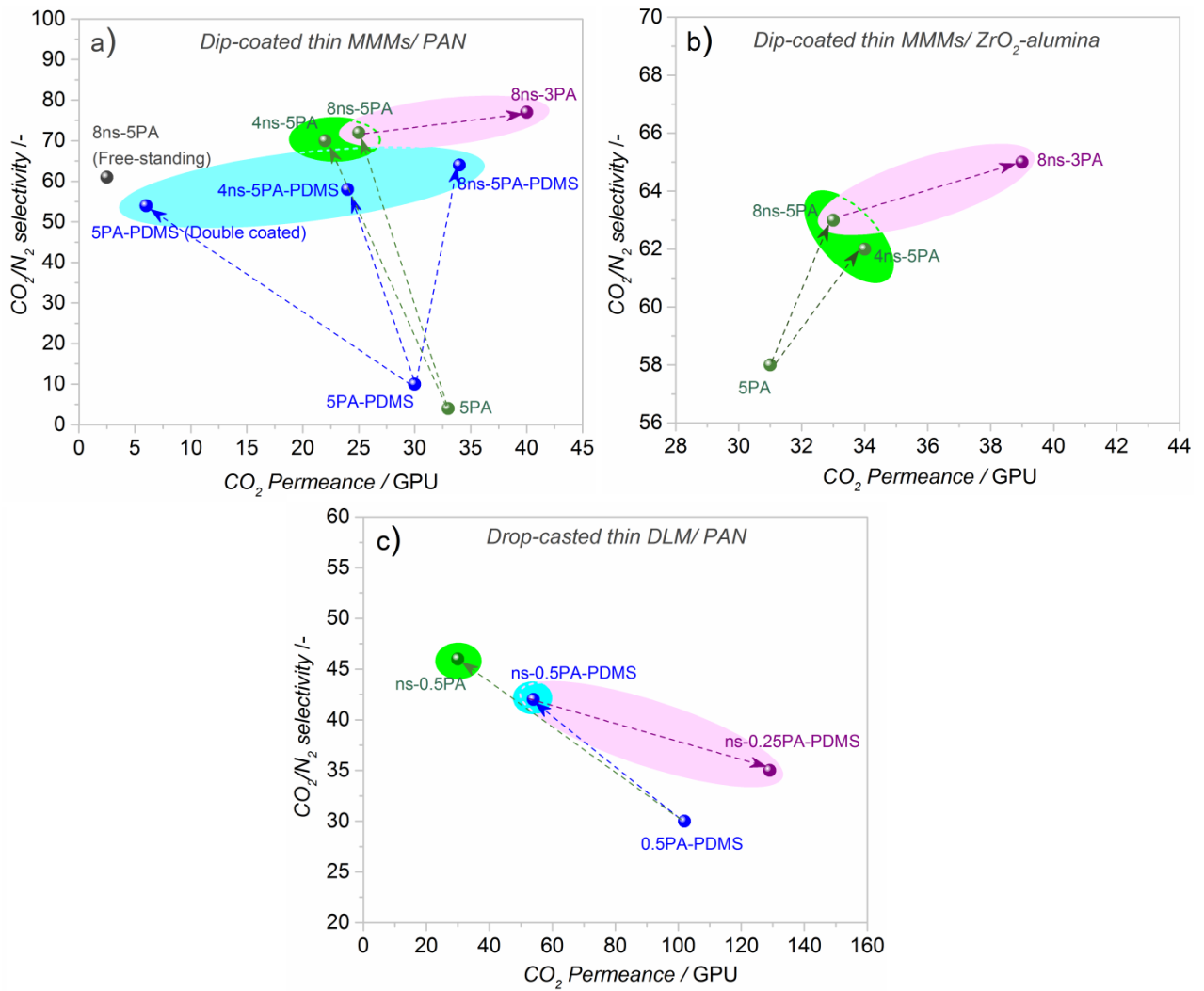
**Figure 5.9.** $CO_2$ and $N_2$ separation performance of dip-coated thin MMMs on (a) PAN, and (b) $ZrO_2$-alumina support, (c) thin dual layer membranes drop-casted on PAN support at 298 K and 2 bar absolute feed pressure (mixed gases). In the sample identification x represents the weight percent of nanosheets based on polymer and y refers to the polymer concentration in the coating solution.
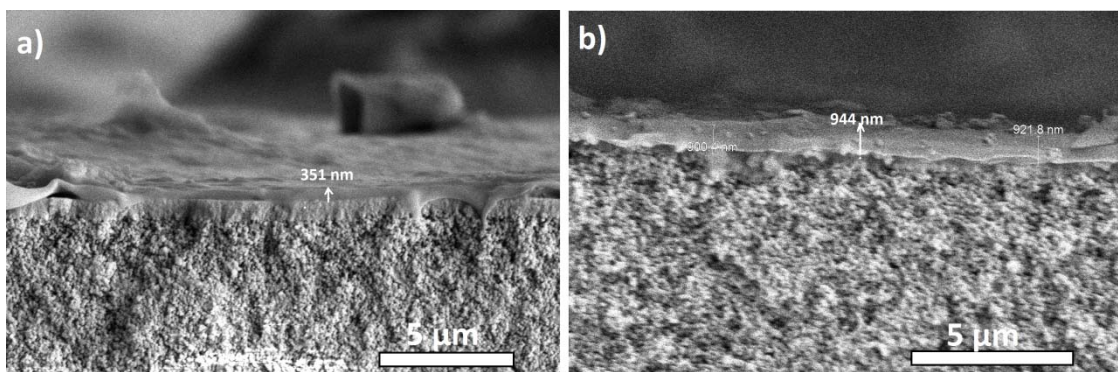


**Figure 5.10.** Cross-sectional FE-SEM images of thin MMMs coated on $ZrO_2$-alumina prepared by dip-coating using mixture of 8 wt.% nanosheets dispersed in 3 wt.% a) and 5 wt.% b) of Polyactive™ solution (the thickness of the thin MMMs are shown).

### 5.3.1 Comparison of thin membrane performance vs. Robeson upper bound

Historical analysis indicates that there is a trade-off between permeability and selectivity of the free-standing membranes (Robeson upper bound) which shows the limits of separation performance quality. Park *et al.* reported the method of calculating an upper bound for thin supported membranes in which the contribution of the support in the overall permeation performance of the composite membranes were incorporated.[1] By taking the following assumptions and applying a series model (Eq. 3a, 3b) the upper bound limit for thin PAN supported membranes was calculated; (*i*) 1 µm thin layer on top of the support, (*ii*) Knudsen diffusion through the porous support (Eq. 4) and (*iii*) using the Robeson upper bound relation (Eq. 5) where $P_i^C$ and $P_i^S$ are the permeance of species *i* in composite membrane and the support, respectively. Moreover, $M_i$ and $\delta_A$ are the molecular weight of species *i* and the thickness of selective layer (F) . By applying Knudsen diffusion relation (Eq. 4), the $CO_2$ permeance of the PAN support based on the experimental $N_2$ permeance ($P_{N2} \sim$ 45776 GPU at 1 bar and 25 °C) was calculated. Figure 5.11 shows the calculated upper-bound for 1 µm thin membranes on the PAN support.

$$P_{CO_2}^C = \left( \frac{\delta_F}{P_{CO_2}^F} + \frac{1}{P_{CO_2}^S} \right)^{-1} , \quad P_{N_2}^C = \left( \frac{\delta_F}{P_{N_2}^F} + \frac{1}{P_{N_2}^S} \right)^{-1} \qquad (3a, 3b)$$

$$P_{CO_2}^S = P_{N_2}^S \times \sqrt{\frac{M_{N_2}}{M_{CO_2}}} = 0.798 \times P_{N_2}^S \qquad (4)$$

$$P_{CO_2}^R = 30,967,000 \times \left( \alpha_{CO_2,N_2} \right)^{-2.888} \qquad (5)$$

Comparison with reported MOF based thin supported and asymmetric MMMs, the thin membranes in this study showed a superior $CO_2/N_2$ separation performance when utilizing high aspect ratio nanosheets, even in combination with a selective polymer (Table 5.2). The selectivity of the studied membranes exceeded most of the reported values of MOF based thin MMMs. Although different types of MOF fillers were incorporated in the glassy and rubbery polymer matrix, the results show that by using small pore size ZIFs and high aspect ratio nanosheets in rubbery polymers the selectivity can be enhanced. This is attributed to the defect covering properties of the nanosheets and their perpendicular orientation towards gas permeation when homogeneously dispersed in the MMM.
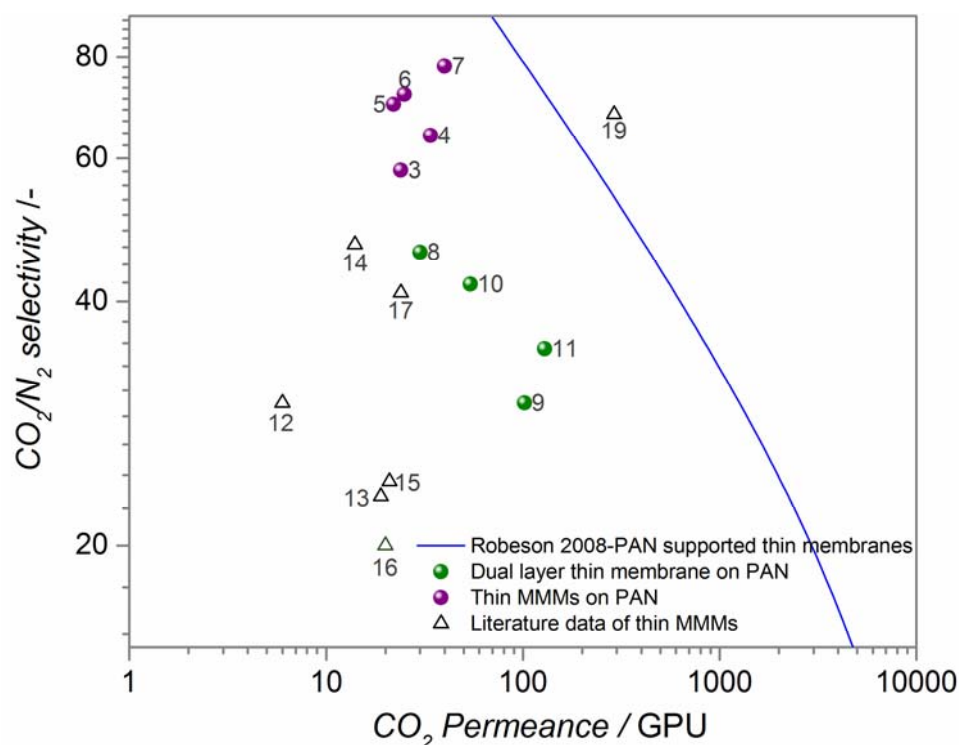
**Figure 5.11.** Effective Robeson limit of $CO_2$ / $N_2$ separation performance of PAN supported thin membranes (*blue line*, calculation in SI) and the comparison of thin supported MMMs (*purple circles*) and dual layer membranes (*green circles*) at 298 K and 2 bar absolute feed pressure ($CO_2/N_2$ mixed gases 15/85 by volume). Experimental and literature data of MOF-based thin supported and asymmetric MMMs are shown for comparison and listed in Table 2 (*open symbols*) and Table S1 (*closed symbols*).

**Table 5.2.** Separation performance of MOF based thin supported and asymmetric MMMs reported in literature and the comparison with this study.

| Thin MOF based MMMs | Feed conditions $p$(bar), $T$($^0$C) | Feed gas $CO_2/N_2$ ratio | $CO_2$ Permeance (GPU) | $\alpha_{CO2/N2}$ - | Data no.[3] | Ref |
|---|---|---|---|---|---|---|
| Cu-MOF/POZ (1500 nm) | 2, 25 | Single gas | 6 | 30 | 12 | [52] |
| Cu-BTC/Matrimid (asymmetric) | 5, 35 | 35/65 | 19 | 23 | 13 | [53] |
| Cu-MOF/Pebax (1500 nm) | 2, 25 | Single gas | 14 | 47 | 14 | [54] |
| MIL-53/Matrimid (asymmetric) | 5, 35 | 35/65 | 21 | 24 | 15 | [53] |
| ZIF-8/Matrimid (asymmetric) | 5, 35 | 35/65 | 20 | 20 | 16 | [53] |
| S-MIL-53/Ultem(asymmetric) | 5, 25 | Single gas | 24 | 41 | 17 | [55] |
| ZIF-7/ Pebax (500 nm) | 3.5, 25 | Single gas | 291 | 67 | 19 | [56] |
| Dual layer Cu-BDC/Polyactive (600 nm)[1] | 2 , 25 | 15/85 | 129 | 35 | 11 | This study |
| MMM Cu-BDC/Polyactive (700 nm)[2] | 2 , 25 | 15/85 | 40 | 77 | 7 | This study |

1 With PDMS as gutter layer on PAN support (ns-0.25PA-PDMS)
2 Without PDMS as gutter layer on PAN support (8ns-3PA)
3 Data number refers to Figure 5.11.

For the other extreme, the fully segregated polymer and nanosheet layers in the dual layer membrane, their permeance was promising in comparison with most reported thin MOF-based MMMs, although the selectivity was lower than for the homogeneous MMM.

### 5.4 Conclusions

In summary, utilizing Cu-BDC nanosheets prepared in a scaled-up synthesis and the selective Polyactive™ polymer to fabricate supported thin MMMs and DLMs was demonstrated to results in membranes with improved separation performance. The main role of nanosheets was found to cover the defects during the thin membrane formation, making a gutter layer superfluous, and improving the $CO_2/N_2$ selectivity of the thin membranes up to 77.

Mixed matrix and dual-layer thin membranes of Cu-BDC nanosheets and polymer, prepared via dip-coating and drop-casting, were compared as two extreme systems with homogeneously mixed or completely segregated components for their separation performance. Using Cu-BDC nanosheets well dispersed in thin supported mixed matrix membranes significantly improved the selectivity, even higher than identical free-standing membranes (77 *vs.* 60), and the $CO_2$ permeance to 40 GPU.

Comparison of PAN and $ZrO_2$-alumina as supports shows that pore size, porosity and thickness affect the obtained separation layer thickness and their resistance can negatively affect the $CO_2/N_2$ selectivity. The findings in this study are relevant in development of optimized preparation methods of defect-free thin supported MMMs.

# References

[1]     H.B. Park, J. Kamcev, L.M. Robeson, M. Elimelech, B.D. Freeman, Maximizing the right stuff: The trade-off between membrane permeability and selectivity, Science, 356 (2017) 1-10.

[2]     X. He, Membranes for Natural Gas Sweetening, in: E. Drioli, L. Giorno (Eds.) Encyclopedia of Membranes, Springer Berlin Heidelberg, Berlin, Heidelberg, 2016, pp. 1266-1267.

[3]     C.A. Scholes, M.T. Ho, A.A. Aguiar, D.E. Wiley, G.W. Stevens, S.E. Kentish, Membrane gas separation processes for CO2 capture from cement kiln flue gas, International Journal of Greenhouse Gas Control, 24 (2014) 78-86.

[4]     E. Sjöberg, L. Sandström, O.G.W. Öhrman, J. Hedlund, Separation of CO2 from black liquor derived syngas using an MFI membrane, Journal of Membrane Science, 443 (2013) 131-137.

[5]     J.M.S. Henis, M.K. Tripodi, The Developing Technology of Gas Separating Membranes, Science, 220 (1983) 11-17.

[6]     R.W. Baker, Membrane technology and application, second ed., John Wiley & Sons.Ltd, 2004.

[7]     H. Strathmann, P. Scheible, R.W. Baker, A rationale for the preparation of Loeb-Sourirajan-type cellulose acetate membranes, Journal of Applied Polymer Science, 15 (1971) 811-828.

[8]     W.J. Lau, A.F. Ismail, N. Misdan, M.A. Kassim, A recent progress in thin film composite membrane: A review, Desalination, 287 (2012) 190-199.

[9]     Y. Shen, H. Wang, X. Zhang, Y. Zhang, MoS2 Nanosheets Functionalized Composite Mixed Matrix Membrane for Enhanced CO2 Capture via Surface Drop-Coating Method, Acs Appl Mater Inter, 8 (2016) 23371-23378.

[10]    M. Karunakaran, R. Shevate, M. Kumar, K.V. Peinemann, CO2-selective PEO-PBT (PolyActive[trade mark sign])/graphene oxide composite membranes, Chem Commun, 51 (2015) 14187-14190.

[11]    Y. Cheng, X. Wang, C. Jia, Y. Wang, L. Zhai, Q. Wang, D. Zhao, Ultrathin mixed matrix membranes containing two-dimensional metal-organic framework nanosheets for efficient CO2/CH4 separation, Journal of Membrane Science, 539 (2017) 213-223.

[12]    J. Peter, K.V. Peinemann, Multilayer composite membranes for gas separation based on crosslinked PTMSP gutter layer and partially crosslinked Matrimid® 5218 selective layer, Journal of Membrane Science, 340 (2009) 62-72.

[13]    P. Bernardo, E. Drioli, G. Golemme, Membrane Gas Separation: A Review/State of the Art, Ind Eng Chem Res, 48 (2009) 4638-4663.

[14]    T.T. Moore, W.J. Koros, Non-ideal effects in organic–inorganic materials for gas separation membranes, Journal of Molecular Structure, 739 (2005) 87-98.

[15]    Z. Dai, L. Ansaloni, L. Deng, Recent advances in multi-layer composite polymeric membranes for CO2 separation: A review, Green Energy & Environment, 1 (2016) 102-128.

[16]    A. Sabetghadam, X. Liu, M. Benzaqui, E. Gkaniatsou, A. Orsi, M.M. Lozinska, C. Sicard, T. Johnson, N. Steunou, P.A. Wright, C. Serre, J. Gascon, F. Kapteijn, Influence of Filler Pore Structure and Polymer on the Performance of MOF-Based Mixed-Matrix Membranes for CO2 Capture, Chemistry – A European Journal, 24 (2018) 7949-7956.

[17] S. Zhao, X. Cao, Z. Ma, Z. Wang, Z. Qiao, J. Wang, S. Wang, Mixed-Matrix Membranes for CO2/N2 Separation Comprising a Poly(vinylamine) Matrix and Metal–Organic Frameworks, Ind Eng Chem Res, 54 (2015) 5139-5148.

[18] Y. Chen, L. Zhao, B. Wang, P. Dutta, W.S. Winston Ho, Amine-containing polymer/zeolite Y composite membranes for CO2/N2 separation, Journal of Membrane Science, 497 (2016) 21-28.

[19] A. Halim, Q. Fu, Q. Yong, P.A. Gurr, S.E. Kentish, G.G. Qiao, Soft polymeric nanoparticle additives for next generation gas separation membranes, J Mater Chem A, 2 (2014) 4999-5009.

[20] C. Zou, Q. Li, Y. Hua, B. Zhou, J. Duan, W. Jin, Mechanical Synthesis of COF Nanosheet Cluster and Its Mixed Matrix Membrane for Efficient CO2 Removal, Acs Appl Mater Inter, 9 (2017) 29093-29100.

[21] Y. Ban, Y. Li, Y. Peng, H. Jin, W. Jiao, X. Liu, W. Yang, Metal-Substituted Zeolitic Imidazolate Framework ZIF-108: Gas-Sorption and Membrane-Separation Properties, Chemistry – A European Journal, 20 (2014) 11402-11409.

[22] T. Brinkmann, C. Naderipour, J. Pohlmann, J. Wind, T. Wolff, E. Esche, D. Müller, G. Wozny, B. Hoting, Journal of Membrane Science, 489 (2015) 237-247.

[23] W. Yave, A. Car, J. Wind, K.-V. Peinemann, Nanometric thin film membranes manufactured on square meter scale: ultra-thin films for CO 2 capture, Nanotechnology, 21 (2010) 395301-395308.

[24] M. Etxeberria-Benavides, O. David, T. Johnson, M.M. Łozińska, A. Orsi, P.A. Wright, S. Mastel, R. Hillenbrand, F. Kapteijn, J. Gascon, High performance mixed matrix membranes (MMMs) composed of ZIF-94 filler and 6FDA-DAM polymer, Journal of Membrane Science, 550 (2018) 198-207.

[25] A. Sabetghadam, X. Liu, A.F. Orsi, M.M. Lozinska, T. Johnson, K.M.B. Jansen, P.A. Wright, M. Carta, N.B. McKeown, F. Kapteijn, J. Gascon, Towards High Performance Metal–Organic Framework–Microporous Polymer Mixed Matrix Membranes: Addressing Compatibility and Limiting Aging by Polymer Doping, Chemistry – A European Journal, 24 (2018) 12796-12800.

[26] M.H.-O. Rashid, S.F. Ralph, Carbon Nanotube Membranes: Synthesis, Properties, and Future Filtration Applications, Nanomaterials, 7 (2017) 99-127.

[27] R.K. Joshi, S. Alwarappan, M. Yoshimura, V. Sahajwalla, Y. Nishina, Graphene oxide: the new membrane material, Applied Materials Today, 1 (2015) 1-12.

[28] Z. Han, X. Qiang, G. Xianghai, L. Najun, K. Prashant, R. Neel, J.M. Young, A.-T. Shaeel, N. Katabathini, B.S. Nasir, T. Berna, O.F. J., M.C. W., M.K. Andre, T. Michael, Open-Pore Two-Dimensional MFI Zeolite Nanosheets for the Fabrication of Hydrocarbon-Isomer-Selective Membranes on Porous Polymer Supports, Angewandte Chemie International Edition, 55 (2016) 7184-7187.

[29] Y. Peng, Y. Li, Y. Ban, H. Jin, W. Jiao, X. Liu, W. Yang, Metal-organic framework nanosheets as building blocks for molecular sieving membranes, Science, 346 (2014) 1356-1359.

[30] K. Varoon, X. Zhang, B. Elyassi, D.D. Brewer, M. Gettel, S. Kumar, J.A. Lee, S. Maheshwari, A. Mittal, C.-Y. Sung, M. Cococcioni, L.F. Francis, A.V. McCormick, K.A. Mkhoyan, M. Tsapatsis, Dispersible Exfoliated Zeolite Nanosheets and Their Application as a Selective Membrane, Science, 334 (2011) 72-75.

[31] C. Sunho, C. Joaquin, J. Edgar, O. Weontae, N. Sankar, O. Frank, S.D. F., T. Michael, Layered Silicates by Swelling of AMH-3 and Nanocomposite Membranes, Angewandte Chemie International Edition, 47 (2008) 552-555.

[32] A. Sabetghadam, B. Seoane, D. Keskin, N. Duim, T. Rodenas, S. Shahid, S. Sorribas, C.L. Guillouzer, G. Clet, C. Tellez, M. Daturi, J. Coronas, F. Kapteijn, J. Gascon, Metal Organic Framework Crystals in Mixed-Matrix Membranes: Impact of the Filler Morphology on the Gas Separation Performance, Advanced Functional Materials, 26 (2016) 3154-3163.

[33] A. Pustovarenko, M.G. Goesten, S. Sachdeva, M. Shan, Z. Amghouz, Y. Belmabkhout, A. Dikhtiarenko, T. Rodenas, D. Keskin, I.K. Voets, B.M. Weckhuysen, M. Eddaoudi, L.C.P.M. de Smet, E.J.R. Sudhölter, F. Kapteijn, B. Seoane, J. Gascon, Nanosheets of Nonlayered Aluminum Metal–Organic Frameworks through a Surfactant-Assisted Method, Advanced Materials, 30 (2018) 1707234-1707242.

[34] T. Rodenas, I. Luz, G. Prieto, B. Seoane, H. Miro, A. Corma, F. Kapteijn, I.X.F.X. Llabres, J. Gascon, Metal-organic framework nanosheets in polymer composite materials for gas separation, Nat Mater, 14 (2015) 48-55.

[35] A. Corma, V. Fornes, S.B. Pergher, T.L.M. Maesen, J.G. Buglass, Delaminated zeolite precursors as selective acidic catalysts, Nature, 396 (1998) 353-356.

[36] Y. Hernandez, V. Nicolosi, M. Lotya, F.M. Blighe, Z. Sun, S. De, I.T. McGovern, B. Holland, M. Byrne, Y.K. Gun'Ko, J.J. Boland, P. Niraj, G. Duesberg, S. Krishnamurthy, R. Goodhue, J. Hutchison, V. Scardaci, A.C. Ferrari, J.N. Coleman, High-yield production of graphene by liquid-phase exfoliation of graphite, Nature Nanotechnology, 3 (2008) 563-568.

[37] M. Choi, K. Na, J. Kim, Y. Sakamoto, O. Terasaki, R. Ryoo, Stable single-unit-cell nanosheets of zeolite MFI as active and long-lived catalysts, Nature, 461 (2009) 246-249.

[38] G. Hu, N. Wang, D. O'Hare, J. Davis, One-step synthesis and AFM imaging of hydrophobic LDH monolayers, Chem Commun, (2006) 287-289.

[39] T. Rodenas, M. van Dalen, P. Serra-Crespo, F. Kapteijn, J. Gascon, Mixed matrix membranes based on NH2-functionalized MIL-type MOFs: Influence of structural and operational parameters on the CO2/CH4 separation performance, Micropor Mesopor Mat, 192 (2014) 35-42.

[40] M. Shete, P. Kumar, J.E. Bachman, X. Ma, Z.P. Smith, W. Xu, K.A. Mkhoyan, J.R. Long, M. Tsapatsis, On the direct synthesis of Cu(BDC) MOF nanosheets and their performance in mixed matrix membranes, Journal of Membrane Science, 549 (2018) 312-320.

[41] Y. Yang, K. Goh, R. Wang, T.-H. Bae, High-performance nanocomposite membranes realized by efficient molecular sieving with CuBDC nanosheets, Chem Commun, 53 (2017) 4254-4257.

[42] X. Li, Y. Cheng, H. Zhang, S. Wang, Z. Jiang, R. Guo, H. Wu, Efficient CO2 Capture by Functionalized Graphene Oxide Nanosheets as Fillers To Fabricate Multi-Permselective Mixed Matrix Membranes, Acs Appl Mater Inter, 7 (2015) 5528-5537.

[43] B. Zornoza, A. Martinez-Joaristi, P. Serra-Crespo, C. Tellez, J. Coronas, J. Gascon, F. Kapteijn, Functionalized flexible MOFs as fillers in mixed matrix membranes for highly selective separation of CO2 from CH4 at elevated pressures, Chem Commun, 47 (2011) 9522-9524.

[44]    D. Grosso, How to exploit the full potential of the dip-coating process to better control film formation, Journal of Materials Chemistry, 21 (2011) 17033-17038.

[45]    M. Shan, B. Seoane, E. Andres-Garcia, F. Kapteijn, J. Gascon, Mixed-matrix membranes containing an azine-linked covalent organic framework: Influence of the polymeric matrix on post-combustion CO2-capture, Journal of Membrane Science, 549 (2018) 377-384.

[46]    L. Ma, F. Svec, T. Tan, Y. Lv, Mixed Matrix Membrane Based on Cross-Linked Poly[(ethylene glycol) methacrylate] and Metal–Organic Framework for Efficient Separation of Carbon Dioxide and Methane, ACS Applied Nano Materials, 1 (2018) 2808-2818.

[47]    X. Wang, C. Chi, K. Zhang, Y. Qian, K.M. Gupta, Z. Kang, J. Jiang, D. Zhao, Reversed thermo-switchable molecular sieving membranes composed of two-dimensional metal-organic nanosheets for gas separation, Nature Communications, 8 (2017) 14460-14470.

[48]    M. Kattula, K. Ponnuru, L. Zhu, W. Jia, H. Lin, E.P. Furlani, Designing ultrathin film composite membranes: the impact of a gutter layer, Scientific Reports, 5 (2015) 15016-15025.

[49]    W.Z. F. Kapteijn, J.A. Moulijn, T.Q. Gardner, Zeolite membranes: modeling and application, in: J.A.M. A. Cybulski (Ed.) Structured catalysts and reactors, CRC Taylor & Francis, USA, (2006) 700-746.

[50]    F.T. de Bruijn, L. Sun, Ž. Olujić, P.J. Jansens, F. Kapteijn, Influence of the support layer on the flux limitation in pervaporation, Journal of Membrane Science, 223 (2003) 141-156.

[51]    T. Rodenas, M.v. Dalen, E. García-Pérez, P. Serra-Crespo, B. Zornoza, F. Kapteijn, J. Gascon, Visualizing MOF Mixed Matrix Membranes at the Nanoscale: Towards Structure-Performance Relationships in CO2/CH4 Separation Over NH2-MIL-53(Al)@PI, Advanced Functional Materials, 24 (2014) 249-256.

[52]    S.Y. Lim, J. Choi, H.-Y. Kim, Y. Kim, S.-J. Kim, Y.S. Kang, J. Won, New CO2 separation membranes containing gas-selective Cu-MOFs, Journal of Membrane Science, 467 (2014) 67-72.

[53]    S. Basu, A. Cano-Odena, I.F.J. Vankelecom, MOF-containing mixed-matrix membranes for CO2/CH4 and CO2/N2 binary gas mixture separations, Separation and Purification Technology, 81 (2011) 31-40.

[54]    J. Kim, J. Choi, Y. Soo Kang, J. Won, Matrix effect of mixed-matrix membrane containing CO2-selective MOFs, Journal of Applied Polymer Science, 133 (2016) 42853-42861.

[55]    H. Zhu, L. Wang, X. Jie, D. Liu, Y. Cao, Improved Interfacial Affinity and CO2 Separation Performance of Asymmetric Mixed Matrix Membranes by Incorporating Postmodified MIL-53(Al), Acs Appl Mater Inter, 8 (2016) 22696-22704.

[56]    T. Li, Y. Pan, K.-V. Peinemann, Z. Lai, Carbon dioxide selective mixed matrix composite membrane containing ZIF-7 nano-fillers, Journal of Membrane Science, 425-426 (2013) 235-242.

# 6

# Summary and outlook

## 6.1 Summary

Membrane separation is an energy efficient technology with a small physical footprint in which the membrane is the core of process. Membranes need to be further developed to be specifically applied in the field of gas separation. The most challenging target in designing membranes is to improve the permeation and selectivity, simultaneously. This goal cannot be achieved without acquiring the knowledge of material science to tune the membrane material properties. This PhD thesis focusses on designing mixed matrix membranes (MMMs) by using a new class of crystalline materials known as metal organic frameworks (MOFs) as filler. In combination with polymers as continuous phase it was expected to improve both the processability and separation performance of this composite material in comparison with the polymer only. This work has been performed in the framework of the FP7-EU project M$^4$CO$_2$ ('MOF-based Mixed Matrix Membranes for energy efficient CO$_2$ capture', *grant agreement* n° 608490). Therefore the focus in this thesis was on, but not limited to, membranes for the separation of CO$_2$ from N$_2$, as a model for stack gases in coal combustion ('post-combustion separation').

To this aim, the overall concept of this thesis is divided into three parts in which the most relevant aspects of design in mixed matrix membranes are carefully studied. Part I (Chapter 2) elucidated the influence of MOF pore structure and topology on the MMMs separation performance. In part II (Chapter 3 and 4) the effect of MOF morphology and polymer free volume is studied. Finally, part III (Chapter 5) reports a study on free-standing and thin supported MOF nanosheet based membranes by using industrially viable methods. The summary of each Chapter in this thesis is presented as follows.

Chapter 1 presents a general introduction to membrane technology. The concept of MOF based MMMs is introduced and the role of chemical compatibility, filler morphology and topology on the CO$_2$ separation performance were thoroughly discussed. Finally, challenges in fabricating thin MMMs and the solutions to overcome those challenges are presented based on studies published in literature.

Chapter 2 focuses on the influence of MOF topology and pore structure. In this Chapter, eight different composites were studied by combining four types of MOFs and two polymers. NH$_2$-MIL-53(Al), MIL-69(Al), MIL-96(Al) and ZIF-94 with various chemical functionalities, topologies, and pore dimensionalities were employed as fillers, while two typical polymers with different permeability-selectivity properties (6FDA-DAM and Pebax 1657) were deliberately selected as matrices. The best performing MOF-polymer composites were prepared by loading 25 wt.% of MIL-96(Al) as filler in both 6FDA-DAM and Pebax polymers. The observed differences in membrane performance in the separation of CO$_2$ from N$_2$ were explained on the basis of gas solubility, diffusivity properties and compatibility between the filler and polymer phases.

The results suggest that the large adsorption capacity of MOF fillers under moderate pressure and high porosity endows the 6FDA-DAM based MMMs with enhanced gas solubility and, consequently, an improved $CO_2$ permeability ánd selectivity. The different topology of the MOF fillers, especially regarding their pore dimensionality, was responsible for the various performance modifications. Addition of the nonflexible, small pore 1D MOF MIL-69 results for both polymers in a slight increase in selectivity at almost constant permeability. In case of $NH_2$-MIL-53, with a similar topology but a flexible structure, interaction with the polymer results either in a decrease in permeability (Pebax) attributed to polymer penetration into the MOF structure or in an increase in permeability (6FDA-DAM) with hardly any improvement in selectivity, most likely related to a partial opening of the structure by the solvent upon membrane preparation. Addition of the narrow pore, rigid, 2D-porous MIL-96 increases both permeability and selectivity for the two polymers. Finally, the 3D-porous ZIF-94 filler displays the largest increase in permeability for both polymers with a slight increase in selectivity only when Pebax is used as continuous phase. These results suggest that the MOF topology, dimensionality of porosity and interaction with the continuous polymer phase play key roles in determining membrane performance. The improved selectivity along with permeability (except for $NH_2$-MIL-53(Al)-Pebax) moves the MMM performance closer to the Robeson upper bound.

Part II of the thesis (Chapters 3 and 4) focuses on the importance of polymer filler interactions at the micro-scale. In Chapter 3, different morphologies of $NH_2$-MIL-53(Al) such as nanoparticles, nanorods and microneedles were synthesized by using various routes. To quantify the effect of different morphologies on the permeation performance of the membrane, two polymers with low (Matrimid®) and high (6FDA-DAM) free volume were selected as the continous matrix in MMMs. The synthesized membranes have been tested in the separation of $CO_2$ from $CH_4$ in an equimolar mixture. Incorporation of $NH_2$-MIL-53(Al) nanoparticles in Matrimid® led to the largest improvement compared to nanorods and microneedles morphologies. This study revealed that the particle morphology has an impact on the permeation results. The incorporation of the best performing filler, *i.e.* $NH_2$-MIL-53(Al) nanoparticles, to the highly permeable 6FDA-DAM had a larger effect (85% increase in permeability), giving rise to the membranes with a performance very close to the 2008 Robeson limit for $CO_2/CH_4$ separation. Furthermore, a new non-destructive technique based on Raman spectroscopy mapping was introduced in this chapter to assess the homogeneity of the filler dispersion in the polymer matrix. The determined homogeneity of the MOF distribution in the polymer was confirmed by FIB-SEM analysis.

Following the scope of part II of the thesis and assessing the micro-scale properties of MOF based MMMs, Chapter 4 focuses on the modification of the polymer matrix in MMMs to enhance the MMMs separation performance and to limit the ageing of ultra highly permeable membranes.

In this regard, doping a highly porous polymer of intrinsic microporosity (PIM-1) with small amounts of a glassy polymer (Matrimid®) shed light on the preparation of MOF-based MMMs with superior separation properties in dry and humidified conditions. This modification mainly contributed to the enhancement in the selectivity of the membranes, which interestingly pushed the permeation performance above Robeson upper bound. The results indicated $NH_2$-MIL-53(Al) as a promising MOF filler in terms of enhancing polymer and filler interaction due to its amine functional groups. Therefore, the superior permeation performance of these MMMs with $NH_2$-MIL-53(Al) as filler, surpassing $CO_2/N_2$ Robeson upper bound, was maintained even after 17 months of ageing. The versatility of the developed method was evidenced by using different MOF fillers.

In Chapter 5, fabrication of defect-free thin supported MMMs via conventional methods was investigated using MOF nanosheets with a large aspect ratio produced by a scaled-up synthesis. One of the challenging facets of thin membrane fabrication is producing a selective layer on a support without nanoscale defects. This is even more challenging when fillers are incorporated in the thin layer. The influence of utilizing Cu-BDC nanosheets in a highly selective Polyactive™ polymer was studied for supported dual layer (drop-casting) and mixed matrix (dip-coating) thin composite MMMs,. The high aspect ratio filler potentially covered the defects of thin, neat Polyactive™ membranes. Further, the separation performances of free-standing and thin supported MMMs were compared and evaluated for the $CO_2/N_2$ separation. The thin supported MMMs showed a superior separation performance in terms of $CO_2/N_2$ selectivity (up to 77) while the thin dual layer membranes demonstrated a significant improvement (doubling) in permeance.

The above results confirm the promise that MOF based MMMs hold for $CO_2$ separation. The work illustrates the elements that require further developments in this rapidly progressing field and emphasises the importance of parallel engineering of MOF and polymer matrix in order to attain industrially applicable gas separation membranes.

## 6.2 General remarks and outlook

Taking into account the role of MOF fillers in permeation performance of MMMs, there are several aspects that should be considered in using MMMs in gas separation. In order to benefit further from MOF properties in the MMMs, high loading of MOFs in the polymer matrix are desired. The highest possible loading of MOFs in the blended polymers (high and low free volume) was up to 25 wt.% without defect formation and becoming too brittle. These results in this thesis showed a promising strategy of blending polymers to obtain flexible sheets of the MMMs with high loading of MOFs. Further increase in MOF loading turned out to be possible by using rubbery polymers such as Pebax. This could further enhance the permeation properties of MMMs significantly.[2] Therefore, incorporating a porous structure in rubbery polymers at high

loading while avoiding defect formation and agglomeration as much as possible can result in large enhancement in permeation performance of MMMs.

To get insight into the role of MOFs in improving the MMMs permeation performance, $CO_2$ adsorption experiments of the MMMs led us towards understanding of solubility and diffusivity properties of MMMs. These studies were evaluated based on single gas measurements. Although MOFs are the porous structures which potentially are expected to facilitate diffusion of the molecules, most of the studies showed that MOFs contributed mostly in enhancement of the $CO_2$ solubility in the MMMs. This is due to the selective interaction of $CO_2$ molecules with the $CO_2$-philic sites of the MOFs. This interaction could influence the mobility of $CO_2$ and consequently, reduce the $CO_2$ permeation. On the other hand the increased concentration in the MOF can compensate for this, as has clearly been demonstrated for zeolite membranes, and the net result can be positive or negative, depending on the MOF.

Ageing is one of the main obstacles to use the high performance membranes in the long term operation. Particularly, ultra high permeable PIM-1 membranes suffer from rapid ageing in a few weeks after preparation. Several strategies have been made to overcome this phenomenon and to limit the polymer chains relaxation over time. The most effective strategy is to incorporate a second polymer or filler to the PIM-1 matrix to limit the chains relaxation and decrease in free volume. Therefore, the best candidates could be a second polymer/filler which not only contributes in limiting the ageing, but also enhances the filler and polymer interactions by making a bridge between filler and PIM-1 matrix. Incorporating of those components together in highly permeable polymers would result in a sharp improvement in MMM separation performance (see Chapter 4).

One of the most important facets of high performance MMMs is the homogeneous dispersion of the fillers in the polymer matrix. To assess this criterion, homogeneity and reproducibility of the MMM samples should be quantified. Homogeneity of the membranes could be analysed by performance testing and non-destructive characterization of different samples of the same sheet of the membrane.[1] Further, the reproducibility of the preparation method should be validated by testing and characterizing different batches of the fabricated membranes under the same conditions. In this PhD project, supported by a collaborative interlaboratory experiments known as Round Robin tests, we could perform several gas separation experiments independently on the samples prepared under the same conditions and using the same method.[1]

Regarding gas permeation tests to evaluate the separation performance of the membranes, another aspect that should be taken into account is the validation of the gas separation setup and the gas flow concentrations. To this aim, not only the concentration of permeate but also the feed and retentate flow should be analysed.

In this regard, the experimental errors due to the accuracy of the MFC, BPC, GC, etc. measurement tools and the uncertainty in membrane thickness and area must be estimated and taken into account in reporting the membrane separation performance if they are significant.

Apart from the experimental aspect of MMM preparation, characterization and testing, rigorous modelling of the filler and polymer, particularly at their interface, is essential.[3, 4] These models should facilitate understanding of filler and polymer interface at the nanoscale and shed light on the selection of compatible and appropriate fillers and polymers for making highly efficient MMMs for $CO_2$ capture.

# References

[1]   J. Sánchez-Laínez, B. Zornoza, S. Friebe, J. Caro, S. Cao, A. Sabetghadam, B. Seoane, J. Gascon, F. Kapteijn, C. Le Guillouzer, G. Clet, M. Daturi, C. Téllez, J. Coronas, Influence of ZIF-8 particle size in the performance of polybenzimidazole mixed matrix membranes for pre-combustion CO2 capture and its validation through interlaboratory test, Journal of Membrane Science, 515 (2016) 45-53.

[2]   A. Sabetghadam, N. Steunou, Jorge Gascon, Freek Kapteijn, High loading mixed matrix membranes containing MIL-96(Al) and Pebax polymer, In preparation.

[3]   R. Semino, J.C. Moreton, N.A. Ramsahye, S.M. Cohen, G. Maurin, Understanding the origins of metal–organic framework/polymer compatibility, Chemical Science, 9 (2018) 315-324.

[4]   S. Hwang, R. Semino, B. Seoane, M. Zahan, C. Chmelik, R. Valiullin, M. Bertmer, J. Haase, F. Kapteijn, J. Gascon, G. Maurin, J. Kärger, Revealing the Transient Concentration of CO2 in a Mixed-Matrix Membrane by IR Microimaging and Molecular Modeling, Angewandte Chemie International Edition, 57 (2018) 5156-5160.

**6**

# Samenvatting & Vooruitblik

## 6.1 Samenvatting

Membraanscheiding is een technologie die energie-efficiënt is met een kleine ecologische voetafdruk waarbij het membraan het hart van het proces is. Membranen moeten echter verder ontwikkeld worden zodat ze specifiek kunnen worden toegepast in het domein van de scheiding van gassen. De grootste uitdaging bij het ontwerpen van membranen is om tegelijkertijd zowel de flux door het membraan (permeatie) als de selectiviteit te verbeteren.  Deze verbeteringen in performance kan niet worden bereikt zonder materiaalkennis om de membraaneigenschappen aan te passen. Dit proefschrift focust op het ontwerpen van zogenoemde Mixed Matrix membranen (MMMs) waarbij een nieuwe klasse van kristallijne materialen, namelijk Metal Organic Frameworks (MOFs), wordt gebruikt als vulmiddel ('filler') ingebed in een continue matrix van een polymeer. Van deze combinatie werd verondersteld dat zowel de bewerkbaarheid als de scheidingsprestatie in vergelijking met het pure polymeermembraan verbeterde.  Dit werk is gedaan in de context van het FP7-EU project genaamd M4CO2 ('MOF-gebaseerde Mixed Matrix Membranes voor de energie-efficiënte afvang van $CO_2$', projectnr. 608490). De nadruk van het onderzoek beschreven in dit proefschrift lag op de ontwikkeling van dit soort membranen geschikt voor de scheiding van $CO_2$ van $N_2$ als een modelsysteem van rookgas van steenkoolverbranding ('post-combustion' scheiding).

Dit proefschrift kan worden verdeeld in drie delen waarin de meest relevante aspecten van het ontwerpen van Mixed Matrix membranen zorgvuldig zijn bestudeerd. Deel I (Hoofdstuk 1 en 2) geeft inzicht in de invloed van de structuur en de porietopologie van de MOFs op de scheidingsprestatie van de MMMs. In deel II (Hoofdstuk 3 en 4) wordt het effect van de morfologie en het vrije volume van het polymeer bestudeerd. Ten slotte worden in deel III (Hoofdstuk 5) membranen bestudeerd gebaseerd op MOF nanosheets daarbij gebruik makend van industrieel toepasbare bereidingsmethodes. De samenvatting van elk Hoofdstuk in dit proefschrift volgt hieronder.

Hoofdstuk 1 presenteert een algehele introductie van membraantechnologie. Het concept van MOF-gebaseerde MMMs wordt geïntroduceerd en de invloed van chemische compatibiliteit, filler morfologie en topologie op de $CO_2$ scheidingsprestaties worden uitgebreid besproken. Tenslotte worden de uitdagingen van het maken van dunne MMMs en hoe deze aan te pakken gepresenteerd, gebaseerd op onderzoek dat is gepubliceerd in literatuur.

Hoofdstuk 2 focust op de invloed van de MOF topologie en poriestructuur op de MMM performance. In dit hoofdstuk worden acht verschillende combinaties bestudeerd door vier MOF types te combineren met twee polymeren.

NH$_2$-MIL-53(Al), MIL-69(Al), MIL-96(Al) en ZIF-94, met diverse chemische functionaliteiten, topologieën en poriedimensies, werden gebruikt als fillers, terwijl twee typische polymeren met verschillende permeabiliteit-selectiviteit eigenschappen (6FDA-DAM en Pebax 1657) zijn geselecteerd als matrix. De MOF-polymeer composieten met de beste performance zijn verkregen met 25 gewichtsprocent MIL-96(Al) in zowel 6FDA-DAM en Pebax polymeren. De waargenomen verschillen in de membraanprestaties voor het scheiden van CO$_2$ en N$_2$ zijn verklaard op basis van de oplosbaarheid- en diffusiviteits-eigenschappen van de gassen en de compatibiliteit van de polymeer en de filler.

De resultaten suggereren dat de hoge adsorptiecapaciteit van de MOF fillers onder matige druk en hoge porositeit zorgt voor een hogere CO$_2$ oplosbaarheid voor 6FDA-DAM-gebaseerde MMMs met een verbeterde CO$_2$ permeabiliteit en selectiviteit tot gevolg. De verschillende topologieën van de MOF fillers, en in het bijzonder hun poriedimensionaliteit, waren verantwoordelijk voor de veranderingen in de membraanprestaties. Het toevoegen van de inflexibele MIL-96, met kleine poriën en een 1D poriestructuur, resulteert in een lichte toename in selectiviteit bij een nagenoeg constante permeabiliteit voor beide polymeren. In het geval van NH$_2$-MIL-53, met een vergelijkbare topologie maar een flexibele structuur, resulteert de interactie met het polymeer in een verminderde permeabiliteit (Pebax), toegeschreven aan penetratie van het polymer in de MOF structuur, of in een toegenomen permeabiliteit (6FDA-DAM) met een geringe toename in selectiviteit, wat waarschijnlijk gerelateerd is aan een gedeeltelijke opening van de strucuur door het oplosmiddel tijdens de bereiding van het membraan. Het toevoegen van MIL-96, een rigide MOF met kleine poriën en een 2D poriestructuur, resulteert in een toename van zowel de permeabiliteit als de selectiviteit voor beide polymeren. Tot slot laat ZIF-96, met een 3D-poriestructuur, de grootste toename in permeabiliteit zien voor beide polymeren met een geringe toename in de selectiviteit in het geval dat Pebax wordt gebruikt als de continue fase. Deze resultaten suggereren dat zowel de topologie, poriedimensionaliteit en de porositeit van de MOF alsook de interactie met de continue polymeerfase een sleutelrol hebben in het bepalen van de membraanprestaties. De simultane toename van selectiviteit en permeabiliteit (behalve in het geval van NH$_2$-MIL-53(Al)-Pebax) zorgt ervoor dat de prestatie van de MMM meer richting de zogenaamde Robeson bovengrens gaat.

Deel II van het proefschrift (hoofdstuk 3 en 4) focust op het belang van de interactie van de polymeer filler op een micro-schaal. In hoofdstuk 3 zijn verschillende morfologieën, zoals nanodeeltjes, nanostaafjes en micronaalden van NH$_2$-MIL-53(Al) gesynthetiseerd via verschillende routes.

Om het effect van de verschillende morfologieën op de permeatieprestaties van het membraan te kwantificeren, zijn twee polymeren geselecteerd als de continue matrix in de MMMs, met een klein (Matrimid®) of een groot vrij volume (6FDA-DAM). De gesynthetiseerde membranen zijn getest voor de scheiding van $CO_2$ van CH4 in een equimolair mengsel. Het inbedden van de $NH_2$-MIL-53(Al) nanodeeltjes in Matrimid® gaf de beste resultaten in vergelijking met de andere twee morfologieën. Dit laat duidelijk zien dat deeltjesmorfologie invloed heeft op de scheidingseigenschappen. Het toevoegen van de best presterende filler, $NH_2$-MIL-53(Al) nanodeeltjes, aan het zeer permeabele 6FDA-DAM had zelfs een groter effect (85 % toename in permeabiliteit), wat membranen opleverde met een prestatie die erg dicht tegen de 2008 Robeson bovengrens aan ligt voor $CO_2/CH_4$ scheiding. Bovendien is er een nieuwe niet-destructieve techniek geïntroduceerd in dit hoofdstuk, gebaseerd op mapping met Raman spectroscopie, om de homogeniteit van de dispersie van de filler in de polymeermatrix te beoordelen. De bepaalde homogeniteit van de MOF distributie in het polymeer werd bevestigd door FIB-SEM analyse.

Als vervolg op de scope van deel II van het proefschrift in combinatie met het beoordelen van eigenschappen van MOF-gebaseerde MMMs op microschaal, is hoofdstuk 4 gericht op het modificeren van de polymeermatrix in MMMs om de scheidingsprestatie te verbeteren en om de veroudering van membranen die een zeer hoge permeabiliteit hebben tegen te gaan.

In dit verband resulteerde het toevoegen van kleine hoeveelheden van een glasachtige polymeer (Matrimid®) aan een zeer poreus polymeer met intrinsieke microporositeit (PIM-1) in MOF-gebaseerde MMMs met superieure scheidingseigenschappen zowel onder droge als vochtige condities. De modificatie droeg voornamelijk bij aan de verbetering van de selectiviteit van de membranen, wat leidde tot een permeatieprestatie boven de Robeson bovengrens. De resultaten wezen $NH_2$-MIL-53(Al) aan als een veelbelovende MOF filler wat betreft het verbeteren van de polymeer-filler interactie vanwege de functionele amine groepen. Daarom was de superieure permeatieprestatie van de MMM met $NH_2$-MIL-53(Al) als filler die de Robeson bovengrens overschreed, zelfs na 17 maanden veroudering behouden gebleven. De veelzijdigheid van deze ontwikkelde methode is verder bewezen door het gebruik van verschillende MOF fillers.In hoofdstuk 5 is de bereiding via conventionele methoden van defectvrije, dunne gedragen MMMs onderzocht, gebruik makend van MOF nanosheets met een grote lengte-dikte verhouding die gemaakt zijn via een opgeschaalde synthese.

Eén van de uitdagingen van het maken van dunne membranen is het produceren van een selectieve laag op een ondersteunende laag zonder nano-defecten. Dit is nog uitdagender wanneer fillers zijn opgenomen in de dunne laag.

De invoed van het gebruik van Cu-BDC nanosheets in een zeer selectief polymeer (Polyactive™) is bestudeerd voor gedragen dubbellaagse (verkregen via drop-casting) en mixed matrix (verkregen via dip-coating) dunne composiet MMMs. De fillers met hun grote lengte-dikte verhouding bedekten mogelijk de defecten die aanwezig waren in pure Polyactive™ membranen. Verder werden de scheidingsprestaties van vrijstaande en dunne gedragen MMMs vergeleken en geëvalueerd voor $CO_2/N_2$ scheiding. De dunne gedragen MMM vertoonde een superieure scheidingsprestatie op het gebied van $CO_2/N_2$ selectiviteit (tot 77) terwijl de dunne dubbellaagse membranen een significante verbetering (verdubbeling) lieten zien van de permeance.

Bovengenoemde resultaten bevestigen dat MOF-gebaseerde MMMs veelbelovend zijn voor $CO_2$ scheiding. Dit werk geeft de elementen aan die verdere ontwikkeling nodig hebben in dit zich snel ontwikkelende veld, en het benadrukt het belang van tegelijkertijd zowel de MOF als de polymeer matrix te ontwerpen om tot industrieel toepasbare membranen voor de scheiding van gassen te komen.

## 6.2 Algemene opmerkingen en vooruitblik

Wat betreft de rol van MOF fillers op de permeatieprestatie van MMMs zijn er verschillende aspecten die beschouwd moeten worden bij het gebruik van MMMs voor gasscheiding. Om nog meer te profiteren van de MOF eigenschappen in MMMs, is een hoge belading van de MOF in de polymeer matrix gewenst. De hoogst mogelijke fractie van MOFs in de gemengde polymeren (groot en klein vrij volume) was 25% zonder dat defecten werden gevormd of dat ze te broos werden. Dit proefschrift presenteert een veelbelovende strategie waarbij polymeren worden gemengd om zo flexibele MMM sheets te krijgen met een hoge fractie MOFs. Een verdere verhoging van de MOF-belading bleek mogelijk door het gebruik van rubberachtige polymeren zoals Pebax. Dit zou kunnen resulteren in een significante verdere verbetering van de permeatie-eigenschappen van de MMMs [2]. Daarom kan bij een hoge belading de combinatie van een poreuze structuur met rubberachtig polymeer, zodat de vorming van defecten en agglomeraten zo veel mogelijk wordt tegengegaan, resulteren in een grote verbetering van de permeatieprestatie van een MMM.

Om een beter beeld te krijgen van de rol van MOFs in het verbeteren van de permeatieprestatie van de MMM, brachten $CO_2$ adsorptieexperimenten van de MMM meer begrip van de oplosbaarheids- en diffusiviteits-eigenschappen van MMMs. Deze studies werden gedaan gebaseerd op single gas metingen. Hoewel MOFs de poreuze structuren zijn waarvan verwacht wordt dat deze mogelijk de diffusie van moleculen faciliteren, lieten de meeste studies zien dat MOFs voornamelijk een bijdrage leverden aan de verbetering van $CO_2$ oplosbaarheid in de MMMs. Dit komt door de selectieve interactie van de $CO_2$ moleculen met de $CO_2$-fiele adsorptieplaatsen van de MOFs. Deze interactie kan de mobiliteit van $CO_2$ beïnvloeden met een afname van de $CO_2$ permeatie als gevolg. Aan de andere kant, kan de toegenomen concentratie in de MOF hiervoor compenseren, zoals duidelijk is aangetoond voor zeolietmembranen, zodat het netto resultaat positief en negatief kan zijn, afhankelijk van de MOF.

Veroudering is één van de voornaamste obstakels voor het langdurig gebruik van high-performance membranen. Vooral PIM-1 membranen, die over een ultrahoge permeabiliteit beschikken, hebben last van snelle veroudering binnen een paar weken na vervaardiging. Verschillende strategieën zijn bedacht om dit fenomeen te onderdrukken en de relaxatietijd van de polymeerketens te limiteren. De meest effectieve strategie is het combineren van een tweede polymeer als filler in een PIM-1 matrix om zowel de relaxatie van de polymeerketens te limiteren als de afname in vrij volume. De beste kandidaten zijn polymeer-fillers die niet alleen een bijdrage leveren aan het limiteren van de veroudering, maar ook aan de toename van de filler-polymeer interacties, door het maken van een brug tussen de filler en de PIM-1 matrix. Het toevoegen van deze componenten aan polymeren met een hoge permeabiliteit zou resulteren in een drastische verbetering van de MMM scheidingsprestatie (zie hoofdstuk 4).

Eén van de belangrijkste facetten van MMMs met een hoge performance is een homogene dispersie van de filler in de polymeermatrix. Om dit criterium te beoordelen, moeten de homogeniteit en de reproduceerbaarheid van de MMM monsters worden gekwantificeerd. Homogeniteit van de membranen kan worden geanalyseerd door het testen van de performance en door non-destructive karakterisering van verschillende monsters van hetzelfde membraan[1]. Bovendien moet de reproduceerbaarheid van de bereidingsmethode gevalideerd worden door het testen en karakteriseren van verschillende batches van het membraan onder dezelfde condities. In dit PhD project, ondersteund door een samenwerkingsverband tussen verschillende laboratoria waarmee zogenaamde 'Round-Robin' testen werden uitgevoerd, konden we verschillende onafhankelijke gasscheidingsexperimenten uitvoeren op monsters die zijn gemaakt onder dezelfde condities, gebruik makend van dezelfde methode [1].

Met betrekking tot de gaspermeatieproeven die zijn gedaan om de scheidingsprestaties van de membranen te evalueren, moet ook rekening gehouden worden met een ander aspect: het valideren van de gasscheidingsapparatuur en de concentraties van de gasstromen. Daartoe moet niet alleen de concentratie van het permeaat worden geanalyseerd, maar ook de voeding- en retentaat-stroom.

In dit opzicht, moeten zowel de experimentele onzekerheden vanwege de nauwkeurigheid van de meetinstrumenten zoals MFC, BPC, GC, etc., alsook de onzekerheden in membraandikte en -oppervlakte worden geschat. Deze moeten ook in beschouwing worden genomen in de rapportage van de membraanscheidingsprestaties.

Afgezien van het experimentele aspect van het maken, karakteriseren en testen van MMMs, is het rigoreus modelleren van de filler en de polymeer, en met name het grensvlak, essentieel [3,4]. Deze modellen zouden moeten helpen bij het inzicht in het filler-polymeer grensvlak op nanoschaal en de selectie van goed bij elkaar passende geschikte fillers en polymeren moeten vereenvoudigen.

## Referenties

[1]  J. Sánchez-Laínez, B. Zornoza, S. Friebe, J. Caro, S. Cao, A. Sabetghadam, B. Seoane, J. Gascon, F. Kapteijn, C. Le Guillouzer, G. Clet, M. Daturi, C. Téllez, J. Coronas, Influence of ZIF-8 particle size in the performance of polybenzimidazole mixed matrix membranes for pre-combustion $CO_2$ capture and its validation through interlaboratory test, Journal of Membrane Science, 515 (2016) 45-53.

[2]  A. Sabetghadam, N. Steunou, Jorge Gascon, Freek Kapteijn, High loading mixed matrix membranes containing MIL-96(Al) and Pebax polymer, in preparation.

[3]  R. Semino, J.C. Moreton, N.A. Ramsahye, S.M. Cohen, G. Maurin, Understanding the origins of metal–organic framework/polymer compatibility, Chemical Science, 9 (2018) 315-324.

[4]  S. Hwang, R. Semino, B. Seoane, M. Zahan, C. Chmelik, R. Valiullin, M. Bertmer, J. Haase, F. Kapteijn, J. Gascon, G. Maurin, J. Kärger, Revealing the Transient Concentration of $CO_2$ in a Mixed-Matrix Membrane by IR Microimaging and Molecular Modeling, Angewandte Chemie International Edition, 57 (2018) 5156-5160.

## *About the Author*

Anahid Sabetghadam was born on 27th of April 1983 in Tehran. She followed the major of mathematics and physics in highschool and pursued her interest in music next to her studies by joining the choral group of Pars Music Orchestra. After graduating from highschool, she was accepted in the university entrance exam in Tehran to start chemical engineering studies. She got her MSc degree from Iran University of Science and Technology in 2009 with the thesis title of "Nanocomposite membranes for ethanol purification" and her studies were published in two peer-reviewed papers in international journals. After her graduation, she joined the Research Institute of Petroleum Industry as a researcher to work on the fabrication of nanocomposite membranes for natural gas sweetening in presence of $H_2S$. From 2010 to 2013, she worked in Pentane Chemistry manufacturing company as a project engineer where she focused on distillation column internals engineering and design. In 2014, she had this opportunity to start her PhD studies under supervision of Prof.dr. Freek Kapteijn and Prof.dr. Jorge Gascon in the Catalysis Engineering group in TUDelft. Her PhD project was part of the M4CO2 European project in collaboration with academic and industrial partners and its outcome is presented in this thesis. From Sep 2018, she joined the MEMBER project, pursuing her studies in mixed matrix membrane modeling as a post-doctoral researcher under guidance of Prof.dr. Freek Kapteijn.

# List of Publications and Presentations

**H index 10**

**Total number of Citation 294**

### PhD publications in chronological order

- *Anahid Sabetghadam, Beatriz Seoane, Damla Keskin, Nicole Duim, Tania Rodenas, Salman Shahid, Sara Sorribas, Clément Le Guillouzer, Guillaume Clet, Carlos Tellez, Marco Daturi, Joaquin Coronas, Freek Kapteijn, Jorge Gascon, "*Metal Organic Framework Crystals in Mixed-Matrix Membranes: Impact of the Filler Morphology on the Gas Separation Performance", *Advanced functional materials 26 (**2016**), 3154-3168.*

- *Mihail Mihaylov, Kristina Chakarova, Stanislava Andonova, Nikola Drenchev, Elena Ivanova, Evgeny Pidko, Anahid Sabetghadam, Beatriz Seoane, Jorge Gascon, Freek Kapteijn, Konstantin Hadjiivanov,"Adsorption of $CO_2$ on MIL-53(Al): FTIR evidence of the formation of dimeric $CO_2$ species", Chemical Communications 52 (**2016**), 1494-1497.*

- *Mihail Mihaylov, Kristina Chakarova, Stanislava Andonova, Nikola Drenchev, Elena Ivanova, Anahid Sabetghadam, Beatriz Seoane, Jorge Gascon, Freek Kapteijn, Konstantin Hadjiivanov, "Adsorption Forms of $CO_2$ on MIL-53(Al) and $NH_2$-MIL-53(Al) As Revealed by FTIR Spectroscopy", The Journal of Physical Chemistry C, 120 (**2016**), 23584-23595.*

- *Javier Sanchez-Lainez, Beatriz Zornoza, Sebastian Friebe, Jürgen Caro, Shuai Cao, Anahid Sabetghadam, Beatriz Seoane, Jorge Gascon, Freek Kapteijn, Clement Le Guillouzer, Guillaume Clet, Marco Daturi, Carlos Tellez, Joaquín Coronas, "Influence of ZIF-8 Particle Size in the Performance of Polybenzimidazole Mixed Matrix Membranes for Pre-combustion $CO_2$ Capture and its Validation Through Interlaboratory Test", Journal of Membrane Science, 515 (**2016**), 45-53.*

- *Sumit Sachdeva, Sander JH Koper, Anahid Sabetghadam, Dimitri Soccol, Dirk J Gravesteijn, Freek Kapteijn, Ernst JR Sudhölter, Jorge Gascon, Louis CPM De Smet," Gas Phase Sensing of Alcohols by Metal Organic Framework–Polymer Composite Materials", ACS applied materials & interfaces, 9 (**2017**), 24926-24935.*

- *Marvin Benzaqui, Renjith S Pillai, Anahid Sabetghadam, Virginie Benoit, Perine Normand, Jerome Marrot, Nicolas Menguy, David Montero, William Shepard, Antoine Tissot, Charlotte Martineau-Corcos, Clémence Sicard, Mihail Mihaylov, Florent Carn, Isabelle Beurroies, Philip L Llewellyn, Guy De Weireld, Konstantin Hadjiivanov, Jorge Gascon, Freek Kapteijn, Guillaume Maurin, Nathalie Steunou, Christian Serre, "Revisiting the Aluminum Trimesate-Based MOF (MIL-96): From Structure Determination to the Processing of Mixed Matrix Membranes for $CO_2$ Capture", Chemistry of Materials, 29 (**2017**), 10326-10338.*

- *Anahid Sabetghadam, Xinlei Liu, Marvin Benzaqui, Effrosyni Gkaniatsou, Angelica Orsi, Magdalena M Lozinska, Clemence Sicard, Timothy Johnson, Nathalie Steunou, Paul A Wright, Christian Serre, Jorge Gascon, Freek Kapteijn, "Influence of Filler Pore Structure and Polymer on the Performance of MOF-Based Mixed-Matrix Membranes for $CO_2$ Capture", Chemistry–A European Journal, 24 (**2018**), 7949-7956.*

- *Xinlei Liu, Xuerui Wang, Anastasiya Bavykina, Liangyong Chu, Meixia Shan, Anahid Sabetghadam, Hozanna Miro, Freek Kapteijn, Jorge Gascon, "Molecular-Scale Hybrid Membranes Derived from Metal-Organic Polyhedra for Gas Separation", ACS applied materials & interfaces, 28 (**2018**), 21381-21389.*

- *Anahid Sabetghadam, Xinlei Liu, Angelica F Orsi, Magdalena M Lozinska, Timothy Johnson, Kaspar MB Jansen, Paul A Wright, Mariolino Carta, Neil B McKeown, Freek Kapteijn, Jorge Gascon, "*Towards High Performance Metal–Organic Framework–Microporous Polymer Mixed Matrix Membranes: Addressing Compatibility and Limiting Aging by Polymer Doping", *Chemistry–A European Journal, 24 (**2018**), 12796-12800.*

- *Anahid Sabetghadam, Xinlei Liu, Soraya Gottmer, Liangyong Chu, Jorge Gascon, Freek Kapteijn, "*Thin Mixed Matrix and Dual Layer Membranes Containing Metal-Organic Framework Nanosheets and Polyactive™ for CO2 capture", *Journal of Membrane Science, 570 (**2018**), 226-235.*

- *Anahid Sabetghadam, Nathalie Steunou, Jorge Gascon, Freek Kapteijn*, "High loading mixed matrix membranes containing MIL-96(Al) and Pebax polymer", *In preparation*.

## Oral presentations

- *Anahid Sabetghadam, Beatriz Seoane, Freek Kapteijn, Jorge Gascon,* "Applying High Free-Volume Polymers (PIM-1 & 6FDA-DAM) and MOFs (NH$_2$-MIL-53) in Mixed Matrix Membranes", M4CO2 consortium meeting, **DECHEMA, Germany, Jun 2014.**

- *Anahid Sabetghadam, Beatriz Seoane, Jorge Gascon, Freek Kapteijn,* "Investigation on Monomer Purification and 6FDA-DAM Polymer Scale-up Synthesis for Mixed Matrix Membrane Fabrication", M4CO2 consortium meeting, **University of Zaragoza, Spain, Dec 2014.**

- *Anahid Sabetghadam, Eli Elderkamp, Beatriz Seoane, Jorge Gascon, Freek Kapteijn,* "Influence of Feed Conditions on Membrane Separation Performance and 1$^{st}$ Round Robin Inter-Laboratory Gas separation Experiments, M4CO2 consortium meeting, **Tecnalia, Spain, June 2015.**

- *Anahid Sabetghadam, Frederico Martins, Beatriz Seoane, Freek Kapteijn, Jorge Gascon,* "Investigation on Reproducibility and Homogeneity of Mixed Matrix Membranes Preparation and the Influence of Heat-treatment on Functionalized UiO-66(COOH) Pore Structure, M4CO2 consortium meeting, **University of Versailles, France, Dec 2015.**

- *Anahid Sabetghadam, Damla Keskin, Beatriz Seoane, Freek Kapteijn, Jorge Gascon, "*Influence of Particle Morphology on Mixed Matrix Membrane Separation Performance and 2$^{nd}$ Round Robin Inter-laboratory Gas Separation Experiments", M4CO2 consortium meeting, **University of Edinburgh, UK, June 2016.**

- *Anahid Sabetghadam, Xinlei Liu, Marvin Benzaqui, Effrosyni Gkaniatsou, Angelica Orsi, Magdalena M Lozinska, Clemence Sicard, Timothy Johnson, Nathalie Steunou, Paul A Wright, Christian Serre, Jorge Gascon, Freek Kapteijn, "*Influence of Filler Pore Structure on Mixed Matrix Membrane Performance, M4CO2 consortium meeting, **Bulgarian Academy of sciences, Bulgaria, Dec 2016.**

- *Anahid Sabetghadam, Xinlei Liu, Angelica F Orsi, Magdalena M Lozinska, Timothy Johnson, Kaspar MB Jansen, Paul A Wright, Mariolino Carta, Neil B McKeown, Freek Kapteijn, Jorge Gascon, "*Effect of MOF Loading and Polymer Blending on Mixed Matrix Membranes Ageing and Separation Performance", M4CO2 consortium meeting, **Leibniz University, Germany, June 2017.**

- *Anahid Sabetghadam, Xinlei Liu, Soraya Gottmer, Liangyong Chu, Jorge Gascon, Freek Kapteijn,* "Scale-up Synthesis of Cu-BDC Nanosheets and Thin Supported Mixed Matrix Membrane Fabrication", M4CO2 consortium meeting, **DECHEMA, Germany, Dec 2017.**

- *Anahid Sabetghadam, Xinlei Liu, Marvin Benzaqui, Effrosyni Gkaniatsou, Angelica Orsi, Magdalena M Lozinska, Clemence Sicard, Timothy Johnson, Nathalie Steunou, Paul A Wright, Christian Serre, Jorge Gascon, Freek Kapteijn,* "Influence of MOF Topology and Polymer Free-volume on Mixed Matrix Membrane Separation Performance", Euromembrane 2018 conference, **University of Valencia, Spain, July 2018.**

- *Anahid Sabetghadam, Xinlei Liu, Soraya Gottmer, Liangyong Chu, Jorge Gascon, Freek Kapteijn,* "Thin Mixed Matrix and Dual Layer Membranes Containing Metal-Organic Framework Nanosheets and Polyactive™ for $CO_2$ Capture", IZMM 2019 conference, **Lulea University of Technology, Sweden, June 2019.**

## Poster presentations

- *Anahid Sabetghadam, Beatriz Seoane, Jorge Gascon, Freek Kapteijn,* "Energy Efficient MOF-based Mixed Matrix Membranes for $CO_2$ Capture (M4CO2)", DPTI Annual Event**, Rotterdam, The Netherlands, November 2014.**

- *Anahid Sabetghadam, Eli Elderkamp, Beatriz Seoane, Jorge Gascon, Freek Kapteijn,* "Applying High Free-volume Polymers (PIM-1 & 6FDA-DAM) and MOFs ($NH_2$-MIL-53) in Mixed Matrix Membranes", EMG Annual event, **Apeldoorn**, **The Netherlands, June 2016.**

- *Anahid Sabetghadam, Beatriz Seoane, Damla Keskin, Nicole Duim, Tania Rodenas, Sara Sorribas, Clément Le Guillouzer, Guillaume Clet, Carlos Tellez, Marco Daturi, Joaquin Coronas, Freek Kapteijn, and Jorge Gascon*, "Application of Engineered MOF Crystals to Mixed-Matrix Membranes", DPTI Annual Event, **The Hague, The Netherlands, May 2016.**

- *Anahid Sabetghadam, Xinlei Liu, Marvin Benzaqui, Effrosyni Gkaniatsou, Angelica Orsi, Magdalena M Lozinska, Clemence Sicard, Timothy Johnson, Nathalie Steunou, Paul A Wright, Christian Serre, Jorge Gascon, Freek Kapteijn,* "Influence of Filler Pore Structure and Polymer on the Performance of MOF-Based Mixed-Matrix Membranes for $CO_2$ Capture", EuroMOF 2018, **TUDelft, The Netherlands, October 2017 (best poster award).**

# Acknowledgements

*"It is not joy that makes us grateful, it is gratitude that makes us joyful."*

*David Steindl-Rast*

Now that I look back to the last few years, I see my PhD experience as a great achievement for the rest of my life. I call it new beginning since it has changed tremendously my perspective towards life. I am so grateful to have this chance to grow and learn more. This chance was given to me by my promotor Prof.dr. Freek Kapteijn who trusted me to be his PhD student in M4CO2 project. Freek, it may not possible to express my gratitude by words, but how deeply you care about your student's improvement and success is something that I will never forget. You always gave me the feeling of confidence in myself and my work. Your great wisdom, leadership and looking deep in science influenced me a lot and your endless support encouraged me to be the best of who I am. Freek, thank you for all these years of tireless supervision.

Jorge, I had this great opportunity to have your guidance and constructive comments in my research and I really appreciate it. I learned from you that publishing the research results is possible if I learn the rules and do research in a systematic manner. Even if sometimes there was not a successful step, you showed me that this is just part of the game. I appreciate your great support and even criticism which makes me go forward faster and improved my abilities. Thank you for providing me this opportunity.

My PhD research would not reach to the end without guidance and kind technical assistance of technicians. Bart, thank you very much for being always there when I was stuck in my gas separation experiments and thank you for your positive attitude to help me to solve the issues in the lab. Harrie, thank you for your assistance in the gas separation setup construction and your great help to run it accurately. Willy, I always had some samples with mysterious properties and you always skillfully helped me figuring out which conditions for adsorption are the best and your complete explanation was truly helpful. Liliana, I was one of those PhD students that always came to you with a trouble in GC analysis and you were always tirelessly showed me how to manage the problem. Ben, thank you for your assistance for running the new XRD machine on my supported samples and helping me interpreting the data optimally. Marcel, you always kindly accepted my request to try AFM on the new materials, thank you for your support and assistance. Duco, thank you for teaching to use the SEM machine and for your assistance in ATR measurements. Hozanna, I really appreciate your help and support to train me to work with the FIB-SEM machine. You were always available even by phone whenever I had a problem. Bart (Boshuizen), thank you for your support in developing the LabVIEW sofware for the controllers of the gas separation setup.

I would like to take the chance to say a big thank you to our secretaries in the CE group; Els and Caroline. Els, I never forget your warm welcome in my first day in CE group. You are always welcome to everyone and you never disappointed me regarding the issues. Caroline, thank you very much for your help and support to send my samples to the project partners. Monique, thank you for your advice about the future and career as a woman. Michiel, thank you for the discussions about the mixed matrix membranes (MMMs) performance. I hope the fillers will be more efficient than salt and pepper!

I am sincerely thankful and appreciate the invaluable support from Beba and Xinlei during my PhD studies. Beba, it was a great chance for me to start my PhD when you were in the CE group. You thought me a lot and you brought me to the world of polymer and MOF synthesis and chemistry. Thank you so much for organizing all those meetings, discussions and guidance. Xinlei, it was my great opportunity that you joined our group. You gave me plenty of advice for doing efficient research and writing a paper. I am so grateful for your scientific support and for being always open for discussion and listening to my questions. I am also very thankful to Salman for sharing his experiences in membrane modeling and also his assitance in doing re-crystalization experiments.

I believe my PhD project was a great opportunity for me since I had this chance to be part of the M4CO2 big family which provides me with invaluable experiences. I would like to take the chance to express my deep gratitude to the project partners and for their great input in my research. John, Nathalie, Lino, Neil, Marvin, Timothy, Angelica, Paul, Clemence, Christian thank you so much for your collaborations in my thesis. The M4CO2 meetings was a great pleasure for me which helped me to learn more and broadened my knowledge. It also gave me the opportunity to share my results with pioneering researchers to have their comments.

In my PhD research, I was not alone. There was a number of smart Bachelor and Master students that I would like to thank them. Eli, I think you were a true talented student with challenging questions in the head. Sometimes, I needed to read more to find an answer to your questions and it helped both of us. Frederico, you were for a short time in the Netherlands, but you did a great job in both modelling and experimental studies thank you for accompanying me in part of my researches. Marije, your hard work led you to become fully expert in spin coating techniques and thin membrane preparation which is a quite challenging topic. We both learned a lot during doing those experiments. And Soraya, you were the last student during my PhD studies. You did a great master thesis including both experimental and modeling of the MMMs. You were also my language coach in learning Dutch. I would like to say a big thank you for your help in translating the summary and propositions of my thesis in Dutch.

In all these years, it was wonderful to be a part of the Catalysis Engineering group (CE) with all the enthusiastic people where we could share our experiences in both work and life and I would like to take this chance to say a big thank you to all. Meixia, thank you for accompanying me to re-assemble the gas separation setups during the moving from the old building. Also, thank you for all those relaxing Chinese tea time and the nice chats. Eduardo, thank you for all the memorable events that you initiated in the group even when you were in the shadow! We were officemate from the beginning of our PhD and I remember how fast you could trap a bee in the cup in the office! as a fencer there is no doubt that you can. Dima, your positive attitude was always stimulating. Thank you for suggesting and accompanying us for the perfect dinner in Prague. Lide, thank you for the the fun times that we had in the kingsday and a lot of nice memories. Maria, I will never forget your exciting BBQ parties in summertime. It was a real fun, playing the game of repeating the sounds, thank you for making all those nice memories. Xuerui, thank you for all the scientific discussions. Your suggestions were always really helpful. Ina, thank you for accompanying me for organizing the first international dinner and for your big hug when I had a hard day. Sumit, thank you very much for helping me to use the spin-coating machine and our nice collaboration. Miren, we were together in TUDelft, M4CO2, Euromembrane conference and this is not all, we are also together in MEMBER project, and during all these times you were always a great friend. Tim, thank you for your suggestions for writing the thesis. We still need to arrange a day trip to Kinderdijk. Alexey, thank you for all the scientific and historical chats. You have a special sense of humor in correlating things together! Yixiao, thank you so much for all the cute gifts from China and being such a kind friend. Jara, thank you for your positive energy and being such a enthusiastic person. Damla, we started our research together and I am so thankful for your great help and collaborations. Emanuel, thank you for sharing your experiences and perfect suggestions for using effectively the scientific search engines. Nastya, thank you for making the memorial clip of the group activities during the moving. Stefano, thank you for introducing the very useful softwares for showing crystal structures. Lorena, thank you for the process design suggestions to answer the reviewer's comments. Adrian, thank you for showing me how to switch on the heating in the office, but it is still puzzling if it really works. Robert, thank you for motivating me to go to the gym. Riming thank you for the beautiful souvenir from China. Davide, Constantino, Chengchung, Shrindhi, Guana, Agi, Alla, Irina, Elena, Filipe, Martijn, Fran, Alma and other group members thank you all for making CE enjoyable.

Fahime, you always gave me a positive energy. I am so happy that we were both in the ChemE department and we could share our experiences in Persian. Maryam, we found again each other here in Netherlands. I really enjoyed all the pleasant Christmas dinners together. Fatima, thank you for suggesting the nice trip to the island in Spain. I also really enjoyed all those breakfast we had together in the weekend.